

1999

Organic Thin Films for Photonics Applications

**Technical
Digest**

September 24-26, 1999

Santa Clara Marriott
Santa Clara, California



OSA
Optical Society of America

Postconference Edition

DISTRIBUTION STATEMENT A
Approved for Public Release
Distribution Unlimited

Jointly sponsored by
Optical Society of America
and the
American Chemical Society (POLY/PMSE)

REPORT DOCUMENTATION PAGE

AFRL-SR-BL-TR-01-

Public Reporting burden for this collection of information is estimated to average 1 hour per response, including the time for review, maintaining the data needed, and completing and reviewing the collection of information. Send comment regarding this burden estimate including suggestions for reducing this burden, to Washington Headquarters Services, Directorate for Information Operations and Services, Paperwork Reduction Project (0704-0188), Washington, DC 20503.

0020

1. AGENCY USE ONLY (Leave Blank)		2. REPORT DATE December 15, 2000		3. REPORT TYPE AND DATES COVERED Final Report 01/08/99 - 07/31/00	
4. TITLE AND SUBTITLE Organization of 1999 Organic Thin Films For Photonics Applications Topical Meeting				5. FUNDING NUMBERS US Air Force Office of Scientific Research F49620-99-1-0302	
6. AUTHOR(S) John A. Thorne					
7. PERFORMING ORGANIZATION NAME(S) AND ADDRESS(ES) Optical Society of America 2010 Massachusetts Ave., NW Washington DC 20036				8. PERFORMING ORGANIZATION REPORT NUMBER	
9. SPONSORING / MONITORING AGENCY NAME(S) AND ADDRESS(ES) AFOSR 801 N. Randolph St. Rm. 732 Arlington VA 22203-1977				10. SPONSORING / MONITORING AGENCY REPORT NUMBER	
11. SUPPLEMENTARY NOTES The views, opinions and/or findings contained in this report are those of the author(s) and should not be construed as an official Department of the Army position, policy or decision, unless so designated by other documentation.					
12 a. DISTRIBUTION / AVAILABILITY STATEMENT Approved for public release; distribution unlimited.				12 b. DISTRIBUTION CODE	
13. ABSTRACT (Maximum 200 words) The Organic Thin Films for Photonics Applications Topical Meeting provided an interdisciplinary forum for the presentation and discussion of new and previously unpublished results on advanced organic thin films materials with potential applications for photonics. Materials synthesis, fabrication, and processing were covered in depth and related to chemical, physical and optical properties. Theoretical and experimental studies regarding these properties were described. Particular emphasis was given to materials exhibiting electroluminescence; electrically and/or optically controlled optical functions; second-order, third-order, and photorefractive nonlinear optical properties; and other properties suitable for applications in optics. Both active and passive photonic device applications were discussed with a focus on the relationship between device performance and materials properties.					
14. SUBJECT TERMS				15. NUMBER OF PAGES	
				16. PRICE CODE	
17. SECURITY CLASSIFICATION OR REPORT UNCLASSIFIED	18. SECURITY CLASSIFICATION ON THIS PAGE UNCLASSIFIED	19. SECURITY CLASSIFICATION OF ABSTRACT UNCLASSIFIED	20. LIMITATION OF ABSTRACT UL		

NSN 7540-01-280-5500

Standard Form 298 (Rev.2-89)
Prescribed by ANSI Std. Z39-18
298-102

20010227 067

Organic Thin Films for Photonics Applications

**Technical
Digest**

September 24–26, 1999

Santa Clara Marriott
Santa Clara, California

Postconference Edition



OSA.
Optical Society of America

Jointly sponsored by
Optical Society of America
2010 Massachusetts Avenue, NW
Washington, DC 20036-1023
and the
American Chemical Society (POLY/PMSE)

Articles in this publication may be cited in other publications. To facilitate access to the original publication source, the following form for the citation is suggested:

Name of Author(s), "Title of Paper," in *Organic Thin Films for Photonics Applications*,
OSA Technical Digest (Optical Society of America, Washington DC, 1999), pp. xx-xx.

Optical Society of America

ISBN

Conference Edition	1-55752-580-3
Postconference Edition	1-55752-589-7
1999 Technical Digest Series	1-55752-584-6

Library of Congress Catalogue Card Number

Conference Edition	98-83002
Postconference Edition	99-64346

Copyright © 1999, Optical Society of America

Individual readers of this digest and libraries acting for them are permitted to make fair use of the material in it, such as to copy an article for use in teaching or research, without payment of fee, provided that such copies are not sold. Copying for sale is subject to payment of copying fees. The code 1-55752-584-6/99/\$15.00 gives the per-article copying fee for each copy of the article made beyond the free copying permitted under Sections 107 and 108 of the U.S. Copyright Law. The fee should be paid through the Copyright Clearance Center, Inc., 21 Congress Street, Salem, MA 01970.

Permission is granted to quote excerpts from articles in this digest in scientific works with the customary acknowledgment of the source, including the author's name and the name of the digest, page, year, and name of the Society. Reproduction of figures and tables is likewise permitted in other articles and books provided that the same information is printed with them and notification is given to the Optical Society of America. In addition, the Optical Society may require that permission also be obtained from one of the authors. Address inquiries and notices to Director of Publications, Optical Society of America, 2010 Massachusetts Avenue, NW, Washington, DC 20036-1023. In the case of articles whose authors are employees of the United States Government or its contractors or grantees, the Optical Society of America recognizes the right of the United States Government to retain a nonexclusive, royalty free license to use the author's copyrighted article for United States Government purposes.

Printed in the U.S.A.

Contents

Agenda	v
FA Second-Order NLO Materials: 1	1
FB Electro-Optic Devices: 1	15
FC Second-Order NLO Materials: 2	29
FD Light-Emitting Devices	45
SaA Electro-Optic Devices: 2	53
SaB Photostability	65
SaC Polymer Optical Fibers/Photorefractive Materials	79
SaD Second/Third Order Nonlinear Optical Effects: 1	97
SaE Poster Session	119
SuA Polymer Integrated Optics: 1	159
SuB Polymer Integrated Optics/2-Photon Absorption	173
SuC Polymer Integrated Optics: 2	187
SuD Second/Third Order Nonlinear Optical Effects: 2	201
SS Special Invited Speaker Presentation	227
Key to Authors and Presiders	229

Technical Program Committee

William H. Steier, *Univ. Southern California, USA, General Chair*

Robert Twieg, *Kent State Univ., USA, General Chair*

Alex K-Y. Jen, *Northeastern Univ., USA, Program Chair*

Robert A. Norwood, *Photon-X, Inc., USA, Program Chair*

Paul Ashley, *US Army Missile Command, USA*

Larry Dalton, *Univ. of Washington, USA*

Louay Eldada, *AlliedSignal Inc., USA*

Susan Ermer, *Lockheed Martin Missiles & Space, USA*

Steve Forrest, *Princeton Univ., USA*

Zakya Kafafi, *Naval Res. Lab., USA*

Yasuhiro Koike, *Keio Univ., Japan*

Mark G. Kuzyk, *Washington State Univ., USA*

Hilary S. Lackritz, *Gemfire Corp., USA*

George F. Lipscomb, *Lightwave Microsystems, USA*

Robert D. Miller, *IBM Almaden Res. Ctr., USA*

Nasser Peyghambarian, *Univ. of Arizona, USA*

Xina Quan, *Lucent Tech./Bell Labs., USA*

Yongqiang Shi, *TACAN Corp., USA*

George I. Stegeman, *Univ. of Central Florida, USA*

Yang Yang, *Univ. of California, Los Angeles, USA*

Joseph Zyss, *École Normale Supérieure de Cachan, France*

International Advisory Committee

Richard Friend, *Cavendish Lab., UK*

Peter Günter, *Inst. of Quantum Electronics, ETH Zurich, Switzerland*

Alan Heeger, *Univ. of California, Santa Barbara, USA*

Toshikuni Kaino, *Tohoku Univ., Japan*

Barrie Keyworth, *JDS Fitel Inc., Canada*

Wolfgang Knoll, *Max-Planck-Inst. Für Polymerforschung, Germany*

Seizo Miyata, *Tokyo Univ. of Agriculture & Tech., Japan*

Almeria Natansohn, *Queen's Univ., Canada*

André P. Persoons, *Univ. of Leuven, Belgium*

Hiroyuki Sasabe, *RIKEN, Japan*

Agenda

■ Friday

■ September 24, 1999

8:15am-8:30am

California Ballroom Salons 4&5

Opening Remarks

8:30am-10:00am

California Ballroom Salons 4&5

FA ■ Second-Order NLO Materials 1

Larry R Dalton, Univ. of Washington, Presider

FA1 8:30am (Invited)

Comparison of simple theory and experiment on the electro-optic coefficient of high dipole moment materials, Bruce H. Robinson, Larry R. Dalton, Univ. Washington, USA

Intermolecular electrostatic interactions among chromophores inhibit the introduction of acentric chromophore order (ACO) by electric field poling. We outline a statistical-mechanical approach to estimating the ACO and the effects of molecular shape. Examples are compared to theory and shown to improve ACO. (p. 2)

FA2 9:00am

High performance side-chain aromatic polyquinolines for E-O devices, Alex K.-Y. Jen, Hong Ma, Jianyao Wu, Xiaoming Wu, Sen Liu, Northeastern Univ., USA; Seth Marder, Univ. Arizona, USA; Larry Dalton, Univ. Washington, USA

High performance side-chain NLO polyquinolines with high E-O activity and a good combination of thermal, optical, electrical and mechanical properties have been developed. (p. 3)

FA3 9:15am

Second-harmonic generation in single-crystal thin-films of 3-methyl-4-methoxy-4'-nitrostilbene (MMONS), Shida Tan, Achintya Bhowmik, Sunil Sodah, Mrinal Thakur, Auburn Univ., USA

Single-crystal thin-films of MMONS have been grown, and the effective d-coefficient for light propagating perpendicular to the film has been measured to be ~180 pm/V. (p. 6)

FA4 9:30am

Quadrupolar molecular nonlinear optics, V.

Ostroverkhov, O. Ostroverkhova, R.G. Petschek, K.D. Singer, Case Western Reserve Univ., USA; L. Sukhomlinova, R.J. Twieg, Kent State Univ., USA

We describe a new approach to second order nonlinear optics that can be activated in macroscopic media by non-polar axial alignment. (p. 8)

FA5 9:45am

Intermolecular interactions of highly nonlinear optical molecules for electro-optic polymer applications, I.

Liakatas, C. Cai, M. Bösch, M. Jäger, Ch. Bosshard, P. Günter, Swiss Federal Institute of Technology, Switzerland; Cheng Zhang, Larry R. Dalton, Univ. Southern California, USA

The molecular optical nonlinearity of highly nonlinear optical molecules, their intermolecular interactions and the effect of the environment on their nonlinearity are presented and discussed. (p. 11)

10:00am-10:30am

California Ballroom Foyer

Coffee Break

10:30am-12:00pm

California Ballroom Salons 4&5

FB ■ Electro-Optic Devices: 1

Alex K.-Y. Jen, Northeastern Univ., Presider

FB1 10:30am (Invited)

Can drive voltages of less than one volt be systematically achieved for polymeric electro-optic devices?

Larry R. Dalton, Univ. Washington, USA

It is generally conceded that to systematically achieve electro-optic device operational voltages of 1 volt or less will require that such devices be fabricated from materials characterized by electro-optic coefficients of 75 pm/V or greater at the operational wavelength. If currently available organic second order nonlinear optical chromophores could be assembled into perfect acentric lattices, macroscopic electro-optic coefficients of many hundred picometers/volt would result. Values are systematically exceeding 75 pm/V. (p. 16)

FB2 11:00am

Polymer waveguides for second-order nonlinear-optical effects at telecommunication wavelengths, *Tomas Pliska, Wook-Rae Cho, Vincent Ricci, Joachim Meier, Anne-Claire Le Duff, Michael Canva, George I. Stegeman, Univ. Central Florida, USA; Paul Raymond, François Kajzar, Centre d'Études de Saclay, France*

Modal dispersion phase matched second-harmonic generation at 1.55 μm wavelength is demonstrated in multiple layer waveguide structures using transparent nonlinear-optical polymers. (p. 17)

FB3 11:15am

Microstrip line-slot ground electrode for high-speed optical push-pull polymer modulators, *Yongqiang Shi, Weiping Lin, David J. Olson, James H. Bechtel, TACAN Corporation, USA; Wenshen Wang TRW Inc., USA*
A new electrode circuit is designed for poling and driving high-speed optical push-pull electrooptic polymer modulators. Numerical simulation and experiments showed a wideband frequency response. (p. 20)

FB4 11:30am

A compact optical branch, composed of a half-mirror and a rectangularly crossed waveguide, *Jiro Toyama, Takeshi Yamada, Yasuhiro Kubota, Ichiro Takatsu, NOK Corp., Japan*
A novel optical waveguide branch, made of fluoride polyimide is reported. Mass-productivity and cost reduction are expected by the compact design. (p. 23)

FB5 11:45am

Bragg gratings by photo-bleaching in polymer waveguides, *Vadim Chuyanov, Araz Yacoubian, Sean Garner, William H. Steier, Univ. Southern California, USA; Dmitry Starodubov, Jack Feinberg, D-STAR Technologies, USA; Antao Chen, Lucent Technologies, USA*
We present results of the measurements of optical and thermo-optical properties of Bragg gratings produced by photobleaching in nonlinear optical polymer based waveguides. (p. 26)

NOON-1:30pm

Lunch on your own

1:30pm-3:00pm

California Ballroom Salons 4&5

FC ■ Second-Order NLO Materials: 2

James R. Heflin, Virginia Polytechnic Inst., President

FC1 1:30pm (Invited)

Ultrafast optoelectronics using poled polymers, *Ajay Nahata, AlliedSignal Inc, USA; Tony F. Heinz, Columbia Univ., USA*

We describe the use of nonlinear non-resonant interactions in poled polymers for the generation and detection of ultrashort electrical transients, with an inherent response time limited only by the duration of the optical pulse. We discuss applications to high speed circuit characterization and coherent THz spectroscopy. (p. 30)

FC2 2:00pm

Characterization of dye-containing polymers ability to be optically oriented, *Michel Dumont, Michel Fischer, Laboratoire de Photonique Quantique et Moléculaire ENS de Cachan, France*
The study of photoinduced anisotropy gives a simple characterization of the ability of chromophores to be oriented optically for nonlinear optics. Experiments and theoretical model are presented. (p. 32)

FC3 2:15pm

Efficient poling-low induced losses tradeoff for efficient SHG in poled-polymer waveguides at 1.55 microns, *Vincent Ricci, George Stegeman, Univ. Central Florida, USA; Kwok Pong Chan, Molecular OptoElectronics Corporation, USA*

Matching glass transition temperatures yields an increased parallel plate poling efficiency by 3.5. A tradeoff between poling-induced losses and high poling efficiency is identified. (p. 35)

FC4 2:30pm

Nonlinear optical films formed layer-by-layer using alternating polyelectrolyte deposition, *M. Joseph Roberts, Naval Air Warfare Center, USA*

The formation of acentric films using alternating polyelectrolyte deposition (APD) has been achieved on hydrophobic and hydrophilic glass substrates. (p. 38)

FC5 2:45pm

Nonlinear optical study of chiral 1,1'-binaphthyl based helical polymers, *Sven Van Elshocht, Thierry Verbiest, Martti Kauranen, André Persoons, K.U. Leuven, Belgium; Liang Ma, Hua Cheng, Kwon Y. Musick, Lin Pu, Univ. Virginia, USA*

We have determined the nonlinear optical response and the Langmuir-Blodgett forming properties of a series of chiral 1,1'-binaphthyl based helical polymers. (p. 41)

3:00pm-3:30pm

California Ballroom Foyer

Refreshment Break

3:30pm-5:30pm

California Ballroom Salons 4&5

FD ■ Light-Emitting Devices

Alex K-Y. Jen, Northeastern Univ., Presider

FD1 3:30pm (Invited)

Interfacial issues in organic light emitting diodes,

Neal R. Armstrong, Univ. Arizona, USA

This talk will review recent work from this group on two-component, small molecule OLEDs, and the characterization of the energetics of the critical interfaces in these devices. (p. 46)

FD2 4:00pm (Invited)

Patterning and electrochemical deposition of conjugated and conducting polymers in light emitting devices, *Daniel B. Roitman, Hewlett Packard, USA; Seiji Inaoka, Rigoberto Advincula, Univ. Alabama, USA*

We have recently discovered a novel electrochemical

approach for depositing very high quality films for conducting and conjugated polymers. (p. 48)

FD3 4:30pm (Invited)

Device performance and polymer morphology in polymer light emitting diodes, *Y. Shi, J. Liu, Y. Yang, Univ. California*

The performance of MEH-PPV based light emitting diodes is strongly affected by the morphology of spin-coated polymer films, which can be controlled by varying the solvent and concentration of the polymer solution as well as the spin-speed. (p. 49)

FD4 5:00pm (Invited)

Progress in organic electroluminescent devices with air stable cathodes, *Ghassan E. Jabbour, Univ. Arizona, USA*

Different air stable cathode structures that allow the better electron injection, which leads to the fabrication of brighter and more efficient organic light-emitting devices, will be presented. (p. 51)

7:00pm-9:00pm

California Ballroom Salons 4&5

Special Invited Speaker

SS1 7:00pm (Invited)

Spatial light modulator using high T_g poled polymers, *T. Yatagai, Univ. Tsukuba, Japan*

A high-speed electrically-addressed spatial light modulator with a resonant structure is designed using poled polymers of DR1-PMPD and PMPD. (p. 228)

Postdeadline Paper Session

■ **Saturday**
■ **September 25, 1999**

8:30am-10:00am

California Ballroom Salons 4&5

SaA ■ Electro-Optic Devices: 2

William H. Steier, Univ. of Southern California, Presider

SaA1 8:30am (Invited)

High-speed electro-optic modulators based on organic waveguides, *Feng Pan, Molecular Optoelectronics Corp., USA*

Organic crystals with improved dielectric and electro-optic properties were used to make high speed EO-devices. The techniques for coupling the organic crystal waveguides with polished fibers to create high speed EO-devices are summarized. A new class of chiral polymers were also evaluated for long term EO stability. (p. 54)

SaA2 9:00am

Demonstration of 5 MHz single-pass electro-optic modulators using single-crystal thin-films of organic molecular salts, *Achintya K. Bhowmik, Ayayi C. Ahyi, Alpina Mishra, Mrinal Thakur, Auburn Univ., USA*
Single-pass electro-optic modulators operating at 5.63 MHz have been demonstrated using DAST and SPCD single-crystal thin-films. (p. 55)

SaA3 9:15am

Young's fringe dual slab waveguide sensor, *Graham H. Cross, Yitao Ren, Univ. Durham, UK; Neville J. Freeman, Benharret Bouattou, Fairfield Sensors, Ltd., UK*
Two vertically integrated polymer slab waveguides form an optical sensor. Far-field output patterns provide Young's fringes from phase changes can be measured. (p. 57)

SaA4 9:30am

Fabrication and characterization of electro-optic polymeric e-field sensors, *Ram Sivaraman, Stephen J. Clarson, Kevin Burcham, David Naghaski, Joseph T. Boyd, Univ. Cincinnati, USA*
Optical waveguides, also known as dielectric waveguides are the structures that are used to confine and guide the light in the guided-wave devices and circuits of integrated optics. A well known waveguide is an optical fiber which has a circular cross section. In contrast guides of interest to integrated optics are usually planar structures such as planar films or strips. The concept of integrating an electro-optic polymer into a reverse poled Mach-Zehnder modulator to be used as an electrode-less E-field sensor is discussed in this work. The two possible core layers (PMMA and PPO), and the upper cladding layer (HMDS) will be the guide layers. (p. 60)

SaA5 9:45am

Waveguide polarizers and polarization splitters with a buried birefringent polymer, *Min-Cheol Oh, Myung-Hyun Lee, Hyung-Jong Lee, Electronics and Telecommunications Research Institute, Korea*

By incorporating birefringent polyimide in low-loss fluorinated polymer waveguides, we demonstrate a pair of TE-pass and TM-pass polarizers and polarization splitters by using the polyimide as a buried rib. (p. 62)

10:00am-10:30am

California Ballroom Foyer
Coffee Break

10:30am-12:15pm

California Ballroom Salons 4&5

SaB ■ Photostability

George Stegeman, Univ. of Central Florida, USA, Presider

SaB1 10:30am (Invited)

Systematics of NLO chromophore photochemical stability, *Tony C. Kowalczyk, Xuan Q. Zhang, Hilary S. Lackritz, Gemfire Corporation, USA; Adriana Galvan-Gonzalez, Michael Canva, George I. Stegeman, Univ. Central Florida, USA; Robert Twieg, Kent State Univ., USA; Seth Marder, S. Thayumanavan, Univ. Arizona, USA*
The design of chromophores for high performance electro-optic devices demands not only outstanding optical, nonlinear, and thermal stability properties, but also photochemical stability. In this paper, we report on evaluating photochemical stability of nonlinear optical dyes. (p. 66)

SaB2 11:00am (Invited)

Effect of environmental factors on the photodegradation of azobenzene doped polymers, *George I. Stegeman, Adriana Galvan-Gonzalez, Michael Canva, Univ. Central Florida, USA; Robert Twieg, Kent State Univ., USA; Tony C. Kowalczyk, Hilary S. Lackritz, Gemfire Corporation, USA; Seth Marder, S. Thayumanavan, Univ. Arizona, USA*
We investigated the photodegradation of azobenzene-based electro-optic polymers and its dependence on different donors and acceptors, temperature, atmosphere and guest-host versus side-chain. (p. 67)

SaB3 11:30am

Effects of the host matrix on near infrared red tail absorption of chromophore doped polymer waveguides, *Anne-Claire Le Duff, Vincent Ricci, Tomas Pliska, Michael Canva, George Stegeman, Univ. Central Florida, USA; K. Pong Chan, Molecular Optoelectronics Corporation, USA; Robert Twieg, Kent State Univ., USA*
The choice of host polymer has a dramatic impact on the absorption tail in the near-infrared of electro-optic chromophores and their associated waveguide loss. (p. 70)

SaB4 11:45am

Photochemical stability of highly nonlinear optical chromophores for electro-optic applications, *M. Bösch, C. Fischer, C. Cai, I. Liakatas, M. Jäger, Ch. Bosshard, P. Gunter, Swiss Federal Institute of Technology, Switzerland*
The photochemical stability of highly nonlinear optical bithiophene chromophores is investigated. Experiments in guest-host systems indicate that these chromophores are excellent candidates for electro-optic applications. (p. 73)

SaB5 NOON

Observation of environmentally sensitive photoluminescence from highly polar chromophores, *Marek Szablewski, Yasuyuji Kagawa, David Bloor, Mosurkal Ravi, Graham H. Cross, Univ. Durham, UK*
Matrix dependant photoemission was observed for highly polar derivatives of TCNQ. Fluorescent emission is enhanced in environments which hinder conformational change in the chromophore. (p. 76)

NOON-1:30pm

Lunch (on your own)

1:30pm-3:00pm

California Ballroom Salons 4&5

SaC ■ Polymer Optical Fibers/Photorefractive Materials

Robert Twieg, Kent State Univ., Presider

SaC1 1:30pm

Single-mode electrooptic polymer optical fiber, *David J. Welker, Dennis W. Garvey, C. D. Breckon, Sentel Technologies L.L.C., USA; Mark G. Kuzyk, Washington State Univ., USA*

We report on single mode polymer optical fiber with embedded electrodes, including polling the nonlinear core and phase modulating the light in the waveguide. (p. 80)

SaC2 1:45pm

Propagating mode attenuation and coupling characteristics of graded-index POF, *Takaaki Ishigure, Mariko Kano, Yasuhiro Koike, Keio Univ., Japan*

It was clarified for the first time that the power distribution of modes formed by the mode dependent attenuation was the dominant factors of the higher bandwidth of the GI POF than theoretically predicted bandwidth, while the effect of the mode coupling was small. (p. 83)

SaC3 2:00pm

Thermal stability of high bandwidth GI POF, *M. Sato, M. Hirai, T. Ishigure, Y. Koike, Keio Univ., Japan*
The progress of PMMA-dopant system graded-index polymer optical fiber (GI POF) for high thermal stability in both bandwidth and attenuation is described. (p. 86)

SaC4 2:15pm

Paper withdrawn.

SaC5 2:30pm

Extended dihydropyridine chromophores for photorefractive polymers, *D. Wright, J. D. Casperson, Univ. California, San Diego, USA; F. You, R. J. Twieg, Kent State Univ., USA; W. E. Moerner, Stanford Univ., USA*
We describe photorefractive polymer composites based on poly (n-vinylcarbazole) doped with representatives from a new class of high-figure-of-merit extended dihydropyridine chromophores. (p. 90)

SaC6 2:45pm

Dual grating photorefractive polymer, *L. Michael Hayden, Shane J. Strutz, Univ. Maryland Baltimore County, USA*
We will present materials capable of storing quasi-permanent photochemical and erasable photorefractive holographic gratings simultaneously in the same volume and discuss their application. (p. 93)

3:00pm-3:30pm

California Ballroom Foyer

Refreshment Break

3:30pm-5:45pm

California Ballroom Salons 4&5

SaD ■ Second/Third Order Nonlinear Optical Effects: 1

Joseph W. Perry, Univ. of Arizona, Presider

SaD1 3:30pm (Invited)

Novel approaches to ionically self-assembled nonlinear optical thin films, *J.R. Heflin, C. Figura, P.J. Neyman, M.A. Murray, R.M. Davis, Virginia Tech. USA; D. Marciu, M. Miller, F&S, Inc., USA*
Ionically self-assembled monolayers produce spontaneously noncentrosymmetric nonlinear optical films. Detailed studies of the structure of these films and methods for increasing order are described. (p. 98)

SaD2 4:00pm

Acoustic spectrum analysis using polymer integrated optics, *Araz Yacoubian, Vadim Chuyanov, Sean M. Garner, Hua Zhang, William H. Steier, Albert S. Ren, Galina Todorova, Larry R. Dalton, Univ. Southern California, USA*
We present nonlinear optical polymer based acoustic spectrum analyzer in a scanning heterodyne geometry. The system has the potential to measure sub-micron amplitude vibrations at GHz frequencies. (p. 101)

SaD3 4:15pm (Invited)

Circular-difference effects in second-harmonic generation from thin films, *Thierry Verbiest, Sven Van Elshocht, Sonja Sioncke, Martti Kauranen, Andre Persoons, K. U. Leuven, Belgium*

Circular-difference effects in second-harmonic generation from chiral anisotropic films are studied. We demonstrate that chirality- and anisotropy-contributions to the circular-difference effects can be separated. (p. 104)

SaD4 4:45pm

High frequency demodulation of multi-photon fluorescence in femtosecond hyper-Rayleigh scattering experiments at both 800 and 1300 nm, *Geert Olbrechts, Koen Clays, Kurt Wostyn, Andre Persoons, Univ. Leuven, Celestijnenlaan, Belgium*

The Fourier content of a femtosecond laser pulse is used to measure the fluorescence-free first hyperpolarizability value of fluorescent chromophores by hyper-Rayleigh scattering. (p. 107)

SaD5 5:00pm

Hyper-Rayleigh scattering of nonlinear optical chromophores at 1064 nm and 1907 nm, *Jeffrey N. Woodford, C.H. Wang, Univ. Nebraska-Lincoln, USA; Alex K.-Y. Jen, Northeastern Univ., USA*

The first hyperpolarizabilities of novel optical chromophores have been measured using a two-photon scattering technique. Relationships between the first hyperpolarizabilities and molecular structure will be elucidated. Theoretical methods for explaining the dispersion effect of the first hyperpolarizability will be discussed. (p. 110)

SaD6 5:15pm

Remarkable enhancement of first hyperpolarization of polynorbornenes studied by Hyper-Rayleigh scattering, *Chia-Chen Hsu, Tzer-Hsiang Huang, Sean Liu, Fen-Fen Yeh, National Chung Cheng Univ.; Bih-Yaw Jin, Jitendra A. Sattigeri, Chung-Wai Shiau, Tien-Yau Luh, National Taiwan Univ., Taiwan*

The Hyper-Rayleigh scattering (HRS) was employed to study the second order nonlinear optical properties of polynorbornenes that contain nonlinear optical chromophores as pendant groups. Remarkable enhancement of first hyperpolarizabilities (β) of the polynorbornenes was observed as a result of the rigidity of the polymer backbone. The HRS results showed that the polymers should adopt a syndiotactic structure, which agrees with the open force field calculations. (p. 113)

SaD7 5:30pm

Determining the fifth order nonlinear optical susceptibility of a polydiacetylene film, *Ke Yang, Jayant Kumar, Sukant Tripathy, Univ. Massachusetts at Lowell, USA; Woohong Kim; Samsung Central Research Inst. of Chemical Technology, Korea*

The dispersion of the fifth order nonlinear optical susceptibility of a spin coated polydiacetylene film (poly(BPOD)) was determined through electroabsorption spectroscopy. (p. 116)

5:45pm-7:00pm

California Ballroom Salons 1,2&3

SaE ■ Poster Session

SaE1

Design guidelines for molecules with large hyperpolarizabilities for third-order nonlinear optics, *U. Gubler, Ch. Bosshard, P. Günter, R. Martin, R. R. Tykwinski, F. Diederich, Swiss Federal Institute of Technology ETH, Switzerland; V. Alain, M. Blanchard-Desce, Ecole Normale Supérieure, France*

We present new optimization rules and refinements of established guidelines for optimization of third-order nonlinear optical properties and demonstrate them on various molecular systems. (p. 120)

SaE2

Polymer enhanced diffraction efficiency in an azo-dye doped liquid crystal, *Gene Carlisle, Manlin Pei, Young-Jing Wang, Texas A&M Univ., USA*

Using degenerate four-wave mixing experiments, a five-fold enhancement in the diffraction efficiency (12%) was observed for a dye- and polymer-doped liquid crystal. (p. 123)

SaE3

New states of light in nonlinear organic thin films and polymeric waveguides, *V.M. Chapela, J. Percino, V.N. Serkin; Benemerita Univ.; Eduard Schmidt, Friedrich-Schiller Univ.; T. L. Belyaeva, Lomonosov Moscow State Univ., Russia*
The optical video solitons, which is a stable solitary electromagnetic wave without high-frequency field components, is predicted in the strong nonlinear organic polymer. (p. 126)

SaE4

Soliton attractors in polymer film waveguides, *V.M. Chapela, J. Percino, V.N. Serkin, Benemerita Univ.; T.L. Belyaeva, Lomonosov Moscow State Univ., Russia*
It is shown that strong high order cubic-quintic nonresonant electronic nonlinearity combined with two-photon absorption lead to the soliton attractor generation in the organic polymer crystals and polymer waveguides. (p. 129)

SaE5

Measurement techniques for the real and imaginary part of the third-order nonlinear optical susceptibility, U. Gubler, Ch. Bosshard, P. Günter, *Swiss Federal Institute of Technology ETH, Switzerland*; R. Negres, D. Hagan, *Univ. Central Florida, USA*

We introduce three experimental techniques to measure real and imaginary part of third-order nonlinear optical properties including time resolution, leading to a complete material characterization. (p. 132)

SaE6

Photoinduced birefringence in poled azo dyes doped side-chain polymers at 632.8 nm, Myung-Hyun Lee, Hyung-Jong Lee, Min-Cheol Oh, *Telecommunication Basic Research Lab, ETRI, Korea*

The photoinduced changes in the electro-optic coefficients of poled azo dye-doped side-chain polymers are reported. The trans-cis photoisomerization occurs at the 632.8 nm wavelength. (p. 135)

SaE7

Optical polymer-amplifier enhanced with photo-induced periodic gain profile, Satoshi Tanaka, Takanori Kemanai, Heihachi Sato, *National Defense Academy, Japan*; Seiichiro Hayakawa, *Mitsubishi Chemical Corporation, Japan*
Inducing a periodic gain-profile onto dye-doped organic polymer by using the interference-pattern of Nd:YAG (532 nm) laser, an extremely high-gain is selectively obtained at a specific wavelength near 585 nm. (p. 138)

SaE8

Unique two-dimensional effects in the first hyper-polarizability of molecules with carbazole donor groups, G. Berkovic, G. Meshulam, Z. Kotler, *Soreq NRC, Israel*; A. Ben-Asuly, L. Shapiro, V. Khodorkovsky, Ben-Gurion Univ. Negev, Israel

Substitution of a carbazole donor group in conjugated organic molecules induces a negative β_{xxx} hyper-polarizability which can cancel out the long axis β_{zzz} coefficient. (p. 141)

SaE9

Synthesis and nonlinear optical properties of high glass transition polyimides and poly(maleimide-styrene)s, Celest Samyn, Kurt Van den Broeck, Thierry Verbiest, André Persoons, *Univ. Leuven, Celestijnenlaan, Belgium*

New nonlinear optical polyimides and polymaleimides were synthesized, they showed T_g 's : 189-275°C, $d_{33}(0)$ -values up to 12.5 pm/V and remaining NLO-efficiency up to 90% at 125°C during 1000h. (p. 144)

SaE10

Organic photosensors for ferroelectric liquid crystal spatial light modulators, Scott Dickey, Blake Eliasson, Garret Moddel, *Univ. Colorado, USA*

A bi-layer organic photosensor has been developed with sufficiently high hole mobility to drive ferroelectric liquid crystal optically addressed spatial light modulators. (p. 147)

SaE11

Bistable optical transmittivity in an ultrathin film of oriented molecular aggregates, Karl-Heinz Feller, Holger Glaeske, *Physikalische, Germany*; Victor Malyshev, *Vavilov State Optical Institute, Russia*

A theoretical study of the nonlinear optical response of a thin film comprised of oriented linear Frenkel chains is carried out, and realizability of bistability effects is discussed. (p. 150)

SaE12

Paper withdrawn.

SaE13

Optical anisotropy of all optically induced $\chi^{(2)}$ polar structures, Naoto Tsutsumi, Masanori Imamura, Yoshiki Ikeyama, Jun Yamamoto, Wataru Sakai, *Kyoto Institute of Technology, Japan*

We present optical anisotropy of noncentrosymmetric NLO dipolar orientation ($\chi^{(2)}$ structures) induced by the cubic interference waves in the NLO polymeric materials. (p. 154)

SaE14

Photorefractive mechanisms in liquid crystal and polymer composites, Oksana Ostroverkhova, Jingwen Zhang, Kenneth D. Singer, *Case Western Reserve Univ., USA*; Ludmilla Sukhomlinova, Robert J. Twieg, *Kent State Univ., USA*

We report on temperature and structure dependent measurements of photorefractive properties revealing trapping and orientational electro-optic properties. (p. 157)

7:00pm-8:30pm

California Ballroom Salons 4&5
Conference Reception

■ **Sunday**
■ **September 26, 1999**

8:30am-9:45am

California Ballroom Salons 4&5

SuA ■ Polymer Integrated Optics: 1

Robert A. Norwood, Photon-X, Inc., Presider

SuA1 8:30am (Invited)

Rare earth doped polymer optical amplifiers, *R. Gao, A.F. Garito, Univ. Pennsylvania, USA*

Based on recent advances in polymer optical waveguides and fibers, we are investigating rare earth doped polymers for optical amplification. (p. 160)

SuA2 9:00am

Photochromic media with sensitivity in the visible spectra, *Igor Chapurin, Stephan Robu, State Univ. Moldova; Kazutaka Oba, Yehaiahu Fainman, Univ. California, San Diego, USA*

We report a new photochromic composite polymer consisting of poly-epoxypropylcarbazole (PEPC) host with a spiropyran (SP) dye dopant. The experimental measurements are evaluated in conjunction with its potential applications for optical holographic recordings in the visible spectral range. (p. 163)

SuA3 9:15am

Fabrication of polymeric large-core optical waveguides using a rubber molding process, *Byung-Tak Lee, Min-Suk Kwon, Jun-Bo Yoon, Sang-Yung Shin, Korea Advanced Institute of Science and Technology, Korea*
We report simple and low-cost fabrication of polymeric large-core (47 μ m x 41 μ m) optical waveguides using a rubber molding process. (p. 166)

SuA4 9:30am

Polarization sensitive surface relief gratings formed on amorphous azopolymer films, *Nirmal K. Viswanathan, Jayant Kumar, Sukant K. Tripathy, S. Balasubramanian, Univ. Massachusetts at Lowell, USA*
Polarized read beams probe unique optical properties of the surface relief gratings (SRG). Specific applications to fabricate polarization discriminators and polarization beamsplitters will be discussed. (p. 169)

9:45am-10:15am

California Ballroom Foyer
Coffee Break

10:15am-11:45am

California Ballroom Salons 4&5

SuB ■ Polymer Integrated Optics/2-Photon Absorption

Lisa Dhar, Lucent Technologies, Presider

SuB1 10:15am (Invited)

Materials for two-photon 3D lithography, *Joseph W. Perry, Sundaravel Ananthavel, Kevin Cammack, Stephen M. Kuebler, Seth R. Marder, Mariacristina Rumi, Univ. Arizona, USA; Brian H. Cumpston, Ahmed A. Heikal, Jeffrey E. Ehrlich, Lael L. Erskine, Michael D. Levin, Matthew Lipson, Diane McCord-Maughon, Harald Rockel, CalTech, USA*
Conjugated organic chromophores with large two-photon absorption cross-sections have been developed and employed to prepare highly-sensitive nonlinear photopolymer systems, which can be used for 3D-microfabrication and optical data storage. (p. 174)

SuB2 10:45am

Two-photon photoinitiated polymer processing and microfabrication, *Kevin D. Belfield, Xiaobin Ren, David J. Hagan, Eric W. Van Stryland, Vladislav Dubikovsky, Edward J. Miesak, Univ. Central Florida, USA*
The near-IR two-photon induced polymerization of methacrylate monomers using a commercially available photoinitiator system is reported. Several microstructures have been fabricated via two-photon photoinitiated polymerization. (p. 178)

SuB3 11:00am

Molecular hyperpolarizability in the two-photon resonance regime: Measurement and analysis, *G. Berkovic, G. Meshulam, Z. Kotler, Soreq NRC, Israel*
Enhancement of molecular hyperpolarizability near the two photon resonance is analyzed experimentally and theoretically using a modified two level model including damping and inhomogeneous broadening. (p. 181)

SuB4 11:15am (Invited)

Polymer photonic components for WDM, *Claire L. Callender, J.-F. Viens, J.P. Noad, Communications Research Centre, Canada; L. Eldada, R.A. Norwood, AlliedSignal Inc., USA*
Design, fabrication and characterization of polymer-based arrayed waveguide grating components for broad-band and dense WDM applications are described. (p. 184)

11:45am-1:30pm

Lunch on your own

1:30pm-2:45pm

California Ballroom Salons 4&5

SuC ■ Polymer Integrated Optics: 2

Louay Eldada, AlliedSignal, Inc., USA, Presider

SuC1 1:30pm (Invited)

Photopolymer media for holographic data storage,

Lisa Dhar, Arturo Hale, Melinda Schnoes, Marcia Schilling, Howard Katz, Carol Boyd, Kevin Curtis, Michael Tackitt, William Wilson, Adrian Hill, Lucent Technologies, USA

We discuss the design and fabrication of high dynamic range, high optical quality, thick photopolymer media for digital holographic data storage. (p. 188)

SuC2 2:00pm

Reliable polymers for OADM applications, Constantina

Poga, Robert Andrew Norwood, AlliedSignal Inc., USA

Reliability issues for polymeric components for optical telecommunications are addressed. The reliability program is outlined and material and component environmental tests are presented. (p. 191)

SuC3 2:15pm

Reversible structuring of optical waveguides using optical switch molecules, M. Jäger, S. Lecomte, U. Gubler, Ch. Bosshard, P. Günter, L. Gobbi, F. Diederich, Swiss Federal Institute of Technology, Switzerland

We investigate the linear and nonlinear optical properties of optical switch molecules in solution and polymeric films. The reversible structuring of optical waveguides is demonstrated. (p. 194)

SuC4 2:30pm

Low-loss polymer waveguide applications based on crosslinked fluorinated poly(arylene ether)s, Hyung-Jong Lee, Myung-Hyun Lee, Min-Cheol Oh, Joo-Heon Ahn, Wol-Yon Hwang, Seon Gyu Han, Telecommunication Basic Research Lab. Electronics and Telecommunications Research Institute, Korea

Thermally crosslinked fluorinated poly(arylene ether) derivatives are synthesized and characterized for low loss polymer optical waveguide devices such as thermo-optic switches and wavelength filters. (p. 197)

2:45pm-3:15pm

California Ballroom Foyer

Refreshment Break

3:15pm-5:15pm

California Ballroom Salons 4&5

SuD ■ Second/Third Order Nonlinear

Optical Effects: 2

Andre Pierre Persoons, Univ. of Leuven, Presider

SuD1 3:15pm

Heterocyclic liquid crystals designed for optical light emitting diode applications, R. J. Twieg, S. Gu, L.

Sukhomlinova, Kent State Univ., USA; G.G. Malliaras, R. Fan, D. Culjkovic, Cornell Univ., USA

We have prepared heterocyclic mesogens that function as electron transport agents and lumiphores. Preliminary results on diodes fabricated from these materials will be presented. (p. 202)

SuD2 3:30pm

Monte carlo modeling method for light transport in organic thin film light-emitting devices, Aldo Badano, Jerzy Kanicki, Univ. Michigan, USA

We describe a Monte Carlo modeling method to study the effect of light transport processes on the optical performance of organic thin film light-emitting devices. The method is based on the tracking of individual photons through statistically described scattering events. Preliminary simulation results indicate that surface roughness can double the photon extraction efficiency, and that absorption at the top electrode can decrease the device diffuse reflectance by a factor of 20. (p. 205)

SuD3 3:45pm

Spectroscopy of the instantaneous all-optical switching nonlinearity of thin films, F.P. Strohkendl, R.J. Larsen, L. R. Dalton, Univ. Southern California, USA; Z.K. Kafafi, Naval Research Laboratory, USA

We demonstrate widely tunable ultrafast nearly-degenerate four-wave mixing to measure the instantaneous electronic third-order nonlinear optical response in thin films under resonant conditions. (p. 208)

SuD4 4:00pm

Nonlinear optical properties of phthalocyanine aggregates, James S. Shirk, Steven R. Flom, Richard G.S. Pong, Dawn D. Dominguez, Arthur W. Snow Naval Research Laboratory, USA; Heino Heckmann, Michael Hanack; Eberhard-Karls Univ., Germany

The nonlinear optical properties of phthalocyanines are strongly influenced by aggregation. The photophysical consequences are discussed. New materials that address the problems are demonstrated. (p. 211)

SuD5 4:15pm

Nonlinear optical properties of pTS near the band edge, *Steven R. Flom, J.R. Lindle, F.J. Bartoli, Naval Research Laboratory, USA; Mingguo Liu, George I. Stegeman, Univ. Central Florida, USA*

Transient absorption, nonlinear transmission and degenerate four-wave mixing measurements have been performed on single crystals of pTS. Stimulated Raman scattering and population of the excited state are observed. **(p. 214)**

SuD6 4:30pm

Mechanism of noncentrosymmetric alignment in spin-coated carbazole polymer films, *Hiromi Kimura-Suda, Yadong Zhang, Japan Science and Technology Corporation, Japan; Takafumi Sassa, Institute of Physical and Chemical Research, Japan; Tatsuo Wada, Hiroyuki Sasabe, Japan Science and Technology Corporation, and, Institute of Physical and Chemical Research, Japan*

Noncentrosymmetric alignment of carbazole polymers was achieved without an electric field by spin coating under one-dimensional flow. **(p. 217)**

SuD7 4:45pm

Ultrafast nonlinear switching and logic based on nonlinear tunnelling of optical solitons through organic thin films, *V.M. Chapela, J. Percino, V.N. Serkin, Benemerita Univ. Autonoma de Puebla; T.L. Belyaeva, Lomonosov Moscow State Univ., Russia*

Numerical simulations of nonlinear soliton tunnelling through thin films of polydiacetylene para-toluene sulfonate predict a "reaction-like" phenomenon in which new colored solitons are formed. **(p. 220)**

SuD8 5:00pm

Fully atomistic modeling of a poled nonlinear optical polymer, *L. Michael Hayden, Won-Kook Kim, Univ. Maryland, Baltimore County, USA.*

Fully atomistic molecular modeling is performed on a poled nonlinear optical polymer at two different densities. The degree of orientation, shape of the swept volume, and poling mechanism will be discussed. **(p. 223)**

Organic Thin Films for Photonics Applications

Second-Order NLO Materials: 1

Friday, 24 September 1999

Larry R. Dalton, University of Washington, USA
Presider

FA

8:30am–10:00am

California Ballroom Salons 4&5

Comparison of simple theory and experiment on the electro-optic coefficient of high dipole moment materials

Larry R. Dalton, Bruce H. Robinson, Univ. Washington, USA.

Intermolecular electrostatic interactions among chromophores inhibit the introduction of acentric chromophore order (ACO) by electric field poling. We outline a statistical-mechanical approach to estimating the ACO and the effects of molecular shape. Examples are compared to theory and shown to improve ACO.

High Performance Side-Chain Aromatic Polyquinolines for E-O Devices

Alex K.-Y. Jen*, Hong Ma, Jianyao Wu, Xiaoming Wu, and Sen Liu

Department of Chemistry, Northeastern University, 360 Huntington Ave., Boston, MA 02115

ajen@lynx.neu.edu

Larry R. Dalton

Department of Chemistry, University of Washington, Seattle, WA 98195-2120

Seth R. Marder

Department of Chemistry, University of Arizona, Tucson, AZ 85721

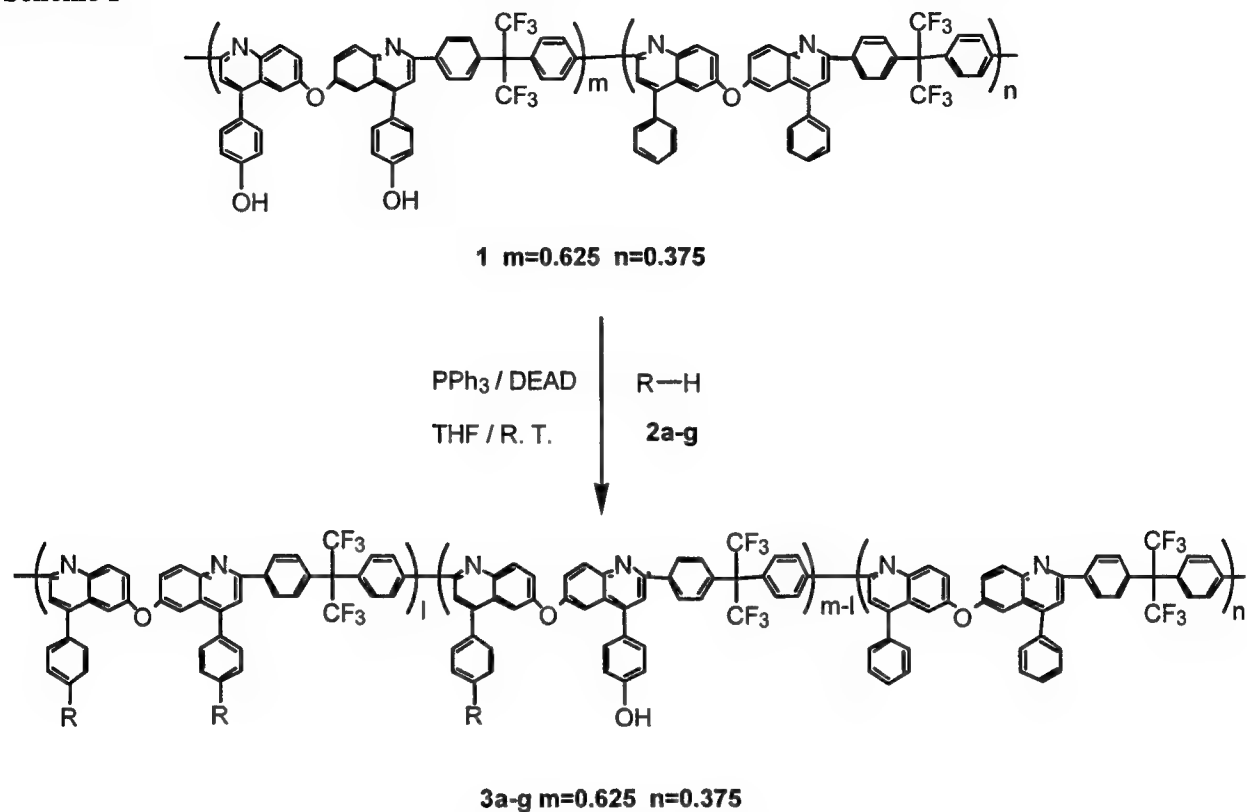
Organic polymeric second-order nonlinear optical (NLO) materials have attracted considerable attention due to their potential applications in telecommunications, optical signal processing, computing and data storage. However, in order to develop practical devices suitable for commercial semiconductor processes, the greatest challenge is to achieve excellent tradeoffs in all the properties of the NLO polymers (i. e., E-O coefficients, thermal, chemical and photochemical stability, temporal dipole alignment stability, optical loss, dielectric constant, and mechanical properties). Most recently, we have developed three efficient approaches to gain a good balance of molecular nonlinearity, thermal and chemical stability.¹⁻³ Concurrent with these developments, we have explored utilizing polyquinolines as a new optical polymer system for second-order NLO applications. Our previous studies of their electro-optic properties have shown very promising results for both guest/host⁴ and side-chain polyquinoline systems.⁵⁻⁶ However, the general applicability of those synthetic methodologies to make NLO side-chain polyquinolines is limited by the stringent acidic polymerization conditions employed in the synthesis of those polymers, in which many chromophores can not survive. In order to alleviate this problem, we have developed a versatile approach for the synthesis of NLO side-chain aromatic polyquinolines.⁷

This was accomplished through a modular approach by preparing a hydroxy-containing polyquinoline, followed by the covalent bonding of chromophores onto the pendent phenyl moieties of the polyquinoline via a very mild Mitsunobu reaction⁸ (Scheme 1). This methodology allowed us to synthesize NLO side-chain aromatic polyquinolines with a broad variety of polymer backbones and flexibility in selecting NLO chromophores. In addition, by locating the hydroxyl group on the pendent phenyl side group instead of on the polyquinoline backbone, a higher efficiency of chromophore attachment could be achieved. It is also noteworthy that a phenyl spacer between the polymer backbone and the NLO chromophores facilitated the process for high electric field poling of the NLO polyquinolines compared to polyquinolines with chromophores directly attached on the polymer backbone.

The covalent bonding of the chromophore onto the backbone of the polymer could be effected easily via very mild Mitsunobu condensation between the hydroxy group on the chromophores and the pendent phenol group on the precursor copolyquinolines. The high efficiency of chromophore attachment allowed us to adjust the loading level of the side-chain chromophores and fine-tune the electro-optic and the thermal properties of the final NLO polymers. The chromophore loading levels of these polyquinolines were controlled to be in the range of 20 wt% to 30 wt% in order to prevent potential chromophore aggregation which may lead to the increase of optical loss in the polymers due to light scattering. Moreover, the very mild conditions of the condensation provided us great flexibility in choosing chromophores. A great variety of chromophores with a hydroxy group, such as tricyanovinyl and phenyl-tetracyanobutadienyl electron acceptor containing chromophores, polyene conjugated π -bridge containing chromophores, and chromone-type chromophores, could be incorporated easily onto the pendent phenyl groups of the polyquinoline. These side-chain NLO polyquinolines demonstrate high electro-optic (E-O) activity (up to 35 pm/V at 830 nm and 22 pm/V at 1300 nm, respectively)

and a good combination of thermal, optical, electrical and mechanical properties (Table 1).

Scheme 1



R:

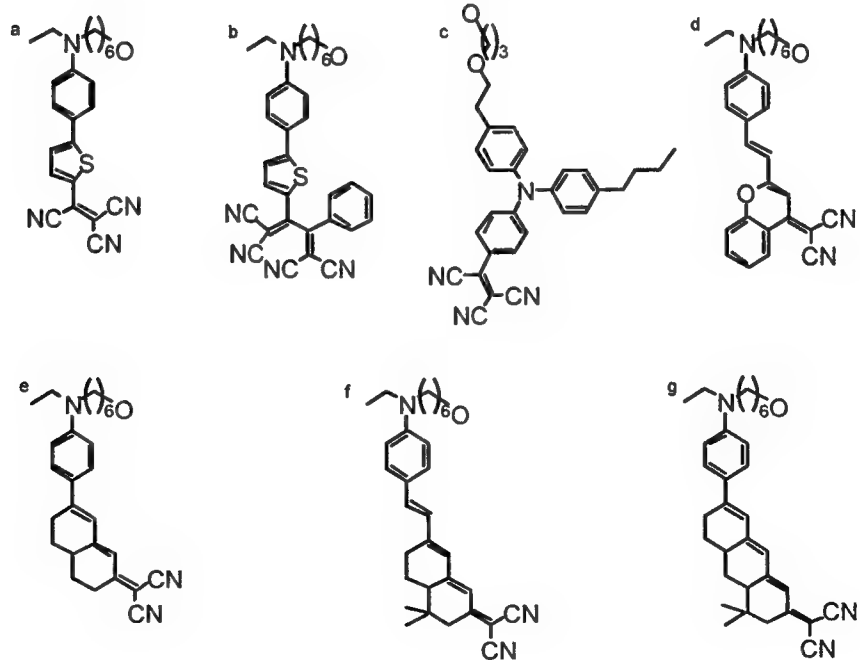


Table 1. Linear and Nonlinear Optical Properties of NLO Side-Chain Polyquinolines

Polymers	Chromophore density [w/w%]	λ_{\max} (nm)	r_{33} (pm/V) ^a	n^b	loss (dB/cm) ^b
3a	29	640	22	1.667	2.5
3b	27	604	20	1.641	2.2
3c	23	538	19	1.661	1.9
3d	22	529	20	1.658	2.3
3e	27	535	17	1.654	2.1
3f	24	556	35	1.655	1.5
3g	20	548	15	1.649	6.7

^a Measured at 1300 nm for polymer **3a**, **3b** and at 830 nm for polymer **3c-3g** after poling. ^b Measured at 1300 nm for polymer **3a**, **3b** and at 830 nm for polymer **3c-3g** before poling.

References

1. Jen, A. K.-Y.; Liu, Y. Q.; Zheng, L. X.; Liu, S.; Drost, K. J.; Zhang, Y.; Dalton, L. R. *Adv. Mater.* **1999**, in press.
2. Wu, X. M.; Wu, J. Y.; Liu, Y. Q.; Jen, A. K.-Y. *J. Am. Chem. Soc.* **1999**, *121*, 472.
3. Shu, C. F.; Shu, Y. C.; Gong, Z. H.; Peng, S. M.; Lee, G. H.; Jen, A. K.-Y. *Chem. Mater.* **1998**, *10*, 3284.
4. Cai, Y. M.; Jen, A. K.-Y. *Appl. Phys. Lett.* **1995**, *117*, 7295.
5. Chen, T.-A.; Jen, A. K.-Y.; Cai, Y. M. *Chem. Mater.* **1996**, *8*, 607.
6. Jen, A. K.-Y.; Wu, X.-M.; Ma, H. *Chem. Mater.* **1998**, *10*, 471.
7. Ma, H.; Wang, X. J.; Wu, X. M.; Liu, S.; Jen, A. K.-Y. *Macromolecules* **1998**, *31*, 4049.
8. Mitsunobu, O. *Synthesis* **1981**, January, 1.

Second-Harmonic Generation in Single-Crystal Thin-Films of 3-Methyl-4-Methoxy-4'-Nitrostilbene (MMONS)

Shida Tan, Achintya Bhowmik, Sunil Sodah, and Mrinal Thakur

Photonic Materials Research Lab, 202 Ross Hall, Auburn University, Auburn AL 36849

Tanshd@eng.auburn.edu, bhowmak@eng.auburn.edu, mthakur@eng.auburn.edu

Organic single-crystals have received significant research attention because of their exceptionally large optical nonlinearities. Among the materials studied, 3-methyl-4-methoxy-4'-nitrostilbene (MMONS) is well known for its large d -coefficients.¹ The d_{33} of MMONS has been shown to be larger than the largest d -tensor element of *N*-(4-nitrophenyl)-*L*-prolinol (NPP). In this work, we report the growth of single-crystal thin-films of MMONS, polarization dependent UV-visible absorption, and preliminary results on measurements of second-order susceptibilities.

Single-crystal thin-films of MMONS were prepared by modified shear method. The shear method has been discussed in previous methods.^{2,3} Large-area ($\sim 50 \text{ mm}^2$), single-crystal films with excellent optical quality were grown. The thickness can be controlled by appropriate pressure during crystal growth. Polarized optical microscopy and x-ray diffraction measurements were used to characterize the single-crystal films. The preliminary results indicate a [100] surface orientation of the films.

Polarization dependent UV-visible absorption measurements of the films have shown a high dichroism. The absorption spectra of the films for polarizations along and perpendicular to the polar axis were measured on a Hitachi U-2000 spectrophotometer (Fig. 1). The wavy patterns in the off-resonant part of the spectra are due to multiple reflections in the films, which were found to be consistent with the film thickness of $2 \mu\text{m}$. The optical density of the films for polarization along the polar axis was significantly higher than that along the direction perpendicular to it. The high dichroism is because the molecular polar axis lies essentially along the film plane.

The transverse second-harmonic generation technique^{3,4} was applied to determine the effective d -coefficients of the films. A mode-locked Nd:YAG laser, producing $\sim 100 \text{ ps}$ pulses at 1064 nm wavelength and a repetition rate of 82 MHz was used as the source of the fundamental radiation in the SHG experiments. Single-crystal thin-films of 2-cyclooctylamino-5-nitropyridine (COANP) and 4-Aminobenzophenone (ABP), nonlinear optical coefficients of which were previously measured,^{3,4} were used as the standards. The beam was propagated perpendicular to the film while the film was rotated about the beam propagation direction. The SHG intensity was measured by the lock-in detection technique as a function of the orientation of the polar axis with respect to the incident polarization. Figure 2 shows the SHG intensity measured as a function of the rotation of the polar axis. The expression for the effective second-order optical coefficient, d_{eff} , was derived by a matrix transformation scheme of the induced polarization from the rotating crystal to the fixed laboratory frame.

The dependence of the d_{eff} on θ (angular orientation of polar axis of the film with respect to the incident polarization) is consistent with the calculated results. Comparing the experimentally obtained results from the sample and reference films, the effective d -coefficient of MMONS single-crystal film was estimated to be $\sim 180 \text{ pm/V}$ at 1064 nm .

In summary, excellent optical quality single-crystal thin-films of MMONS were grown. The films were characterized by polarized optical microscopy, X-ray diffractometry, and UV-visible absorption spectroscopy. The films were found to have a large dichroism. From SHG measurements, the magnitude of the effective d -coefficient for propagation normal to the film was determined to be ~ 180 pm/V. The results indicate that these films are promising for applications in frequency conversion and electro-optics.

Acknowledgement

We thank Ms. P. Mitchel and Dr. J. Shaw for assistance with X-ray diffraction. This work was supported by NSF and DOE/EPSCOR.

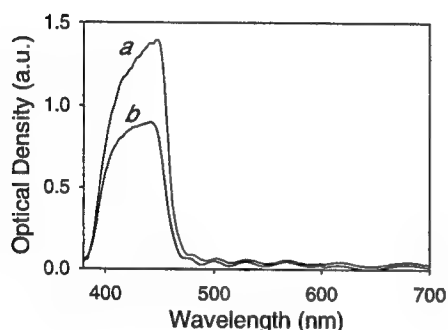


Fig. 1. Absorption spectra of MMONS single-crystal films, measured with light polarized: (a) parallel, and (b) perpendicular to the polar axis.

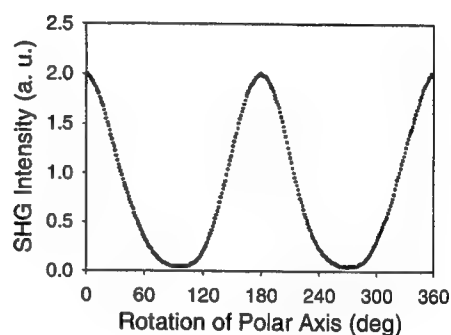


Fig. 2. Effective SHG intensity measured as a function of the orientation of the polar axis of the film with respect to the incident polarization.

References

1. J. D. Bierlein, L. K. Cheng, Y. Wang, and W. Tam, *Appl. Phys. Lett.* **56**, 423 (1990).
2. M. Thakur and S. Meyler, *Macromolecules* **18**, 2341 (1985); M. Thakur, Y. Shani, G. C. Chi, and K. O'Brien, *Synth. Met.* **28**, D595 (1989).
3. R. Quintero-Torres and M. Thakur, *Opt. Lett.* **19**, 87 (1994).
4. A. K. Bhowmik and M. Thakur, *Polym. Preprints* **39**, 1038 (1998).

Quadrupolar molecular nonlinear optics

V. Ostroverkhov, O. Ostroverkhova, R.G. Petschek, and K.D. Singer

Department of Physics, Case Western Reserve University, Cleveland, OH 44106

Tel: +(216)-368-4017, email: kds4@po.cwru.edu

L. Sukhomlinova and R.J. Twieg

Department of Chemistry, Kent State University, Kent, Ohio 44242

Tel: (330) 672-2791, Email: rtwieg@lci.kent.edu

Second order nonlinear optics requires a noncentrosymmetric material. Consequently, much effort has gone into developing polar materials that exploit the dipolar (vector) component of the molecular hyperpolarizability. Polar crystals, poled polymers, and polar Langmuir-Blodgett films comprised of push-pull chromophores are examples. However, it has been recognized for a long time that even isotropic fluids containing chiral molecules can exhibit second order nonlinear optical effects.[1] Second harmonic generation is not observed in such isotropic chiral media, but may be observed in materials with minimal additional imposed symmetries. Since one would like to avoid the difficulties of fabricating and maintaining polar structures, the question arises then as to what symmetry group allows the easiest fabrication of macroscopic media exhibiting second harmonic generation. The symmetry group D_∞ , which consists of a nonpolar axis and no mirror planes, is the simplest. The group D_2 , which has three two-fold axes and no mirror planes, is also a candidate. The D_∞ symmetry can be fabricated by a single axial stretch of a polymer containing chiral molecules, and is characteristic of a nematic or smectic A liquid crystal. The D_2 symmetry can be attained using a two-axis stretch or shear alignment of a polymer containing chiral molecules, and is characteristic of a smectic C or other biaxial phases of liquid crystals. Thus, these symmetries may be easily and robustly fabricated.

The question then arises as to how to optimize molecular properties in these chiral media. To analyze this we examine how the molecular hyperpolarizability is expressed in terms of the irreducible rotation group. It is found that a quadrupolar, second-rank pseudotensor component makes the only contribution in the case of D_∞ symmetry while both the quadrupolar and octupolar (third-rank traceless symmetric tensor) contribute in the D_2 case. This quadrupolar component exists in non-Kleinman symmetric materials, and chiral, multidimensional π -electron containing chromophores.[2]

In this study, we describe our efforts aimed at measuring and understanding the features of appropriate chromophores exhibiting this quadrupolar character. We have looked at a quantum mechanical model in the two-level approximation in order to elucidate the basic design features for active chromophores. We find that molecules with transition moments perpendicular to the change in dipole moment between the ground and excited state maximize this optical nonlinearity.

We have measured the rotational invariants associated with Kleinman disallowed components using nonlinear light (hyper-Rayleigh) scattering. The intensity of second harmonic light scattered from isotropic solutions of the nonlinear molecules is defined by the rotational average of squared molecular hyperpolarizability tensor $\langle \beta\beta^* \rangle$. The latter can be rewritten as a

sum of rotationally invariant tensors multiplied by scalar figures of merit that characterize the hyperpolarizability tensor and are essentially the values being measured in the experiment.

The rotationally invariant tensors are solely functions of incoming and outgoing polarization vectors, which are controlled by appropriate polarizer and retarder orientations. The intensity of the scattered light is measured as a function of the polarization state of the incoming and generated light. The raw data is then Fourier-transformed, and the set of invariants are found by fitting the measured Fourier components to ones calculated theoretically. These invariants describe figures of merit for polar (vector), quadrupolar (second-rank pseudotensor), and octupolar (traceless, symmetric third-rank tensor) processes, and thus fully characterize second-order nonlinear optical interactions.

The compounds measured include pNA **1**, camphorquinone derivative **2** [2], crystal violet **3**, recently synthesized camphor derivatives **4-6** and the steroid derivative **7**. The structures and results for all of the figures of merit for the rotational invariants are given in Table 1. The spectral content of the scattered light was measured to verify that multiphoton fluorescence was not problematic at the measured wavelengths. We find that the molecular features for large quadrupolar response are generally consistent with the quantum model. For example, the nearly one-dimensional pNA **1** is nearly Kleinman symmetric and exhibits no quadrupolar component. The chiral camphor derivatives **4-6** are largely dipolar. Thus, the angle between the dipole moment change and the transition moment are somewhat different but not large enough to provide for a large quadrupolar component. However, these are chiral π -electron systems and may be combined to form more active chromophores. For example, the lambda-shaped Q-BNH **2** containing two camphorquinone moieties, exhibits a substantial quadrupolar component since this shape provides for a large angle between the change in dipole moment and the transition moment. The role of symmetry is thus obvious when comparing Q-BNH to the other camphorquinones. Crystal violet **3** exhibits large quadrupolar and octupolar components relative to a nonzero dipolar component therefore the symmetry of crystal violet is more complicated than is drawn. The large overall magnitude of the crystal violet signal indicates that crystal violet is an interesting candidate for use in quadrupoled materials if a single enantiomer could be resolved. These results point out directions for optimization of the quadrupolar molecular nonlinear response.

Support by the NSF under Science and Technology Center Advanced Liquid Crystalline Optical Materials grant DMR89-20147 is acknowledged.

1. J. A. Giordmaine, "Nonlinear Optical Properties of Liquids", *Phys. Rev.* **138**, 1599-1606 (1965).
2. S.F. Hubbard, R.G. Petschek, K.D. Singer, N. D'Sidocky, C. Hudson, L.C. Chien, C. C. Henderson, and P.A. Cahill, "Measurements of Kleinman-disallowed Hyperpolarizability in Conjugated Chiral Molecules", *J. Opt. Soc. Am. B* **15**, 289-301 (1998).

Material	$\beta_{1mm}^2/\beta_{1ss}^2$	$\beta_{1sm+}^2/\beta_{1ss}^2$	$\beta_{1sm-}^2/\beta_{1ss}^2$	$\beta_{2mm}^2/\beta_{1ss}^2$	$\beta_{3ss}^2/\beta_{1ss}^2$	λ , nm
PNA 1	0.16±0.08	-0.02±0.03	0.17±0.02	0.04±0.04	0.54±0.04	1064
Q-BNH 2	0.15±0.10	-0.06±0.07	0.13±0.03	0.19±0.05	0.47±0.04	1064
CV 3	1.2±0.2	-1.3±0.1	0.08±0.03	0.8±0.2	1.7±0.2	1064
4	0.22±0.04	0.11±0.02	-0.05±0.01	0.11±0.05	0.52±0.03	1064
5	0.05±0.01	0.04±0.01	0.04±0.01	0.11±0.06	0.47±0.01	1340
6	0.11±0.02	0.13±0.01	0.01±0.01	0.00±0.01	0.40±0.01	1340
7	0.13±0.03	0.10±0.02	0.15±0.02	0.08±0.02	0.51±0.02	1064

Table 1. HRS results. The 1ss, 1sm+, 1sm- are polar (vector) components, 2mm the quadrupolar component, and 3ss the octupolar component. All are referenced to 1ss components. All HRS measurements were performed in acetone as solvent.

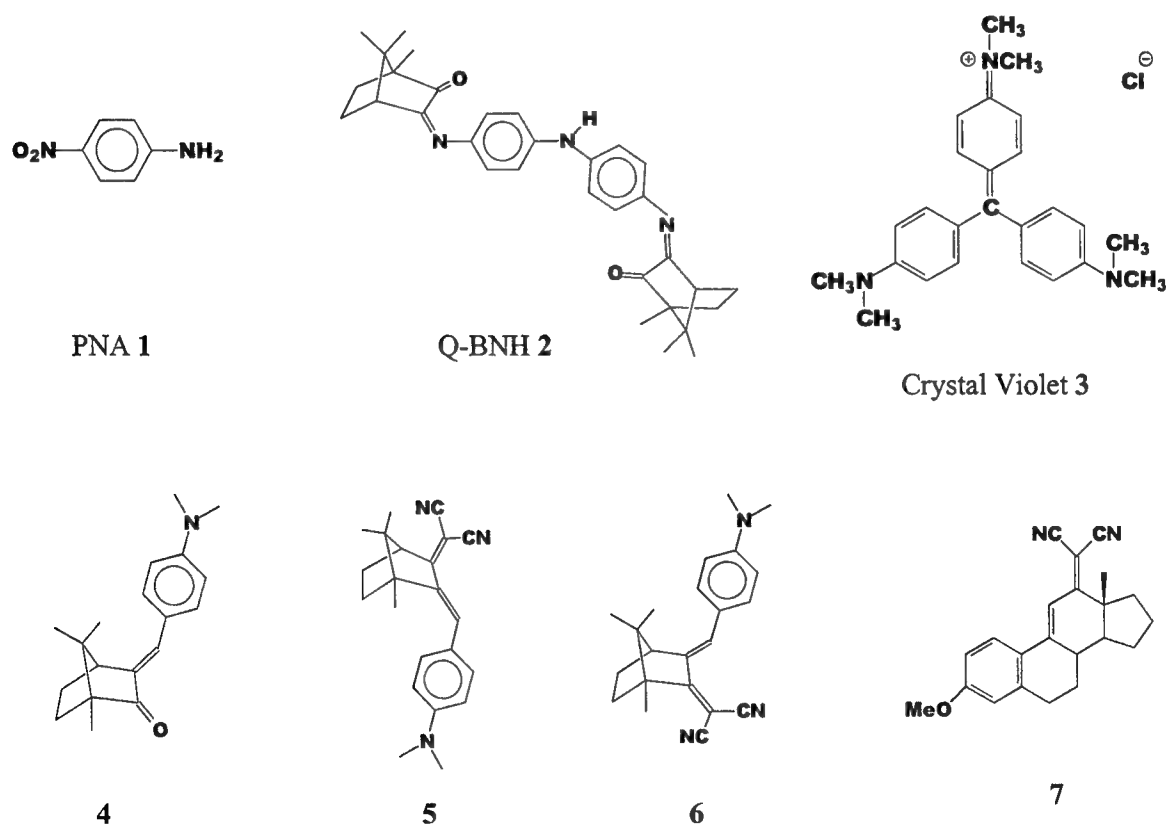


Figure 1. Compounds used in this study

Intermolecular Interactions of Highly Nonlinear Optical Molecules for Electro-Optic Polymer Applications

I. Liakatas, C. Cai, M. Bösch, M. Jäger, Ch. Bosshard, and P. Günter
 Swiss Federal Institute of Technology, ETH-Hönggerberg HPF, 8093, Zürich, Switzerland
 liakatas@iqe.phys.ethz.ch, bosshard@iqe.phys.ethz.ch

Cheng Zhang and Larry R. Dalton
 Department of Chemistry and Loker Hydrocarbon Research Institute
 University of Southern California, Los Angeles, CA 90089-1062, USA
 chengz@aludra.usc.edu

The research activities in the field of electro-optic polymers are focused on the development of nonlinear optically active molecules, appropriate polymer matrices to host these molecules, and devices using these polymer systems. In the framework of our ongoing research on these three aspects, we have synthesized two series of high performance molecules and investigated their molecular optical nonlinearity, their intermolecular interactions and the effect of the environment on the optical nonlinearity.

The CC series[1] (see Table 1) is based on the amino donor and tricyano acceptor bridged by the phenylbithiophene stilbene. The incorporation of monothiophene rings to the molecule's backbone and the use of the strong electron withdrawing tricyano group has led to high molecular as well as macroscopic nonlinear optical properties[2]. By using bithiophene instead of monothiophene as a bridge we have obtained enhanced optical nonlinearities and very good physical properties. The product of the molecule's dipole moment μ times the first-order hyperpolarizability extrapolated to infinite wavelengths β_0 is a figure of merit for electro-optic applications and has been measured by electric field induced second harmonic generation (EFISH) performed at 1.907 μm in solution. Molecule CC176 containing two double bonds in its backbone has one of the highest reported $\mu\beta_0$ for molecules of similar length and molecular weight. Its value of $\mu\beta_0 = 9300 \cdot 10^{-69} \text{ Cm}^5/\text{V}$ is more than eight times larger than that of Disperse Red 1 (DR1), a standard molecule for polymer electro-optic applications. The molecules of the CC series are thermally stable up to at least 200 °C and exhibit an excellent photostability.

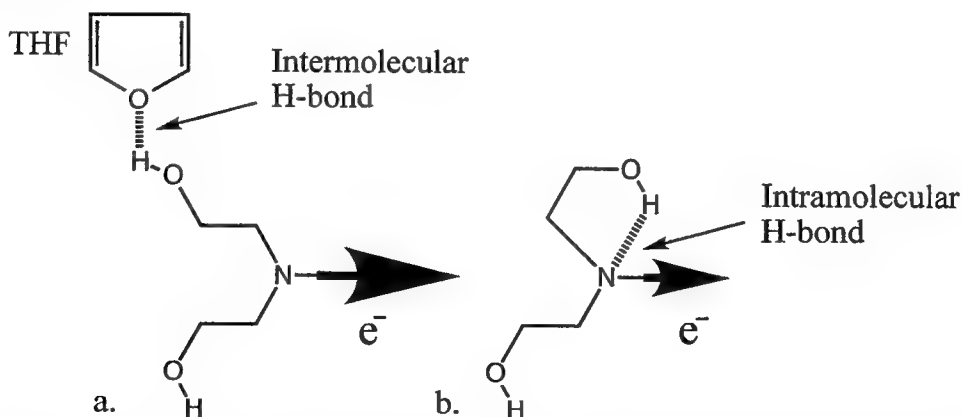


Fig. 1: Influence on the electron donating strength a) of an intermolecular hydrogen bond formation in the presence of an oxygen-containing solvent (tetrahydrofuran) and b) of an intramolecular hydrogen bond formation in a solvent without oxygen (chloroform).

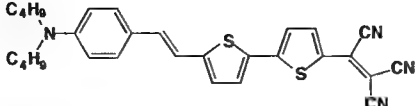
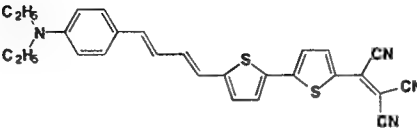
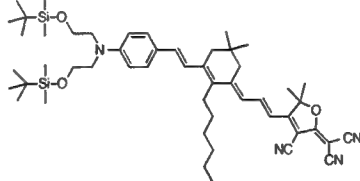
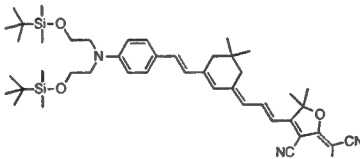
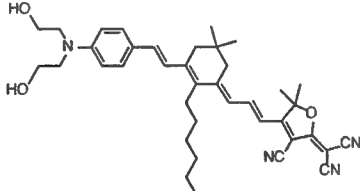
Name	Structure	Solvent	λ_{\max}	$\mu\beta$ (10^{-69} Cm^5/V)	$\mu\beta_0$ (10^{-69} Cm^5/V)
CC172		Dioxane	611	14740	6650
CC176		Dioxane	655	19960	9300
CLD III-1p		THF	649	18140	8620
CLD II-4		THF	648	13500	6430
CLD III-1		THF	650	14320	6780
		Chloroform	661	10760	4920

Table 1: Chemical structures of the synthesized molecules, their wavelength of maximum absorption λ_{\max} and results on their molecular second-order nonlinearities determined by EFISH measurements at 1907 nm. For comparison, $\mu\beta$ of Disperse Red 1 measured in Dioxane is $1580 \cdot 10^{-69} \text{ Cm}^5/\text{V}$. The estimated experimental error is 2%. (THF: tetrahydrofuran)

The CLD series[3] based on the phenyltetraene bridge exhibits large $\mu\beta_0$ values and very good solubility. Moreover, by varying the substituents of the chromophores the effect of the intermolecular interaction between the chromophores and their matrices can be studied systematically. $\mu\beta_0$ of molecule CLD III-1 is higher when measured in THF than in chloroform. This increase of 38% is probably due to the hydrogen bond formation between the hydrogen atom of the hydroxy (-OH) group and the oxygen atom of the THF molecule. This reduces the formation of an intramolecular hydrogen bond (O-H \cdots N) with the nitrogen atom of the donor which would result –as in the case of chloroform– in a decrease of the electron donation strength. (see Fig. 1) The attachment of the bulky TBDMS group to the donor (CLD III-1p compared to CLD III-1) eliminates the intramolecular hydrogen bond formation. Moreover it can reduce the intermolecular electrostatic interaction which may cause aggregation. A more effective way to reduce the formation of aggregates is by adding a carbon side-chain perpendicular to the conjugate backbone of the molecule. The use of such a side-chain (CLD III-1p compared to CLD II-4) keeps the individual molecules away from each other and greatly reduces the formation of dipole couples and leads to enhanced solubility and optical nonlinearity.

Two chromophores (CC172 and CLD II-4) with similar $\mu\beta_0$ were mixed in polymethylmethacrylate (PMMA) and polyquinoline (PQ100, kindly provided by Hitachi Chemical Europe GmbH) in order to investigate the behaviour of the molecules in the polymer matrix. Solutions of wt.15% chromophore loading were spun to form thin films of 2-3 μm thickness on ITO substrates. After the deposition of the top gold electrodes, the samples were poled near the glass transition temperature under the application of an electric field of 100 V/ μm . The electro-optic coefficient r_{33} was measured using the reflection technique at the wavelength of 1.55 μm . The results of the measurements under the same experimental conditions are given in Table 2.

Molecule	Polymer host	r_{33} (pm/V)
CC172	PMMA	9.5 ± 2
CC172	PQ100	4.5 ± 2
CLD II-4	PMMA	18.5 ± 3
CLD II-4	PQ100	12 ± 3

Table 2: Electro-optic coefficients of selected molecules in polymethylmethacrylate (PMMA) and polyquinoline (PQ100) host matrices measured with the reflection technique at 1.55 μm . The molecular concentration in the polymer was 15% by weight, and the poling field was 100 V/ μm .

Despite the comparable $\mu\beta_0$ of molecules CC172 and CLD II-4, in both polymer matrices the latter exhibits a larger electro-optic coefficient. This is probably due to the bulky side chains in CLD II-4 which greatly reduces the aggregation of the chromophores. The increase of the electro-optic coefficient of molecule CLD II-4 is linear up to a chromophore loading of at least 25% where it has a value of $r_{33}=30$ pm/V. For molecule CC172 a strong red shift of 70 nm of the wavelength of maximum absorption λ_{max} in PMMA compared to that of solution in dioxane also indicates the existence of strong intermolecular interactions.

In summary, molecules with large first-order hyperpolarizabilities and good thermal- and photostability have been synthesized. The combination of two thiophene rings and two double bonds in the conjugate bridge together with a strong acceptor, in the case of CC176, and the combination of the phenyltetraene bridge with a bulky group at the donor side and a carbon side-chain, in the case of CLD II-4, led to $\mu\beta_0$ values in the order of $9000 \cdot 10^{-69} \text{ Cm}^5/\text{V}$, which are among the highest for molecules of similar weight and length. It was shown that the formation of intramolecular hydrogen bonds on the amino donor group may decrease the molecular nonlinear optical properties and can be reduced by the formation of intermolecular hydrogen bonds with neighboring solvent molecules. For the reduction of aggregation, we propose the use of the bulky TBDMS substituted donor group. The use of a side-chain perpendicular to the molecule's conjugate bridge further keeps the molecules apart and reduces the aggregation. Electro-optic coefficients of such highly nonlinear optical molecules (CLD II-4) in PMMA are as high as 30 pm/V at 1.55 μm .

References

- [1] Cai, C.; Liakatas, I.; Wong, M-S.; Bosshard, Ch.; Günter, P., *Polymer Preprints*, 1998, 39 (2), 1111.
- [2] (a) Rao, V. P.; Jen, A. K-Y.; Wong, K. Y.; Drost, K. J., *J. Chem. Soc., Chem. Commun.*, 1993, 1118, (b) Cai, Y. M.; Jen, A. K-Y., *Appl. Phys. Lett.* 67 (3), 1995, 299.
- [3] Zhang, C.; Ren, A. S.; Wang, F.; Dalton, L. R.; Lee, S-S.; Garner, S. M.; Steier, W. H., *Polymer Preprints*, 1999, 40 (1), 49.

Organic Thin Films for Photonics Applications

Electro-Optic Devices: 1

Friday, 24 September 1999

Alex K-Y. Jen, Northeastern University, USA
Presider

FB

10:30am-NOON

California Ballroom Salon 4&5

Can drive voltages of less than one volt be systematically achieved for polymeric electro-optic devices?

Larry R. Dalton
Department of Chemistry, Box 351700
University of Washington
Seattle, WA 98195-1700
tel. (206) 543-1686
e-mail: dalton@chem.washington.edu

It is generally conceded that to systematically achieve electro-optic device operational voltages of 1 volt or less will require that such devices be fabricated from materials characterized by electro-optic coefficients of 75 pm/V or greater at the operational wavelength. If currently available organic second order nonlinear optical chromophores could be assembled into perfect acentric lattices, macroscopic electro-optic coefficients of many hundred picometers/volt would result. Unfortunately, intermolecular electrostatic interactions involving NLO chromophores act to inhibit the realization of perfect acentric order and the problem becomes much more severe with increasing chromophore numberdensity. The exact extent of inhibition depends on upon chromophore shape. Chemical modification of chromophore structures along the lines suggested by statistical mechanical theories has result in significant (factor of 2) increases in macroscopic electro-optic activity. Values are systematically exceeding 75 pm/V.

Polymer Waveguides for Second-Order Nonlinear-Optical Effects at Telecommunication Wavelengths

Tomas Pliska, Wook-Rae Cho, Vincent Ricci, Joachim Meier, Anne-Claire Le Duff*, Michael Canva*, and George I. Stegeman

*School of Optics / Center for Research and Education in Optics and Lasers, University of Central Florida,
P.O. Box 162 700, 4000 Central Florida Blvd., Orlando, FL 32816-2700, USA
Tel.: +1-407-823-6860, Fax: +1-407-823-6955, e-mail: pliska@steglab.creol.ucf.edu*

** permanent address: Laboratoire Charles Fabry, Institut d'Optique Théorique et Appliquée,
Université d'Orsay / Paris-Sud, 91403 Orsay Cedex, France*

Paul Raymond and François Kajzar

Commissariat à l'Énergie Atomique, Centre d'Études de Saclay, 91191 Gif sur Yvette Cedex, France

Organic materials exhibit large optical nonlinearities and, hence, are attractive for parametric interactions [1]. We envision using polymers in $\chi^2:\chi^2$ -cascading based optical processes at telecommunication wavelengths.

Cascading of second-order nonlinear-optical processes has been shown to provide new possibilities for all-optical signal processing as $\chi^2:\chi^2$ -cascading can mimic third-order (Kerr-type) nonlinearities [2]. Because the figure-of-merit for the cascaded nonlinear phase shift is identical to the one for second-harmonic generation given by d_{eff}^2/n^3 where d_{eff} denotes the effective nonlinear-optical coefficient and n the index of refraction, devices exhibiting large second-harmonic conversion efficiencies are also candidates for cascading.

Normalised conversion efficiencies for second-harmonic generation at 1.55 μm comparable to inorganic materials were obtained in 4-dimethylamino-4'-nitrostilbene (DANS) waveguides [3]. However, the absolute conversion efficiency was limited by the high loss of several tens of dBcm^{-1} at the second-harmonic wavelength. To reduce the loss of polymer waveguides used for second-order nonlinear effects at telecommunication wavelengths, materials with low intrinsic absorption between 0.6 and 1.6 μm have to be combined with techniques allowing one to form waveguides with low scattering losses.

Traditionally, ultraviolet photobleaching has been the technique of choice for fabricating waveguides in nonlinear-optical polymers. With the prospective use of polymers with enhanced photostability and low absorption, alternative techniques may be required as materials with high bleaching efficiencies in the ultraviolet tend to have fast photodegradation rates also when exposed to near-infrared radiation, e.g. DANS [4]. Plasma etching offers a versatile tool for micromachining with a high degree of process control [5]. Polymers can be etched in O_2 or O_2/CF_4 plasmas containing He or Ar as a buffer gas.

Here we report on material characterisation, waveguide fabrication, and second-harmonic generation measurements using two different transparent nonlinear side-chain polymers, namely 4-diethylamino-1-nitrobenzyl-methyl methacrylate (DANB-MMA, 67 % weight chromophore loading) and 4[N-ethyl-N-(2 hydroxyethyl)] amino-4'-nitrozobenzene-methyl methacrylate (disperse red 1, DR1-MMA, 24 % weight loading). The absorption spectra of DANB-MMA and DR1-MMA are shown in Fig. 1 with fitted inhomogeneously broadened absorption profiles [6]. To estimate the absorption in the 0.6-1.6 μm band, where transmission spectroscopy through a thin film does not provide sufficient resolution, we measured the loss in unpoled DANB-MMA and DR1-MMA slab waveguides of 1.5 μm thickness spin coated on silicon oxide. The results of these measurements which provide an upper limit for the absorption coefficient are shown by diamonds in Fig. 1. Both polymers show very low losses at the second-harmonic wavelength of 0.78 μm , more than an order of magnitude smaller than the absorption reported for DANS [6].

The nonlinear-optical coefficients of poled DANB-MMA and DR1-MMA films were measured by the Maker fringe technique at a wavelength of 1.58 μm . Using $d_{11}(\text{quartz}) = 0.29 \text{ pmV}^{-1}$ as a reference we found for DANB-MMA $d_{31} = (1.5 \pm 0.2) \text{ pmV}^{-1}$ and $d_{33} = (4.5 \pm 0.5) \text{ pmV}^{-1}$ and for DR1-MMA $d_{31} = (2.2 \pm 0.3) \text{ pmV}^{-1}$ and $d_{33} = (6.6 \pm 0.7) \text{ pmV}^{-1}$ at a poling field of 100 $\text{V}\mu\text{m}^{-1}$.

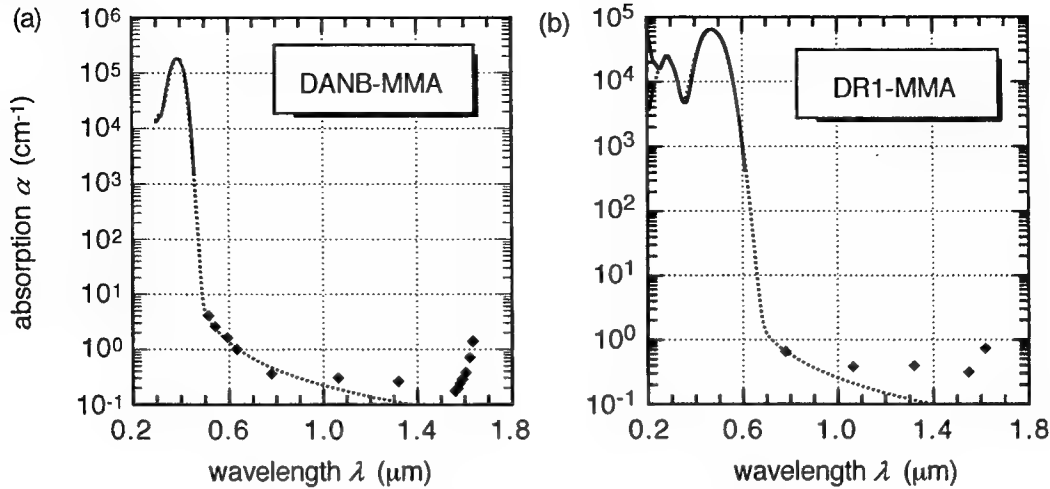


Fig. 1: Absorption spectra of (a) 4-diethylamino-1-nitrobenzyl-methyl methacrylate (DANB-MMA) and (b) disperse red 1-methyl methacrylate (DR1-MMA) side chain polymers, showing data obtained by transmission spectroscopy using a photospectrometer (—) and by loss measurements in planar waveguides (♦). The dotted lines (.....) indicate fitted inhomogeneously broadened absorption spectra. The chromophore loading is 67 % in weight for DANB-MMA and 24 % in weight for DR1-MMA.

In a next step, we developed fabrication processes for waveguides of different geometries. The process starts with spin coating of polymer layers on a substrate. A suitable mask is then patterned by standard photolithography on the top layer for oxygen plasma etching of raised channel or strip-loaded guides.

Modal-dispersion-phase-matching was shown to be a suitable scheme for efficient parametric processes in polymer waveguides [7]. This type of phase matching, schematically displayed in Fig. 2, is based on an interaction between the lowest order mode at the fundamental wavelength and a higher order mode at the second-harmonic. Therefore, special multiple layer structures need to be devised in order to avoid interference effects across the waveguide that cancel the overlap integral for second-harmonic generation (inverse effective cross section). Figure 2a shows the basic structure for the $TM_0^\omega \rightarrow TM_1^{2\omega}$ interaction. The core is composed of the nonlinear polymer layer and an index matched linear layer, sandwiched between low index buffer and cladding layers. Figures 2b and 2c schematically show the field profiles of the TM_0^ω and $TM_1^{2\omega}$ modes and the nonlinearity, respectively. When the electric field of the second-harmonic mode changes sign across the waveguide, the nonlinearity is turned off resulting in a nonvanishing overlap integral.

Test samples for second-harmonic generation were prepared for both nonlinear polymers discussed. Figure 3 shows the second-harmonic tuning curve obtained with a mode-locked color center laser tunable between 1.50 and 1.65 μm for a DANB-MMA planar waveguide of 7 mm length. The comparison between calculated and measured second-harmonic bandwidth shows that phase-matching was obtained over the whole sample length of 7 mm. At this stage we did not optimise the focusing into the planar waveguide which resulted in a rather low conversion efficiency of approximately $10^{-3} \%W^{-1}$. Figure 4 displays the second-harmonic tuning curve obtained in a 2 mm long plasma etched DR1-MMA ridged channel waveguide (inset of Fig. 4). The peak normalised conversion efficiency was $0.1 \%W^{-1}$ ($2.5 \%W^{-1}\text{cm}^{-2}$). The measured propagation loss was 6 dBcm^{-1} at the fundamental and 10 dBcm^{-1} at the second-harmonic wavelength. From these data, we estimate an nonlinear coefficient of 6 pmV^{-1} , corresponding to an effective poling field of $90 \text{ V}\mu\text{m}^{-1}$, which is identical to the applied external field across the polymer stack.

Our current work focuses on further reduction of the waveguide loss, improvement of the poling procedure to increase the poling field up to $200 \text{ V}\mu\text{m}^{-1}$, and design of waveguide structures with optimised effective cross sections. For improved waveguide structures with transparent polymers, we estimate that conversion efficiencies of more than $25 \%W^{-1}$ in 1 cm long guides are attainable.

This research was supported by STTR (BMDO) and JPL (AFOSR) grants.

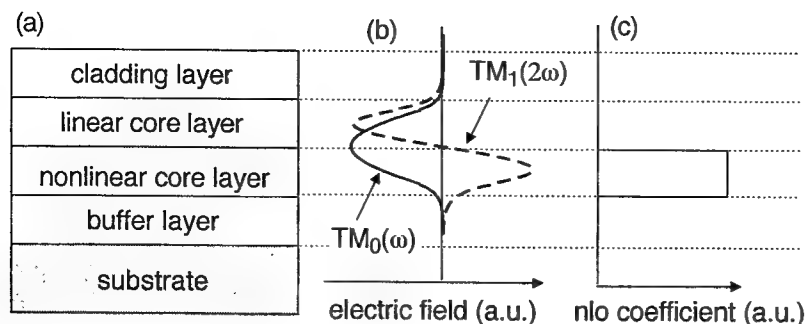


Fig. 2: (a) Basic waveguide structure for modal-dispersion-phase-matched second-harmonic generation. (b) Schematic of the optical fields for the $TM_0^\omega \rightarrow TM_1^{2\omega}$ interaction. (c) Schematic of the optical nonlinearity.

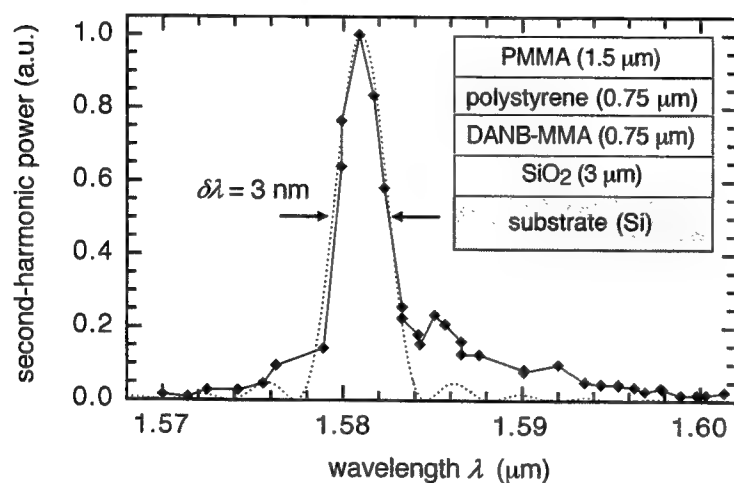


Fig. 3: Second-harmonic power as a function of wavelength measured in a planar DANB-MMA waveguide (inset) of 7 mm length. The full-width-half-maximum bandwidth of 3 nm of the measured tuning curve corresponds to the one of the calculated curve indicated by the dotted line. The waveguide core consists of a nonlinear DANB-MMA and a linear polystyrene layer, respectively, sandwiched between SiO_2 buffer and PMMA cladding layers.

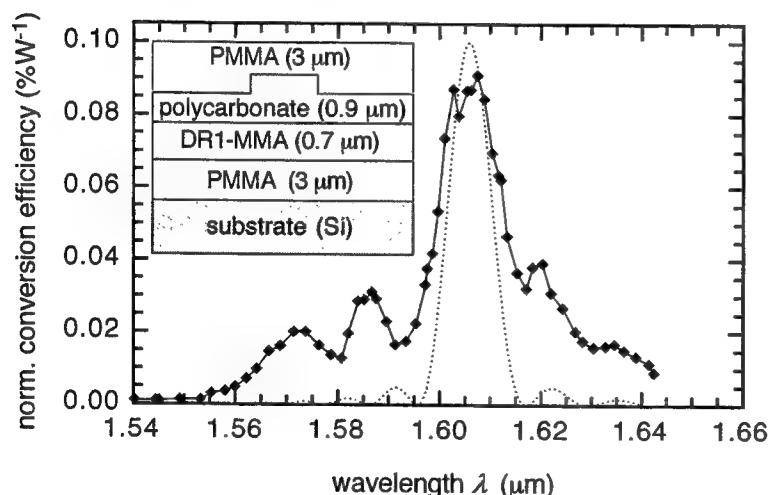


Fig. 4: Normalised second-harmonic conversion efficiency as a function of wavelength measured in a DR1-MMA ridged channel waveguide (inset) of 2 mm length. The waveguide core is formed by a nonlinear DR1-MMA and a linear polycarbonate layer. PMMA is used as the buffer and cladding material. The ridge height, etched by an oxygen plasma, is 0.4 μm . The dotted indicates the theoretical tuning curve.

- [1] H.S. Nalwa and S. Miyata, Eds., *Nonlinear Optics of Organic Molecules and Polymers*, CRC Press, Boca Raton (1997)
- [2] G.I. Stegeman, D.J. Hagan, and L. Torner, *Opt. Quantum Electron.* **28**, 1691 (1996)
- [3] M. Jäger et al., *J. Opt. Soc. Am. B* **15**, 781 (1998)
- [4] Q. Zhang, M. Canva, and G.I. Stegeman, *Appl. Phys. Lett.* **73**, 912 (1998)
- [5] D.M. Manos and D.L. Flamm, Eds., *Plasma Etching*, Academic Press, San Diego (1989)
- [6] A. Otomo et al., *Appl. Phys. Lett.* **69**, 1991 (1996)
- [7] W. Wirges et al., *Appl. Phys. Lett.* **70**, 3347 (1997)

Microstrip line-slot ground electrode for high-speed optical push-pull polymer modulators

Yongqiang Shi, Weiping Lin, David J. Olson, and James H. Bechtel
 TACAN Corporation, 2330 Faraday Avenue, Carlsbad, California 92008
 Tel. 760-438-1010, Fax 760-438-2412
 Yqshi2@aol.com

Wenshen Wang
 TRW Inc., D1/1024, One Space Park, Redondo Beach, CA 90278
 Tel. 310-812-8364, Fax 310-812-8983
 wenshen.wang@trw.com

Optical push-pull poling and modulation can dramatically reduce the halfwave voltage of an electrooptic (EO) modulator [1-2]. However, additional processing steps are often required to fabricate high-speed push-pull EO polymer modulators with microstrip line (MSL) electrodes, because push-pull poling requires three electrodes while MSLs provide only two. Therefore, a set of intermediate poling electrodes are defined to carry out electric field poling and are later removed for MSL fabrication. In addition, due to high field strength during electric field poling, inert gas protection or a pulsed power supply is required to minimize electric discharge through air gaps. These additional processes complicate the device fabrication and materials selections, particularly for crosslinkable materials systems.

To simplify the optical push-pull modulator fabrication, we have designed a modified MSL electrode structure [3] that can be used for both poling and modulation. The circuit consists of three sections: a MSL top electrode, and two half-infinite planes separated by a slot underneath MSL, as shown in Figure 1. Electric field poling is achieved by applying appropriate potentials on three sections. For finished modulators, the modulation signals will be applied to the top MSL electrode and the two planes separated by the slot are grounded.

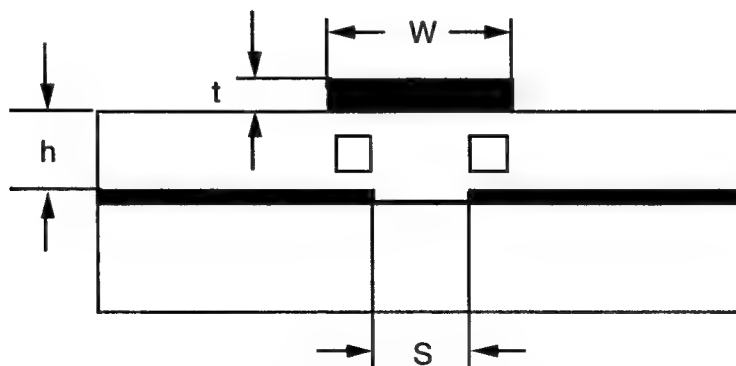


Fig. 1 Cross section view of the microstrip line-slot ground electrode.

The microwave properties of the MSL-slot ground electrode structure can be estimated using standard approaches, although all require extensive numerical calculation. We have used a commercial software package based on the method of moments to model this circuit. The calculated characteristic impedance and propagation loss coefficient are shown in Figure 2 for selected parameters $\epsilon_r=3.0$, $W=50\text{ }\mu\text{m}$, $S=30$

μm , $t=10\text{ }\mu\text{m}$, and $h=10\text{ }\mu\text{m}$. The numerical modeling showed a very flat characteristic impedance over broad frequency range. The impedance can be fine tuned by changing the width W and height t of the MSL circuit.

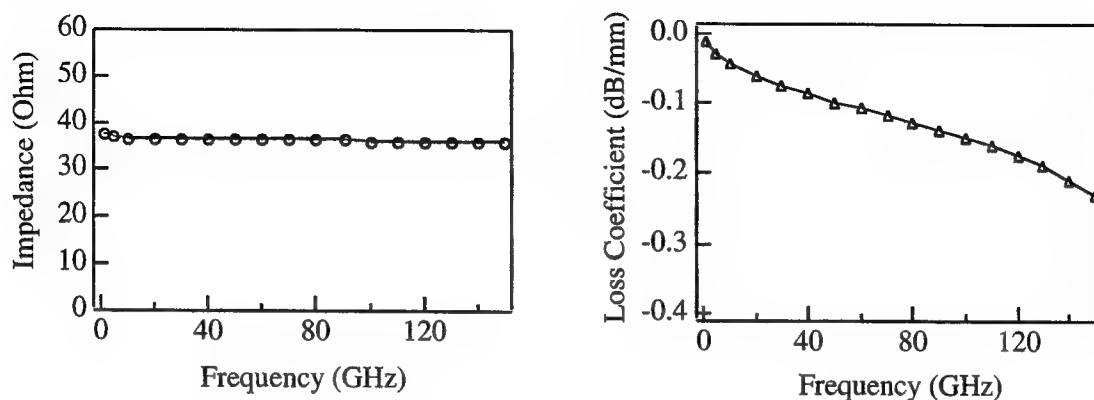


Fig. 2 Numerical simulation of (a) microwave loss coefficient, and (b) characteristic impedance.

One major advantage of this electrode design is that the electrodes with highest potential difference are covered by thick ($\sim 10\text{ }\mu\text{m}$) polymer layers. Therefore, the air discharge between the electrode gap can be effectively suppressed. In our experiment, a poling voltage $>1000\text{ V}$ (average field $>50\text{ V}/\mu\text{m}$) can be easily achieved using the MSL-slot ground electrode layout. This voltage is sufficient in our device poling due to a controlled conductivity distribution among cladding and active polymer layers. In comparison, when the poling electrodes are directly exposed in air, the air discharge started at $\sim 400\text{ V}$ across a $30\text{ }\mu\text{m}$ separation. Optical push-pull poling has been tested using thin gold layer electrodes similar to the Figure 1 structure. With 2 cm long interaction length and $\sim 10\text{ }\mu\text{m}$ electrode gap distance, halfwave voltage of 5 V and 8 V were obtained from polymers containing FTC [4] and Disperse Red 19 [5] chromophores, as shown in Figure 3.

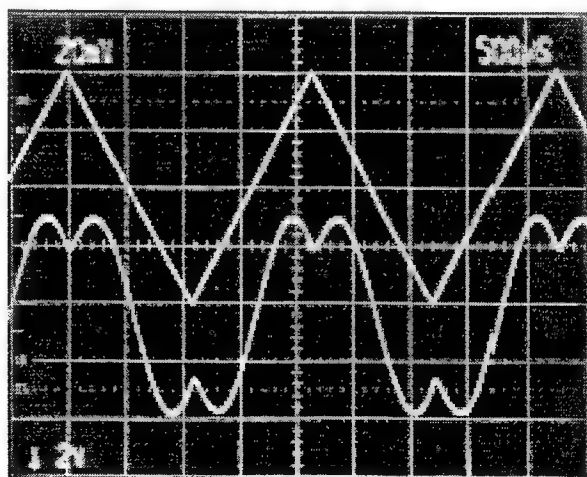


Fig. 3 Halfwave voltage measurement from a push-pull poled a FTC containing polyurethane sample.

The microwave properties of the MSL-slot ground electrode were tested using standard network analyzers shown in Figure 4 (a) and (b). For a 2.5 cm long test electrode, the total transmission loss at 20 GHz was

6.5 dB, which corresponding to a loss coefficient of $0.6 \text{ dB/cm/GHz}^{1/2}$. The reflection was below -15 dB over almost entire bandwidth.

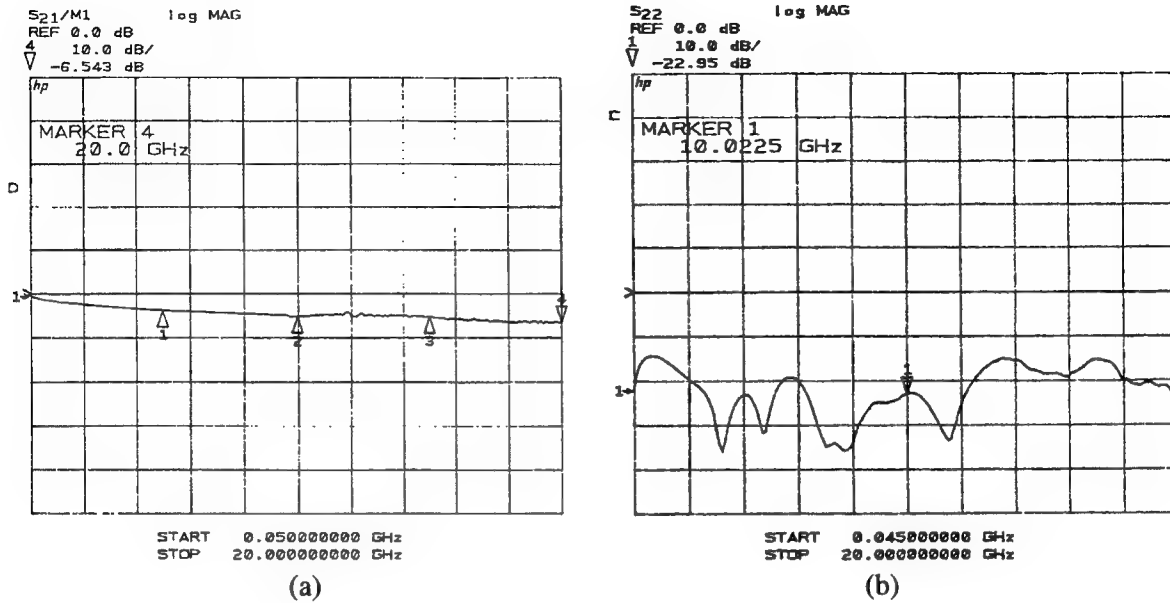


Fig. 4 (a) microwave transmission and (b) reflection parameters of testing electrode.

In conclusion, a microstrip line-slot ground microwave electrode is proposed and constructed for optical push-pull type EO polymer modulator. The new electrode design can perform both electric field poling and modulator driving functions. Numerical simulation and experimental test results showed that the new electrode design has a wide frequency response. It also allows high poling field and can simplify fabrication process for push-pull type EO polymer modulators.

References:

1. W. Wang, Y. Shi, D. J. Olson, W. Lin, J. H. Bechtel, *IEEE Photon. Technol. Lett.*, **11**, 51, (1999).
2. T. A. Tumolillo, Jr., P. R. Ashley, *IEEE Photon. Technol. Lett.*, **4**, 142 (1992).
3. H. R. Janson, *Arch. Elektronik u. Übertragungstechn.*, **32**, 485 (1978).
4. H. R. Fetterman, D. Chen, A. Udupa, S. Lee, A. Chen, W. H. Steier, in *Organic Optics and Optoelectronics, 1998 IEEE/LEOS Summer Topical Meeting Tech. Dig.*, p. 9.
5. Y. Shi, W. H. Steier, M. Chen, L. Yu, L. R. Dalton, *Appl. Phys. Lett.*, **60**, 2577 (1992).

A compact optical branch, composed of a half-mirror and a rectangularly crossed waveguide

Jiro Toyama, Takeshi Yamada, Yasuhiro Kubota and Ichiro Takatsu

NOK Corporation, Tsukuba Technical Lab. 25 Wadai, Tsukuba-shi, Ibaraki-ken, 300-4247 Japan

jtoyama@nok.co.jp, ykubota@nok.co.jp, takatu16@nok.co.jp

An optical branch is a key component of an integrated optical circuit, not only obtaining the two-way communication as a passive component but also forming various active components such as a modulator and an optical switch. Although, usually, a Y-shape waveguide is used for the branch, cost of this type is not enough low to be used widely in the FTTH system, because of the longer waveguide and the precise patterning to suppress the transmission-loss (1) (2). To materialize a low cost optical integrated circuit, it may be required to search a tradeoff between performance and cost of a branch. To minimize the cost, it is effective to reduce the size with simple waveguide pattern, and to get a larger amount of components on a wafer at a time. From the point of view, we have developed a compact and simple optical branch, which is composed of a pair of rectangularly crossed waveguides and a half-mirror fabricated in it. The size is reducible below 1mm^2 and the productivity is more than a hundred times that of conventional Y-branch. And to adopt organic waveguide, fluoride polyimide, the fabricating process becomes simple and the matching of refractive index around the half-mirror is easily obtained. And further application of this construction will make 1:N branch and optical switch, in which non-linear polymer is adopted, feasible.

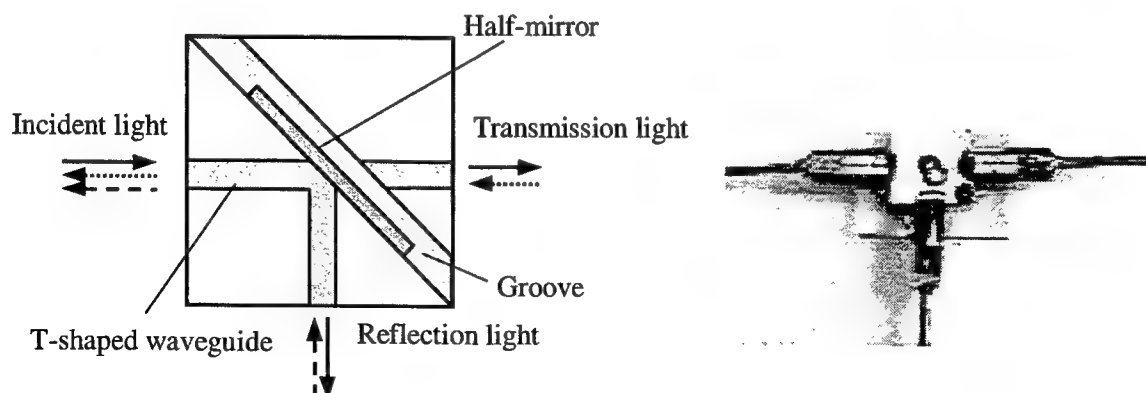


Fig.1 Schematic configuration of a compact branch component with a half-mirror.

The configuration of the 1:2 branch is shown in Fig.1. A set of rectangularly crossed waveguide is formed with polymer on a silicon wafer. A narrow groove is formed at the cross-area by 45 degrees to the axis of both waveguides. A multi-layer half-mirror is fabricated by means of vacuum evaporation on a side of the groove. The groove is buried with polymer of which refractive index is the same as the waveguide's, after fabricating the mirror.

The loss at the groove is estimated as the coupling loss of a radiated beam, from the front-end waveguide to the back-end waveguide, of which Gaussian function gives distribution. The angle of the radiation is estimated by the propagating angle decided by the effective refractive index of the waveguide. The estimation and the experiments are shown in Fig.2, and it is found that the minimum loss is about 1 dB by adopting the moderate combination of refractive indices of the fluoride polyimide core and the cladding of the waveguide.

The other excess loss of this branch, the loss of the half-mirror, is estimated by using published simulation software, and assured by several experiments. In this design, it is desired that the half-mirror should show a low polarized dependent loss (PDL) to be used widely in the FTTH and the structure should be made simple to be fabricated in the narrow groove. A three-layer structure of a silver layer and two zinc-sulfide layers, and sandwiching the silver is preferred for the half-mirror. We have found that the branch ratio can be controlled by the thickness of the silver mainly and the PDL is obtained by deciding the zinc-sulfide's thickness. The Fig.3 shows the simulation and the experiments of this design. They correspond mutually well and indicate that the penetrating loss of 0.41dB and the PDL of 0.024dB at 1:1 branch ratio are achieved. Then the target for the excess loss of this branch is decided as below 3.0dB including propagating loss of the waveguide and the coupling loss to fibers.

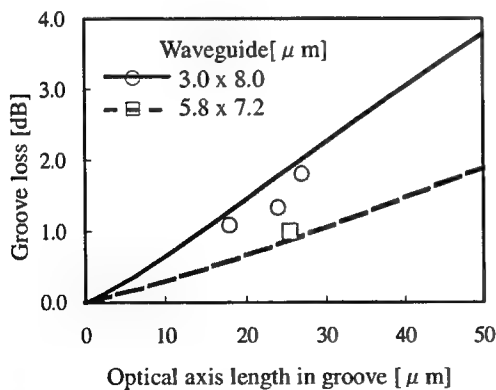


Fig.2 The transmission loss depend on the groove at the cross of waveguide.

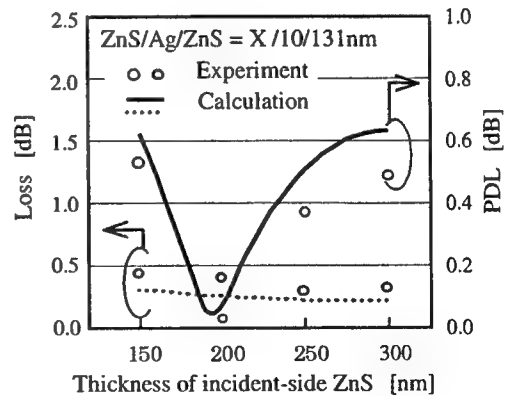


Fig.3 Optical characteristics of the three layer half-mirror, simulated and experimented.

The waveguide is constructed on a 3-inch silicon wafer with fluoride polyimide, OPI-N3000 series of Hitachi Chemical Co.. Two types of polyimide are spin-coated on the wafer to form a cladding layer and a core layer. A T-type waveguide is formed by means of photolithography and dry etching, and after formed the waveguide, the cladding polymer is spin-coated to form the side and the upper cladding. The difference of diffraction index is chosen 0.3 %. The height of waveguide is $5.8 \mu\text{m}$ and the width is $7.2 \mu\text{m}$. A groove is formed at the cross point of T by a dicing saw, at the angle of 45 degrees for the waveguide. The width of groove is $18 \mu\text{m}$, and the depth is $150 \mu\text{m}$. The half-mirror is constructed with a 13 nm thick silver sandwiched by 193 and 119 nm thick zinc sulfide, directly formed by vacuum evaporation to the one side of the groove. The space of the groove is varied with transparent resin of which refractive index is equal to that of the waveguide core. The dimension of the branch in this trial is 5mm square.

The characteristics of the trial branch are as follows:

Excess loss	:	2.8 dB
Branch ratio	:	1:1
Isolation	:	below 30dB
Mode	:	Single-mode

Although the excess loss of 2.8 dB of this new branch is higher than the well performed ordinal Y-branch's, it is considered that it is enough low to be used in the FTTH system and fully satisfy the cost performance. The loss includes 0.9 dB of coupling loss and 0.4 dB of transmission loss and half-mirror loss. Then the loss value would be largely improved by further study. The transmissive bandwidth is assured up to 400 MHz, and further measurement of it is planned to get sufficiently wider bandwidth. And this branch is free from mode disturbance problem and the dimension is reduced to the extent that one can handle the branch in the application. The maximum production run of the branch is over 4000 pieces in our estimation, when the branches are produced separately on a 3-inch silicon plate.

Reference:

- (1) Chu F.S. and Liu P-L, Opt Lett **16**,5,309 (1991)
- (2) M.Seino, N.Mekada and H.Nakajima, IEIC Technical Report. OQE-87,24(1987)

Bragg Gratings by Photo-Bleaching in Polymer Waveguides

Vadim Chuyanov

Department of Electrical Engineering-Electrophysics University of Southern California.
920 West 37th Place, Los Angeles, CA 90089-0483

Dmitry Starodubov

D-STAR Technologies, 725 33rd Street, Manhattan Beach, CA 90266

Antao Chen

Lucent Technologies. Optoelectronic Center 3K-105,
9999 Hamilton Boulevard Breinitsville, PA 18031-9359

Araz Yacoubian, Sean Garner, William H. Steier

Department of Electrical Engineering-Electrophysics University of Southern California.
920 West 37th Place, Los Angeles, CA 90089-0483

Jack Feinberg

D-STAR Technologies, 725 33rd Street, Manhattan Beach, CA 90266

1. Introduction

Recent advances in polymers have resulted in various demonstrations of polymer based devices and components for integrated optics, optical communications, RF photonics and sensors. Among them are Mach - Zender optical modulators, polarization filters vertical polarization and power splitters and many more. There is now significant effort to demonstrate wavelength sensitive planar devices and components. For example among the latest achievements are integrated optical chemical sensor based on Bragg grating [1], tunable optical add/drop multiplexer [2], and sol-gel grating waveguide for distributed Bragg reflector lasers [3].

There are several techniques to produce Bragg gratings, which are usually the basis for such devices, in polymer waveguides. For example gratings can be fabricated by means of replication, molding, stamping, embossing and e-beam writing.

Another way to create a Bragg grating is to use photo-bleaching of nonlinear optical polymers. Photo-bleaching has been utilized for writing polymer waveguides, diffraction gratings, and post-process trimming of active polymer devices. This process has several advantages. As in case of photochemical fabrication it produces bulk changes of the refractive index in the material which increases the reflection efficiency of the grating. The induced anisotropic index change depends on polarization of the writing beam and can be as high as 10^{-2} (see [4]). The only drawback of such materials is the higher optical loss compared to passive polymers which limits the useful length of grating, saturates the reflectivity and increases the FWHM of the reflection peak. Nevertheless our calculations show that a Bragg grating with the length of 0.6 cm in a polymer with loss as high as 3 dB/cm can still have a reflection coefficient as high as 90% and FWHM of less than 0.5 nm at $\lambda=1.3 \mu\text{m}$.

In this article we present fabrication of Bragg gratings in nonlinear optical polymers and studies of their properties.

2. Experimental results

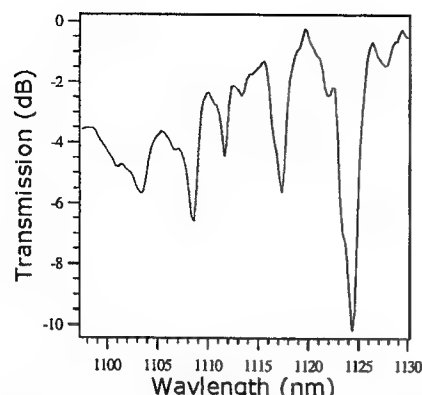


Figure 1. Transmission spectrum of the Bragg grating induced by photo-bleaching in

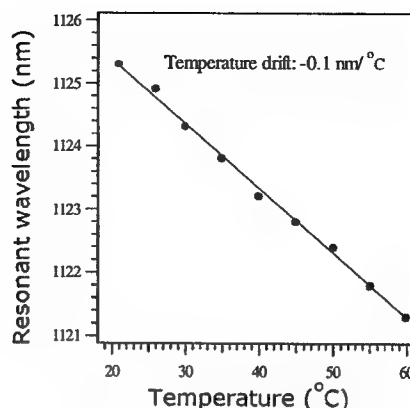


Figure 2. Dependence of resonant wavelength from temperature for fundamental mode of the polymer waveguide

All experiments were performed with 1.5-2 cm long polymer waveguides on silicon substrate with IBM PMMA-DR1 material as a core layer and UV-15D epoxy as upper and lower cladding. Ridge waveguides were produced in 2.5 μm thick core layer by reactive ion etching in oxygen plasma. The etch depth and ridge height were 0.8 μm and 6 μm respectively. Both ends of waveguides were connected with single mode fiber with a cut-off wavelength of 1275 nm.

The Bragg gratings were fabricated by using a phase mask technique using 451 nm light from the argon laser. To increase the length of the grating the beam from laser was expanded to 8 mm in diameter with a telescope. The power of the laser beam was 100 mW which resulted in average intensity of laser radiation on sample of 0.2 W/cm^2 . The typical exposure time was around 200 seconds. The polarization of the laser light was perpendicular to the polarization of both the TE and TM modes so that induced index change would be the same for both TE and TM polarizations. Transmission spectra were recorded with an optical spectrum analyzer using Yb-doped fiber as a source.

Figure 1 shows an example of transmission spectrum of the Bragg grating created in the multimode waveguide. Several minima correspond to reflection of various modes of the waveguide. The highest reflectivity (up to 90%) was observed for fundamental modes of the waveguide. This can be explained by the fact that fundamental mode has the highest overlap integral with the lateral profile of the index change in the core of the waveguide. The measured FWHM for this reflection peak was about 2 nm and probably was a combination of reflection peaks of both TE and TM modes with slightly different center wavelengths. Note that the above reflectivity corresponds to the index change $\Delta n \approx 1.6 \cdot 10^{-4}$.

Figure 2 presents results on temperature tuning of the reflection resonance of the Bragg grating. The temperature sensitivity calculated from the results of this experiment was $-0.1 \text{ nm/}^\circ\text{C}$. The value of dn/dT that can be obtained from this rate is $-1.2 \cdot 10^{-4}/^\circ\text{C}$ which is typical for polymers.

Figure 3 shows the result of a thermal stability test of the Bragg grating using isochronal annealing technique. In this experiment sample was heated up for two minutes at each temperature with increment of 10°C . As one can see significant deterioration of index change starts around 80°C .

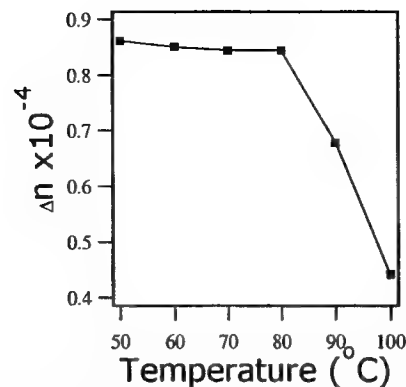


Figure 3. Temperature stability of photo-induced index change

3. Discussion and Conclusion

The initial results show that even in relatively lossy photo-bleached grating, the reflection coefficient can be high and reflection band relatively narrow. Both of these parameters can be improved by optimization of the bleaching process.

To explain the results of the thermal stability experiments one should note that the index change because of photo-bleaching in azo-dye like materials such as DR1 comes from several mechanisms. One of these mechanisms is breaking of the azo-bond, which results in decreased density of the DR1 dye. Another one is realignment of the DR1 dye groups away from the polarization of the writing beam through trans-cis-trans transitions.

The first mechanism creates a more stable index change. To erase it one needs temperature activated diffusion on a relatively large scale unlike the index change produced by photo-induced realignment. The relative contributions for these two mechanisms has to be studied separately. But the fact that significant deterioration of index change happens well above $T_g \approx 60^\circ\text{C}$ allows us to conclude that first mechanism prevails.

In summary nonlinear optical polymer materials used for electro-optical devices can be processed by photo-bleaching. Their photosensitivity opens interesting possibilities of integrating such electro-optical devices with wavelength sensitive components on a single chip. In addition to that post-writing trimming of these devices can be used for the fine tuning of such devices. Bragg gratings induced by photo-bleaching in nonlinear polymers can open new fields of applications for these materials in integrated optics and communications. Further studies of polarization sensitivity, temperature and electro-optic properties are required

Reference

1. Thomas M. Butler, Eishi Igata, and Steve J. Sherad. *Optics Letters* **24**, 525-527 (1999).
2. Louay Eldada, Robert Blomquist, Mac Maxfeld, Deepti Pant, George Boudoughian, Constantina Pogoda, and Robert A. Norwood. *IEEE Photon. Tech. Letters* **11**, 448-450 (1999).
3. M. A. Faradad, H. Lou, Y. Beregovski, and M. Fallahi. *Optics Letters* **24**, 460-462.
4. Sang-Shin Lee, Sean Garner, Antao Chen, Vadim Chuyanov, and William H. Steier. *Appl. Phys. Lett.* **73**, 3052-3054.

Organic Thin Films for Photonics Applications

Second-Order NLO Materials: 2

Friday, 24 September 1999

James R. Heflin, Virginia Polytechnic Institute, USA
Presider

FC

1:30pm–3:00pm

California Ballroom Salons 4&5

Ultrafast Optoelectronics Using Poled Polymers

Ajay Nahata

AlliedSignal Inc., 101 Columbia Road, Morristown, NJ 07962

Tony F. Heinz

Departments of Electrical Engineering and Physics, Columbia University, New York, NY
10025

Over a period of years, high-speed photoconductors have served very well for the conversion of ultrafast optical pulses from modelocked lasers into ultrafast electrical pulses, as well as the measurement and characterization of such electrical pulses. These methods have been developed and applied successfully both to electrical transients guided by transmission lines and to pulses of freely propagating terahertz (THz) electromagnetic radiation. While techniques based on photoconductivity have many attractive features, including excellent efficiency for generation and sensitivity for detection, they exhibit an inherent maximum speed associated with the response time of the photo-excited carriers. For electrical pulses of picosecond to subpicosecond duration, this limitation is not severe if one makes use of the appropriate photoconductive media. However, if one wished to match the time resolution of 10 fs provided by current modelocked lasers, this factor becomes a critical limitation.

With this background in mind, several groups have been developing methods to generate and detect ultrafast electrical fields with laser radiation using a non-resonant material interaction. In principle, such a non-resonant (electronic) interaction can provide an instantaneous response even over the time scale of a 10 fs laser pulse. Electro-optic sampling is one such method that has already been developed in the context of probing transient fields in transmission lines and in circuits. In this approach, an ultrashort optical pulse senses the electric fields present in an appropriate nonlinear medium through a change in birefringence induced by the material's electro-optic response. More recently, this scheme has been extended to sampling of ultrafast electric fields in freely propagating THz electromagnetic pulses [1]. Researchers at RPI have also demonstrated the possibility of using this method for an elegant imaging technique [2] and have shown the possibility of detecting electromagnetic radiation at frequencies as high as 37 THz [3]. Complementary to these detection techniques is the application of the optical rectification process to generate ultrafast electrical transients. This approach relies on precisely the same nonlinear material response as is used in electro-optic sampling, i.e., the second-order nonlinearity, but in this case the ultrafast optical pulse generates a polarization at baseband frequencies. In this paper, we discuss the development and characteristics of a THz spectroscopy system based on a combination of this optical rectification process and free-space electro-optic sampling [4]. One of the key considerations to be examined concerns the role of phase matching of the interactions and how this may best be achieved. We will also discuss the application of these nonlinear optical processes to generate subpicosecond guided wave electrical pulses on

transmission lines [5]. In our most recent work, we have observed sub-200 fs guided wave electrical transients in a poled polymer-based transmission line device [6]. This scheme offers the inherent speed of a non-resonant nonlinear optical process, while producing pulses suitable for circuit applications.

The work at Columbia University was supported the NSF, AFOSR, and JSEP.

- [1] Q. Wu and X.-C. Zhang, Appl. Phys. Lett. 67, 3523 (1995); P.U. Jepson et al., Phys. Rev. E 53, R3052 (1996); A. Nahata, D.H. Auston, T.F. Heinz, and C. Wu, Appl. Phys. Lett. 68, 150 (1996).
- [2] Q. Wu and X.-C. Zhang, Appl. Phys. Lett. 69, 1026 (1996).
- [3] Q. Wu and X.-C. Zhang, Appl. Phys. Lett. 71, 1285 (1997).
- [4] A. Nahata, A.S. Weling, and T.F. Heinz, Appl. Phys. Lett. 69, 2321 (1997).
- [5] A. Nahata and T.F. Heinz, Opt. Lett. 23, 867 (1998).
- [6] A. Nahata, Opt. Lett., submitted for publication.

Characterization of dye-containing polymers ability to be optically oriented

Michel Dumont and Michel Fischer,

Laboratoire de Photonique Quantique et Moléculaire, CNRS,
ENS de Cachan, 61 Av du Président Wilson, F-94235 Cachan cedex, France
Michel.Dumont@LPQM.ENS-Cachan.fr

Three different optical methods have been developed for ordering dye molecules in polymer films, for non linear optics and telecommunication applications.

- Photoinduced anisotropy (PIA) or Weigert effect: birefringence and dichroism are induced by a polarized resonant light excitation
- The photoassisted electrical poling (PAEP): optical pumping increases the mobility of molecules which can be oriented by the field at room temperature[1].
- The all-optical poling (AOP) is the most recent method: The material is coherently pumped by the fundamental frequency and the second harmonic of a laser beam resonant at 2ω [2]. A $\chi^{(2)}$ can be created with non polar molecules (octupolar molecules) and different macroscopic symmetries can be induced [3].

These three methods can be described by the combination of three mechanisms:

1. A selective optical pumping, or angular hole burning (AHB). In PIA, the polarized pumping beam produces an anisotropic depletion of the ground state, according to a $\cos^2\theta$ law (θ is the angle between the transition dipole of the molecule and the polarization of light). In AOP, the depletion is non centrosymmetric. If both beams are linearly polarized in parallel directions, the pumping probability is in $\cos^3\theta$, but with different polarization configurations a more sophisticated tensorial hole burning can be produced. In PAEP anisotropic AHB plays a secondary role.
2. An angular redistribution (AR) in the optical excitation process, during the lifetime of excited levels or in the relaxation process, back to the ground state. These angular redistribution is particularly efficient when a change of the geometrical structure of molecules occurs, i.e. when molecules are subjected to photoisomerization (azo-dyes are the most efficient photoisomerizable molecules). AR is a kind of thermalization of molecules orientation in the excitation process.
3. Angular relaxation in the ground state. This is the usual thermal diffusion. Of course, to built a permanent orientational order, this relaxation must be avoided.

In PIA and in AOP, the angular redistribution is random and isotropic. The orientational order is produced by the depletion of the ground state through AHB. After several cycles of excitation molecules are accumulated in the less pumped directions. Finally the geometry of the pumping light is imposed to the material. Conversely, in PAEP, orientation is produced by the electric field. AR is no more isotropic: the thermalization, during the excitation cycle, occurs in the presence of an electrical torque acting on the permanent dipole of molecules. In PAEP, optical excitation increases the mobility of molecules, like heat in the usual thermal poling method. All these phenomena have been described by a theoretical model [4,5] and their transient behavior can be computed as a function of the optical pumping geometry and of angular diffusion properties in excitation processes and in the ground state.

This paper shows that a very simplified phenomenological description and a simple experiment of PIA permits the rapid characterization of the ability of molecules, in a given polymeric environment, to be oriented by any of the three techniques.

The experimental set up is described in reference 6. It has been built in order to record the time variations of the anisotropy of the optical density of optically pumped dye-containing polymer films, simultaneously on several wavelengths. A wheel with narrow slits rotates in front of the six entrance slits of a modified monochromator. The output beam, constituted of a periodic succession of pulses (≈ 2 ms) of different colors, is used as a probe beam and crosses the polarized pump beam on the sample. The probe beam is then split into parallel and perpendicular polarization components, by a Wollaston prism. A computer synchronized with the slit wheel reconstructs the optical densities $OD_{//}$ and OD_{\perp} for each wavelength. Then the average optical density, S_0 , and the anisotropy, S_2 , are built:

$$S_{0,\lambda} = \frac{1}{3}(OD_{//} + 2OD_{\perp}) = N_g \bar{\sigma}_g(\lambda) + N_e \bar{\sigma}_e(\lambda) \quad (1)$$

$$S_{2,\lambda} = \frac{1}{3}(OD_{//} - OD_{\perp}) = N_g \bar{\sigma}_g(\lambda) a_g(\lambda) \langle P_2 \rangle_g + N_e \bar{\sigma}_e(\lambda) a_e(\lambda) \langle P_2 \rangle_e \quad (2)$$

Where N_g and N_e are the populations of the ground state and of the excited state(s), respectively; $\bar{\sigma}_g$ and $\bar{\sigma}_e$ are the average cross sections, α_g and α_e , the molecular anisotropies and $\langle P_2 \rangle_g$ and $\langle P_2 \rangle_e$ the order parameters (Projection of the angular distributions on the Legendre parameter $P_2(\cos\theta)$). Figure 1 gives an example of time evolution of these quantities for an double azo-dye molecule in PMMA. In that case g is the trans state and e the cis state. The photoisomerization is clearly demonstrated by the decrease of the average optical density at 430 and 481 nm which are in the absorption band of trans and its increase at 392 and 554 nm (absorption band of cis). After the pump is switched off, the relaxation of cis contains a fast component and a very slow one which needs one day for full relaxation. In addition one also observes that there is a blue shift of the absorption band (T_0 decreases slowly at 481 nm, on the red side of trans band, while it increases at 430 nm on the blue side): photoisomerization is probably not the unique photochemical process. Looking at anisotropy curves (lower graphs), one observes successively a very fast variation correlated with that of population (T_0), corresponding to the creation of anisotropy by hole burning. In that period of time, the anisotropy at 554 nm (and also in UV) is positive since cis molecules are excited in the direction parallel to the pump polarization. After a few seconds, T_0 (populations) is stationary but anisotropy continues to increase with a slower slope: this a clear proof of the angular redistribution and of the accumulation of trans molecules in the perpendicular direction. At 554 nm the positive anisotropy of cis decreases and is dominated by the negative anisotropy of trans. After the end of pumping, the anisotropy is rather stable in this material, although it is a guest-host system (much better stability than for the smaller DR1 molecules, but worse than with chromophores grafted to the main chain).

Several other examples will be presented and in some cases, we will show in comparison, some results obtained with PAEP (observed by measuring the growing of Pockels electrooptic effect in an attenuated total reflection experiment [6]) and AOP experiments. A molecule such as that of the above example should be a good candidate for AOP, if it was a non centrosymmetric molecule. Indeed the mechanism of photo-induced rotation is the same in AOP and in PIA. With a non photoisomerizable molecule we have also observed photoinduced anisotropy but in this case there was no angular redistribution and the anisotropy was interpreted as an angular selective photodegradation: this molecule exhibits a small AOP effect explained by the same mechanism. Researches are in progress for finding mechanisms other than photoisomerization for optical organization of chromophores in polymers and in sol-gels.

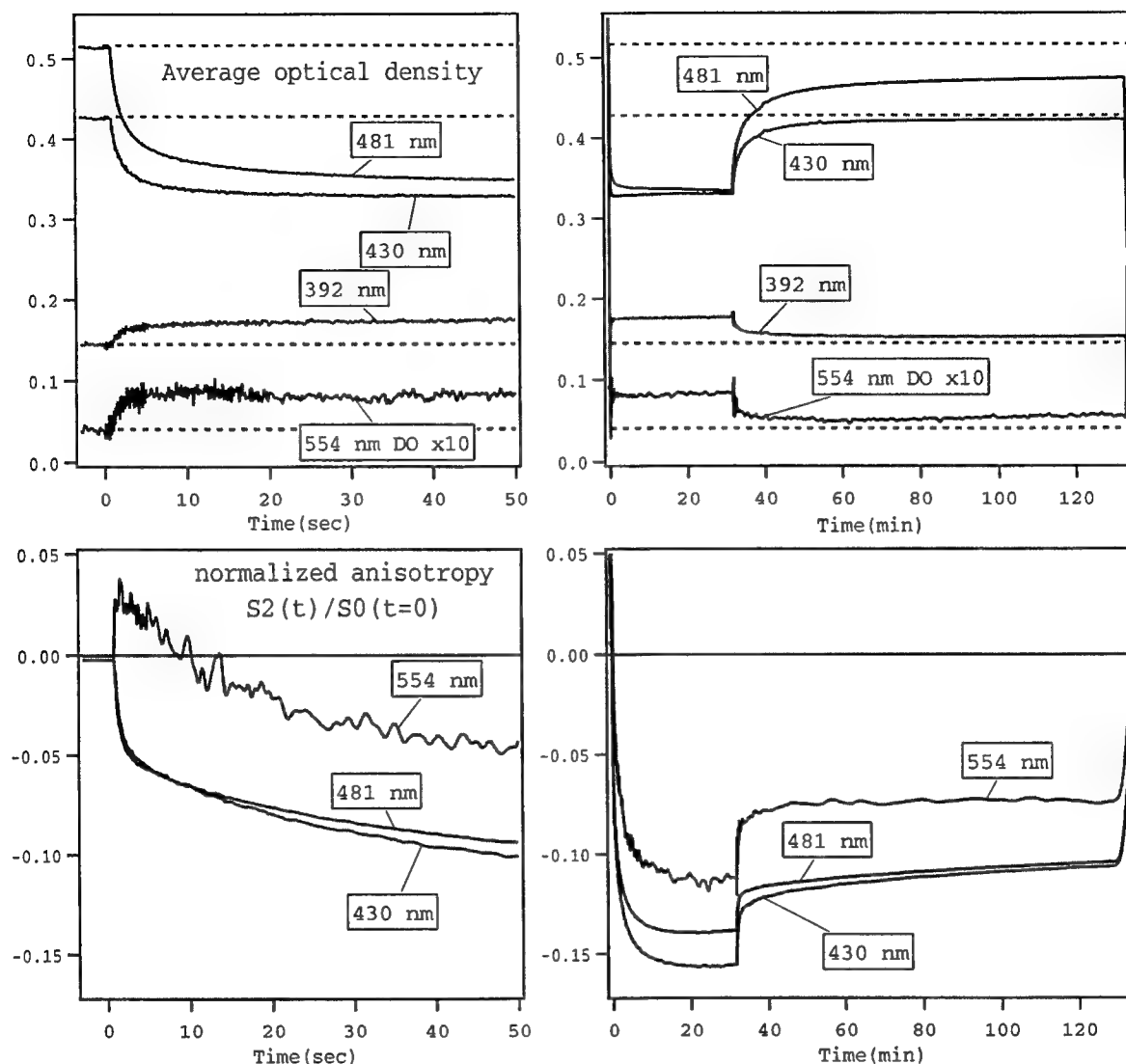


Figure 1. The polarized optical pumping begins at $t=0$ up to $t=32$ minutes ($\lambda=457$ nm, 20 mW/cm²). The left hand graphs show the first 50 s of pumping and the right hand graphs pumping and relaxation.

References

1. Z. Sekkat And M. Dumont, s. **B 54**, pp 486-489, 1992 and, *Mol. Cryst. liq. Cryst. Sci. Technol. secB: Nonlinear Optics*, **2**, pp 359-362, 1992..
2. F. Charra, F.Kajzar, J.M. Nunzi, P. Raimond and E. Idiart, *Optics Lett.* **18**, p 941, 1993.
C. Fiorini, F. Charra, J.M. Nunzi and P. Raimond, *Nonlinear Optics* **9**, p 339, 1995.
J.M.Nunzi, F. Charra, C. Fiorini, J. Zyss, *Chem.Phys. Lett.* **219**, p349, 1994.
3. S. Brasselet, J. Zyss, *Opt. Lett.* **19**, pp 1464-1466, 1997. And , *J. Opt. Soc. Am. B* **15**, pp 257-288, 1998.
4. M.Dumont, in : *Photoactive Organic Molecules, Science and Applications*, F. Kajzar, ed., Nato ASI Series Vol. **9**, pp 501-511, Kluwer Academic Publishers 1996.
M. Dumont, G.Froc and S.Hosotte, *Nonlinear Optics* **9**, pp 327-338, 1995.
5. M. Dumont, *Chemical Physics* , In press (1999)
6. A. El Osman and M. Dumont, *Proc. SPIE* 3417, 36 (1998)

Efficient Poling-Low Induced Losses Tradeoff for Efficient SHG in Poled-Polymer Waveguides at 1.55 μm

Vincent RICCI, George Stegeman

*School of Optics / Center for Research and Education in Optics and Lasers, University of Central Florida,
P.O. Box 162 700, 4000 Central Florida Boulevard, Orlando, FL, 32816-2700, USA
Tel.: +1-407-823-6945, Fax: +1-407-823-6955, email: Vincent @ mail.creol.ucf.edu.*

And Kwok Pong Chan

Molecular OptoElectronics Corporation, 877 25th Street, Watervliet, New York 12189 – 1903.

Ultra-fast switching and frequency shifting devices are important for telecommunications. In that respect, organic polymers are good material candidates since they exhibit large second-order nonlinearities that can be used for second-order parametric interactions, and that can also generate ultra-fast nonlinear phaseshifts via $\chi^{(2)}\chi^{(2)}$ cascading processes [1]. In order to achieve practical waveguide applications, very efficient second harmonic generation (SHG) must first be demonstrated. Besides, SHG shows the same figure of merit as $\chi^{(2)}\chi^{(2)}$ cascading, namely d^2/n^3 , where d is the effective nonlinear coefficient and n the effective index of the waveguide mode.

So far, the best SHG efficiency obtained in a polymer waveguide has been achieved in a photo-bleached channel waveguide of 4-dimethyl-amino-4'-nitrostilbene (DANS), using an intermodal phase-matching scheme. A record SHG efficiency of 0.7 % / W for a 7 mm-long channel was then reported [2]. However, the reported propagation losses at the second harmonic were pretty high, $\alpha(2\omega) = 20 \text{ dB / cm}$, and the reported effective nonlinearity, $d = 5 \text{ pm / V}$, not optimized.

The normalized SHG efficiency is typically broken into four factors involving the polymer macroscopic nonlinearity, the interaction effective cross-section, a detuning term and a loss factor. Most of the research focuses on these factors independently.

We first focused on optimizing the macroscopic nonlinearity, which scales with the degree of orientational order of the optically nonlinear active chromophores. The fabrication technique that we used to align the chromophores is called parallel-plate poling. In parallel plate poling, the polymer stack is sandwiched by two electrodes (ITO and Aluminum in our case). First, the temperature of the structure is raised close to the glass transition temperature (T_g) of the polymer matrix containing the active nonlinear chromophores, thereby increasing the free volume and allowing free rotation of these chromophores. Then, an electric field is applied across the multi-layered, creating a torque on the permanent dipole moments and forcing them to align along the lines of the electric field, this is known as "electric poling". Then, the poling field is maintained while the structure is cooled down to room temperature, thereby freezing the dipole orientation distribution as the free volume decreases. It is important that most of the applied voltage falls across the nonlinear active layer. When the temperature of a polymer gets close to its T_g , its electrical properties can span up to two orders of magnitude. Consequently, matching the glass transition temperature of the different polymer layers (Figure 1) allowed us to

decrease the voltage drop that occurred in the linear Polyetherimide layer $T_g = 190^\circ\text{C}$ [2]. We were able to increase the second-order nonlinearity by a factor of 3.5.

We applied external poling voltages ranging from 1200 V to 1360 V (corresponding to nominal poling fields between $130\text{ V}/\mu\text{m}$ and $180\text{ V}/\mu\text{m}$) to the 2 guiding structures showed figure 1. We report the first SHG Maker Fringes measurements at $1.58\text{ }\mu\text{m}$ carried directly through the multi-layered structure in order to measure the nonlinearity of the guiding device in-situ. This allows a direct measurement of the nonlinearity as opposed to the indirect channel waveguide SHG measurements that includes other factors such as propagation losses, the effective nonlinear cross-section of the interaction and the phase-matching term. In our SHG Maker fringe model, we ignored multiple reflections in the buffer layers, we considered both the absorption in the DANS layer and the poling-induced birefringence σ . We used α -Quartz as a reference with $d = 0.29\text{ pm/V}$. In the case of PC/DANS/PEI-X/PC structure, we measured a phase-matchable d -coefficient of up to 18 pm/V for the DANS layer, together with a poling-induced birefringence of $\sigma = 0.004$ (Figure 2), which is in excellent agreement with reference [3].

In reference [2], a d -coefficient of $d = 5\text{ pm/V}$ was measured. Assuming all other factors of this reference kept constant, our improved poling efficiency would yield an increase of the waveguide normalized SHG efficiency by an order of magnitude above the current record, i.e. $7\text{ \%}/\text{W}$.

Practically, however, the increase of the poling field leads to an increase of the poling current density, which can ultimately induce an electric breakdown in the polymer materials. When the current density increases below the threshold of electrical breakdown, although no terminal breakdown occurs, yet, an increasing number of microscopic discharges occur in the polymer material, leading to propagation losses due to physically damaged areas. For the most efficiently poled samples ($d = 16.5\text{ pm/V}$ with PEI-HM and $d = 18\text{ pm/V}$ with PEID, we could observe cracks through the polymer stacks), after removing the top aluminum electrode, and consequently measured very high propagation losses, $\alpha(\omega) > 90\text{ dB/cm}$. Those losses led to extremely reduced SHG efficiencies. On the other hand, the PC/DANS/PEI-X/PC sample structure poled with a nominal field of $133\text{ V}/\mu\text{m}$, yielded a d -coefficient of 12 pm/V measured by Maker Fringes, with propagation losses, $\alpha(\omega) = 4\text{ dB/cm}$ and $\alpha(2\omega) = 20\text{ dB/cm}$. A normalized SHG efficiency up to $0.6\text{ \%}/\text{W}$ was measured for a 4-mm long, $6\text{-}\mu\text{m}$ wide channel waveguide. In this case, the new larger effective cross-section decreased the SHG efficiency by a factor of 2 compared to reference [2]. This clearly shows the tradeoff between high poling field and high propagation losses.

In conclusion, we showed that glass transition temperature matching is a viable route to increase the poling efficiency and therefore the waveguide SHG efficiency. In-situ Maker-Fringes measurements were performed to assess the magnitude of the macroscopic second-order nonlinearity, up to $d = 18\text{ pm/V}$ for a nominal poling field of $180\text{ V}/\mu\text{m}$. A tradeoff exists between the poling field strength and the magnitude of the corresponding poling-induced losses. Optimization of the poling efficiency should be made in conjunction with monitoring the waveguide propagation losses. Moreover, the effective cross-section is affected by the choice of material indices. As a result, a proper selection of materials should be made so that both the effective cross-section and the poling efficiency are optimized. Finally, we demonstrated a normalized SHG efficiency of the order of $0.6\text{ \%}/\text{W}$ for a 4-mm long, $6\text{-}\mu\text{m}$ wide phase-matched channel with a measured $d = 12\text{ pm/V}$ nonlinearity, losses at the second harmonic of $\alpha(2\omega) = 20\text{ dB/cm}$ and an non-optimized effective cross-section of $256\text{ }\mu\text{m}^2$. We would like to

acknowledge the AFOSR and M. Diemeer from Akzo-Nobel for supplying us with the DANS and PC polymers.

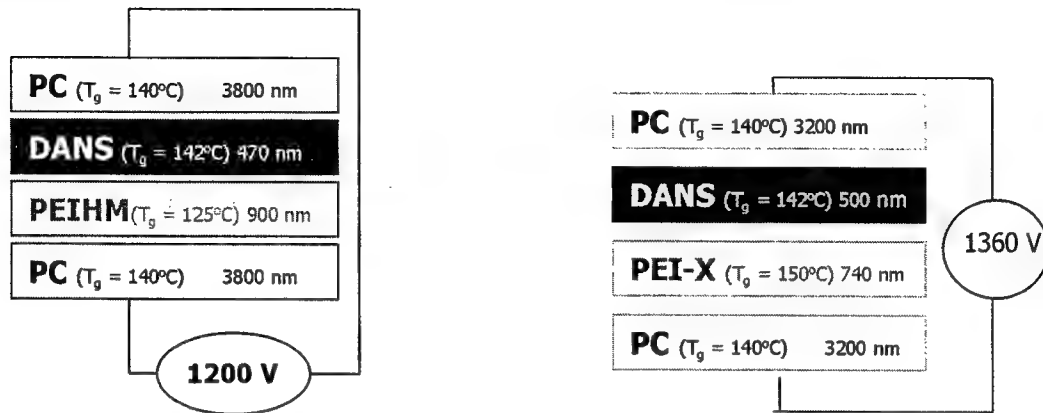


Figure 1: Multi-layered structures studied: upper and bottom cladding layers are made of polycarbonate PC ($T_g = 140^\circ\text{C}$). The core is made of a nonlinear layer, DANS ($T_g = 142^\circ\text{C}$) and a linear layer, polyetherimide derivative PEI-HM ($T_g = 125^\circ\text{C}$) or PEI-X (HM ($T_g = 150^\circ\text{C}$)). To achieve poling, contact electrodes were used. The bottom PC cladding was deposited on a transparent ITO electrode, respectively coated on top of a fused silica substrate. A top Aluminum electrode was also deposited on top of the upper PC-cladding for poling and then removed before taking the SHG Maker-Fringes measurement. In each case, d_{33} and d_{31} were measured given the external poling voltages. Left structure: nominal poling field = $133\text{ V}/\mu\text{m}$, $d_{33} = 3d_{31} = 16.5\text{ pm/V}$. Right structure: nominal field = $180\text{ V}/\mu\text{m}$, $d_{33} = 3d_{31} = 18\text{ pm/V}$.

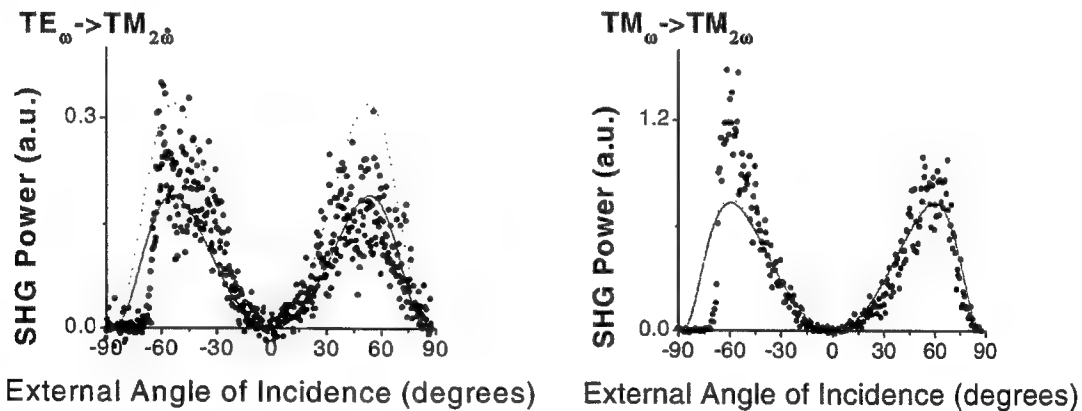


Figure 2: black circles are data points from the Maker Fringes Measurements of PC/DANS/PEIX/PC structure (nominal poling field $180\text{ V}/\mu\text{m}$). The left graph is obtained for a TE fundamental input and a TM second harmonic output. The right graph is obtained for a TM fundamental input and a TM second harmonic output. The dotted curves are the theoretical fit assuming no induced birefringence, the straight lines correspond to a poling-induced birefringence $\sigma = 0.004$. Both theoretical fits are obtained for $d_{33} = 3d_{31} = 18\text{ pm/V}$ with the reference α -Quartz ($d = 0.29\text{ pm/V}$).

- [1] T. Gase, W. Karthe, "Quasi-Phase-Matched cascaded second-order processes in poled organic polymer waveguides", *Optics Communication*, **133**, 1997.
- [2] M. Jaeger et al., "Modal dispersion phase-matching over 7 mm length in overdamped polymeric channel waveguides", *Appl. Phys. Lett.*, Vol. **65**, pp. 1205-1207, 1994.
- [3] M. Jager, "Efficient second harmonic generation in poled-polymer waveguides using co-propagating geometries", *Ph.D. dissertation*, university of central Florida, 1997.

NONLINEAR OPTICAL FILM FORMED LAYER-BY-LAYER USING ALTERNATING POLYELECTROLYTE DEPOSITION

M. JOSEPH ROBERTS

Naval Air Warfare Center, Materials and Chemistry Division, Code 4T4220D, 1 Administration Circle, China Lake, CA 93555, Phone: (760)939-1394, Fax: (760)939-1617, Email: RobertsMJ@navair.navy.mil

Alternating polyelectrolyte deposition (APD) is a room temperature self-assembly technique for the formation of multilayer stacks without the need for expensive equipment.¹ A multilayer film is formed by alternately immersing the substrate in aqueous solutions of a polyanion and a polycation. Since the thickness of each layer is on the order of 2 nanometers, APD allows precise control of the overall film thickness. APD films of thousands of layers have been reported. Coulombic forces are responsible for the formation of the APD films so the resulting structure is very robust. Polishing is necessary for removal of an APD film from the substrate.

Noncentrosymmetric chromophore orientation has been observed in APD films by several research groups.⁷⁻⁹ Uniform NLO APD films have been deposited with SHG increasing quadratically with film thickness over one hundred bilayers, although $\chi^{(2)}$ values were modest and comparable to quartz.¹⁰⁻¹¹ More recently, our group has made NLO APD films in which both the polyanion and the polycation contain polarizable chromophores and the results suggest that both polyelectrolytes contribute to the observed SHG signal.¹² Also, our group has demonstrated that the chromophore orientation in NLO APD films is stable at temperatures up to 150 °C.¹³

Recent efforts have focussed on a polyepichlorohydrin substituted with a side-chain stilbazolium chromophore (SPECH) (Figure 1). This paper is a report our recent progress with the APD of SPECH with polystyrene sulfonate, SPECH with polyacrylic acid, and SPECH with polyvinylsulfonate.

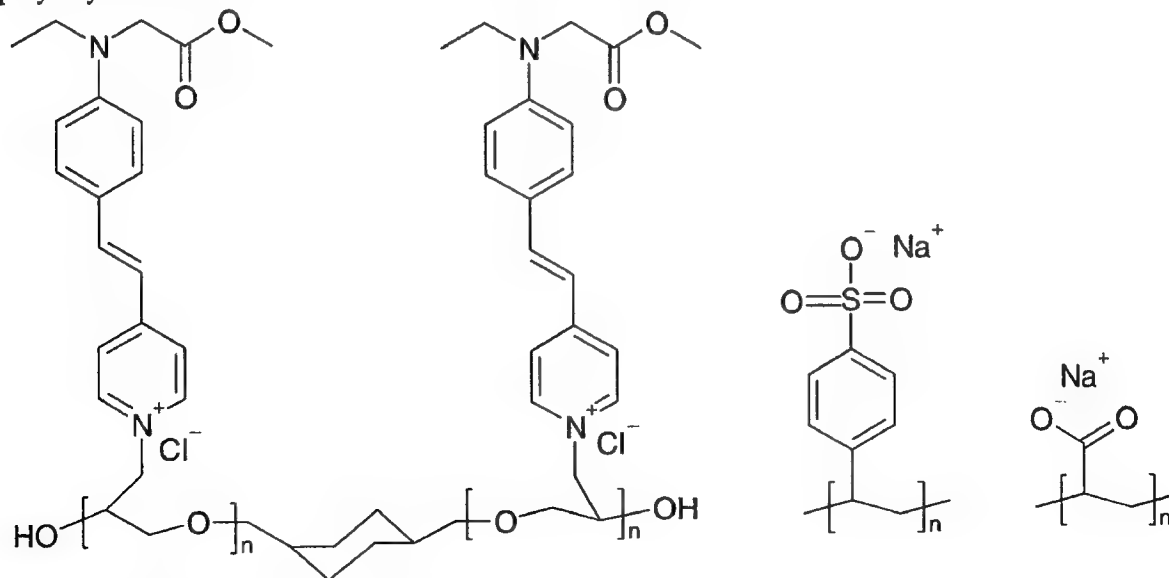


Figure 1. NLO-active water-soluble polycation, SPECH, (left), inactive water-soluble polyanions, PSS, (middle), and PAA, (right) used to make polar films by APD. For SPECH, $n=4-5$; for PSS, $n=300-370$; and for PAA, $n=750-800$.

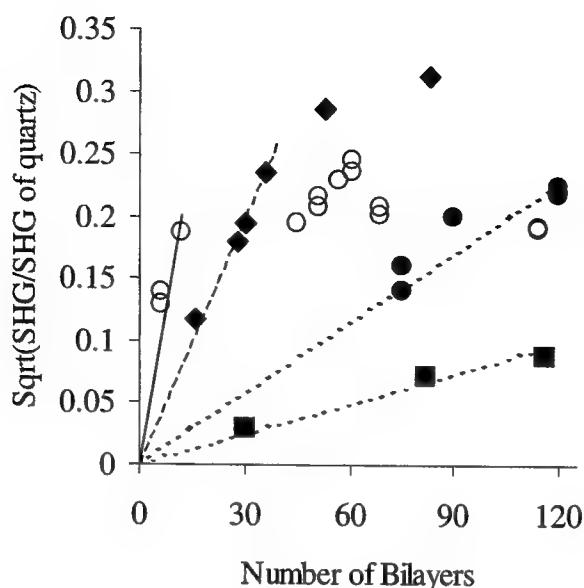


Figure 2. SHG intensity versus the number of SPECH/PSS bilayers deposited on hydrophobic glass (filled symbols) and SPECH/PAA on hydrophilic glass (open circles). Data for SPECH/PSS films in which the adsorption time of SPECH was 30 minutes (filled squares), 40 minutes (filled circles), and 50 minutes (filled diamonds) is shown.

The SPECH is a low molecular weight polyelectrolyte and so most likely adopts a chain-extended conformation. However, the side chain chromophores of the SPECH represent the greatest fraction of the total mass of any complete SPECH molecule. The stilbazolium side-chain chromophores in SPECH possess a strong ground state dipole moment. Adjacent stilbazolium chromophores will electrostatically repel one another yet they are covalently bound to the main chain so the net result is a 'bottle-brush' conformation of the SPECH in dilute aqueous solution. The SPECH is expected to adsorb to the surface in an extended conformation.

The length of the PSS chain is greater than its estimated persistence length (15 nm) and so is expected to be an expanded random coil in solution. Computational molecular modeling calculated distance between charges along the chain in the extended conformation is approximately 0.62 nm for both SPECH and PSS. The distance between charges for PAA was not calculated. The adsorption of the first layers of SPECH and PSS on a hydrophobic substrate has been figuratively described previously.⁹

The SPECH adsorbs rapidly from solution onto base-washed glass. Adsorption of the first layer is complete within 5 minutes of immersion. Also the adsorbed SPECH exhibits relatively strong polar order within the same short period of time. Apparently, the positive charges of the pyridinium end of the chromophores in SPECH quickly forms ion pairs with the O⁻ sites at the surface of base-washed glass. The process is facilitated by the extended conformation of the SPECH in solution plus the chromophores may easily tilt up away from the plane of the substrate to accommodate the later adsorbing SPECH chains.

At pH 6.5, most of the carboxylic acid groups are converted to the sodium salt and so each PAA polymer chain is highly charged. PAA adsorbed from pH 6.5 solutions has been shown to form layers less than 0.3 nm thick with minimal RMS roughness.¹⁷ In contrast to the adsorption of PSS onto SPECH layers on hydrophilic glass which disrupts the polar order of the SPECH layer,⁹ PAA does not disturb the SPECH layer to any measurable extent. This allowed the

formation of multilayers of SPECH and PAA with quadratic increase of SHG and linear increase of UV-visible absorbance as the film thickness increased up to 10 bilayers. Further deposition resulted in continued linear increase in UV-Visible absorbance but the SHG intensity did not continue to increase quadratically (Figure 2).

Although the deposition process is slower, uniform SPECH/PSS films up to 120 bilayers thick have been made. The UV-visible absorbance in transmission through the films is linear as a function of the number of deposited bilayers. The SHG intensity follows the expected quadratic dependence when the immersion time for each layer of SPECH is 30 or 40 minutes (Figure 2). At immersion times less than 30 minutes the SHG signal was below the detection limit.

In this work, thin films with polar ordered chromophores were obtained by APD. The best results were obtained alternating SPECH with PSS on hydrophobic substrates and SPECH with PAA on hydrophilic substrates. Future work will include further characterization of the APD films by Kelvin probe microscopy, ellipsometry, and azimuthal SHG measurements. Design and synthesis of new polymer systems is underway. Work is now focussed on improving the $\chi^{(2)}$ of the APD films by extending the uniform deposition of the SPECH/PAA to greater film thickness.

REFERENCES

- 1) G. Decher, Y. Lvov, J. Schmitt, *Thin Solid Films* **244**, 772 (1994).
- 7) X. Wang, S. Balasubramanian, L. Li, X. Jiang, D. J. Sandman, M. F. Rubner, J. Kumar, S. K. Tripathy, *Macromol. Rapid Commun.* **18**, 451 (1997).
- 8) A. Delcorte, P. Bertrand, E. Wischerhoff, A. Laschewsky, *Langmuir* **13**, 5125 (1997).
- 9) M. J. Roberts, J. D. Stenger-Smith, P. Zarras, G. A. Lindsay, R. A. Hollins, A. P. Chafin, R. Y. Yee, K. J. Wynne, *Proceedings of the SPIE* **3281**, 126 (1998).
- 10) J. R. Heflin, Y. Liu, C. Figura, D. Marciu, R. O. Claus, *Technical Digest of the OSA/ACS Conference on Organic Thin Films for Photonics Applications*, 78 (1997).
- 11) K. M. Lenahan, Y. Wang, Y. Liu, R. O. Claus, J. R. Heflin, D. Marciu, C. Figura, *Advanced Materials* **10**(11), 853, (1998).
- 12) G. A. Lindsay, M. J. Roberts, J. D. Stenger-Smith, P. Zarras, R. A. Hollins, A. P. Chafin, R. Y. Yee, K. J. Wynne, *Proceedings of the SPIE* **3474**, 63 (1998).
- 13) M. J. Roberts; W. N. Herman; G. A. Lindsay; K. J. Wynne, *Journal of the American Chemical Society* **120**, 11202 (1998).
- 14) G. A. Lindsay, M. J. Roberts, J. D. Stenger-Smith, P. Zarras, R. A. Hollins, A. P. Chafin, R. Y. Yee, K. J. Wynne, *Journal of Materials Chemistry*, in press.
- 15) J.J. Tanahatloe, M. E. Kuil, *Macromolecules* **30**, 6102 (1997).
- 16) V. V. Tsukruk, V. N. Bliznyuk, D. Visser, A. L. Campbell, T. J. Bunning, W. W. Adams, *Macromolecules* **30**, 6615.
- 17) S. S. Shiratori, M. F. Rubner, *Technical Report of the Institute of Electronics, Information, and Communications Engineers OME98-106*, 32, (1998).

Nonlinear optical study of chiral 1,1'-binaphthyl based helical polymers

Sven Van Elshocht, Thierry Verbiest, Martti Kauranen, and André Persoons

Center for Research on Molecular Electronics and Photonics, Department of Chemistry, KU Leuven,
Celestijnenlaan 200 D, B-3001 Heverlee, Belgium
sven.vanelshocht@fys.kuleuven.ac.be

Tel : ++32-16-32.71.71

Fax : ++32-16-32.79.82

Liang ma, Hua Cheng, Kwon Y. Musick, and Lin Pu

Department of Chemistry, University of Virginia, Charlottesville,
Virginia 22901, USA

The main problem in the field of nonlinear optics is the lack of materials needed for the development of optoelectronic devices. Therefore a lot of effort has been put into the study of all kinds of classes of materials to identify suitable materials. It has become clear that organic materials, especially polymers, could be useful for second- and third order materials. They offer several advantages such as easy structural modification to improve their properties and easy, low cost processing.

Materials for second-order nonlinear optics have to be noncentrosymmetric on a molecular and macroscopic scale^[1]. On a molecular scale the noncentrosymmetry is usually achieved by the construction of a D- π -A system, i.e. an electron donor and acceptor substituted π -conjugated system. On a macroscopic scale different techniques can be used to break the centrosymmetry such as electric field poling, the Langmuir-Blodgett technique, crystal growth and self-assembly. An alternative approach is the use of chiral materials. Chiral materials exist in two forms, enantiomers, that are mirror images of each other. They lack mirror planes, are noncentrosymmetric on both the microscopic and macroscopic scales, and therefore suitable for second-order nonlinear optics^[2]. In addition, it has been demonstrated that chirality can enhance the nonlinear optical efficiency^[3].

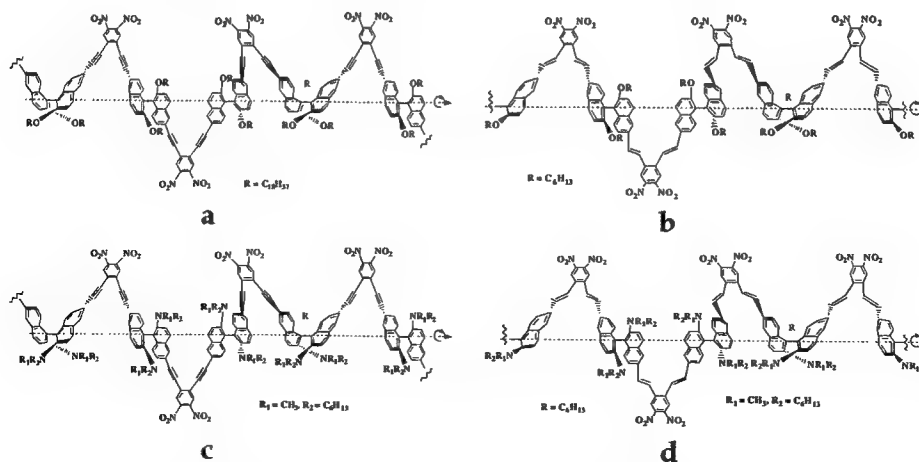


Fig. 1 The molecular structure of the studied chiral 1,1'-binaphthyl based helical polymers.

We have studied a series of chiral 1,1'-binaphthyl based helical polymers. The monomeric units were optimized for nonlinear optics by adding a Π -conjugated bridge and electron donor and acceptor groups^[4]. The monomer units can be considered as an ensemble of rigid electric-dipole units that form a propeller-like three-dimensional conformation due to the chirality of the binaphthyl units. We made Langmuir-Blodgett (LB) films of these polymers and studied their nonlinear optical response.

Surface pressure isotherms were recorded for all polymers by spreading a dilute chloroform solution onto the water subphase of a KSV minitrough. After complete evaporation of the solvent, the monolayer was compressed at a rate of $0.01 \text{ nm}^2 / (\text{min repeat unit})$. All polymers show rather featureless isotherms. Only polymer a shows an inflection point around 0.35 mN/m where probably a double layer is formed.

To construct multilayer LB-films, the monolayers were compressed to surface pressures between 10 mN/m and 30 mN/m . After stabilization the monolayer was transferred onto a glass substrate. The substrates were made hydrophobic through silanization with octadecyltrichlorosilane. To transfer the monolayers onto the substrate the horizontal dipping technique was used. The vertical dipping technique was not suitable because the monolayer on the water was too rigid. The hole that resulted around the substrate during the dipping procedure could not be closed by the barriers. The transfer ratios were around 1 indicating that monomolecular layers were transferred to the glass slides.

The nonlinear optical properties were studied with second harmonic generation (SHG). A Q-switched Nd:YAG laser (10 nsec, 50Hz, 1064 nm) incident at 45 degrees was used to excite the samples and the intensity of the frequency doubled light (532 nm) was detected with a photomultiplier tube.

The film quality of the samples was also verified with SHG by verifying that the second harmonic signal increased quadratically with the number of layers. Three of the four polymers demonstrated a very good optical quality. Polymer c appeared to be unsuitable for the construction of LB-films. Large holes could be observed by the naked eye throughout the entire film.

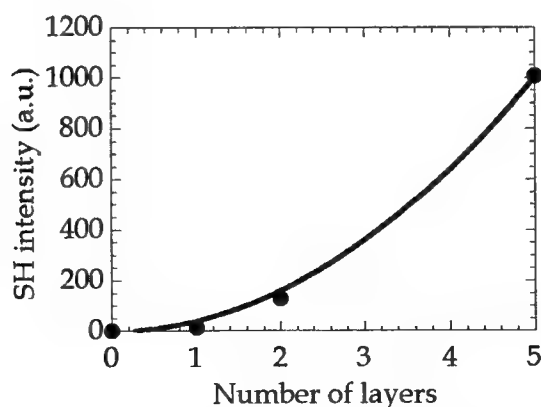


Fig. 2 The second harmonic intensity is plotted as a function of the number of layers. The solid line is a quadratic fit of the datapoints (dots).

Polymer **a** and **b** show a comparably weak SHG intensity. Furthermore, the SH signal generated by polymer **b** decreased when it was irradiated with the infrared laser light. The signal decreased to 75 % from its initial value within a few minutes. Polymer **c** showed a SH signal that was a factor of 50 higher than for polymers **a** and **b**. However the lack of a long alkylchain or a double bond, for some degree of flexibility, resulted in poor quality LB-films. Finally, for polymer **d** the $-N(CH_3)(C_6H_{13})$ sidegroup was kept but the triple bond, from polymer **c**, was replaced by a double bond. This resulted in a polymer that gives excellent quality LB-films with a SH-efficiency a factor of 200 higher compared to the original polymers **a** and **b**.

The symmetry of the samples was also determined with SHG. The SH intensity was measured while the sample was rotated around the surface normal. The SH intensity was independent of the position of the sample which is an indication that the sample is isotropic in the plane of incidence. All samples were found to be C_{∞} with the surface normal as the z -fold axis. To analyze the nonlinear optical response, the polarization dependence of the second harmonic signal was studied. The polarization of the fundamental beam was continuously varied with a quarter waveplate and the SH s - and p -polarized signals were detected. A mathematical analysis of these patterns allows us to determine the second order susceptibility tensor components^[5]. The values of the susceptibility were calibrated using a quartz wedge^[6]. We found that the second harmonic signal was dominated by the zzz component of the second order susceptibility which has for polymer **d** a respectable value of 35 pm/V. Note however that this value is resonantly enhanced. The chirality of the polymers manifests itself in a large circular difference effect, i.e. the difference between the SH intensity when irradiated with left and right circularly polarized light, between 25 and 60 % although there are no large chiral contribution to the second order susceptibility. The chiral xyz component, 2 pm/V, is very small compared to the dominating zzz component.

In conclusion, we studied chiral 1,1'-binaphthyl based helical polymers. We found that these polymers can have interesting NLO-properties and give rise to a respectable second order susceptibility. We also found that these polymers can be used to construct high quality LB-films. The chirality of the polymers gives rise to large CD-effects and a nonnegligible, although small, xyz susceptibility component.

References

- [1] R.W. Boyd, *Nonlinear Optics*, Academic Press, Sand Diego, 1992.
- [2] P.M. Rentzepis, J.A. Giordmaine, K.W. Wecht, *Phys. Rev. Lett.*, **16**, 792, 1966.
- [3] T. Verbiest, S. Van Elshocht, M. Kauranen, L. Hellemaans, J. S. Nauwaert, C. Nuckolls, T.J. Katz, and A. Persoons, *Science*, **282**, 913, 1998.
- [4] (a) Liang Ma, Qiao-Sheng Hu, Dilrushi Vitharan, Chi Wu, Chi Man Simon Kwan, and Lin Pu, *Macromolecules*, **30**, 204, 1997. (b) Hua Sheng and Lin Pu, *Macromolecular Chem. Phys.*, In press. (c) Kwon Y. Musick, Qiao-Sheng Hu, and Lin Pu, in preparation.
- [5] J.J. Maki, M. Kauranen, and A. Persoons, *Phys. Rev. B*, **51**, 1425, 1995.
- [6] D. Roberts, *IEEE J. Quantum Electron.*, **28**, 2057, 1992.

Organic Thin Films for Photonics Applications

Light-Emitting Devices

Friday, 24 September 1999

Alex K-Y. Jen, Northeastern University, USA

Presider

FD

3:30pm–5:30pm

California Ballroom Salons 4&5

I-1 Interfacial Issues in Organic Light Emitting Diodes†

Neal R. Armstrong

Departments of Chemistry/Optical Sciences, University of Arizona, Tucson, Arizona 85721
nra@u.arizona.edu

Summary

Recent studies here at the University of Arizona (Optical Sciences, Chemistry, Physics) of two-component, small molecule OLEDs, such as those based upon Alq₃/TPD, have been directed toward the optimization of the energetics and rates of charge injection at the anode and cathode and at the organic/organic' heterojunction in the center of the device (1-7). We have recently taken the point of view that the critical charge injection and recombination processes can be understood from a mainly "molecular perspective." Combinations of solution electrochemical studies of the individual components of the OLED, and UPS/XPS studies of thin films of these materials, can allow characterization of the offsets in frontier orbital energies of each set of components, and indicate how enhancing the energy differences between the charged states of the hole transport and lumophore materials in the center of the device can lead to higher luminescence efficiencies.

UPS/XPS studies have indicated that the difference in frontier orbital (HOMO) energies at the TPD/Alq₃ interface is ca. 0.4 eV, with a comparable estimate of differences in electron affinities (LUMO) (3). There would appear to be two competing reactions which could occur at the TPD/Alq₃ interface: 1) direct injection of a hole into the Alq₃ layer (oxidation of Alq₃ to its cation radical state; 2) reaction of anion radicals of Alq₃ (Alq₃^{•-}) with cation radicals of TPD (TPD^{•+}), i.e. a "cross-reaction" (Alq₃^{•-}/TPD^{•+}) an electron transfer reaction which leads to the emissive state, Alq₃* (1,2). Reaction 1 may also lead to an emissive Alq₃* state, through direct reactions of Alq₃^{•-} and Alq₃^{•+}, but is also likely to lead to degradation of Alq₃, as shown recently by Popovic and coworkers (8). Increasing the first solution oxidation potential of TPD, through judicious choice of added substituents, can increase the driving force for Reaction 1 in solution, and also appears to increase the probability for this reaction in the condensed phase, improving efficiencies of various OLEDs (1,2,5). Differences in transport and differences in injection efficiency and wetting of the ITO interface with the TPD derivatives also appear to influence these efficiency enhancements. Recent studies of the stability of the cation and anion radical species in such OLEDs suggest that optimization of the Reaction 2 will be essential in improving the stability of the OLED(9). Coupling reactions are likely to occur for the cation radicals of various TPD derivatives, which result in the release of protons. Since the chemical stability of Alq₃^{•-} species is low (1,8), and proton release by TPD coupling reactions are likely to lower this stability even further (9).

This talk will focus on a review of these issues, as well as recent attempts to modify the composition of both the anode and cathode interfaces in such OLEDs, to enhance both materials compatibility and charge injection rates.

† Work supported by the Office of Naval Research, through the MURI-Center for Advanced Multifunctional Polymers and Molecular Assemblies for Photonics (CAMP)

References

- 1) "Electrochemistry and Electrogenenerated Chemiluminescence Processes of the Components of Aluminum Quinolate/Triarylamine, and Related Organic Light Emitting Diodes," J.D. Anderson, E.M. McDonald, P.A. Lee, M.L. Anderson, E.L. Ritchie, H.K. Hall, T. Hopkins, A. Padias, S. Thayumanavan, S. Barlow, S. Marder, G.E. Jabbour, S. Shaheen, B. Kippelen, N. Peyghambarian, R.M. Wightman, N.R. Armstrong, *J. Amer. Chem. Soc.*, **120**, 9646 (1998).
- 2) "Electrochemical models for the radical annihilation reactions in organic light-emitting diodes," J. Anderson, P.A. Lee, E. McDonald, R.M. Wightman, H.K. Hall, T. Hopkins, A. Padias, S. Thayumanavan, S. Barlow, S. Marder, N.R. Armstrong, in "Organic Light Emitting Devices II," Z. Kafafi, ed. SPIE **3476-29**, 178, (1998).
- 3) "Determination of Frontier Orbital Alignment and Band Bending at an Organic Semiconductor Heterointerface by Combined X-ray and Ultraviolet Photoemission Measurements," with R. Schlaf, B.A. Parkinson, P.A. Lee, K.W. Nebesny, *Appl. Phys. Lett.* **73**, 1026 (1998)
- 4) "Investigation of the Electronic Structure of LiF Coated Al and Pt Electrodes by Photoemission Spectroscopy," R. Schlaf, B.A. Parkinson, P.A. Lee, K.W. Nebesny, G. Jabbour, B. Kippelen, N. Peyghambarian, N.R. Armstrong, *Journal of Applied Physics*, **84**, 6729 (1998).
- 5) "Organic Light-Emitting Diode with 20 Lumens /Watt Efficiency Using a Triphenyldiamine Side-Group Polymer as the Hole Transport Layer" S.E. Shaheen, G.E. Jabbour, B. Kippelen, N. Peyghambarian, J.D. Anderson, N.R. Armstrong, E. Bellman, S.R. Marder, and R.H. Grubbs, *Applied Physics Letters*, (in press).
- 6) "Energy and Charge Transfer in Organic Light-Emitting Diodes: A Soluble Quinacridone Study," S.E. Shaheen, Y. Kawabe, J.-F. Wang, J.D. Anderson, E.A. Mash, P.A. Lee, N.R. Armstrong, B. Kippelen, N. Peyghambarian, *Journ. Appl. Phys* (in press).
- 7) "Aluminum Composite Cathodes: A New Method for the Fabrication of Efficient and Bright Organic Light Emitting Devices," G.E. Jabbour, S.E. Shaheen, M.M. Morrell, B. Kippelen, N.R. Armstrong, N. Peyghambarian, *Optics and Photonics News*, **10**, 25, (1999).
- 8) H. Aziz, Z.D. Popovic, N.-X. Hu, A.M. Hor, G. Xu, *Science*, **283**, 1900, (1999)
- 9) J.D. Anderson, S. Thayumanavan, S. Barlow, S. Marder, J.-P. Dodelet, N.R. Armstrong, manuscript in preparation.

Patterning and Electrochemical Deposition of Conjugated and Conducting Polymers in Light Emitting Devices

Daniel B. Roitman

Hewlett-Packard Laboratories, 3500 Deer Creek Rd., Palo Alto, CA 94303
daniel_roitman@hpl.hp.com

Seiji Inaoka

University of Alabama at Birmingham, Chemistry Department, Birmingham, AL 35294-1240
seiji@uab.edu, inaokas@hpl.hp.com

Rigoberto Advincula

University of Alabama at Birmingham, Chemistry Department, Birmingham, AL 35294-1240
gobet@uab.edu

Device structuring represents a real challenge in the fabrication of polymer light emitting devices (P-OLEDs). The various materials that comprise their structure are typically spin cast, but unlike resists, they are not amenable to photolithography. Several approaches have been proposed, such as laser ablation and jet-printing, to pattern monochrome, multicolor and full color displays. In this presentation we will discuss the use of traditional DNQ/novolac resists, in conjunction with electroluminescent polymers, for patterning monochrome displays, as well as the introduction of novel electrochemical film deposition techniques with potential applications in multicolor and full color devices.

In the case of monochrome passive-addressed P-OLED we established that structuring poly(paraphenylene vinylene) (PPV) and polyfluorenes (PF) can be achieved using resists to protect the active areas and plasma etching to open vias. Surprisingly, both materials were found to be compatible with the harsh process of image reversal for creating inverted tapered walls for cathode patterning. However since most EL polymers are sensitive to air and water-based processing, the use of resist technology is generally not desirable. Furthermore, it is anticipated that it will be difficult to pattern different colors in the micron and submicron pixel sizes using this approach. Therefore our group decided to explore the method of "directing" the film deposition onto desired areas of the substrate using electrochemical means.

Electrochemical polymerization from monomer solutions has not been used in the past for the fabrication of POLED's presumably due to the difficulty in depositing pinhole-free films with good mechanical characteristics. We addressed this problem by designing polymer precursors and deposition conditions that led to the formation of extended molecular networks during deposition. This resulted in smooth homogeneous films with excellent mechanical characteristics. As a demonstration of this approach, we fabricated a P-OLED on ITO with two pixels each containing a different hole-transport polymer: a poly(vinylcarbazole) (PVK) derivative, and a poly(fluorene) (PF) derivative respectively. Both pixels shared a top layer of a green light-emitting polymer [courtesy of Cambridge Display Technology (CDT)] and a Ca cathode. Each pixel showed distinctive light-bias and current-bias responses. In addition to hole-transport polymers, we also deposited conducting polymer "network" films of poly(pyrrole) (PPy) on ITO, and fabricated devices using the CDT polymer as the emissive layer. Their efficiencies were in the range of 0.5 to 1 Cd/A, which is lower than standard spin cast PEDT [poly(thiophene)]-based devices (5 to 10 Cd/A), but the doping levels of PPy and its work-function were not optimized.

Device Performance and Polymer Morphology in Polymer Light Emitting Diodes

Y. Shi, J. Liu, and Y. Yang*

Department of Materials Science and Engineering
University of California

Abstract

The performance of MEH-PPV based light emitting diodes is strongly affected by the morphology of spin-coated polymer films, which can be controlled by varying the solvent and concentration of the polymer solution as well as the spin-speed.

Summary

We have demonstrated in this manuscript that the aggregation states of a spin-coated polymer film can be roughly classified as unaggregated and aggregated species. It is found that these species have different emission spectra and different electroluminescence quantum efficiency. The former generally shows a strong yellow emission at ~ 580 nm and the latter has an orange-red color with $\lambda_{\text{max}} = 630$ nm. It is generally observed that in aromatic solvents or cyclohexanone, low polymer concentration and/or high spin-speed usually result in more unaggregated species, and *vice versa*. This has been contributed to the centrifugal force, which tends to tear apart the polymer aggregates and also to stretch the polymer chains to the more linear states. When higher polymer concentrations and/or lower spin-speed is used, the film is predominated by the aggregated species. These aggregates give an excimer-like excited state and have higher electroluminescence quantum efficiency than the unaggregated species. In non-aromatic solvent such as tetrahydrofuran (THF), the resulted polymer films show a reversed effect on their emission spectra. It is observed that polymer films

coated at low spin-speeds show the strong yellow emission while those coated at higher spin speeds give the orange-red emission spectrum. It is also found that the turn on voltages for the polymer films coated using THF solutions are always higher than those coated using aromatic solvents and cyclohexanone. The surface energies of such films are also different. These observations can be qualitatively explained by solvation effect. Aromatic solvents (or cyclohexanone) can solvate the polymer backbone (also aromatic) better than the side chains, and therefore the side chains will tend to stay closer to each other to lower the energy. It is thus expected that these solvents will result in an "aromatic faced out" (with side-chains trapped inside) type of aggregates. In contrast, THF can solvate the side chains better than the aromatic moiety. It is thus expected that a "side chains pointed out" type of conformations will be resulted. Since these saturated side chains are good insulators, it is thus not surprising that these films have higher turn-on voltages. On the other hand, such conformations also hinder the π - π overlapping and thus decrease the red emission. At higher spin-speed, the polymer chains are significantly stretched by the centrifugal force. This may allow a conformational change to favor the π - π overlapping in the excited state, which results in an enhanced red emission.

Progress in organic electroluminescent devices with air stable cathodes

Ghassan E. Jabbour
Optical Sciences Center
The Department of Materials Science and Engineering
The University of Arizona
Tucson, AZ 85721

Email: gej@optics.arizona.edu
Phone: 520-626-8324, FAX 520-621-4442

Different air stable cathode structures that allow for better electron injection, which leads to the fabrication of brighter and more efficient organic light-emitting devices, will be presented.

Organic Thin Films for Photonics Applications

Electro-Optic Devices: 2

Saturday, 25 September 1999

William H. Steier, University of Southern California, USA
Presider

SaA

8:30am–10:00am

California Ballroom Salons 4&5

High-speed electro-optic modulators based on organic waveguides

Feng Pan

Molecular OptoElectronics Corp (MOEC), 877 25th St., Watervliet, NY 12189

Tel: 518-270 8203, Fax: 518-273 5701, E-mail :pan@mocc.com

Abstract

Organic crystals with improved dielectric and electro-optic properties were used to make high speed EO-devices. The techniques for coupling the organic crystal waveguides with polished fibers to create high speed EO-devices are summarized. A new class of chiral polymers were also evaluated for long term EO stability.

Summary:

High performance electro-optic (EO) modulators require large electro-optic modulation bandwidth and low drive power. These requirements are dominated by the electro-optical coefficient, dielectric constant, transparency, and linear refractive index of the active material within the modulator. Compared to inorganic ionic electro-optic crystals, such as LiNbO₃, organic crystals and polymers have large electro-optic coefficients, high modulation bandwidths, and low drive powers making them ideal materials for EO applications. The organic salt crystal DAST[®] (4-N,N-dimethylamino-4'-N'-methyl-stilbazolium tosylate) has a bandwidth of 140 GHz and a figure of merit ($n^7 r_{\text{eff}}^2 / \epsilon$) about 20 times higher than that of LiNbO₃. We report the formation of thin film waveguides of organic DAST[®] crystals by precision optical polishing and the fabrication of an electro-optic intensity modulation device. The modulator is based on coupling the thin film DAST[®] waveguide with a side-polished fiber (SPF). Electrodes were added to the SPF/DAST[®] overlay architecture and intensity modulation was observed out to 18 GHz. Calculations suggest that the device frequency response extends beyond 100 GHz. [1]

The same SPF device architecture can also be used with thin film waveguides fabricated from highly efficient EO-polymers. Novel chiral EO-thermoplastics were developed and characterized for long term EO stability. The EO- properties the dye doped chiral thermoplastics were four times as stable as an identical non-chiral (racemic) thermoplastic. The chiral polymer has nearly identical material properties such as ductility, high-temperature performance, and T_g.

- [1] F. Pan, K. McCallion and M. Chiappetta "Waveguide Fabrication and Fast Electro-optical In-line Modulation in Organic Crystal 4-N,N-dimethylamino-4'-N'-methyl-stilbazolium ", *Appl. Phys. Lett.* **74** (4) 492, (1999)

Demonstration of 5 MHz Single-Pass Electro-Optic Modulators Using Single-Crystal Thin-Films of Organic Molecular Salts

Achintya K. Bhowmik, Ayayi C. Ahyi, Alpana Mishra, and Mrinal Thakur

Photonic Materials Research Lab, 202 Ross Hall, Auburn University, AL 36849

bhowmak@eng.auburn.edu, claude@eng.auburn.edu, alpanam@eng.auburn.edu,

mthakur@eng.auburn.edu

Organic molecular salts with stilbazolium chromophores as the cation are known to have extremely large second-order susceptibilities. Very large electro-optic effects have been reported in crystals of salts 4'-dimethylamino-*N*-methyl-4-stilbazolium tosylate (DAST) and styrylpyridinium cyanine dye (SPCD). Recently, we have shown that good optical quality single-crystal thin-films of DAST have larger electro-optic coefficients ($r_{11} = 530$ pm/V at 720 nm) than bulk crystals.¹ We have provided the first demonstration of a single-pass modulator based on DAST single-crystal films (3 μm thick).¹ The modulation depth was 20% at a low *ac* field (1 V/ μm at 4 kHz). In this work, we demonstrate higher speed of operation and a larger modulation depth for single-pass electro-optic modulators using single-crystal thin-films of DAST and SPCD based on field-induced birefringence geometry.

Excellent optical quality single-crystal films of DAST and SPCD were grown using the modified shear method.² X-ray diffraction and polarized optical microscopic studies established the single-crystallinity of the films. Polarization dependent UV-visible absorption measurements showed that the films were strongly dichroic.

A Ti-Sapphire laser, tunable over 720-850 nm, and a He-Ne laser at 632.8 nm were used as the light sources in the electro-optic measurements. Thin-film electro-optic modulator devices were constructed by depositing gold electrodes on the single-crystal films across the polar axes. *AC* electric fields were applied along the polar axis of the device, while the laser beam was propagated normal to the film. Measurements were performed with applied fields of 2 V/ μm at 2 and 4 kHz, 0.7 V/ μm at 40 kHz, and 0.25 V/ μm at 5.63 MHz frequencies. The incident light was polarized at 45° with respect to the polar axis on the film, and an analyzer was placed at the output. The modulated signal was detected using a fast photodetector, and displayed on a high bandwidth oscilloscope and a spectrum analyzer. This device configuration is directly relevant to applications.

Fig. 1 shows the oscilloscope trace of light modulation obtained using a DAST thin-film modulator at 750 nm, for an applied field of 2 V/ μm at 4 kHz. The modulation depth at this wavelength, defined as $(I_{\text{max}} - I_{\text{min}})/I_{\text{avg}}$, is about 50%. The results were also verified by measurements using the lock-in detection technique. The signal modulation at the frequency of 5.63 MHz, recorded on a high speed spectrum analyzer, is shown in Fig. 2. The response was found to be independent of the frequency of applied field over the measurement range (2 kHz - 5.6 MHz). Large electro-optic effect, comparable to that of DAST, was also measured in SPCD. The measured electro-optic coefficients of DAST single-crystal films are in the range of 300-600 pm/V as the wavelength is varied from 850 nm to 632.8 nm.

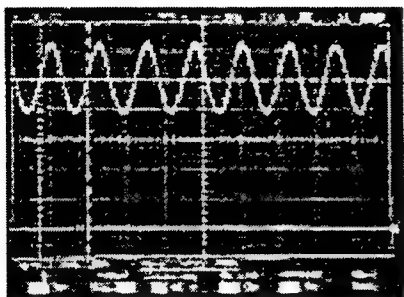


FIG. 1. Oscilloscope trace of light modulation at 750 nm using DAST single-crystal film for an *ac* voltage of 2 V/μm at 4 kHz. Modulation depth ~ 50%.

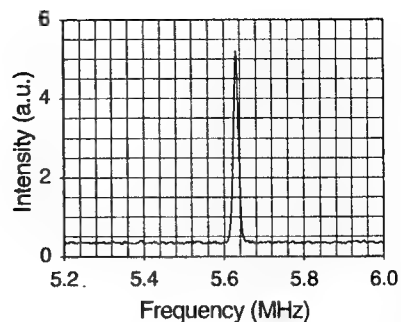


FIG. 2. Display of the modulated signal on a spectrum analyzer. The drive field was 0.25 V/μm at 5.63 MHz.

In conclusion, electro-optic modulators based on a single-pass field-induced birefringence geometry have been constructed using single-crystal thin-films of the molecular salts DAST and SPCD. Modulation depth in excess of 50% was demonstrated for light propagating perpendicular to the film. The performance of the devices was observed to be independent of frequency from 2 kHz to 5.63 MHz. The observed effect is clearly electronic. These modulators involve negligible losses compared to waveguide structures, and have significant potential for various applications in high speed optical signal processing in the free-space interconnect geometry. The device configuration is as simple as a liquid crystal modulator and yet offers many orders of magnitude higher speed than liquid crystals.

References

1. M. Thakur, J. Xu, A. Bhowmik, and L. Zhou, *Appl. Phys. Lett.* **74**, 635 (1999).
2. M. Thakur and S. Meyler, *Macromolecules* **18**, 2341 (1985); M. Thakur, Y. Shani, G. C. Chi, and K. O'Brien, *Synth. Met.* **28**, D595 (1989).

Young's Fringe Dual Slab Waveguide Sensor

Graham H. Cross and Yitao Ren

University of Durham, Department of Physics,
South Road, Durham, DH1 3LE, U.K.

Tel : +44 191 374 2577

FAX : +44 191 374 3848

g.h.cross@durham.ac.uk

Neville J. Freeman and Benharret Bouattou

Farfield Sensors Ltd., Unit 51, Salford University Business Park, Leslie Hough Way, Salford, Greater
Manchester M6 6AJ, U.K.

Tel : +44 161 925 8210

FAX : +44 161 925 8211

neville.freeman@farfieldsensors.freemove.co.uk

Summary

Optical methods of detection for gases and vapours can utilise a range of optical response functions the most general of which is a change in the refractive index of the sensing material. Interferometry can then be used to detect the induced phase changes of the propagating light. Optical waveguide formats can offer a compact system yet are often rather complicated in their fabrication and operation.

We have fabricated a simple multiple layer waveguide system, comprising two vertically displaced slab waveguides (figure 1). Optical coupling to the modes of the structure is made by uniformly illuminating the input end-face of the sensor with a coherent polarised laser source. The structure spatially filters the light to produce two discrete distributions of optical power propagating in the slab waveguide modes which emerge as two closely separated sources at the sensor output end-face (figures 2 and 3). Young's fringes are measured in the far-field due to interference from these two closely spaced 'apertures'.

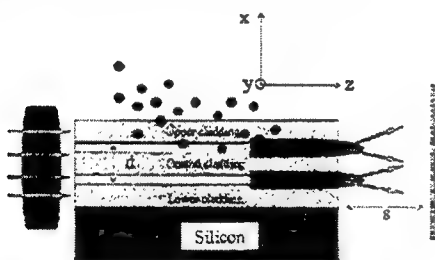


Figure 1 : Schematic diagram of the multiple stack slab waveguide sensor chip and method of optical coupling. Vapour enters through the top surface and diffuses through the structure. In the preferred design, the central cladding layer is of a material impervious to the analyte vapour.

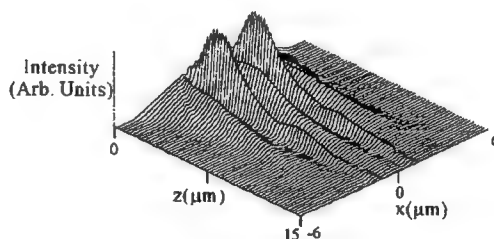


Figure 2: Simulation of the propagation of field intensity in two vertically stacked slab waveguides. The transverse direction is shown along x and the propagation direction is along z .

In these initial studies we used substrates with a $1\text{ }\mu\text{m}$ layer of SiO_2 ($n = 1.46$) as the lower cladding layer. The second and fourth waveguide layers were the water sensitive polymer, P-4VP ($0.9 - 1\text{ }\mu\text{m}$, $n = 1.57$) whilst the central layer was a commercial polyolefin polymer (Zeonex 480R, Nippon Zeon, $n = 1.52$) of thickness between 2.5 and $2.8\text{ }\mu\text{m}$. This layer is impervious to water vapour and acts to isolate the lower P-4VP layer from water taken up in

the top waveguide layer. No extra top cladding layer was used (i.e. we take the air to be the top cladding layer).

Short lengths (approx. 10 mm) of waveguide substrate were formed by cleaving of the silicon wafer substrate. Light from a helium neon laser was focused onto the input end facet of the waveguide using a microscope objective lens. The propagated light was then allowed to diffract out from the output facet of the guide and onto either a screen or camera, for direct observation, or onto a pin-holed silicon photodiode.

Fringes obtained experimentally from a typical hybrid structure are shown in figure 4. The Young's fringe condition, $a = \lambda z/d$, is verified as follows. At a distance to the screen, z , of 9.6 cm we observed a separation between adjacent fringe maxima, a , of 1.76 cm. At a wavelength, λ , of 632.8 nm this gives a waveguide centre separation for this sample, d , of $3.45 \mu\text{m}$. This compares extremely favourably with the expected separation of between $3.4 - 3.8 \mu\text{m}$ and thus within experimental error.

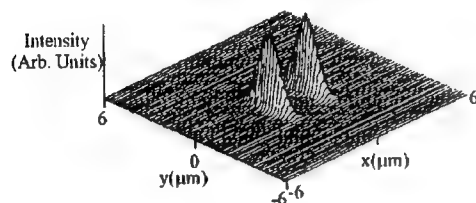


Figure 3 : Calculated field intensity distribution in the xy plane of the device after a propagation distance of $120 \mu\text{m}$.

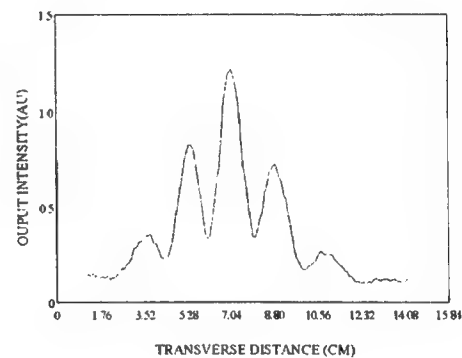


Figure 4 : The measured vertical intensity distribution of fringes produced from a 'hybrid' system at a distance from the device end-face of 9.6 cm.

In these structures we have measured a nearly linear phase change response from these devices to water vapour concentrations from above 1000 ppm down to 30 ppm (see figure 5). The lower limit is determined by the method of observing and recording phase shifts. Greater precision can be obtained by scanning the whole pattern using a linear array photodiode and calculating the accumulated phase shift. This method is used in the prototype commercial instrument¹. We have developed a data logging algorithm for these sensors which will offer a measurement resolution of better than 0.01 radians of phase. This corresponds to a detection limit in the current structures of around 400 ppb.

An impression of the speed of response can be seen in the pin-hole detected intensity versus time to exposure of 1100 ppm of water vapour (figure 6). At $t = 0$ the valve is operated and the observed time delay before the onset of the response is governed by the flow rate, the length of the tube leading to the sample chamber and the remaining 'dead volume' in the equipment. The sample then responds to the vapour to produce around 9π of phase shift and the time taken to reach equilibrium is around 150 s. This response time is found to be largely independent of the partial pressure of water in the mobile phase which implies that the dynamics for mass transfer follow simple rules².

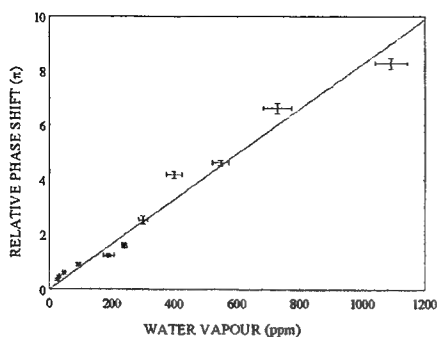


Figure 5 : Relative phase shift versus humidity concentration for a 'hybrid' device.

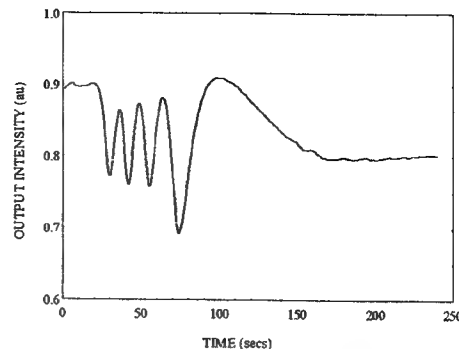


Figure 6 : Response of the 'hybrid' structure to 1100 ppm of water vapour as a function of time. The measured response is taken from a point in the vertical intensity distribution.

Repeatability is an issue when considering the functioning of an absorptive mode sensor such as this. We have adapted the design of the basic sensor structure such that the first four layers defining the two slab waveguides are fabricated from silicon dioxide. The top-most cladding layer is the water-sensitive polymer. The evanescent field component of the uppermost part of the supermodes of the structure transduces index changes into phase changes and by optimising the design can give an efficiency dn_{eff}/dn (where n_{eff} is the effective index, n is the cladding index) of over 30 %. The relative phase change to 95 ppm of water vapour is shown below (figure 7). The response shows excellent reversibility which is assumed to be a consequence of the relatively weak binding of water in the polymer.

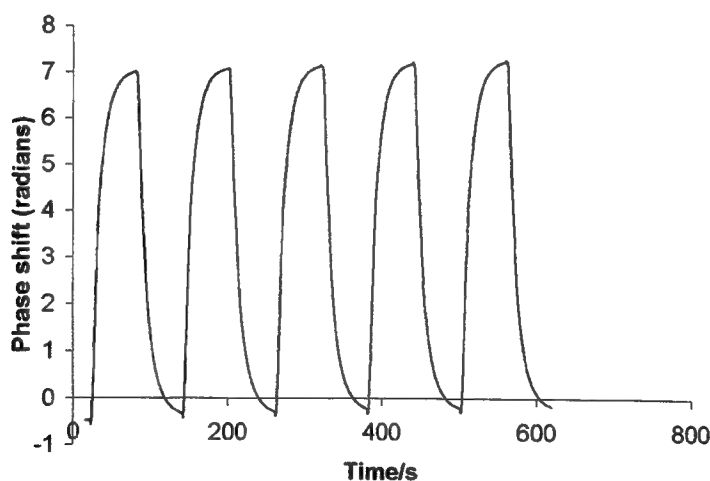


Figure 7 : Response of an evanescent wave sensor to 95 ppm water vapour in a nitrogen flow.

References

- ¹ "Analight EVA/500" vapour detection system (Farfield Sensors Ltd.)
- ² International encyclopaedia of heat and mass transfer, G.F. Hewitt, G.L. Shives, Y.V. Polezhaev (Eds.), (CRC, New York, 1997)

Fabrication and Characterization of Electro-Optic Polymeric E-Field Sensors

R. Sivaraman and S.J. Clarson

Department of Materials Science and Engineering, University of Cincinnati, Cincinnati, OH 45221.
sivarar@email.uc.edu, sclarson@uceng.uc.edu

K. Burcham, D. Naghschi and J.T. Boyd

Department of Electrical, Computer Engineering and Computer Science, University of Cincinnati, Cincinnati, OH 45221.
burchake@email.uc.edu, naghskdh@email.uc.edu, jboyd@ececs.uc.edu

Optical waveguides, also known as dielectric waveguides are the structures that are used to confine and guide the light in the guided-wave devices and circuits of integrated optics. A well known waveguide is an optical fiber which has a circular cross section. In contrast guides of interest to integrated optics are usually planar structures such as planar films or strips. A polymer optoelectronic device would have significant cost and performance advantages over the current lithium niobate devices used in the communications and electronics industry. First, the polymer has a significantly lower dielectric constant than lithium niobate, a ferroelectric, implying that the internal electric field, and thus the sensitivity, could be about 20 times as high as with lithium niobate. Second, the substrate and the polymer materials could be engineered to overcome the drift and thermal problems associated with the pyroelectric effect in LiNbO_3 . The optical polymers, which are made in solution, can readily be formed into thin films and waveguides, which offer an advantage over crystalline LiNbO_3 . Spin-coating techniques used with electro-optic polymers can easily be adapted for use with current electronic processing, therefore devices made with optical polymers could be both inexpensive and easy to construct. Devices using optical waveguide circuits in polymeric electro-optic thin films would offer improved performance and lower manufacturing cost.

A Mach-Zehnder modulator was fabricated from a channel waveguide with an electro-optic polymer core (guest host system of polymethylmethacrylate (PMMA) doped with dimethylamino nitrostilbene (DANS), (Aldrich Chemicals, USA) chromophore.). The light is coupled in through the left side and is split equally in two directions through the separate branches of the waveguide. For an electric field sensor, it is beneficial to design a Mach-Zehnder that does not use the electrodes as a way to create the phase shift in the arms of the device. Therefore, one of the arms in the Mach-Zehnder is reverse poled with respect to the other arm. The reverse poling of one interferometer arm provides the opposing phase change in the presence of an external electric field. This leads to the varying output intensity which can be related to the magnitude of the electric field present (ref. Figure 1).

Initial loss measurements have yielded very promising loss numbers. To test the optical loss of the polymer thin-films, an end-fire coupled waveguiding test was used. The loss measured with an 834 nm laser beam was 6 dB/cm (ref. Figure 2). This is an acceptable loss for initial feasibility demonstration. Practical loss measurements would be less than 2 dB/cm.

Polymers such as DANS/PMMA must be poled before they exhibit the electro-optic effect. Samples of DANS-PMMA on ITO glass were successfully poled with voltages of 100 V/mm at a temperature of 100-110°C. Poling of the device is currently underway.

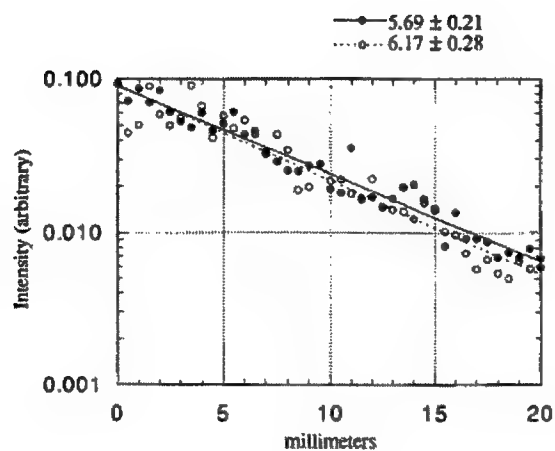
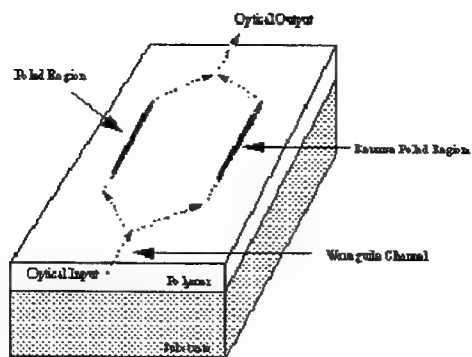


Figure 1. Schematic showing the poled and reverse poled regions

Figure 2. Loss measurements for PMMA-DANS planar guide. Loss is 6 db/cm.

Waveguide Polarizers and Polarization Splitters with a Buried Birefringent Polymer

Min-Cheol Oh, Myung-Hyun Lee, and Hyung-Jong Lee

Electronics and Telecommunications Research Institute

161 Kajong-dong, Yusong, Taejeon, 305-350, Korea, mincheoloh@hanmail.net

I. Introduction

Waveguide devices controlling the polarization state of the guided-light have been widely investigated in LiNbO_3 , especially relying on the proton exchange process which can provide very large birefringence [1], [2]. Recently, we have demonstrated a series of polarization controlling devices in the polymer waveguides based on the poling-induced birefringence of poled polymers [3]-[5]. However, the device should be improved to have low insertion loss and long-term reliability for the practical application. In this work, we demonstrate a pair of integrated optic polarizers and a polymeric polarization splitter in the low-loss fluorinated polymer waveguides utilizing a highly birefringent polyimide. Compared to the previous polymeric polarization controlling devices based on the poling-induced birefringence, the devices with a buried birefringent polymer exhibit a couple of improvements such as the lower insertion loss, the higher extinction ratio, and the easier fabrication.

II. Device configuration and design

The devices consist of three kinds of fluorinated polymers, polyimide, fluorinated poly(ether ketone) (FPEK), and perfluorocyclobutane (PFCB). The FPEK polymer used as the core layer is a crosslinkable fluorinated polymer possessing low absorption loss and excellent stability [6]. The PFCB polymer is also a crosslinkable fluorinated polymer supplied from DOW chemical. The polyimide with a product name of UD9020D is commercially available from Amoco Co. By virtue of the thermal and mechanical stability of these three polymers, the device will have good reliability even at high temperature. To find polymers with appropriate refractive indices, we have carefully measured the refractive indices of various polymer materials as shown in Table 1 by using a prism coupling method at an wavelength of $1.55 \mu\text{m}$. The polyimide has the higher refractive index for the TE polarization than that for the TM polarization, and it has much larger birefringence than FPEK. Hence, we can exploit the polyimide to determine the polarization of the guided light depending on the shape of the

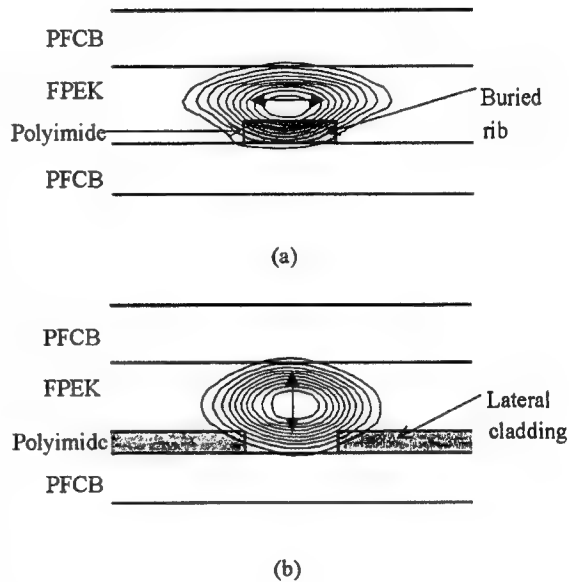


Fig. 1. The cross-sections and corresponding mode contours of the waveguide polarizers: (a) the TE-pass polarizer, and (b) the TM-pass polarizer.

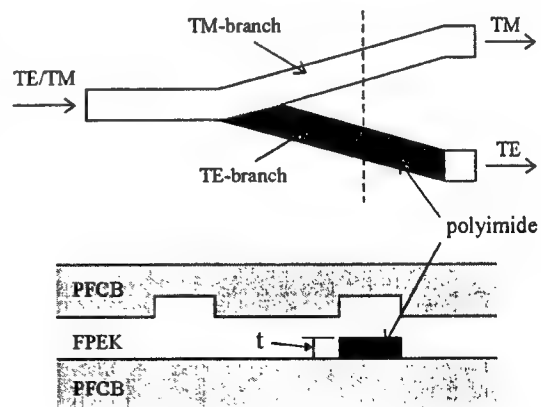


Fig. 2. Top and cross-section views of the polymer waveguide polarization splitter.

polyimide layer.

For the TE-pass polarizer, as shown in Fig. 1 (a), the polyimide layer is patterned as a rib structure and buried into the core layer of FPEK. The buried waveguide with the polyimide rib has a large birefringence so that the effective index of the waveguide core is enhanced for the TE polarization while decreased for the TM polarization. Then the TE mode is guided by the waveguide, while the TM mode is radiated out into the core layer. The contour graph of the TE-polarized guided-mode is drawn over the cross-section of Fig. 1 (a).

For the TM-pass polarizer, the polyimide layer is inserted at the two sides of the waveguide as shown in Fig. 1 (b). Because the polyimide has the lower index than FPEK for the TM polarization, the proposed structure forms an inverted-rib waveguide with the core of FPEK for the TM mode. Otherwise the TE mode will be radiated out into the polyimide layer. The contour graph of the TM-polarized guided-mode is drawn over the cross-section of Fig. 1 (b).

A schematic diagram of the polymeric polarization splitter based on an asymmetric Y-branch is shown in Fig. 2. The polyimide strip lies under one branch of the Y-branch waveguide consisting of the PFCB and FPEK polymers. For convenience, the waveguide branch with the polyimide strip is called as a TE-branch, while that without the polyimide strip as a TM-branch. The polyimide strip with a large optical birefringence enhances the birefringence of the TE-branch. Then, for the TE polarization, the effective refractive index of the TE-branch becomes higher than that of the TM-branch so that the TE mode will propagate through the polyimide branch by the mode evolution effect. On the other hand, the TM mode evolves to the TM-branch which has the higher effective refractive index than the TE-branch for the TM polarization.

III. Experimental results

For the wavelength of 1.55 μm , the guided mode profiles were observed by a CCD camera. The guided modes were well-confined on the waveguide core region, and the mode size was not so different as that of the optical fiber. To measure the insertion loss and the polarization extinction ratio (PER), the device was aligned between two single mode fibers. The polarization of the input light was adjusted to a certain state by using a fiber-optic polarization controller connected between the light source and the device. The PER was given by the ratio of the transmitted light intensities for the TE and TM polarizations. For the devices with different waveguide widths, the PERs were measured as shown in Fig. 4. The PER of the TM-pass polarizer was as high as 40 dB for all the devices regardless of the waveguide width. The TE-pass polarizer exhibited the PER of 35 dB for the devices with the width of 6 and 7 μm . In the TE-pass polarizer, the scattered light from the input facet was observed at the output end so that the PER depended on the amount of the scattered light coupled to the output fiber. The insertion losses of TE-pass polarizers with a length of 7.0 mm were from 3.5 to 4.0 dB, and that of TM-pass polarizers with a length of 6.2 mm were from 2.7 to 3.3 dB.

Polymers	$n(\text{TE})$	$n(\text{TM})$	birefringence
Polyimide	1.5270	1.5007	0.0263
FPEK	1.5171	1.5140	0.0031
PFCB	1.4895	1.4872	0.0023

Table 1. Refractive indices of the polymer materials for the wavelength of 1.55 μm .

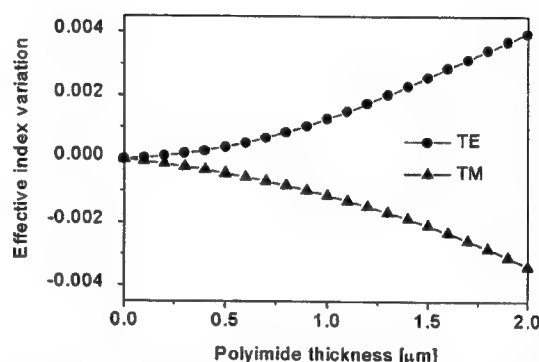


Fig. 3. Calculated effective index of the planar waveguide for the TE and TM polarizations as the function of the polyimide thickness.

For the input light adjusted to the TE or TM polarization, we measured the output light intensities of the two branches. Then the crosstalk was given by the ratio of the light intensities of the two output waveguides for each polarization state. The measured crosstalks of eight devices are plotted in Fig. 5. For the devices with the branch angles of $1/400$ radian, we obtained the crosstalks less than -20 dB when the TE polarized light was launched. However, the devices showed the crosstalks of about -16 dB for the TM polarized input light. The devices with the branch angles of $1/200$ radian exhibited crosstalks less than -15 dB for each polarization. These measured crosstalks were much worse than the simulation results by the scalar 2-dimensional BPM. During the mode profile measurement using the CCD, we observed a slight polarization coupling in the device, and it could be one reason of the worse crosstalk.

For the polarization splitters with a length of about 12 mm, the insertion losses were ranged from 3.8 to 4.8 dB for the two polarizations. To find the excess loss induced by the device, the insertion loss was compared to that of the straight channel waveguide adjacent to each device. The excess losses were sufficiently less than 1 dB for all the devices. The fluorinated polymer waveguide usually has the propagation loss of about 0.5 dB/cm. The coupling loss including the end-facet scattering loss would be as large as 2 dB per facet because the guided mode was tightly confined in the vertical direction by the large index contrast between the core and cladding polymers.

References

- [1] P. G. Suchoski, T. K. Findakly, and F. J. Leonberger, *Optics Lett.*, Vol. 13, pp. 172-174, 1988.
- [2] N. Goto, and G. L. Yip, *J. Lightwave Technol.*, Vol. 7, No. 10, pp. 1567-1574, 1989.
- [3] M.-C. Oh, S.-Y. Shin, W.-Y. Hwang, and J.-J. Kim, *IEEE Photon. Technol. Lett.*, Vol. 8, No. 3, pp. 375-377, 1996.
- [4] M.-C. Oh, S.-S. Lee, S.-Y. Shin, W.-Y. Hwang, and J.-J. Kim, *Electron. Lett.*, Vol. 32, No. 4, pp. 324-325, 1996.
- [5] M.-C. Oh, W.-Y. Hwang, and K. Kim, *Appl. Phys. Lett.*, Vol. 17, No. 17, pp. 2227-2229, 1997.
- [6] H.-J. Lee, M.-H. Lee, M.-C. Oh, J.-H. Ahn, and S. G. Han, *J. Polym. Sci.; Part A: Polym. Chem.*, in press.

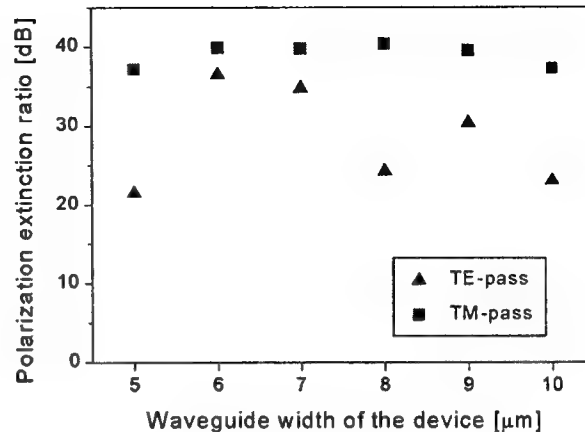


Fig. 4. Measured polarization extinction ratios of the TE-pass and TM-pass polarizers with waveguide widths from 5 to 10 μm .

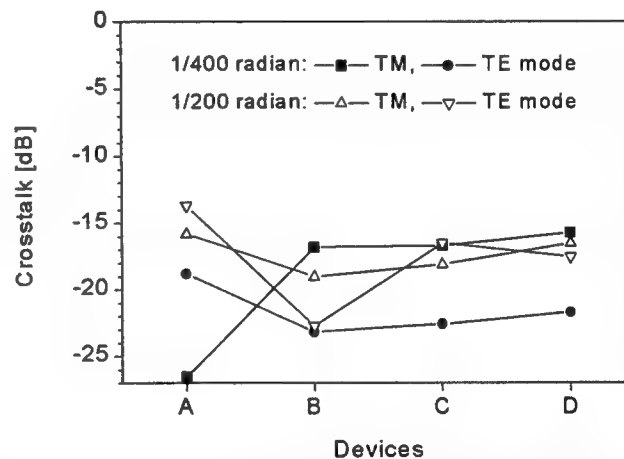


Fig. 5. Measured crosstalks of the polarization splitters with the branch angles of $1/200$ and $1/400$ radians and the waveguide dimensions from 4 to 8 μm .

Organic Thin Films for Photonics Applications

Photostability

Saturday, 25 September 1999

George Stegeman, University of Central Florida, USA
President

SaB

10:30am-12:15pm

California Ballroom Salons 4&5

Systematics of NLO Chromophore Photochemical Stability

Tony C. Kowalczyk, Xuan Q. Zhang, and Hilary S. Lackritz
Gemfire Corporation, 2471 East Bayshore Road, Suite 600
Palo Alto, CA 94303

Adriana Galvan-Gonzalez, Michael Canva and George I. Stegeman
School of Optics and Center for Research and Education in Optics and Lasers (CREOL) University of Central
Florida, 4000 Central Florida Blvd., Orlando, FL32816-2700

Robert Twieg
Department of Chemistry & Liquid Crystal Institute
Kent State University, Kent, OH 44242

Seth Marder and S. Thayumanavan
Dept. of Chemistry, University of Arizona, Tucson, AZ 85721

Many material requirements must be simultaneously satisfied in organic nonlinear optical (NLO) polymers in order to produce efficient devices. Some of the requirements include thermal/temporal stability, nonlinearity, transparency, and processability of material into devices. Steady progress has led to improved NLO polymer systems that possess a balanced optimum of these properties, but new fundamental concerns about photochemical stability relating to device lifetime must now be considered. Until recently, issues pertaining to photochemical stability have been relatively ignored. This fact is particularly surprising given that all devices will be used for optical applications and in some cases preferably used with intense light sources. In addition many modes of photodegradation exist including photobleaching and photoisomerization.

Recent studies have quantified photostability in common NLO dyes such as DR1 and DANS as well as more efficient chromophores¹. Wavelength and power dependence of the photostability have been shown. In addition, photostability may depend on environmental variables in the form of photo-oxidation, and yet by other variables such as polymer host and functionality. Even though wider classes of dyes have been studied, the mechanisms underlying photo-instability are not well understood.

We report our results investigating a homologous series of thermally stable chromophores to elucidate structure-property trends that affect photochemical stability. We believe studies of this sort may assist understanding basic mechanisms of photostability in organic EO materials. Additionally, intrinsic photodegradation measurements will be presented, and compared to device lifetime predictions.

1. A. Galvan-Gonzalez, M. Canva, G.I. Stegeman, S. Marder, S. Thayumanavan, R. Twieg, T.C. Kowalczyk, X.Q. Zhang, and H.S. Lackritz, "Systematics of the Wavelength Dependence of Electro-Optic Chromophore Photostability" submitted for publication

Effect of Environmental Factors on the Photodegradation of Azobenzene Doped Polymers

Adriana Galvan-Gonzalez, Michael Canva*, and George I. Stegeman

School of Optics/Center for Research and Education in Optics and Lasers, Un. of Central Florida

P.O. Box 162 700, 4000 Central Florida Blvd., Orlando, FL 32816-2700, USA

Tel.: +1-407-823-6915, Fax: +1-407-823-6955, e-mail:george@creol.ucf.edu

* permanent address: Laboratoire Charles Fabry, Institut d'Optique Théorique et Appliquée,
Université d'Orsay / Paris-Sud, 91403 Orsay Cedex, France

Robert Twieg

Department of Chemistry & Liquid Crystal Institute, Kent State University, Kent, OH 44242

Tony C. Kowalczyk and Hilary S. Lackritz

Gemfire Corporation, 2471 East Bayshore Road, Suite 600, Palo Alto, CA 94303

Seth Marder and S. Thayumanavan

Dept. of Chemistry, University of Arizona, Tucson, AZ 85721

The azobenzene family of chromophores, doped into polymer hosts has been investigated for a variety of nonlinear photonics applications including electro-optics, second harmonic generation etc.[1,2] To be successful in device formats, their linear and nonlinear optical properties must be stable for periods of years. Standard device operating conditions include continuous illumination with wavelengths ranging from 820 to 1600 nm, a variety of environmental conditions including high temperatures and/or different gas atmospheres. To date there is very little information available about the photostability of the azobenzene polymer family. It has been reported that another similar chromophore, DANS has a strong wavelength dependence to its photostability which improves with increasing wavelength, but leaves it still far from suitable for nonlinear devices.[3] So a key question is what factors affect the photostability of azobenzenes at active device wavelengths, for example a variety of environmental conditions such as temperature and atmospheric environment. The research addresses these important questions.

The charge transfer state which is responsible for the second order nonlinearity is manifest by a strong absorption feature in the blue-green region of the spectrum and the concentration $N_1(t)$ of nonlinear active species present in the polymer is proportional to the charge transfer state absorption coefficient which we measure in its long wavelength tail, at 544 nm. When light is absorbed and the chromophore is raised from its ground to first excited state, it can decay either back to the ground state, or undergo a transformation into a new molecule with the same atomic constituents, for example via trans-cis isomerization, or undergo a chemical reaction producing a totally new molecule, for example via photo-oxidation. Assuming a single dominant transformation process and a quantum efficiency for this to occur of B^{-1} , the local rate of creation of the new photoproduct (concentration $N_2(t)$) can be written as

$$\frac{\partial N_2(t)}{\partial t} = -\frac{\partial N_1}{\partial t} = \left[\frac{B(\lambda)}{\sigma(\lambda)} \right] N_1(t) n \propto -\frac{\partial \alpha(t)}{\partial t} \quad (1)$$

where $n(t)$ is the photon flux, $\sigma(\lambda)$ is the chromophore's molecular absorptivity, $\alpha_1(t)$ is the polymer absorption coefficient and the lifetime of the active species is given by $\tau = B(\lambda)/\sigma(\lambda)n$. Hence $B(\lambda)/\sigma(\lambda)$ is a useful figure of merit for describing the chromophore photostability. The larger the value, the longer the lifetime. The experiment consists of illuminating a thin polymer film at normal incidence with a uniform flux and periodically measuring the transmission with a weak probe laser at 544 nm. From eqn. (1), the initial slope of the increase in transmission with

time gives a direct measure of $B(\lambda)/\sigma(\lambda)$. The experimental details can be found in reference 3.

Varying the input wavelength then allows the wavelength dependence of $B(\lambda)/\sigma(\lambda)$ to be evaluated.

Disperse red one (DR1) is a prototype azobenzene chromophore and it was investigated both as a side chain polymer (24% weight fraction) and as a guest (5% weight fraction) in a PMMA matrix. The measured values for the figure of merit are shown in Figure 1 (left-hand-side). It is clear that at room temperature there is significant difference

between the photostability in PMMA versus the side-chain format. This is demonstrated that side-chains are more stable than the corresponding guest host polymers.

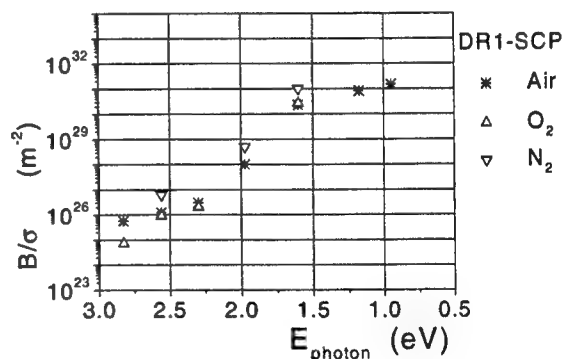
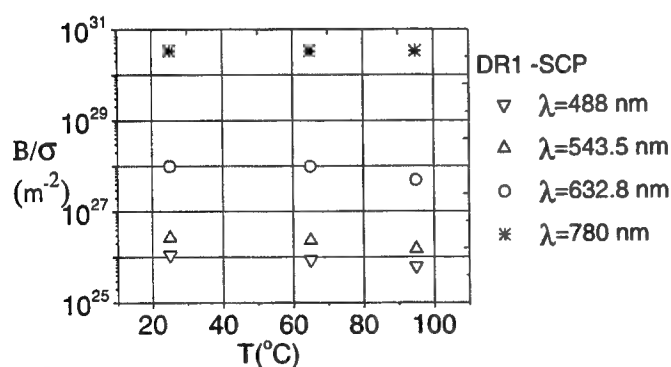
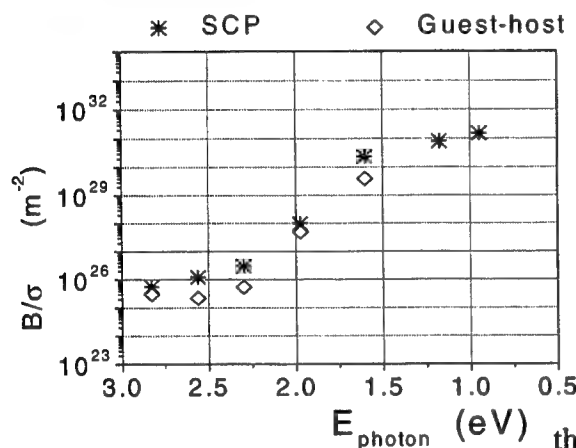


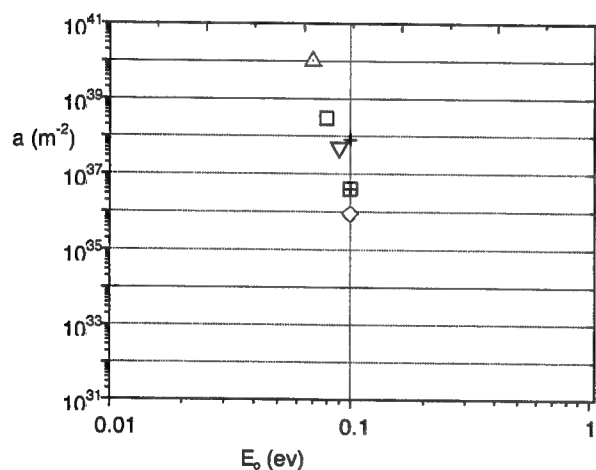
Figure 2 (above, left-hand side) shows the effect on B/σ of increasing the temperature from 25°C to 95°C on the photostability of DR1 at different wavelengths. The degradation is faster at elevated temperatures, the closer the wavelength is to λ_{\max} , the larger the effect of a temperature increase.

In order to investigate the effects of oxygen, when the polymers were in solution prior to spin-coating, either pure oxygen or pure nitrogen was bubbled through the solution for 2 hours.

Then the subsequent spin-coating and degradation mechanisms were all performed in that particular atmosphere. The difference in the photodegradation between these two cases is shown in Figure 3 (previous page, right hand side). Note that the figures of merit for the nitrogen and just air cases are equal to within the experimental uncertainty. There is a clear decrease for the oxygen enrichment case by a factor of at least two in the figure of merit (and hence the lifetime) for the polymer processed in the oxygen versus nitrogen atmosphere. The difference is a factor of 4 at 780 nm.

Note that in the spectral region 500 to 1064 nm the wavelength dependence of $\log[B/\sigma]$ is approximately linear in the photon energy E_{phot} i.e. this dependence can be written as $B/\sigma = a \exp[-E_{\text{phot}}/E_0]$ where "a" and " E_0 " are constants which differ from polymer to polymer. The best photostability is obtained for large "a" and small " E_0 ".

Our experiments on changing the donors and acceptors at the ends of the azobenzene bridge are summarized in this format in Figure 4. Differences of one to two orders of magnitude are reflected there. So it is clear that the choice of the donor acceptor combination has a strong



influence on the photostability. Details will be discussed during the presentation. The best chromophore is 4 (N ethylmethacrylate N-ethyl) amino 4' nitroazobenzene.

In summary, the photostability of chromophores in the azobenzene family depends on a large number of parameters. These include whether the chromophore is in a guest-host or side-chain environment, the temperature, the atmospheric environment in which the polymer was processed and the details of the donor and acceptor used.

Figure 4 "a" versus E_0 for a selection of azobenzenes.

References:

- [1] Y. Shi, W. Wang, J.H. Bechtel, A. Chen, S. Garner, S. Kalhuri, W.H. Steier, D. Chen, H.R. Fetterman, L.R. Dalton and L. Yu, *IEEE J. Quant Electron.* **2**, 289 (1996).
- [2] S. Yilmaz, W. Wirges, W. Brinker, S. Bauer-Gogonea, S. Bauer, M. Jager, G.I. Stegeman, M. Ahlheim, M. Stahelin, F. Lehr, M. Diemeer and M.C. Flipse, *J. Opt. Soc. Am., B* (special issue), **15**, 781 (1998)
- [3] Q. Zhang, M. Canva, and G.I. Stegeman, *Appl. Phys. Lett.* **73**, 912 (1998)

Effects of the Host Matrix on the Near-Infrared Red Tail of the Absorption of Chromophore Doped Polymeric Waveguides

Anne-Claire Le Duff*, Vincent Ricci, Tomas Pliska, Michael Canva*, George Stegeman

CREOL, Center for Research and Education in Optics and Lasers
School of Optics, University of Central Florida
4,000 Central Florida Boulevard, FL 32816-2700 Orlando, USA

* - permanent address: IOTA Institut d'Optique Théorique et Appliquée
LCF, Laboratoire Charles Fabry du CNRS, Centre National de la Recherche Scientifique,
Université d'Orsay Paris Sud, 91403, Orsay France
michael.canva@iota.u-psud.fr

K. Pong Chan

MOEC, Molecular OptoElectronics Corporation
877 25th Street, Watervliet, NY 12189, USA

Robert Twieg

Department of Chemistry, Liquid Crystal Institute
Kent State University
Kent, OH 44242, USA

The potential of organic amorphous materials, in particular chromophore doped polymers, for optics is now well-established. Much effort has been devoted to optimizing the chromophore doped polymer materials, "classic" organic and hybrid inorganic/organic "sol-gel". Many parameters have been considered and several trade-offs have been demonstrated. For example, in poled polymers for second order nonlinear optics, matrices and chromophore/matrix interactions have been extensively studied in view of optimizing the stable nonlinear quadratic coefficients. High T_g matrices were thus developed to retain, at room and device operating temperatures, as much as possible of the anisotropy that can be created during electric field poling at high temperature. However, for devices, the material's figure of merit usually also incorporate, with the same importance as the nonlinear coefficient, the inverse of the absorption losses at the operating wavelength(s). This is in particular the case for materials needed to realize efficient second harmonic generation in waveguides for cascading applications in optical telecommunication systems. We will report at the conference on the systematic study of chromophore structure and matrix composition impact on the near infrared absorption coefficient.

Previously published data suggested that the wavelength dispersion of the absorption in electro-optic doped polymers could be extrapolated by a "straight line behavior" observed on semi-log plots towards longer wavelengths than can be classically measured with thin film optical transmission measurements. The slope of this line can be defined as

$$Slope = \frac{d(\log[\alpha(\lambda)])}{d\lambda}$$

where $\alpha(\lambda)$ is the absorption coefficient of the chromophore doped material and the slope is expressed in nm^{-1} . It is projected that this absorption will dominate propagation losses of waveguides made from this material, as long as the extrapolated absorption value remains large compared to reasonable scattering losses (i.e. $> 1 \text{ dB.cm}^{-1}$). Figure 1 illustrates this point with two well-known materials, DANS (4-dimethylamino-4'-nitrostilbene) and DR1 (Dispersed Red 1) side chain polymers.

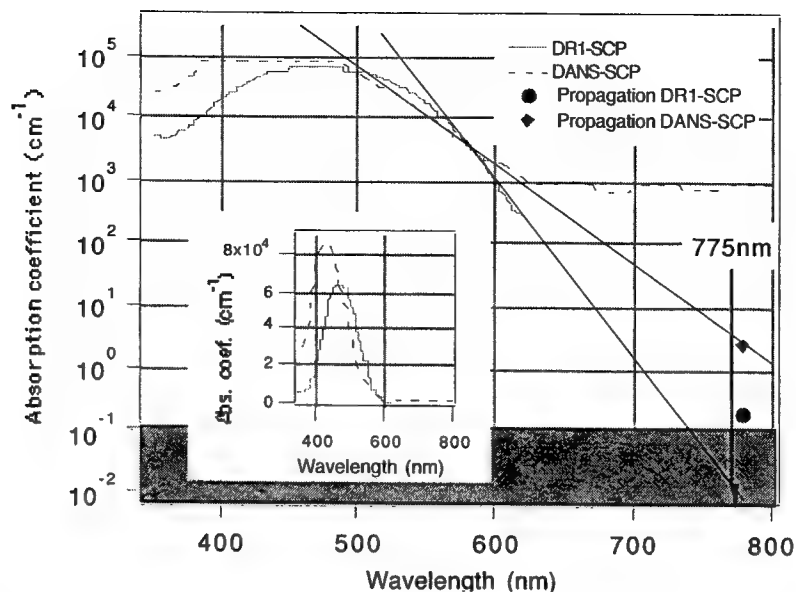


Figure1: Example of the straight-line extrapolation protocol using DANS and DR1 side-chain polymers. Absorption spectrum and waveguide loss measurements were performed on the same thin film samples. (Inset gives a comparison of the DANS and DR1 absorption spectra on a linear scale.)

The two straight lines are fitted to the red part of the absorption spectra measured by thin film transmission; the slopes are much different, -16.10^{-3} and $-21.10^{-3} \text{ nm}^{-1}$ respectively, which more than compensates for the fact that the latter is red shifted by tens of nm compared to the former. As a result the extrapolated absorption at 775 nm is more than two orders of magnitude less for the azobenzene chromophore. The waveguide propagation losses measured around this wavelength support this prediction when reasonable scattering losses are taken into account.

We started our systematic studies using more than a dozen chromophores from well-known families such as stilbenes and azobenzenes. Absorption data from transmission measurements using both doped solution (in ethyl acetate) and solid polymer matrix (PMMA-guest/host) showed, for all chromophores, large differences in "slope" between the two environments. Although only minor differences could be observed on a linear scale (small chromatic shift, small widening of the FWHM, small changes in the absorption cross-section), the differences in red tail absorption that can be seen on a semi-log plot actually correspond to major differences in the "slope" and the extrapolated absorption coefficient for wavelengths several hundreds of nanometers further into the near infrared. The results of doping into PMMA matrices were about two orders of magnitude greater than those doped into solution! For example, at 775 nm, some chromophores which had appeared transparent enough ($\alpha < 0.5 \text{ cm}^{-1}$) from the initial measurement were proven useless in the solid environment ($\alpha > 5 \text{ cm}^{-1}$). Propagation loss measurements on several planar waveguides validated the extrapolation protocol within its already specified limits.

Based on this initial study, we predicted that matrix composition should have a very large impact on such extrapolated absorption coefficients. Moreover, these variations should be much larger than those usually reported for the change in the nonlinear coefficient. Thus, in the cases where absorption has to be taken into account, the variation in absorption losses rather than variation in the nonlinear coefficient would mainly govern the material figure of merit.

To study the impact of changing the matrix, we chose some of the potentially most attractive chromophores, namely "4-(dibutylamino)-4'-nitroazobenzene" (referenced "5"), "4-diethylamino-3'-4'dicyanoazobenzene" (referenced "13") and DR1, together with an initial set of seven polymer matrices. These polymers were namely PMMA, Polystyrene (PS), BPA-Polyethersulfone (PES), BPA-polycarbonate Lexan®, Polyetherimide Ultem®, Pthalazinone-Polyethersulfone (MPIII 34.12), and Poly(butylmetacrylate) PBMA. Figure 2 shows the absorption spectra, normalized to a 10% weight concentration, of the chromophore "5" in these different matrices and in the ethyl acetate solution. A very strong influence on the chromophore absorption due to the polymer environment can be observed. The values of the slope are very different from one matrix to another, ranging from -14.10^{-3} in PES to -21.10^{-3} in PMMA! These different values of the slope result in large differences in the extrapolated values of the absorption coefficient at 775 nm, as shown in Figure 3. For example, there is a difference of almost two orders of magnitude between the predicted absorption coefficient at 780 nm of "5" chromophore in PS (0.2 cm^{-1}) and the predicted absorption coefficient in PES (10 cm^{-1}).

In conclusion, matrix environment is demonstrated to have a dramatic impact on a material figure of merit for use in nonlinear optical devices. This is not only for the magnitude of the anisotropy that can be induced by poling and how much and how long this anisotropy can be retained under operating conditions which is the usual case discussed. But it is also to a larger degree governed by the tail of the absorption in the near infrared. Better detailed understanding and more precise control of this inhomogeneous broadening effect of the chromophore absorption spectra should allow realization of superior nonlinear polymeric materials, taking advantage of new red shifted and more nonlinear chromophore doped material.

This research was funded by STTR (BMDO) and JPL (AFOSR) grants and is supported by international NSF/CNRS bilateral US/French collaboration.

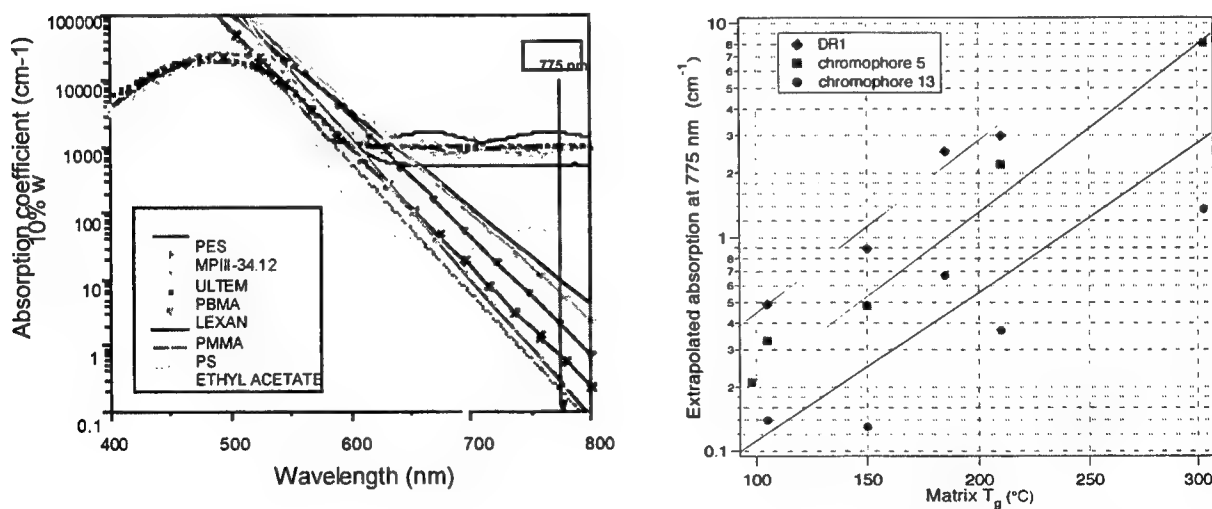


Figure 2 (LHS): The absorption spectrum of a "4-(dibutylamino)-4'-nitroazobenzene" chromophore (referenced "5") in seven different polymeric host matrices and diluted in a liquid solvent.

Figure 3 (RHS): Evolution of the extrapolated absorption loss at 775 nm as a function of the host matrix T_g for three azobenzene chromophores: DR1, "4-(dibutylamino)-4'-nitroazobenzene" (referenced "5") and "4-diethylamino-3'-4'dicyanoazobenzene" (referenced "13").

Photochemical Stability of Highly Nonlinear Optical Chromophores for Electro-Optic Applications

M. Bösch, C. Fischer, C. Cai, I. Liakatas, M. Jäger, Ch. Bosshard, and P. Günter
 Swiss Federal Institute of Technology, ETH-Hönggerberg HPF, 8093 Zürich, Switzerland
 boesch@iqe.phys.ethz.ch, bosshard@iqe.phys.ethz.ch

As nonlinear optical polymeric materials begin to enter the market in e.g. electro-optic modulators, stability issues become more and more important. Whereas the orientational stability of poled polymer systems has been studied extensively over the last decade [1], the photochemical stability of the chromophore dopants in the polymers under working conditions has not been investigated until recently [2-4]. These measurements revealed that one possible candidate for applications, a side-chain polymer with a dimethyl-amino-nitro-stilbene (DANS) developed by Akzo Nobel exhibited a very poor photochemical stability and estimated device lifetimes are not suitable for practical applications. Therefore chromophores with high nonlinearities and sufficient photochemical stability have to be identified.

In our group, we synthesized chromophores based on the phenylbithiophene bridge and a tricyano acceptor (Fig. 1). The molecule CC172 exhibits excellent microscopic nonlinear optical properties as reported previously [5]. Its figure of merit $\mu\beta_0$ is 6 times higher than Disperse Red 1 (DR1). Furthermore, it is thermally stable up to at least 200 °C.

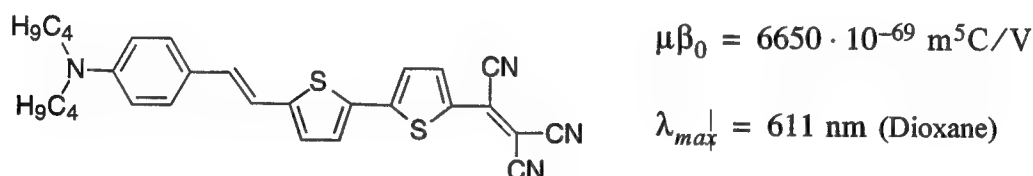


Fig. 1: Structure of the molecule CC172 and its electro-optic figure of merit.

Here, we report on the photochemical stability of CC172 in a guest-host system with polymethylmethacrylate (PMMA), which is very high even when bleached in the absorption band. The inverse photodegradation quantum efficiency B (average number of photons that a molecule absorbs before decomposition) is the main figure of merit to describe photochemical stability based on one photon processes. Our measurement setup depicted in Fig. 2 uses an argon pumped Ti-Sapphire laser tunable between 700 nm and 800 nm as well as a He-Ne probe laser operating at 633 nm. A silicon detector monitors the transmission change of the probe laser as a function of the pump laser photon fluence. For data evaluation and calculation of the inverse quantum efficiency for photodegradation B , we used the model developed by Dubois et al. [6] based on a one photon absorption process. In this model, the dependence of the light transmission $T(E)$ on the pump energy per unit area E is given by

$$T(E) = \frac{T_{\infty}}{1 + (T_{\infty}/T_0 - 1)e^{(-\beta E)}} ,$$

where $T_0 = e^{-\sigma_1 J_0}$ and $T_\infty = e^{-\sigma_2 J_0}$ are the initial and final transmission, respectively, with σ_1 and σ_2 being absorption cross-sections of the bleached and unbleached dyes. J_0 is the number of molecules per unit area and $\beta = \sigma_1 / (h\nu B)$ with h being Planck's constant, ν being the frequency of the pump light and B the desired inverse quantum efficiency for photodegradation.

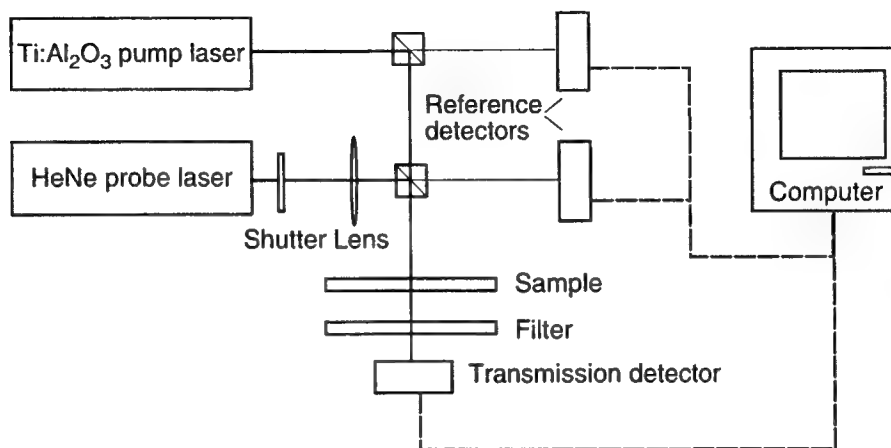


Fig. 2: Experimental set-up to measure photochemical stability of chromophores.

Figure 3 shows a typical bleaching curve for a pump wavelength of 710 nm which is close to the absorption maximum as indicated by the inset showing the absorption spectra of CC172 in PMMA. The sample was prepared using a 15 percent doping of CC172 into PMMA and making a 8 percent solution in dibromomethane. Samples were spin cast onto glass substrates to a thickness of 1.5 micrometers, resulting in an initial probe beam transmission of 5 percent.

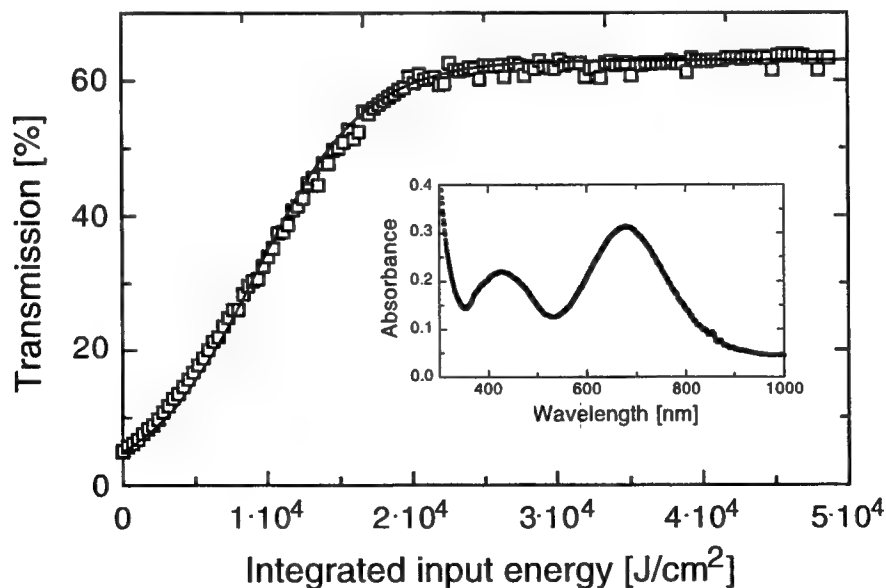


Fig. 3: Typical bleaching curve of CC172 in PMMA at $\lambda = 710$ nm (experimental data points and theoretical curve) and transmission spectrum of the unbleached polymer film (inset).

The results of the bleaching experiments are summarized in table 1. The inverse quantum efficiencies for photodegradation B of a DR1/PMMA guest-host system and the value taken from [3] for a DR1 side-chain polymer are included for comparison. Experiments with DR1 were performed using a bleaching wavelength of 543 nm which is in the absorption band of DR1.

Table 1: Inverse photodegradation quantum efficiency B of studied polymer systems at different bleaching wavelengths.

Polymer system	B
CC172/PMMA (710 nm)	$(1.2 \pm 0.3) \cdot 10^6$
DR1/PMMA (543 nm)	$(0.5 \pm 0.2) \cdot 10^6$
DR1 side-chain (543 nm)	$(2.5 \pm 0.4) \cdot 10^6$

The inverse quantum efficiency for photodegradation B of our bithiophene when bleached in the main absorption peak is $(1.2 \pm 0.3) \cdot 10^6$ which is about twice the value we measured for a DR1/PMMA guest-host system and half the value for DR1 molecules when incorporated into a side-chain as reported by Zhang et al. [3]. Compared to DANS even the guest-host system with CC172 is 40 times better than the DANS side-chain polymer [2]. Considering that the inverse photodegradation quantum efficiency B is expected to increase at least by a factor of 2 when incorporated into a side-chain polymer, the photochemical stability of our bithiophene is very promising.

In conclusion we investigated the photochemical stability of newly synthesized, highly nonlinear optical, bithiophene chromophores. The results indicate that they are excellent candidates for incorporation into side-chain polymers for electro-optic devices.

References:

- [1] P. Prêtre, P. Kaatz, A. Bohren, P. Günter, B. Zysset, M. Ahlheim, M. Stähelin, F. Lehr, *Macromolecules* **27**, 5476 (1994)
- [2] Q. Zhang, M. Canva, G. Stegeman, *Appl. Phys. Lett.* **73**, 912 (1998)
- [3] Q. Zhang, M. Canva, G. Stegeman, CLEO 98 Anaheim, Technical digest, 207 (1998)
- [4] T.C. Kowalczyk, R.J. Twieg, H.L. Lackritz, *Polymer Preprints* **39**, 1015 (1998)
- [5] C. Cai, I. Liakatas, M.S. Wong, Ch. Bosshard, P. Günter, *Polymer Preprints* **39**, 1111 (1998)
- [6] A. Dubois, M. Canva, A. Brun, F. Chaput, J.P. Boilot, *Appl. Opt.* **35**, 3193 (1996)

Observation of environmentally sensitive photoluminescence from highly polar chromophores

Marek Szablewski, Yasuyuki Kagawa, David Bloor, Mosurkal Ravi & Graham H. Cross

University of Durham, Department of Physics,
South Road, Durham DH1 3LE, U.K.
Tel: +44 191 3743909
FAX: +44 191 3743848
Marek.Szablewski@durham.ac.uk

As a result of our work developing novel chromophores for nonlinear optics we have synthesised a range of derivatives of TCNQ (tetracyanoquinodimethane) which were products of the action of amines on TCNQ. Tertiary amines acting as enamines gave highly dipolar “blue” chromophores, (absorption maxima 650-700 nm)¹ with one nitrile group substituted by the amine (Figure 1).

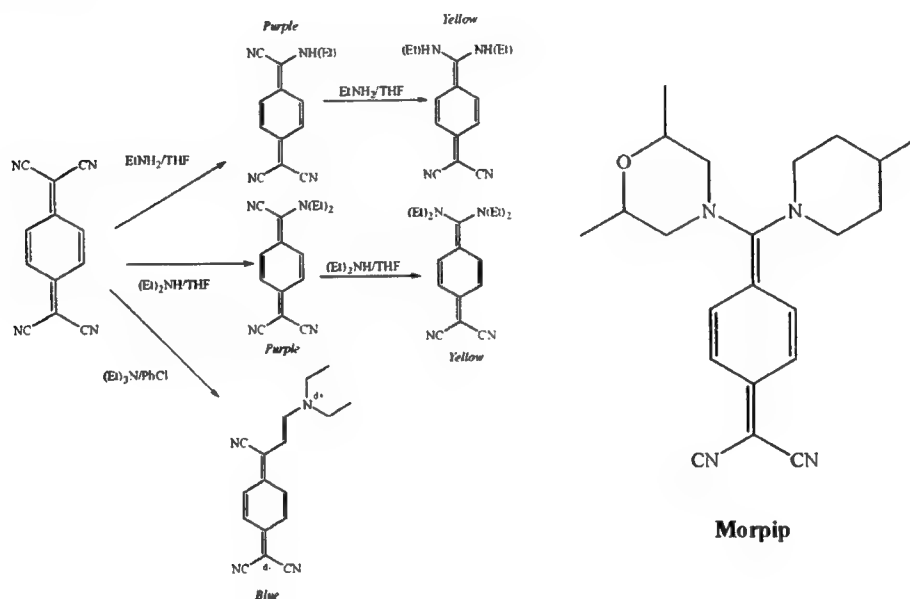


Figure. 1. Amino-substituted TCNQ chromophores.

These compounds have been shown to have a planar structure by X-Ray crystallography². The action of primary and secondary amines which substitute two nitrile moieties results in di-substituted yellow chromophores³ (as shown above) with absorption maxima in the range 350-450 nm. These chromophores are not planar, the plane of substituents is twisted by about 40° with respect to the quinoidal ring in the ground state⁴.

We have observed a strong increase in photoemission⁵ in the twisted materials such as Morpip⁶ (Shown in Figure 1), in comparison to the planar adducts which show little photoemission. The strength of the emission is dependent on the environment in which the chromophore is dispersed. A strong emission is observed in the solid state on exposure under a UV lamp, while the emission from a liquid solution is very weak. The photoemission of several analogues has been studied in a variety of media from the crystalline state, to liquid solutions and solutions in glassy environments over a range of temperatures. Both the quantum efficiency and Stokes' shift are dependent on solvent viscosity. This is best illustrated by the results shown in Table.1 which summarises the data from experiments in

which emission spectra of Morpip solutions were measured in a range of alcohols. The quantum yield for the low viscosity straight chain alcohol solutions increases in a linear manner with decreasing polarity parameter, while the extra hydrogen bonding in diethylene glycol and glycerol causes greatly increased viscosity⁷ and thus a dramatic increase in both quantum yield and Stokes' shift.

Table 1. Stokes' shifts and quantum yields of Morpip in a range of alcohols.

Alcohol	Stokes' shift (cm ⁻¹)	Quantum yield (%)	Δf	Viscosity (nP)
Methanol	5160	0.1	0.309	0.544
Ethanol	4620	0.1	0.290	1.07
1-Propanol	4240	0.4	0.275	1.95
1-Butanol	4150	0.5	0.264	2.54
1-Pentanol	3970	0.7	0.254	3.62
1-hexanol	4010	1.0	0.243	4.58
Diethylene Glycol	5040	1.4	0.266	30.2
Glycerol	5400	11.8	0.265	934

$$\Delta f = \left(\frac{\epsilon - 1}{2\epsilon + 1} \right) - \left(\frac{n^2 - 1}{2n^2 + 1} \right) \quad \Delta f = \text{the polarity parameter}^8.$$

Emission spectra were recorded in the glass forming solvent 2-methyl tetrahydrofuran (THF) over a range of temperatures; these are shown below in Figure 2. The shift in the position of the emission band can be attributed to solvatochromism, brought about by changes in the density of the medium. Formation of a glassy state in 2-methyl THF begins below 200K and is complete between 100-150K. Figure 2 clearly shows changes in behaviour from solution like (low emission intensity) to solid (high emission intensity).

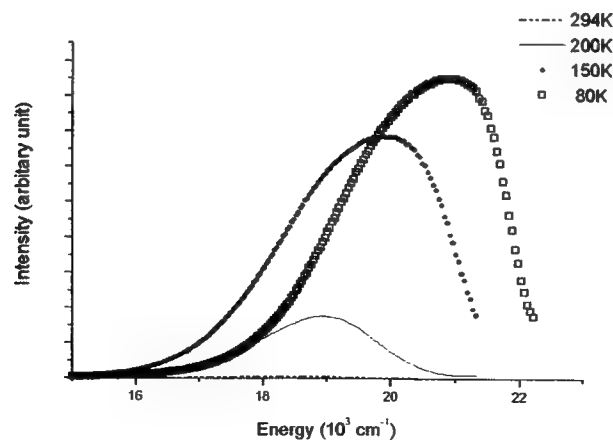


Figure 2. Emission Spectra of Morpip in 2-methyl THF

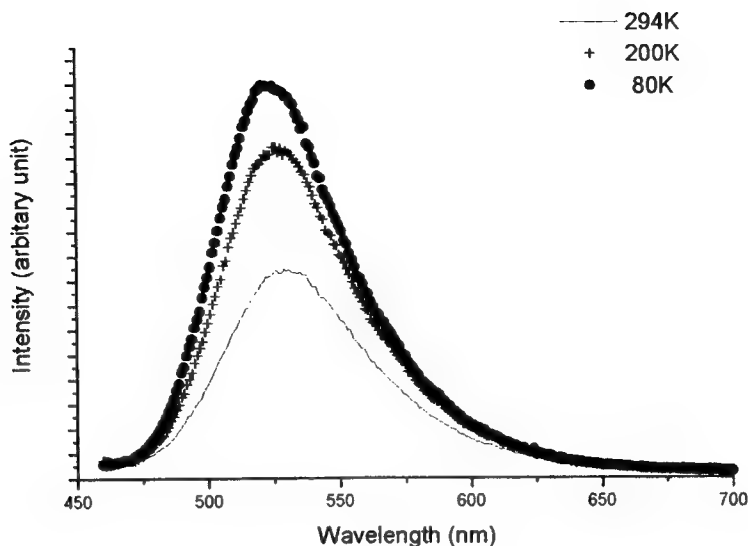


Figure 3. Emission Spectra of Morpip in PMMA

Solid state solutions of Morpip were prepared in PMMA films, and emission spectra were recorded over a range of temperatures (Figure 3), once more the highest emission intensities were recorded at the lower temperatures. In contrast to the glass forming solvent, 2-methyl THF, changes in the density and local environment of PMMA are much smaller at low temperatures, thus the increase in emission intensity could be due mostly to the cut-off of the non radiative decay pathway.

The data obtained for solutions in glass forming solvents and polymers indicate that fluorescent emission is enhanced in environments which hinder conformational change in the chromophore, suggesting that the excited state adopts a more planar conformation than the ground state.

The authors would like to thank Mounir Halim for the Quantum yield measurements.

References

- ¹ M.Szablewski, P.R.Thomas, A.Thornton, D.Bloor, G.H.Cross, J.M.Cole, J.A.K.Howard, M.Malagoli, F.Meyers, J.Brédas, W.Wenseleers, E.Goovaerts, *J.Am.Chem.Soc.*, **119**, 1997, 3144
- ² J.C.Cole, J.A.K.Howard, G.H.Cross, M.Szablewski, *Acta Cryst.*, **C51** 1994, 715
- ³ W.R.Hertler, H.D.Hartzer, D.S.Acker, R.E.Benson, *J.Am.Chem.Soc.*, **84**, 1962, 3387
- ⁴ M.Ravi, D.N.Rao, S.Cohen, I.Agranat, T.P.Radhakrishnan, *Chem.Mater.*, **9**, 1997, 830
- ⁵ Y.Kagawa, M.Szablewski, M.Ravi, G.H.Cross, D.Bloor, A.Beeby, C.Parmer, G.Rumbles, *In preparation.*
- ⁶ Y.Kagawa, M.Szablewski, M.Ravi, N.-A.Hackman, G.H.Cross, D.Bloor, A.S.Batsanov, J.A.K.Howard, *In preparation.*
- ⁷ P.F.Barbara, S.D.Rand, P.M.Rentzepis, *J.Am.Chem.Soc.*, **103**, 1981, 2156
- ⁸ C.F.Zhao, R.Givishi, U.Narang, G.Ruland, P.N.Prasad, *J.Phys.Chem*, **100**, 1996, 4526

Organic Thin Films for Photonics Applications

Polymer Optical Fibers/ Photorefractive Materials

Saturday, 25 September 1999

Robert Twieg, Kent State University, USA
Presider

SaC

1:30pm–3:00pm

California Ballroom Salons 4&5

Single-mode Electrooptic Polymer Optical Fiber

David J. Welker, Dennis W. Garvey, and C. D. Breckon

Sentel Technologies L.L.C., 1610 NE Eastgate Blvd, Pullman, WA 99163

Mark G. Kuzyk*

Department of Physics (*and Materials Science Program), Washington State University
Pullman, WA 99164-2814

Abstract: We report on single mode polymer optical fiber with embedded electrodes, including polling the nonlinear core and phase modulating the light in the waveguide.

The fabrication process for making a polymer optical fiber with a dye-doped core is well enough defined to make a step index single-mode waveguide. [1,2] Graded index fibers have also been demonstrated. [3] Because the core diameter can be made small and dye doping renders the material highly optically nonlinear, such waveguides are well suited for making devices based on the intensity dependent refractive index. [4] In this paper, we report on the successful incorporation of electrodes that can be used to apply an electric field to the fiber core while the fiber is being drawn, and, that these same electrodes can be used to electro-optically modulate light. This makes possible a whole new class of polymer optical fiber devices based on second-order nonlinearity.

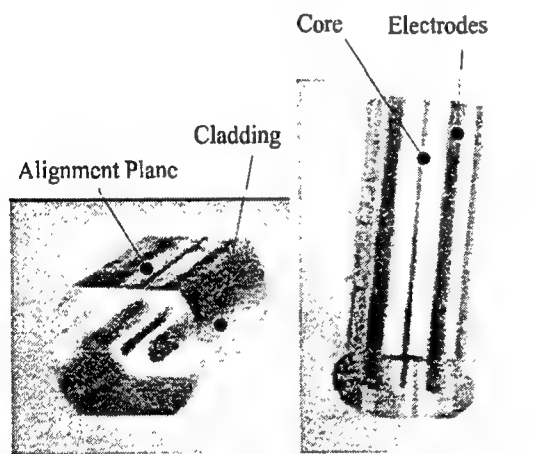


Figure 1. Two views of a preform with a DR1/PMMA core and electrodes.

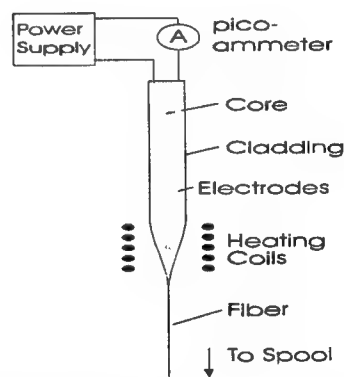


Figure 2. Drawing a fiber while polling with electrodes.

The first step is making the fiber preform from which the fiber is drawn. The process we use is similar to the one for making single mode fiber.[2] Two semicylinders with three grooves - one for the core and two for the electrodes - are pressed together at elevated temperature. Figure 1 shows two views of a preform with a DR1(disperse red #1 azo dye)/PMMA(poly (methyl methacrylate)) core of 800 μm diameter, electrodes each of 2mm diameter, and an outer preform diameter of 12.7 mm. Two alignment planes are machined on the top and bottom of the preform in the PMMA cladding - parallel to the plane containing the electrodes and core.

The preform is pulled into a fiber in a drawing tower, which is above the glass transition temperature of the polymer and above the melting temperature of the electrodes. A high voltage power supply is attached to the electrode so that the dye-doped core can be poled [5] during the drawing process. As the fiber leaves the drawing oven, it cools and the alignment of the chromophores is frozen in place. Figure 2 shows a schematic of the drawing tower. The preform is about 10cm in length and, for a fiber diameter of 125 μm , draws into about 1km of fiber.

The current passing through the electrodes during polling is measured with an ammeter. A short during the polling process results in a spike in the current. Note that a large resistor(not shown), whose resistance is

much lower than the resistance of the PMMA material that is being poled, is placed in series with the ammeter to prevent damage to the poling electronics. A short during the polling/pulling process is self healing, so that a short does not ruin the entire spool, but rather only a short length of the fiber. [6]

Figure 3 shows a side view (illuminated from the other side by a laser source) and an end view of the electrooptic fiber showing the guiding of light. In this fiber the total diameter was 400 microns. The distortion of the electrodes is an artifact caused by the polishing of the ends of the fiber.

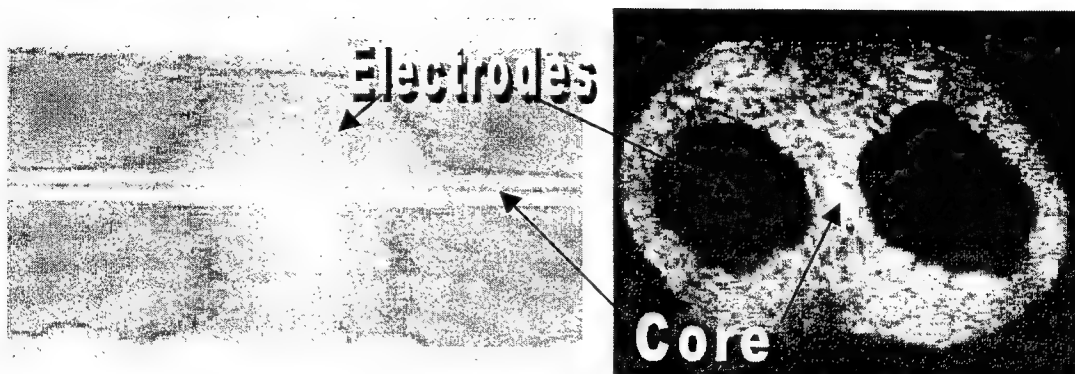


Figure 3. Side and end view of the electrooptic fiber.

The 1km spool of fiber are cut into small pieces for testing. 10cm to 20cm lengths of fiber are attached with epoxy to a plastic planar substrate as shown in figure 4. The plane containing the electrodes is guaranteed to be parallel to the substrate because of the alignment plane. The polymer fiber is micro-machined down to the electrodes so that leads can be attached. A lead is attached near each on of the electrodes with conducting epoxy so that a total of four leads is attached to the piece of fiber.[5] Details of lead attachment process will be described elsewhere.

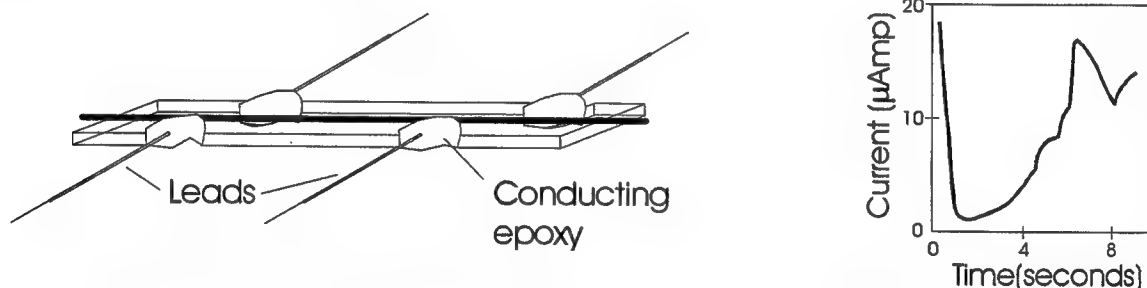


Figure 4. Electrooptic fiber on substrate with leads attached and a plot of current as a function of time after a hot plate turned on.

The continuity of each electrode is measured using the pair of leads attached to either end of an electrode. For 40 μm diameter electrodes, the resistance is always found to be less than 0.1 ohm/cm. The resistance between electrodes during poling (above the glass transition temperature of the polymer) is about 300 M Ω while below the glass transition temperature after poling it is 50,000 M Ω . The degree of poling is measured using thermally stimulated discharge (TSD), where the fiber is placed on a hot plate, and the current is measured as a function of temperature. The main sources of current in a TSD measurement are trapped charges being freed by thermal activation, and, the reorientation of dipoles, which yield a displacement current. Figure 4 also shows a TSD measurement of a poled fiber. The expected current for dipolar reorientation depends on the material number density, degree of poling, and electrode geometry. Based on our samples, we estimate that the current peak should be about 10 μA . This is consistent with the data, implying that fiber core is poled.

The electrooptic effect is demonstrated in an electrooptic fiber by placing the fiber waveguide into one arm of an interferometer (see Figure 5). A glass slide is used to deflect part of the beam to a reference detector so that the intensity of the beam in the interferometer can be monitored. A glass slide on a rotation mount is used to adjust the optical path difference between the two arms of the interferometer. Light intensity is lost in the fiber arm due to coupling and propagation losses. An optical filter is placed in the reference arm to balance the intensities in both arms. The lens on the reference arm is used to adjust the divergence of the beam to match the divergence of the light leaving the microscope objective at the EO fiber. The result is a high contrast set of fringes at the detector. A sinusoidal voltage is applied to the fiber and the resultant modulation amplitude is measured with a photodiode detector. A lock-in amplifier measures the modulation amplitude. The path differences between the two arms are adjusted to maximize the electrooptic signal. Figure 6 shows the modulation amplitude as a function of applied voltage. The linear behavior demonstrates that the linear electrooptic effect is the source of signal in the fiber. We have thus demonstrated electrooptic phase modulation in a polymer optical fiber.

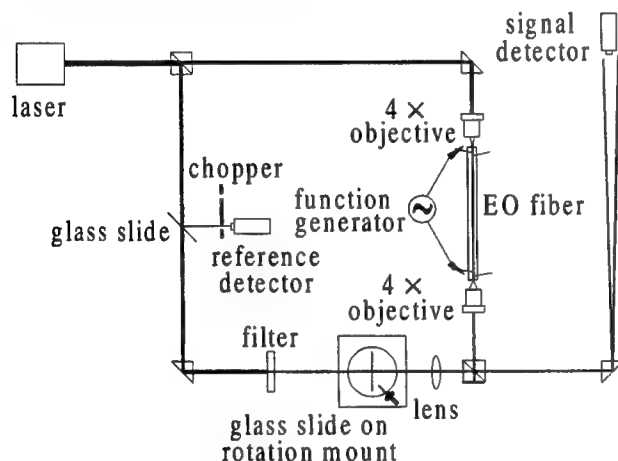


Figure 5. The electrooptic experiment.

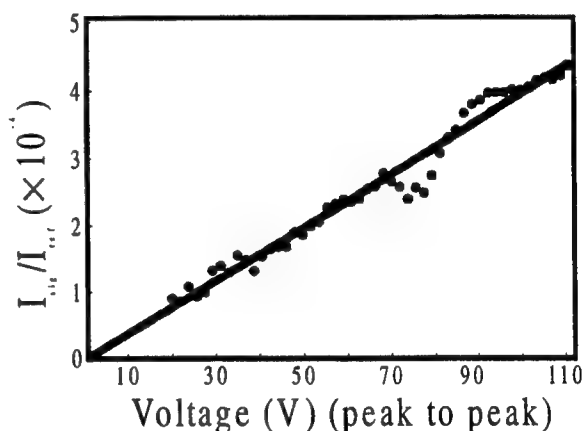


Figure 6. Electrooptic signal as a function of voltage.

In conclusion, we have demonstrated that an electrooptic fiber can be fabricated, poled, and that the dipoles are aligned in the poling as measured with thermally stimulated discharge. Furthermore, the fiber is demonstrated to be a linear phase modulator.

Acknowledgments: We thank the Air Force Office of Scientific Research for generously supporting this work.

References

1. M. G. Kuzyk, U. C. Paek, and C. W. Dirk, "Dye-Doped Polymer Fibers for Nonlinear Optics," *Appl. Phys. Lett.* **59**, 902 (1991).
2. D. W. Garvey, K. Zimmerman, P. Young, J. Tostenrude, J. S. Townsend, M. Lobel, M. Dayton, R. Wittorf, M. G. Kuzyk, J. Sunick, and C. W. Dirk, "A Single-mode Nonlinear-Optical Polymer Fiber," *J. Opt. Soc. Am. B* **13**, 1017 (1996).
3. Y. Koike, N. Tanio, and Y. Ohtsuka, *Macromol.* **22**, 1367 (1989).
4. D. W. Garvey, Q. Li, M. G. Kuzyk, and C. W. Dirk, "Sagnac Interferometric Intensity Dependent Refractive Index Measurements of Polymer Optical Fiber," *Optics Letters* **21**, 104 (1996).
5. K. D. Singer, M. G. Kuzyk, and J. E. Sohn, "A Second Harmonic Generation of Orientationally Ordered Materials," *J. Opt. Soc. Am. B* **4**, 78 (1987).
6. D. J. Welker, J. Tostenrude, D. W. Garvey, B. Canfield, and M. G. Kuzyk, "Fabrication and Characterization of Single-mode Electrooptic Polymer Optical Fiber," *Opt. Lett.* **23**, 1826 (1998).

Propagating Mode Attenuation and Coupling Characteristics of Graded-Index POF

Takaaki Ishigure, Mariko Kano, and Yasuhiro Koike

(1) Faculty of Science and Technology, Keio University, 3-14-1, Hiyoshi, Kohoku-ku YOKOHAMA 223-8522

ishigure@appi.keio.ac.jp

(2) Kanagawa Academy of Science and Technology

1-1-1, Fukuura, Kanazawa-ku, Yokohama 236-0004

Introduction

With increasing demand accessing to Internet with high bit-rate, much attention has been focused on the higher communication bandwidth even in the office and home network. Polymer Optical Fiber (POF) having much larger core than that of silica fiber has been expected to be the office and home-network media because the large core allows the use of inexpensive injection-molded plastic connector, which can drastically decrease the total link cost. To cover the high-bit rate such as several hundred mega bit per second, which must be required even in office and home-network, we proposed the high-bandwidth Graded-Index (GI) POF for the first time¹, and have reported its bandwidth characteristic². Recently interests focused on POF accelerates the research and development of POF particularly in its bandwidth improvement. There have been several reports concerning the dispersion property of GI POF. The theoretical bandwidth properties of the GI POF often have some amount of disagreement with the measured one. The reason of the disagreement is generally explained by the mode coupling. However, the detail modal property has not been analysed.

In this paper, we clarified that the launch condition and mode dependent attenuation are the dominant factors determining the bandwidth of the GI POF. It was also shown that the mode coupling effect on the bandwidth characteristics of the GI POF is considered to be small compared to the above two factors within 100 m. We show a precise bandwidth prediction of the GI POF by considering the power distribution among the propagating modes and differential mode attenuation for the first time, resulting in a good agreement with the experimentally measured property.

Mode Dependence of Output Waveform

We reported that the refractive index profile of the GI POF could be widely controlled by the interfacial-gel polymerization technique². Bandwidth characteristics of the prepared GI POF were analyzed, and we succeeded in predicting the impulse response function of the GI POF having arbitral index profile. In this analysis, uniform launch of all modes is usually assumed because of easy calculation. Fig. 1 shows the experimental and calculated pulse broadening through 100-m PMMA base GI POF. Here, the GI POF whose index profile is slightly deviated from the ideal one was used for measurement in order to clearly observe the pulse broadening. Even for this GI POF, more than 1 GHz of bandwidth for 100m was obtained. The pulsed light signal was launched into the GI POF via a 1-m length, 1-mm core diameter step-index (SI) POF having NA of 0.5 which is much higher than that of the GI POF, in order to realize the uniform excitation of all modes including both meridional and skew modes. A large disagreement is observed between the calculated and measured output waveforms. It was confirmed by the detail analysis that the second peak existing in the calculated waveform shown by the open circle is attributed to the higher order modes having large group delay. On the other hand, an excellent agreement with the measured waveform was observed when the mode dependent attenuation obtained from the near-field power distribution was taken into consideration as shown by close circle.

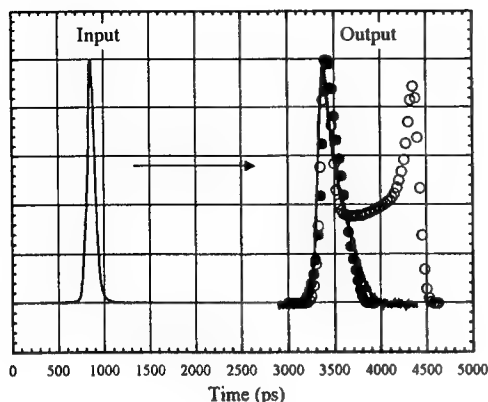


Fig. 1: Pulse Spread through 100 m PMMA base GI POF at 650-nm Wavelength. Solid Line: Experimentally Measured Data O: Calculated Waveform by Considering All Modes are Uniformly Launched. ●: Calculated Waveform by Considering the Mode Dependent Attenuation

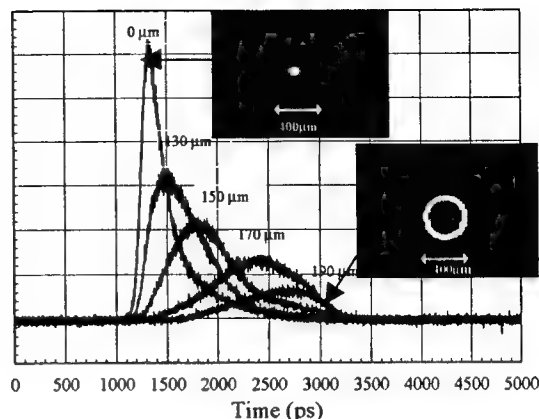


Fig. 2: Measured Result of Differential Mode Delay in 100-m PMMA base GI POF. Core Diameter: 400μm. Photograph: Output Near-Field Pattern from the GI POF, where arrows show the core diameter

Differential Mode Delay

The group delay of each mode in the GI POF was investigated by the measurement of the differential mode delay (DMD). In the DMD measurement, optical pulse is coupled into the GI POF via a 1-m single mode silica fiber in order to launch a specified mode group of the GI POF. By shifting the position of the single mode fiber attaching to the GI POF from the core center to the periphery, each mode from the low order to high order is independently launched. The results of the DMD measurement in 100-m GI POF are shown in Fig.2. Here, the lengths 0 μm, 130μm, ...200 μm shown in Fig. 2 signify the distance from the core center to launching position by the single mode fiber. Output near-field patterns (NFPs), which directly relate to the mode number of transmitted mode, are also shown in Fig.2. When the higher order modes are selectively launched by shifting the launch position 200 μm apart from the core center, the ring pattern is clearly observed, which indicates that the higher order modes are independently transmitted with little energy transfer to the lower order modes. The group delay of each mode in the GI POF was investigated by the measurement of the differential mode delay (DMD). It was observed that with increasing the mode number, larger time delay is observed in which each peak in Fig. 2 is exactly the same as the theoretical value assuming no mode coupling. The fiber length dependence of the DMD is shown in Fig. 3. A linear relation between the DMD and fiber length is observed, and the slope is almost 1, which indicates weak mode coupling.

Generally, the degree of mode coupling in the multi-mode optical fiber is evaluated by the relation between the fiber length and the output pulse width. When the output pulse width is plotted with respect to the fiber length, the slope is an important parameter. The slope close to 1 signifies weak mode coupling, while the slope less than 1 large mode coupling. However, the output pulse width decreases when the higher order modes have very high attenuation, which means that the slope between the fiber length and the output pulse width becomes less than 1 even if the mode coupling is much weak. On the other hand, it was reported that the strong mode coupling changes the output pulse shape from original near triangle shape to Gaussian shape with increasing the transmission distance. This pulse shape change to Gaussian is seen in the result of the conventional step-index type POF even within 50m.

Output pulse shape of the GI POF with respect to the fiber length is shown in Fig. 4. Used fiber is the

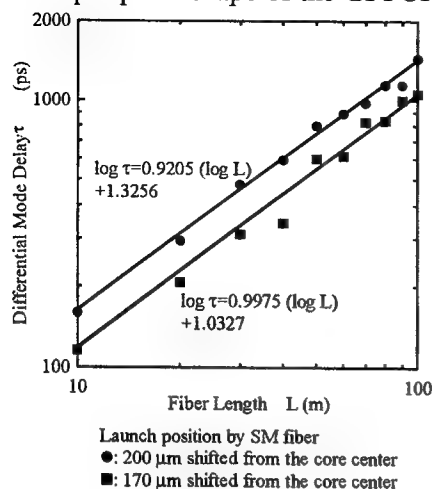


Fig. 3: DMD versus Fiber Length of the GI POF.

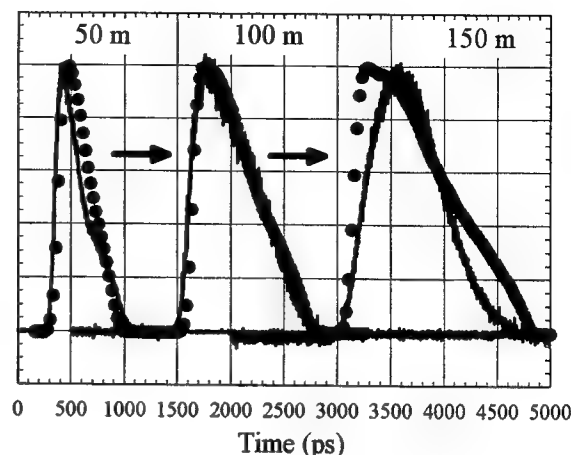


Fig. 4 Fiber Length Dependence of the Output Pulse Spread for the PMMA base GI POF. Solid Line: Measured Results ●: Calculated Results Considering Mode Dependent Attenuation

same as that used in Fig. 2. It is noteworthy that even after 100-m transmission, the steep edge in the leading part of the output pulse, which was originally shown in the input pulse is observed, while after 150-m transmission, it slightly changes to the Gaussian shape. Plots in Fig. 4 signify the calculated waveform in which the mode dependent attenuation was taken into account. It is noteworthy that a good agreement between the measured and calculated waveforms is observed within 100-m transmission although the mode coupling effect was not considered. On the other hand, a slight disagreement between calculated and measured is seen in the waveforms after 150-m transmission. This is considered to be due to the mode coupling. Therefore, it can be concluded that the mode coupling in the SI POF is stronger than that in the GI POF because the core-cladding boundary strongly affects the propagating mode characteristics. It is also concluded that the mode coupling effect on the bandwidth of the GI POF is very small for 100m distance.

Conclusion

It was theoretically and experimentally confirmed that the bandwidth characteristics of the PMMA base GI POF is strongly influenced by the mode dependent attenuation and not by the mode coupling. Calculated bandwidth characteristics of the GI POF has excellent agreement with the measured one by considering the mode dependent attenuation.

Acknowledgement

This work is supported by the research fund of Plastic Optical Fiber Project from Telecommunications Advancement Organization (TAO) of Japan.

References

- /1/ Y.Koike et.al., J. Lightwave Technol., 13, 1475 (1995)
- /2/ T. Ishigure et. al., J. Lightwave Technol., 15, 2095 (1997)

Thermal stability of high bandwidth GI POF

M.Sato, M.Hirai, T.Ishigure and Y.Koike

Faculty of Science and Technology, Keio University, 3-14-1, Hiyoshi, Kouhoku-ku, Yokohama 223, Japan

Email address: m_sato@appi.keio.ac.jp

Introduction

We have already reported large-core, high-bandwidth graded-index polymer optical fiber (GI POF) and 100m, 2.5Gbps data transmission was achieved in PMMA - dopant system GI POF. To achieve high speed data communication even in digital home network by utilizing PMMA base GI POF, thermal stability in both bandwidth and attenuation are important issues. We have already reported thermally stable GI POF even under high humidity atmosphere by selecting suitable dopant. It was confirmed that maintaining high T_g at core center and prohibiting the aggregation of absorbed water molecules in polymer matrix¹ are key issues for high thermal stability. In this paper, we investigated the effect of the high temperature atmosphere on the attenuation of GI POF.

The progress of thermal and humidity stability

We have reported the excess scattering induced by water absorption under high temperature and high humidity atmosphere¹. Although it was found that absorbed water into POF caused excess scattering loss, high attenuation stability under high humidity atmosphere was successfully achieved by selecting suitable dopant which can disperse water molecules in polymer matrix as shown in Fig. 1. Used dopant were benzyl benzoate (BEN), triphenyl phosphate (TPP), diphenyl sulfide (DPS) and diphenyl sulfoxide (DPSO).

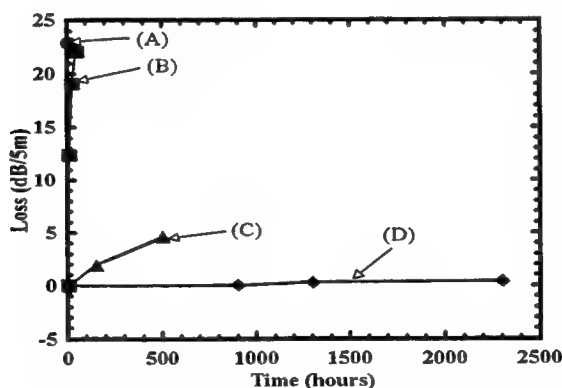


Fig.1 Thermal stability of attenuation of GI POF under 70°C, 95%RH.
 (A): BENdoped GI POF (B):TPP doped GI POF (C): MMA-BzMA copolymer GI POF (D): DPSO doped GI POF

Thermal stability in attenuation

We focused on the stability in attenuation of GI POF in order to clarify the effect of “ high temperature atmosphere “. Even if the GI POF has high temperature resistance at 80°C, abrupt increase of the total transmission loss was observed in some of such GI POFs under high humidity as shown in Fig.1. This increase in the loss may be due to the aggregation of water absorbed into the core of GI POF. The attenuation spectrum of DPS-doped GI POF drawn by high tension as 280gf through 70°C aging is shown in Fig. 2. It should be noted that the increment of loss from the original POF is independent of the wavelength. It is considered that such wavelength independent attenuation increment is considered to be

caused by excess scattering loss due to large heterogeneous structures, imperfection of waveguide structure, or bending loss. Similar wavelength independent attenuation increase was observed when the GI POF is statically bent. As we previously confirmed and reported that no scattering loss increase from PMMA homopolymer and dopant added PMMA was observed through aging at 85 °C for 70 days², attenuation increase shown in Fig.2 is not induced by large size heterogeneous structure formed in GI POF through aging. On the other hand, no attenuation increase was observed in the GI POF drawn by low tension as 45gf under 70 °C aging as shown in Fig.3. It should be noted that the difference between Figs.2 and 3 is drawing condition. Therefore, in order to clarify what is the main reason of the attenuation increase, relation between attenuation increase and length

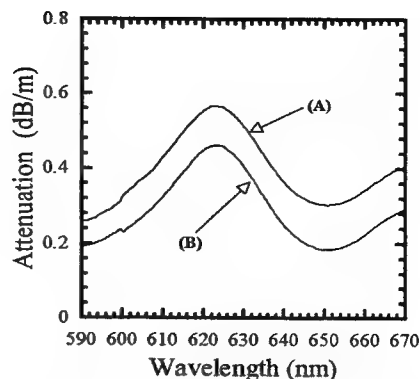


Fig.2 Wavelength dependency of the total attenuation of 11wt.% DPS-doped GI POF at 70 °C. Drawing tension: 280gf (A): Original (B): Aged at 70 °C for 1 day

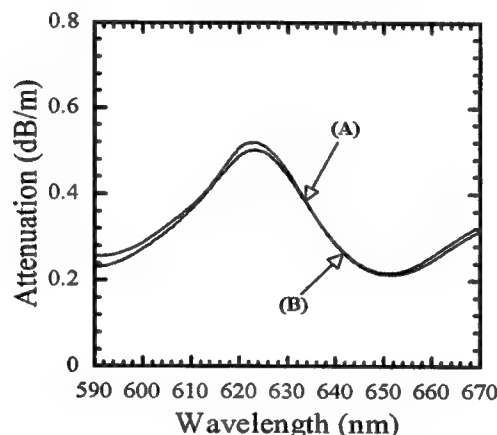


Fig.3 Wavelength dependency of the total attenuation of 11wt.% DPS-doped GI POF at 70 °C. Drawing tension: 45gf (A): Original (B): Aged at 70 °C for 1 day

shrinkage of the GI POF through the aging was investigated. The GI POFs drawn by different drawing tension were tested. Figure 4 shows the relationship between drawing tension and length shrinkage of GI POF after 48 hours aging at 70°C. As the drawing tension corresponds to the orientation degree of polymer chains, the GI POF drawn by high tension tends to show large length shrinkage due to relaxation of orientation as shown in Fig.4. On the other hand, Figure 5 shows thermal stability in attenuation of GI POF at 650nm through aging at 70°C. Attenuation increase is observed only in the GI POF drawn by high tension, while no attenuation increase is observed in the GI POF with little length

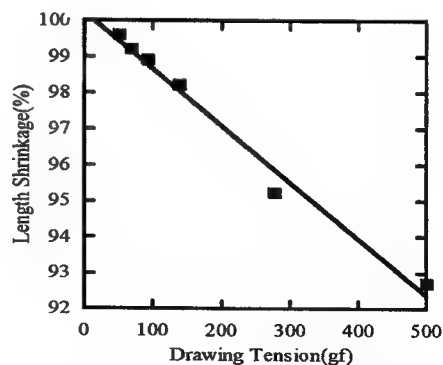


Fig.4 Relationship between drawing tension and length shrinkage of GI POF after 48 hour aging at 70 °C.

shrinkage as shown in Fig.5. The thermal stability in attenuation of GI POF having high NA is shown in Fig.6. It is noteworthy that even in the case of the GI POF drawn by high tension, no attenuation increment was observed through the aging at 70 °C. Therefore, from the results shown in Figs.2, 3, 5, and 6, it is considered that the attenuation increase of the GI POF at high temperature is originated in the bending loss arisen by the random length shrinkage. It is concluded that high NA, which is important property for bending loss, is effective to improve the thermal stability in attenuation as well as drawing tension.

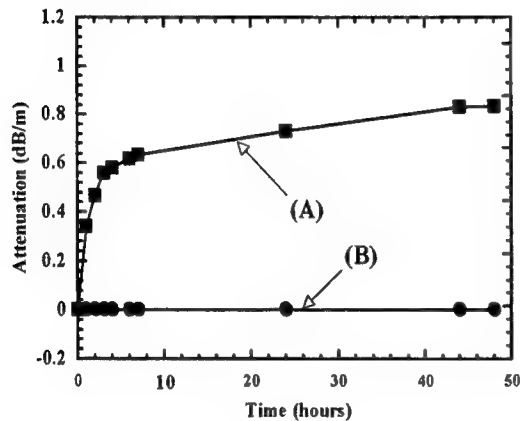


Fig. 5 Thermal stability in attenuation of GI POF whose NA is 0.2 through 70 °C aging. (A): drawing tension: 250gf (B): drawing tension: 50gf

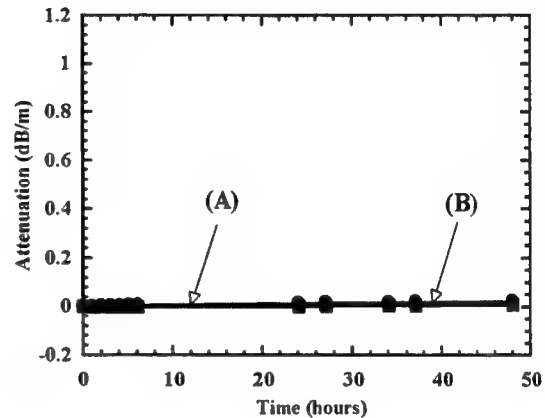


Fig. 6 Thermal stability in attenuation of GI POF whose NA is 0.25 through 70 °C aging. (A): drawing tension: 270gf (B): drawing tension: 50gf

References

1. M.Sato, T.Ishigure, E.Nihei and Y.Koike, Seventh International Plastic Optical Fibers Conference '98 Proceedings pp.109-110, 1998.
2. N. Tanio, H. Kato, Y. Koike, H. E. Bair, S. Matuoka, and L. L. Blyler, Jr, "Physical aging and light scattering of low-loss poly(methyl methacrylate) glass," *Polym. J.*, Vol. 30, No. 1, pp. 56-59, 1998.

Paper withdrawn.

Extended Dihydropyridine Chromophores for Photorefractive Polymers

D. Wright and J. D. Casperson

Department of Chemistry, University of California San Diego
9500 Gilman Drive, M/C 0340
La Jolla, CA 92093-0340
Phone: (619) 822-0243 Fax: (619) 534-7244
dawright@ucsd.edu, jcaspers@ucsd.edu

F. You and R. J. Twieg

Department of Chemistry, Kent State University, Kent, OH 44242
Phone: (330) 672-2791 Fax: (330) 672-3816
fyou@lci.kent.edu, rtwieg@lci.kent.edu

W. E. Moerner

Department of Chemistry, Stanford University, CA 94305-5080
Phone: (650) 723-1727 Fax: (650) 725-0259
w.e.moerner@stanford.edu

Photorefractive materials show promise for several applications including high density optical data storage, image processing (correlation, pattern recognition), phase conjugation, optical limiting, simulations of neural networks and associative memories, and programmable optical interconnections.^{1, 2} Polymeric photorefractive materials provide potential advantages over their inorganic counterparts due to their low cost, processability, and high values of certain photorefractive figures of merit.

Photorefractive polymers have improved greatly since the demonstration of the first photorefractive polymer in 1991.³⁻⁵ To date several materials have shown large gain coefficients (Γ) and diffraction efficiencies (η) at high applied electric fields ($>60\text{V}/\mu\text{m}$).⁶⁻⁸ Recently, several groups have focused on obtaining large Γ and η at lower applied fields ($30\text{-}50\text{V}/\mu\text{m}$).^{9, 10} In other studies at high field, several materials have shown grating growth time constants (τ_g) in the tens of milliseconds,^{8, 11} and more recently several milliseconds at the canonical writing intensity of $1\text{W}/\text{cm}^2$.¹²⁻¹⁴ Unfortunately, no material to date has shown high Γ and η , while having small τ_g at low applied fields, which is what is required for many applications.

Many of the most successful photorefractive polymer composites have used poly(n-vinylcarbazole) (PVK) as a charge transporting host, doped with photorefractive chromophores, charge generators, and plasticizers. Much recent work has concentrated on chromophore optimization guided by the realization that due to the orientational enhancement effect,¹⁵ both the hyperpolarizability and the polarizability anisotropy of the chromophore are critical. In the oriented gas approximation, a figure of merit (FOM) has been derived:^{16, 17}

$$F = \frac{9\mu_g\beta}{M} + \frac{2\mu_g^2\Delta\alpha}{kTM} \quad (1)$$

where μ_g is the ground-state dipole moment, β is the first hyperpolarizability, M is the molar mass, k is Boltzmann's constant, T is the temperature, and $\Delta\alpha$ is the polarizability anisotropy, i.e., the difference in optical polarizability parallel and perpendicular to the molecular axis.

In this work, a new class of extended dihydropyridine chromophores has been synthesized with the goal of optimizing polarizability anisotropy and dipole moment. Representatives from this class have been

doped into PVK along with visible and near-infrared sensitizers. The structure of the chromophores is given in Figure 1.

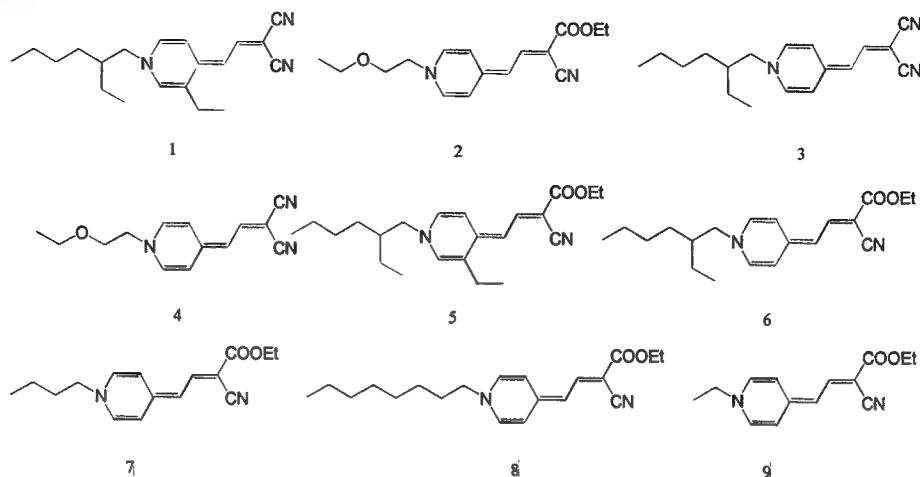


Figure 1. Structures of the extended dihydropyridines studied

In other work, representatives of this class of chromophores have been analyzed by electro-optic absorption measurements to determine the F values.¹⁸ The F values of several members of this class were found to be higher than any chromophore to date. In our measurements, the photorefractive performance of these composites was studied by two-beam-coupling. The gain and loss curves for a sample based on chromophore 3 is given in Figure 2:

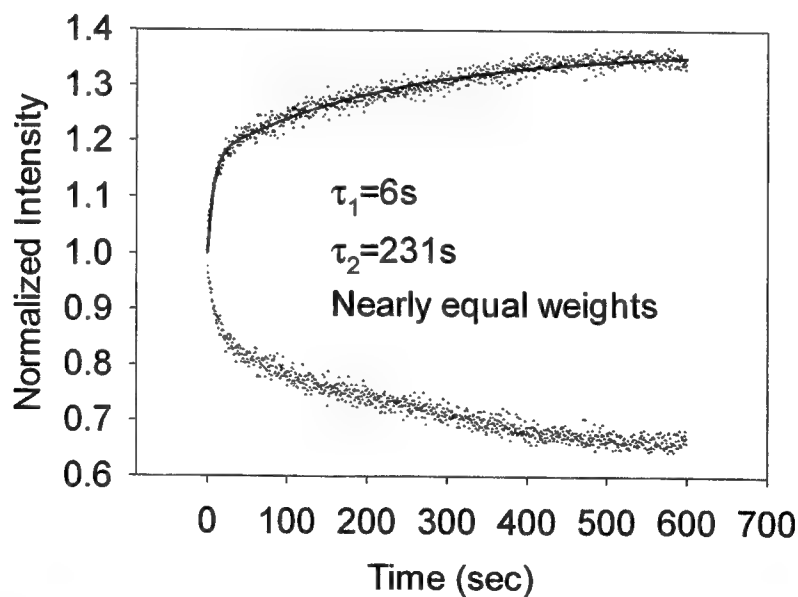


Figure 2. Two-beam-coupling in a composite of PVK/Chromophore 3/BBP/TNFDm at 830nm.

These data were obtained with an intensity of $\sim 300 \text{ mW/cm}^2$ at 830nm, and applied field of $50 \text{ V}/\mu\text{m}$. The solid line is a fit to the gain curve with the sum of two exponentials, giving time constants of 6 and 231

seconds. The steady state Γ is 72cm^{-1} while the absorption coefficient is 55cm^{-1} . This performance may be compared to that for a similar composite with a different chromophore, AODCST, which is a representative of the well-studied dicyanostyrene family. AODCST has been shown to be the most promising of this class because PVK-based composites doped with it have shown large Γ ($>230\text{cm}^{-1}$) and low τ_g values ($\sim 5\text{ms}$) at 647 nm with 1 W/cm^2 writing intensity.¹² At 830 nm with 300 mW/cm^2 writing intensity, the AODCST composite shows $\Gamma = 48\text{ cm}^{-1}$, absorption coefficient 9 cm^{-1} , and observed time constants of 279 ms and 684 ms .

Clearly the composite with the dihydropyridine chromophore needs optimization. Judging from the FOM value alone, the Γ value should be higher than that of the AODCST composite. One possible problem is low photoconductivity, which can lead to less than unity photoconductivity contrast, which in turn weakens the space charge field. Another possible problem is the glass transition temperature value T_g may be higher than room temperature, which can lead to poor chromophore alignment. If chromophores can not align with their local field, the $\mu^2\Delta\alpha$ term of the FOM can not be fully exploited. Future work will focus on increasing the gain coefficient while lowering absorption and time constants.

Acknowledgement: This work was supported in part by the U. S. Air Force Office of Scientific Research Grant No. F49620-96-1-0135 at UCSD and Grant No. F49620-99-1-0032 at Stanford.

References:

- 1 P. Günter and H. J-P., *Photorefractive Materials and Their Applications* (Springer Verlag, Berlin, 1988).
- 2 L. Solymar, D. J. Webb, and A. Grunnet-Jepsen, *The Physics and Applications of Photorefractive Materials* (Clarendon Press, Oxford, 1996).
- 3 S. Ducharme, J. C. Scott, R. J. Twieg, *et al.*, Physical Review Letters **66**, 1846 (1991).
- 4 W. E. Moerner and S. M. Silence, Chemical Reviews **94**, 127 (1994).
- 5 W. E. Moerner, A. Grunnet-Jepsen, and C. L. Thompson, Annual Review of Materials Science **27**, 585 (1997).
- 6 K. Meerholz, B. L. Volodin, Sandalphon, *et al.*, Nature **371**, 497 (1994).
- 7 A. M. Cox, R. D. Blackburn, D. P. West, *et al.*, Applied Physics Letters **68**, 2801 (1996).
- 8 A. Grunnet-Jepsen, C. L. Thompson, R. J. Twieg, *et al.*, Applied Physics Letters **70**, 1515 (1997).
- 9 K. Meerholz, Y. de Nardin, R. Bittner, *et al.*, Applied Physics Letters **73**, 4 (1998).
- 10 B. Kippelen, S. R. Marder, E. Hendrickx, *et al.*, Science **279**, 54 (1998).
- 11 M. E. Orczyk, J. Zieba, and P. N. Prasad, Journal of Physical Chemistry **98**, 8699 (1994).
- 12 D. Wright, M. A. Diaz-Garcia, J. D. Casperson, *et al.*, Applied Physics Letters **73**, 1490 (1998).
- 13 J. A. Herlocker, K. B. Ferrio, E. Hendrickx, *et al.*, Applied Physics Letters **74**, 2253 (1999).
- 14 K. Ogino, T. Nomura, T. Shichi, *et al.*, Chemistry of Materials **9**, 2768 (1997).
- 15 W. E. Moerner, S. M. Silence, F. Hache, *et al.*, Journal of the Optical Society of America B (Optical Physics) **11**, 320 (1994).
- 16 R. Wortmann, C. Poga, R. J. Twieg, *et al.*, Journal of Chemical Physics **105**, 10637 (1996).
- 17 B. Kippelen, F. Meyers, N. Peyghambarian, *et al.*, Journal of the American Chemical Society **119**, 4559 (1997).
- 18 R. Wortmann, C. Glania, P. Kramer, *et al.*, Appearing in Chemical Physics (1999).

Dual grating photorefractive polymer

L. Michael Hayden and Shane J. Strutz

Department of Physics, University of Maryland Baltimore County, Baltimore, MD 21250
hayden@umbc.edu

Photorefractive (PR) polymers are potential replacements for PR crystals. The rapid response times and high diffraction efficiency¹ (>86%) of these polymers, combined with their low cost, has lead to their study for various real-time holography applications, such as phase conjugation,² imaging through distorting media,³ digital data storage,⁴ and the coupling of light into waveguides.⁵

A subset of the PR crystals, $\text{Bi}_{12}\text{SiO}_{20}$,^{6,7} $\text{Bi}_{12}\text{TiO}_{20}$,⁸ and GaP,⁹ have been shown to exhibit a dual grating behavior. In these crystals, photochromic gratings are formed during the photorefractive grating formation process. These dual grating materials are useful for applications which benefit from the interaction between light diffracted from two simultaneous gratings. These applications¹⁰ include, wave front interferometry, image synthesis, logic operations, phase object detection, holographic interferometry, and novel spatial light modulation. Here we introduce a polymer composite capable of simultaneously storing both erasable, photorefractive and quasi-permanent, irreversible photochemical (PC) holograms. Gratings may be formed in the following combinations: PC only (at 675 nm with no external field); PC and PR simultaneously (at 675 nm under the application of an external field); or PR only (at wavelengths longer than 715 nm with an applied field).

Our composite consists of the photoconductor poly(N-vinylcarbazole) (PVK), the plasticizer butyl benzyl phthalate (BBP), the sensitizer/charge generator C₆₀ and the chromophore, (3-(2-(4-(N,N-diethylamino)phenyl)ethenyl)-5,5-dimethyl-1,2-cyclohexenylidene)-propanedinitrile (Lemke-e).¹¹ Lemke-e performs two functions in our composite. First, it is a chromophore with a large PR molecular figure of merit,¹² allowing the formation of efficient PR gratings. Second, it takes part in certain photochemical reactions when triplet sensitized. These photochemical reactions can be used to write PC gratings. The photochemical reaction begins when a photon is absorbed by one of the singlet energy levels (675 nm) of C₆₀, followed by coupling of this energy into a long lived triplet state (795 nm)¹³ through intersystem crossing. The C₆₀ then transfers its energy to a Lemke-e molecule through triplet-triplet energy exchange. Finally, two Lemke-e molecules undergo a 2+2 cycloaddition reaction, resulting in a change in the local absorption of the composite.¹⁴ Interference of two coherent beams of 675 nm light inside the composite results in a local absorption grating (hologram). Recent literature has referred to this reaction as photochromic;^{14,15} however, we will refer to it as photochemical or irreversible photochromic (PC) since the reaction is irreversible. The composites studied in this work consisted of Lemke-e 7%/ C₆₀ 1%/BBP 21-36%/PVK 72-56% (LCBP) by weight.

We verified the PR nature of the LCBP composites by performing asymmetric two-beam-coupling (TBC) experiments and measured the diffraction efficiency of the gratings using a degenerate four wave mixing (DFWM) technique. The PR experiments were performed with either a Ti-Sapphire laser, tunable between 715 and 820 nm or a 675 nm laser diode. An electric field of 82 V/ μm applied to 75 μm thick samples yielded a TBC gain coefficient of, $\Gamma_p = 156 \text{ cm}^{-1}$, for *p*-polarized, 730 nm light. In the DFWM experiments, overmodulation occurred at 110 V/ μm for 730 nm light with a maximum external diffraction efficiency of 53% (Figure 1a inset). As expected, the PR external diffraction efficiency, η_E , of the composite decreases as the glass transition temperature (T_g) of the polymer increases (Figure 1a inset).

The PC grating formation was probed using a DFWM configuration. For these experiments, the polymer was pressed between plain glass slides with the sample normal bisecting the two write beams. A slanted geometry was not required since no field was applied to the sample. A 675 nm laser diode was used to generate the coherent *s*-polarized write beams (1.8 W/cm²), as well as the *p*-polarized read beam (0.05 W/cm²). The initial slopes of the curves in Figure 1a yield the sensitivities of the different composites, defined here as the square root of the diffraction efficiency divided by the exposure. The highest sensitivity, $S = 0.0006 \text{ cm}^2/\text{J}$ ($\lambda = 675 \text{ nm}$), was observed for the $T_g = 26^\circ\text{C}$ system. The sensitivity of the material decreased as the T_g of the material increased. As a result, the time required to write a PC grating increased with the T_g . The increased write time (decreased sensitivity) is due to a decrease in the translational diffusion of the Lemke-e molecules which slows the photochemical process responsible for PC grating formation.

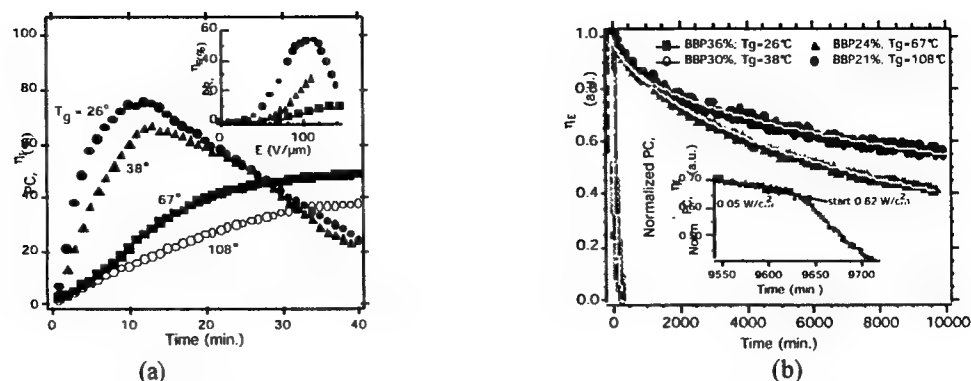


Figure 1 (a) PC write times and PR diffraction efficiencies versus T_g . The main figure shows the internal diffraction efficiency, η_I of the PC gratings. The inset figure shows the T_g dependence of the PR external diffraction efficiency, η_E ; (b) Lifetime of PC holograms. The main figure shows grating decay during sparse reading; the inset during continuous reading.

A maximum internal diffraction efficiency, $\eta_I = 74\%$ ($\eta_E = 20\%$) was reached in the BBP 36% ($T_g = 26^\circ\text{C}$) system after writing for ten minutes. Since the photochemical grating formation process is irreversible, the decrease in η_I after reaching a maximum value in the low T_g systems is not due to overmodulation, as in the PR effect, but due entirely to the translational diffusion of the molecules that formed the grating. Thus, after a grating is formed, translational diffusion causes the grating to deteriorate in low T_g systems. The translational diffusion is reduced in the higher T_g systems. The effect of translational diffusion on the lifetime of the PC gratings is shown in Figure 1b. After writing a PC grating to its maximum efficiency ($\eta_E \approx 20\%$), the decay in the diffraction efficiency of the grating was periodically probed with a low power density (0.05 W/cm^2) read beam of the same wavelength. The $1/e$ times were 24, 91, 11228 (7.7 days), and 26201 minutes (18.2 days) for the 26°C , 38°C , 67°C , and 108°C systems, respectively. Grating decay due to continuous reading can be alleviated by reading with a longer wavelength. For instance, 730 nm light reconstructs PC holograms but does not photochemically alter the material and hence will not cause erasure of the PC holograms. We are currently attempting to increase the dye concentration in our samples by either using dyes with lower absorbance at 675 nm, or by selecting a triplet sensitizer for Lemke-e that allows us to use longer wavelengths. Our early results (Figure 2) show that by using a low absorption chromophore and simply doubling the chromophore concentration, we can increase the sensitivity to $S = 0.003 \text{ cm}^2/\text{J}$ (sample $T_g = 67^\circ\text{C}$), a factor of 5 increase.

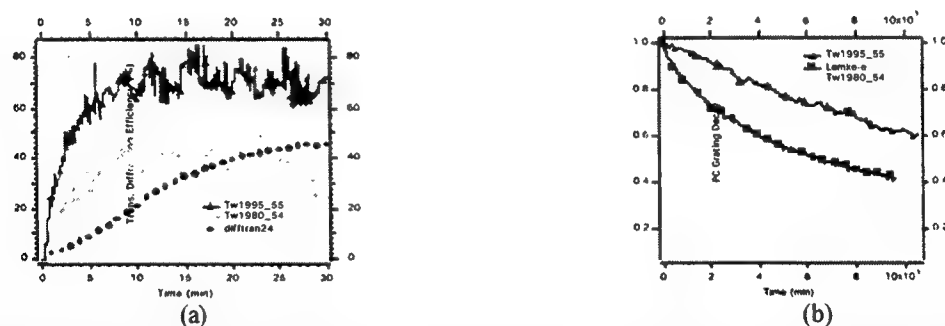


Figure 2. Effect of increased dye concentration and size on PC grating buildup and decay. The T_g of these systems was 67°C . Tw1995-55 and Tw1980-54 (synthesized by R. Twieg of Kent State Univ.) have blue shifted absorption maxima compared to Lemke-e, allowing higher concentrations, while Tw1995-55 is larger and Tw1980-54 is smaller than Lemke-e.

PC and PR holograms can also be stored in the same location. A LCBP (BBP 36%) composite was placed into a holographic storage setup which incorporated a spatial light modulator and multiple wavelength capability. We then stored and recovered holograms from the same location by illuminating the sample with the appropriate wavelength (Figure 3). Illumination by either 675 nm or 730 nm light reconstructed both holograms. However, when the PC hologram was reconstructed by 730 nm light or the PR grating was reconstructed with 675

nm light, the images were diffracted away from the camera. Besides the demonstration shown in Figure 3, we were also able to angle multiplex and recover 10 PC holograms and an erasable, dynamic PR hologram in the same volume, simultaneously.

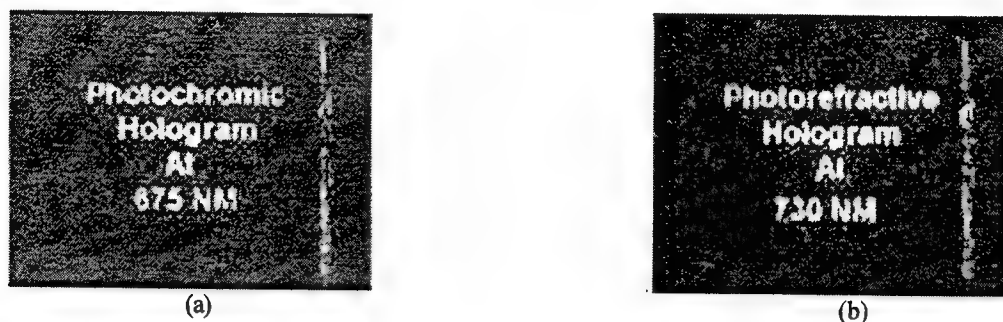


Figure 3. PC and PR holographic storage in the same sample volume. With no electric field applied, the sample was exposed to 675 nm light for two minutes to write the PC image. Exposure for one second at 730 nm with 100 V/ μ m applied recorded the PR image. Subsequent illumination at 675 nm recovered the stored PC image (3a). After reading the PC image, switching wavelengths back to 730 nm retrieved the stored PR image (3b). The reading cycles could be repeated until the gratings were erased in a time similar to those seen in the FWM experiments. The vertical lines in the "H" are 4 pixels wide, each pixel is 15x15 μ m.

The main advantage of our composite is that it is capable of storing both erasable and quasi-permanent holograms in the same location. In addition, the grating formation processes are wavelength selective, allowing for the formation of simultaneous PR and PC gratings or each grating type individually. Using 675 nm light and an external electric field, causes the formation of both grating types, allowing applications such as holographic interferometry, image synthesis, and logic operations to be carried out. Using longer wavelengths, purely PR holographic operations such as optical switching and imaging through distorting media are possible. Finally, long term storage applications like digital data storage may be possible by writing purely PC gratings at 675 nm with no external field.

Acknowledgments. We thank the Earth and Space Data Computing Division at the NASA Goddard Space Flight Center for its support.

References

- 1 K. Meerholz, B. L. Volodin, Sandalphon, B. Kippelen, and N. Peyghambarian, *Nature* **371**, 497 (1994).
- 2 A. Grunnet-Jepsen, C. L. Thompson, and W. E. Moerner, *Science* **277**, 549 (1997).
- 3 B. Kippelen, S. R. Marder, and N. Peyghambarian, *Science* **279**, 54 (1998).
- 4 P. M. Lundquist, C. Poga, R. G. DeVoe, Y. Jia, W. E. Moerner, M.-P. Bernal, H. Coufal, R. K. Grygier, J. A. Hoffnagle, C. M. Jefferson, R. M. Macfarlane, R. M. Shelby, and G. T. Sincerbox, *Optics Letters* **21**, 890 (1996).
- 5 D. Kokron, S. M. Evanko, and L. M. Hayden, *Opt. Lett.* **20**, 2297-2299 (1995).
- 6 P. M. Jeffrey, S. L. Clapham, R. W. Eason, D. A. Eason, D. A. Fish, A. K. Powell, T. J. Hall, and N. A. Vainos, *Optics Communications* **98**, 357 (1993).
- 7 D. A. Fish, A. K. Powell, T. J. Hall, P. M. Jeffrey, and R. W. Eason, *Optics Communications* **98**, 349 (1993).
- 8 J. Frejlich and P. M. Garcia, *Applied physics. A, Solids and surfaces*. **55**, 49 (1992).
- 9 K. Horiuchi and K. Kuroda, *Optics Communications* **113**, 487 (1995).
- 10 N. A. Vainos, S. L. Clapham, and R. W. Eason, *Applied Optics* **28**, 4386-4392 (1989).
- 11 R. Lemke, *Chem. Ber.* **103**, 1894 (1970).
- 12 S. R. Marder, B. Kippelen, and N. Peyghambarian, *Nature* **388**, 845 (1997).
- 13 R. R. Hung and J. J. Grabowski, *J. Phys. Chem.* **95**, 6073-6075 (1991).
- 14 R. Wortmann, P. M. Lundquist, R. J. Twieg, C. Geletneky, C. R. Moylan, Y. Jia, R. G. DeVoe, and D. M. Burland, *Appl. Phys. Lett.* **69**, 1657 (1996).
- 15 A. Akella, S. L. Sochava, and L. Hesselink, *Optic Letters* **22**, 919 (1997).

Organic Thin Films for Photonics Applications

Second/Third Order Nonlinear Optical Effects: 1

Saturday, 25 September 1999

Joseph W. Perry, University of Arizona, USA
Presider

SaD

3:30pm–5:45pm

California Ballroom Salons 4&5

Novel Approaches to Ionically Self-Assembled Nonlinear Optical Thin Films

J.R. Heflin¹, C. Figura¹, P.J. Neyman¹, D. Marciu², M.A. Murray¹,
R.M. Davis³, and M. Miller²

¹Department of Physics, Virginia Tech, Blacksburg, VA 24061-0435

²F&S, Inc., P.O. Box 11704, Blacksburg, VA 24062-1704

³Department of Chemical Engineering, Virginia Tech, Blacksburg, VA 24061-0211
(540)231-4504, fax: (540)231-7511, rheflin@vt.edu

Ionically self-assembled monolayer (ISAM) films are a recently developed,¹ class of materials that allows detailed structural and thickness control at the molecular level combined with ease of manufacturing and low cost. The ISAM method involves the alternate dipping of a charged substrate into an aqueous solution of a cation followed by dipping in an aqueous solution of an anion at room temperature. Since the adsorption is based on the electrostatic attraction of interlayer charges, each layer is self-limiting in thickness and uniform at the molecular level. Using commercial ionic polymer dyes, we have used the ISAM technique to produce a noncentrosymmetric arrangement of nonlinear optical (NLO) chromophores to yield thin films with $\chi^{(2)}$ values comparable to that of quartz.^{2,3} The noncentrosymmetric structure is a spontaneous result of the self-assembly process and is a thermodynamically-stable state. Thus, electric field poling is not required as in the case of electro-optic poled polymers. Importantly, the second harmonic intensity generated by ISAM films exhibits the expected quadratic dependence on film thickness for films as thick as 100 bilayers. This demonstrates that the noncentrosymmetry induced by the ionic deposition technique is uniformly maintained in each successive bilayer. Furthermore, ISAM films exhibit exceptional stability of the $\chi^{(2)}$ response with no measureable decay over a period of greater than two years at room temperature. The second harmonic generation signal decreases by a factor of two when the film is heated to 150° C for 18 hours but fully recovers upon cooling. There is therefore no permanent degradation of chromophore orientation over the course of this heating cycle.

Here, we present detailed studies of the structure of noncentrosymmetric ISAM films as a function of the parameters of the aqueous solutions. These studies indicate that while the thickness of the individual layers can be increased by more than a factor of ten in a controlled manner, the corresponding increase in the amount of NLO chromophore is not always associated with a corresponding increase in $\chi^{(2)}$. There is clearly a separate degree of orientation obtained at the interfaces between adjoining layers as compared to that within the "bulk" of an individual layer. The largest $\chi^{(2)}$ values are observed in the thinnest films since these contain the largest fraction of oriented chromophore. As a result of the understanding obtained from these studies, we have developed several novel approaches to substantially increase the NLO response of ISAM films by reducing the orientational competition between chromophores that is inherent in the basic ISAM structure.

ISAM films are grown monolayer by monolayer by first immersing an initially charged substrate into an aqueous solution containing an oppositely charged polyelectrolyte. This is followed by rinsing and then by immersion of the substrate into a second polyelectrolyte that is of opposite charge to the first. The dipping process can, in principle, be repeated as many times as desired until a film with the chosen number of bilayers has been produced. For the present study, ISAM films were deposited on glass microscope slide substrates. Noncentrosymmetric, ISAM $\chi^{(2)}$ films were produced using the polymeric dye Poly S-119, which consists of a poly(vinylamine) backbone with an ionic azo dye chromophore (from Sigma), as the polyanion and poly(allylamine)

hydrochloride) (PAH), which has no $\chi^{(2)}$ response, for the polycation. The formation of each monolayer is exceptionally rapid with these polymers. Through measurements of absorbance and of film thickness (by ellipsometry) as a function of immersion time, each monolayer is found to be fully deposited in less than one minute of immersion in the polyelectrolyte. This allows the rapid buildup of self-assembled, multilayer films. A series of Poly S-119/PAH ISAM films was made with pH values of 1.5, 2.5, and 3.5 and added NaCl concentrations of 0.0, 0.06, 0.10, and 0.13 M. Each film consisted of 30 bilayers. Lower pH and higher salt molarity result in an increase in small ion concentration in the solutions. The charge screening that results is known to lead to a conformational change in polyelectrolytes from linear to a more three-dimensional, loopy structure.

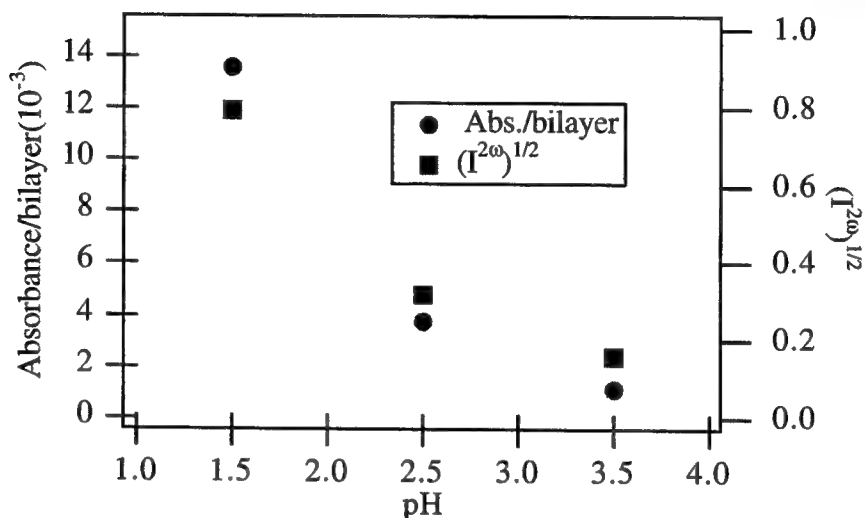


Figure 1. Absorbance per bilayer and square root of the SHG intensity as a function of pH.

For each film, the absorbance at $\lambda=480$ nm (near the peak of the Poly S-119 chromophore), the thickness (determined by a FilmTek 2500 unit), and the second harmonic intensity (with a fundamental wavelength of 1200 nm) were measured. Figure 1 shows the thickness per bilayer

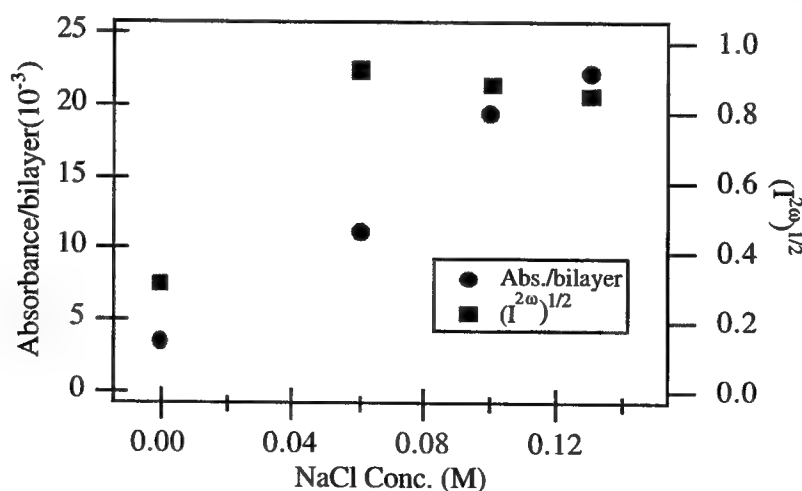


Figure 2. Absorbance per bilayer and square root of the SHG intensity as a function of NaCl concentration at pH=2.5.

and square root of the SHG intensity as a function of pH for solutions that contained no added salt. The amount of Poly S-119 adsorbed into each layer increased by more than a factor of ten as the pH was decreased. While the SHG intensity also increased, the dependence is weaker than that of the absorbance, suggesting that not all of the additional chromophores were properly aligned.

The dependence of absorbance and $(I^{2\omega})^{1/2}$ on ionic strength are illustrated in Figure 2 for a constant pH of 2.5. The absorbance increases strongly with increased NaCl concentration while $(I^{2\omega})^{1/2}$ reaches a plateau. Since increased absorbance without concomitant increase in $(I^{2\omega})^{1/2}$ suggests the additional chromophores are randomly oriented, these results are interpreted in terms of conformational changes in the Poly S-119 from an extended to a more "loopy" structure within a layer in the high ionic strength limit. This would result in thicker layers, but the chromophores within the layer interior would be less likely to be oriented.

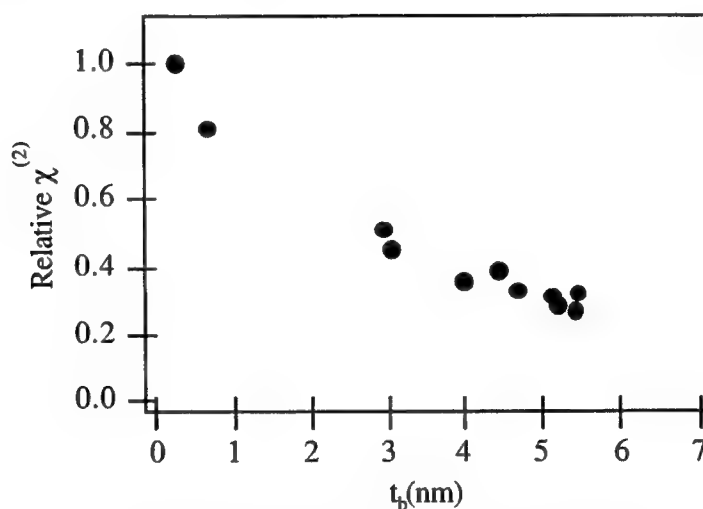


Figure 3. Relative $\chi^{(2)}$ versus thickness per bilayer.

Measurements of the thickness of each film demonstrate a linear dependence between the absorbance and film thickness. The relative $\chi^{(2)}$ value for each film is plotted versus the bilayer thickness in Figure 3. It is seen that $\chi^{(2)}$ decreases monotonically with the bilayer thickness since the material with the "bulk" of the layer adds to the thickness but does not make as strong a contribution to $\chi^{(2)}$ because of reduced chromophore orientation. We will also present results regarding novel ISAM structures including nonpolymeric chromophores as well as biorecognition (as opposed to ionic) interactions. These approaches increase the net orientational chromophore alignment.

1. G. Decher, J.D. Hong, and J. Schmitt, *Thin Solid Films* **210/211**, 831 (1992).
2. J.R. Heflin, Y. Liu, C. Figura, D. Marciu, and R.O. Claus, in *Nonlinear Optical Properties of Organic Materials X*, M.G. Kuzyk, ed., SPIE Vol. **3147**, 10 (1997).
3. J.R. Heflin, C. Figura, D. Marciu, Y. Liu, and R.O. Claus, *Appl. Phys. Lett.* **74**, 495-497 (1999).

Acoustic Spectrum Analysis Using Polymer Integrated Optics

**Araz Yacoubian, Vadim Chuyanov, Sean M. Garner, Hua Zhang,
and William H. Steier**

Department of Electrical Engineering-Electrophysics,
University of Southern California, Los Angeles, CA 90089-0483, (213) 740-7830

Albert S. Ren, Galina Todorova, and Larry R. Dalton

Department of Chemistry, Loker Hydrocarbon Institute,
University of Southern California, Los Angeles, CA 90089-1661, (213) 740-7103

High frequency acoustics is of great importance to analyze fine structures and perform nondestructive evaluation (NDE) of materials opaque to electro-magnetic radiation. An appropriate acoustic sensor should exhibit both the sensitivity and the frequency range required to provide fine spatial resolution. The highest sensitivity is generally achieved using interferometric systems. At high frequencies (GHz range), detectors and electronics are noisy, and have low gain. For example, to analyze submicron structures using acoustic wavelength of $0.1 \mu m$ in a solid with sound velocity of 5 km/s, one needs to analyze 50 GHz vibrations. This frequency is out of the detection range of piezo transducers and direct detection of the output of an interferometer would require photo-detectors and electronics operating at frequencies greater than 100 GHz.

Recently, a technique called picosecond ultrasonics [1] has been used to analyze sub-micron structures. It utilizes a pump-probe geometry and the measurements are done in the time domain with the help of a moving mirror used for optical delay. The system we propose in this paper senses acoustic waves in the frequency domain and is highly sensitive because it is interferometric. It does not have any mechanical moving parts, and is completely electrically controlled. The integrated optical system shown in Fig. 1 utilizes a second order nonlinear polymer as the active component of a heterodyning Michelson interferometer [2, 3].

The phase modulation on the light caused by the vibrating surface beats with the phase modulation due to the EO polymer, is down converted to lower frequencies, and detected by the photo-detector. Immediately after the detector, a low pass (homodyne) or band pass (heterodyne) filter is used. When the beat frequency falls within the filter bandwidth, a high signal is obtained, and when it is out of the range of the filter, a low signal is obtained. Thus, varying the EO modulation frequency yields a scan that corresponds to the acoustic spectrum of the vibrating surface. A simulation of the system with a low pass filter is shown in Fig. 2, calculated using the following equation:

$$I(t) = r(1 - r)I_o \left[2 + 2\cos \left\{ \left(\frac{2\pi}{\lambda} \right) [\Delta_s \cos(2\pi f_s t) - \Delta n_{EO} n_{eff} L \cos(2\pi f_m t) + \phi_d] \right\} \right]$$

where I is the output light intensity, r is the splitting ratio of the directional coupler, I_o is the input intensity, λ is the free space wavelength, Δ_s is the vibration amplitude, L and n_{eff} are the length

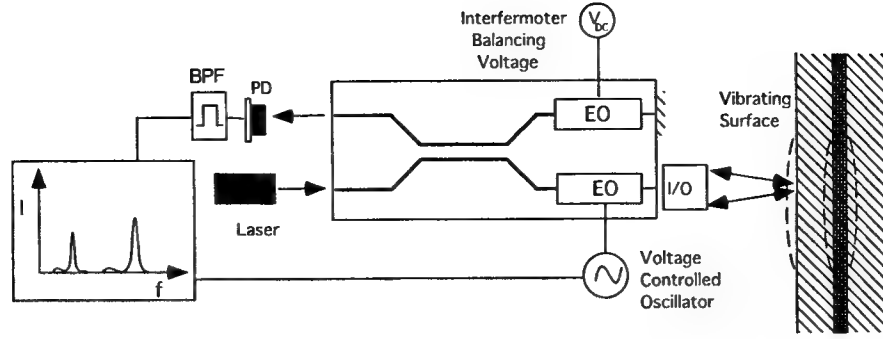


Figure 1: Simplified schematics of polymer integrated optical acoustic spectrum analyzer

and effective index of the EO modulator, respectively, and Δn_{EO} is the change in the index due to EO modulation. f_s and f_m are the acoustic and EO modulation frequencies, respectively, and ϕ_d is the phase difference between the arms of the interferometer, which is set to zero.

The important parameters in acoustic measurements are the frequency of vibration, the amplitude, and the relative phase. The vibration frequency is easily extracted from the spectrum, by the location of the peaks. At high amplitude vibrations (on the order of laser wavelength,) the spectrum shows additional orders, which can be utilized to calculate the amplitude. At low amplitudes, the signal obtained from the scan is linearly proportional to the mirror vibration. The system can be calibrated by comparing the heterodyned amplitude to the amplitude of the EO modulation, which is detected when $2f_m$ falls within the filter bandwidth. The relative phase of the vibration can also be obtained from the shape of the resonant peaks, which will be discussed elsewhere [4].

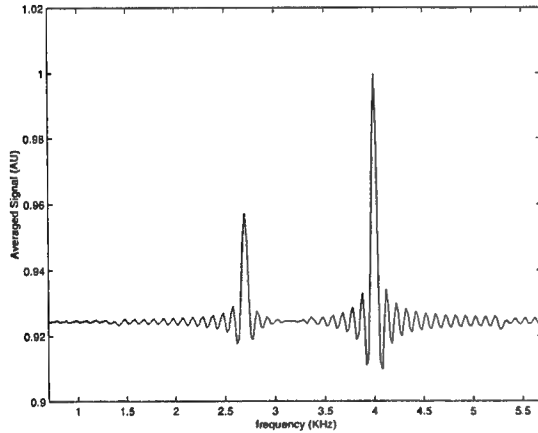


Figure 2: Simulation of the acoustic spectrum analyzer with two vibration frequencies

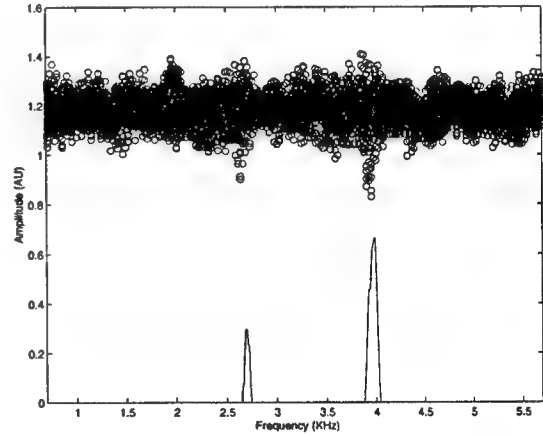


Figure 3: Measurement in heterodyne configuration, with band-pass filter set between 50 and 100 Hz. Cumulative data (circles) over 10 spectral scans, and the post processed data (solid)

The active material used in the device is a thermosetting chromophore/polymer system, FTC [5], which is thermally crosslinked during poling. The $r_{33} = 40 \text{ pm/V}$ at $1.06 \text{ } \mu\text{m}$, and is capable of modulation over 100 GHz [6]. The active layer is sandwiched between an upper and lower cladding.

The waveguides are patterned using UV lithography, and reactive ion etching (RIE). The final device length is 4 cm long. The input/output of the device is provided by fiber pigtails, with the exception of the reference arm, where the endface of the waveguide is Au coated to provide back reflection.

Initial experiments were conducted using a mirrorized low frequency piezo element as an acoustic source. Two drive frequencies were used, 2.7 and 4 KHz, set at different amplitudes. The optical source was a 1.3 μ m diode laser. The system was used in heterodyne configuration, with the band-pass filter set between 50 and 100 Hz. Ten consecutive scans were made, and the cumulative data plotted in Fig. 3 (circles) was post-processed to yield cleaner spectrum (solid line). Because of heterodyning, the 1/f detector noise was eliminated, and the noise due to the slow drift of the interferometer was greatly reduced.

To test system operation in extreme conditions, we used a sample with a directional coupler of 1000:1 ratio, which results to additional 24 dB loss compared to 50:50 splitter. Furthermore, the interferometer was not balanced. In such adverse conditions, we were able to detect signals with SNR = 10, and $\Delta_s = \lambda/10$. When a 50:50 splitter is used, the signal to noise ratio will increase by a factor of 250, and we expect Δ_s to be in the sub-nanometer range.

In conclusion, we have demonstrated a scanning heterodyne acoustic spectrum analyzer using polymer integrated optics, which has the potential to operate from DC to GHz frequencies. Proof of concept experiments show capability of the system to detect multiple acoustic resonances in noisy environments. At the time of the talk, we will present device operation at higher (1-2 GHz) frequencies, and discuss its application for thin film characterization.

References

- [1] G. Tas, R. J. Stoner, H. J. Maris, G. W. Rubloff, G. S. Oehrlein, and J. M. Halbout, "Noninvasive picosecond ultrasonic detection of ultrathin interfacial layers: CF at the Al/Si interface," *Appl. Phys. Lett.* **61**, 1787-1789 (1992).
- [2] C. Gorecki, "Sub micrometric displacements by an all fiber laser heterodyne interferometer using digital phase demodulation," *J. Optics* **26**, 29-34 (1995).
- [3] F. Tian, R. Ricken, and W. Sohler, "High performance integrated acousto-optical heterodyne interferometer in LiNbO₃," *OFS '93 Florence*, 263-266 (1993).
- [4] A. Yacoubian, "High frequency acoustic spectrum analyzer based on polymer integrated optics," Ph. D. dissertation, University of Southern California, in prep.
- [5] F. Wang, "Design, synthesis and characterization of novel organic chromophores and polymers for electro-optic modulator applications," Ph. D. dissertation, University of Southern California (1998).
- [6] D. Chen, H. R. Fetterman, B. Tsap, A. Chen, and W. H. Steier, "Next generation ultra-high frequency integrated EO modulators," *OSA Technical Digest Series* **14**, 224-225 (1997).

Circular-difference effects in second-harmonic generation from thin films

Thierry Verbiest, Sven Van Elshocht, Sonja Sioncke, Martti Kauranen, and André Persoons
Laboratory of Chemical and Biological Dynamics, K. U. Leuven, Celestijnenlaan 200 D, B-3001 Heverlee,
Belgium
Tel: +32-16-32.71.71 Fax: +32-16-32.79.82 Email: thierry@lcbdiris.fys.kuleuven.ac.be

Chirality is equivalent to the lack of mirror planes in a molecule or a material. In linear optics, chiral molecules give rise to optical activity or circular-difference effects, i.e., the interaction with left- and right-hand circularly-polarized light is different. Such effects exist also in nonlinear optics. For example, second-harmonic generation (SHG) from chiral, isotropic surfaces is sensitive to the handedness of incoming circularly-polarized light. Circular difference effects (ΔI) in SHG can be expressed as $\Delta I = I_{\text{left}}(2\omega) - I_{\text{right}}(2\omega)$, where $I_{\text{left}}(2\omega)$ and $I_{\text{right}}(2\omega)$ are the SHG intensities for left- and right-hand circularly-polarized fundamental excitation.

Optical activity is usually associated with the chiral structure of a molecule or a material. However, under certain experimental conditions, even achiral molecules can give rise to optical activity effects. For example, anisotropic achiral surfaces exhibit optical activity in SHG if the experimental geometry does not possess mirror planes. Such optical activity was recently demonstrated in SHG from Langmuir-Blodgett films with C_{1h} symmetry. The observed circular-difference effects reverse sign as the handedness of the experimental geometry is reversed and vanishes when the setup possesses a mirror plane.

In this paper, we investigate circular-difference effects in anisotropic chiral samples. For such samples, both chirality and anisotropy should give rise to circular-difference effects in SHG. The sample studied was a Langmuir-Blodgett film having a chiral C_2 surface symmetry. The sample is mounted on a

rotation stage that allows for rotation around the surface normal (Fig. 1). The azimuthal rotation is characterized by the angle ϕ and the double arrows on the sample in Fig. 1 indicate the two-fold symmetry of the sample. The fundamental laser beam (wave vector k , p- and s-polarized components) is incident on the sample at an angle of 45° . The intensity of the second-harmonic light emanating from the sample is measured for left-and right-hand circularly-polarized fundamental excitation and $\Delta I = I_{\text{left}}(2\omega) - I_{\text{right}}(2\omega)$ is calculated. This procedure is repeated for several azimuthal rotation angles ϕ . Sufficient polarization purity of the experiment is always verified by making sure that no circular-difference effects are observed in the second-harmonic intensity generated from achiral isotropic samples.

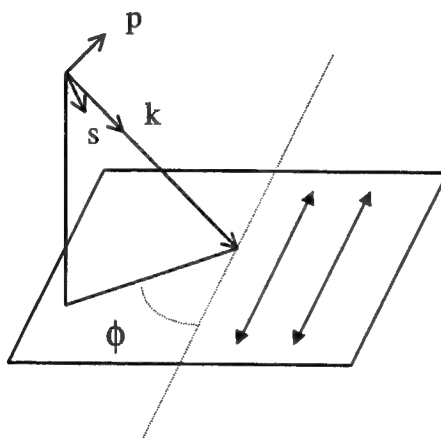


Fig. 1: Experimental geometry.

A plot of ΔI (in arb. units) vs the azimuthal rotation angle ϕ is shown in Fig. 2. It is clear from Fig. 2 that the two-fold symmetry of the sample is reflected in the experimental data and that the circular-difference effects are highly dependent on the azimuthal rotation angle of the sample in the setup. It can be theoretically shown that for a sample belonging to the C_2 symmetry group, the circular-difference effects ΔI can be described by an equation of the type

$$\Delta I = a_\infty + a \sin(2\phi) + b \cos(2\phi) + c \sin(4\phi) + d \cos(4\phi) \quad (1)$$

where a_∞ represents an isotropic contribution to the circular-difference effect. This contribution originates from the chirality of the sample. The other terms represent the anisotropic contribution to the circular-difference effect. A theoretical fit of the experimental data to Eq. 1 (Fig. 2, solid line) gives a nonzero value of a_∞ , indicating the chirality of the sample. Nonzero values of the other terms in Eq. 1 represent the anisotropic contribution to the observed circular-difference effects.

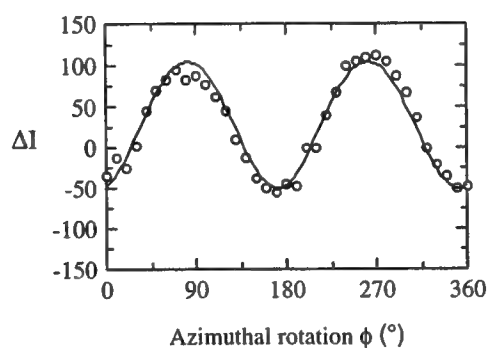


Fig. 2: Circular-difference effect (arb. units) vs azimuthal rotation angle

In conclusion, we have shown that it is possible to discriminate between contributions of chirality and anisotropy to the circular-difference response in SHG from thin films. Besides the fundamental importance of such a study in the field of chirality, we believe that the present study will improve our understanding of nonlinear optical effects in organic thin films.

- [1] J.J. Maki, T. Verbiest, M. Kauranen, S. Van Elshocht, A. Persoons, J. Chem. Phys. **105**, 767 (1996)
- [2] T. Verbiest, M. Kauranen, Y. Van Rompaey, A. Persoons, Phys. Rev. Lett. **77**, 1456 (1996)

High frequency demodulation of multi-photon fluorescence in femtosecond hyper-Rayleigh scattering experiments at both 800 and 1300 nm

Geert Olbrechts, Koen Clays, Kurt Wostyn and André Persoons

Center for Research on Molecular Electronics and Photonics, University of Leuven,

Celestijnenlaan 200D, B-3001 Leuven, BELGIUM

geert.olbrechts@fys.kuleuven.ac.be

tel: +3216327171

fax: +3216327982

Over the last ten years, hyper-Rayleigh scattering (HRS) has been used as a tool to determine the first hyperpolarizability value of organic chromophores in solution^[1]. The molecular second-order properties of several new classes of chromophores, *e.g.* octopoles and ionic chromophores, have been envisaged with this technique since the alternative, Electric Field Induced Second Harmonic Generation (EFISHG), does not allow the characterization of such materials. The EFISHG technique uses an electric field to orient the (dipolar) chromophores in the solution. In this way the centrosymmetry of the solution is broken and a coherent second-harmonic signal can be detected. In the HRS technique, temporal orientational fluctuations of the chromophores in the laser focus result in small deviations from the centrosymmetry. Here, incoherent second-harmonic scattered light is generated from solution. As a result, the first hyperpolarizability value β of each noncentrosymmetric chromophore of whatever symmetry or composition is accessible by this technique. Moreover, the knowledge of the second hyperpolarizability value γ and the dipole moment μ , needed for the calculation of the first hyperpolarizability value from an EFISHG measurement become superfluous. From an HRS measurement an averaged first hyperpolarizability value can be retrieved immediately. Only recently it was realized that multi-photon fluorescence, if present, might influence the measured first hyperpolarizability values^[2]. For some chromophores, the two-photon anti-Stokes band as well as the three photon Stokes band can spectrally overlap with the narrow HRS peak. As the detected signal at the second-harmonic wavelength is then enlarged, the first hyperpolarizability value will be overestimated. Several schemes to correct for this overestimation have been proposed in the literature. It was suggested to shift the fundamental wavelength further in the near infrared region as to move the second-harmonic wavelength away from the absorption bands of the chromophore. As this might work for one chromophore in particular it is not a general solution to the fluorescence problem. A second approach is based on the difference in spectral width. As the fluorescence bands are broad compared to the narrow HRS peak, the fluorescence band can be interpreted as a background and subtracted^[3]. However, this spectral background subtraction technique is reported as time consuming. An elegant solution to the problem is based on the difference in response time between (multi-photon) fluorescence, characterized by a fluorescence lifetime τ , and the immediate hyper-Rayleigh scattering process^[4]. A high frequency amplitude modulation of the fundamental beam will then result in a time delayed (out-of-phase) behaviour of the fluorescence signal whereas the immediate HRS signal will still be in phase. Together with this out-of-phase behaviour an amplitude demodulation will be observed. As such, at sufficiently high amplitude modulation frequencies, the amplitude of the fluorescence signal will tend to zero as the amplitude of the HRS signal remains equal. As a result, the measured signal amplitude at these very high frequencies represents only the HRS process. To obtain these high amplitude modulation frequencies, a high repetition rate femtosecond laser is used instead of an external modulator. As the Fourier spectrum of such a femtosecond pulse train is almost flat over several gigahertz and consists of all harmonics of the repetition rate, a number of amplitude modulation frequencies (harmonics of the repetition frequency) are immediately available from the Fourier spectrum of the short laser pulses. As the

Fourier spectrum of the detected HRS signal at the second harmonic wavelength represents the response of the sample to all amplitude modulation frequencies at the same time, one measurement frequency has to be filtered out. This is done by cross correlation of the whole Fourier spectrum with the desired amplitude modulation frequency electronically generated by a signal generator. As only the harmonics of the repetition rate are available as amplitude modulation frequencies, the selected frequency should be a multiple of the repetition rate. Moreover, as to avoid a dc signal, a small low frequency (700 Hz) shift between the desired amplitude modulation frequency and the frequency generated by the signal generator is introduced. The obtained low frequency signal is then measured by a low frequency lock-in-amplifier (LIA). To avoid phase noise problems, the cavity length, corresponding to the repetition frequency of the laser, is stabilized by the introduction of a piezo mounted cavity mirror. The piezo corrects for any deviation between the actual repetition frequency and the frequency of an ultra stable 80 MHz clock. Moreover, the signal generator used for the cross-correlation detection is synchronized to this 80 MHz clock as well. Figure 1 displays the detailed setup of the experiment.

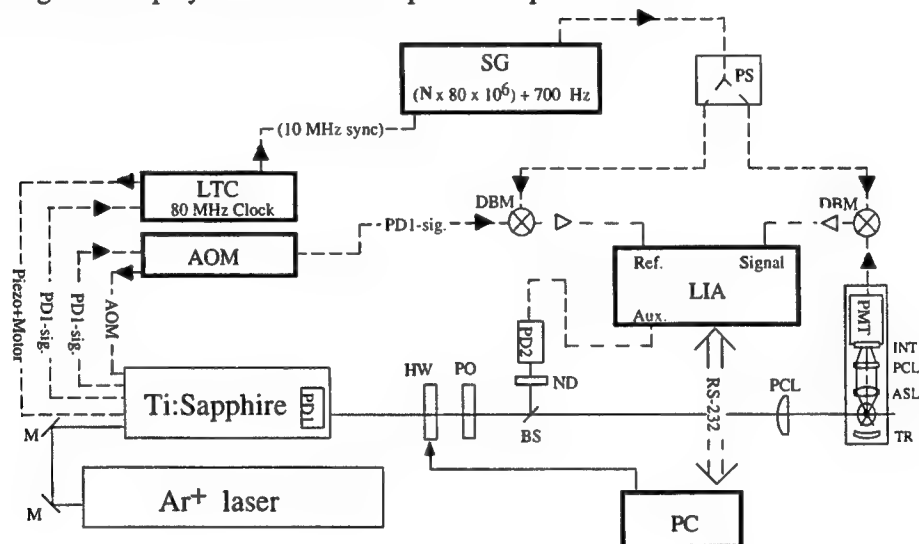


Figure 1: Experimental set-up. LTC: Lok-To-Clock®; AOM: acousto-optic modulator; SG: signal generator; PS: power splitter; LIA: Lock-In-Amplifier; PC: personal computer; PMT: photomultiplier tube; DBM: double balanced mixers; N: harmonic number of the repetition frequency (80 MHz); PD1-sig.: Photodiode signal 1; PD1: photodiode 1; PD2 photodiode 2; ND: neutral density filter; HW: half-wave plate; PO: polarizer; M: routing mirrors; Aux.: auxiliary input of the LIA; Ref.: reference input; BS: beamsplitter; PCL: plano convex lens; INT: interference filter; ASL: aspheric lens; TR: total concave reflector; 10 MHz sync: 10 MHz synchronization circuit

The femtosecond laser (Tsunami, Spectra Physics) uses a Ti:Sapphire crystal. For this medium the wavelength of maximal emission is 800 nm. Whereas some chromophores can be characterized at this wavelength, the second harmonic wavelength (400 nm) is too close to resonance for the majority of chromophores to obtain reliable first hyperpolarizability values. To shift the fundamental wavelength further into the infrared region, an optical parametric oscillator (OPO) was introduced in the setup. This OPO can be tuned between 1150 nm and 1500 nm with two optic sets. Up to now, only measurements at 1300 nm have been performed. The output power of the OPO is about 500 mW, the pulse duration about 100 femtoseconds. The ability of the technique to suppress fluorescence contributions to the HRS signal has been unequivocally demonstrated by measurements on some well known reference compounds as 4-methoxy-4'-nitrostilbene (MONS) and 4-(N,N-dimethylamino)-4'-nitrostilbene (DANS)^[5]. The β -values of

MONS and DANS are $(16 \pm 4) \times 10^{-30}$ and $(110 \pm 10) \times 10^{-30}$ respectively. The capability of the technique to fully explore all HRS advantageous has been demonstrated on an ionic, fluorescent chromophore 4-[4-(N,N-methyl-octadecylamino)styryl]-1-methyl-pyridinium bromide (MO)(Fig.2).

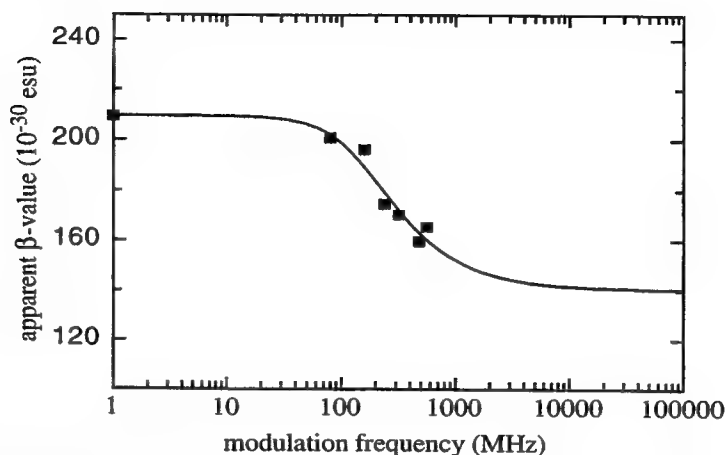


Figure 2: Visual representation of the demodulation of the β -value as a function of the modulation frequency. The full line is the fitted curve which reveals an extrapolated fluorescence-free β -value at high modulation frequencies of $(140 \pm 10) \times 10^{-30}$ esu for the MO chromophore.

The apparent first hyperpolarizability value has been plotted versus the amplitude modulation frequency. As the amplitude modulation frequency increases, the fluorescence signal becomes demodulated. In the limit of very high amplitude modulation frequency, the fluorescence-free hyperpolarizability value results. In the case of MO a fluorescence-free β -value of $(140 \pm 10) \times 10^{-30}$ esu is obtained. If no fluorescence is present, no demodulation would be observed and the apparent hyperpolarizability value would be constant. Recently, the β -values of some subphthalocyanines, *i.e.* chloro[2,3,9,10,16,17-hexa-alkylthiosubphthalocyaninato] boron(III) homologues with as the peripheric alkyl substituent an octyl-, decyl, dodecyl-, or hexadecyl-chain have been measured at 1300 nm as well. The measured β -value was $(190 \pm 30) \times 10^{-30}$ independent of the alkyl chain length whereas the β -value obtained from classical HRS with fluorescence contributions was $(1760 \pm 30) \times 10^{-30}$. Hyperpolarizability values of the popular dimethylaminostilbazolium (DAST) chromophores have been measured as well. Here, the effect of the conjugation length in the NLO moiety on the β -value in the case of ionic, fluorescent chromophores was reenvisioned resulting in a maximum instead of a saturation behaviour.

We have shown that it is possible to suppress multi-photon fluorescence at both 800 nm and 1300 nm. More general, however, it also shows that shifting the fundamental to longer wavelengths is not a general solution to the fluorescence problem in hyper-Rayleigh scattering. Even at these long wavelengths, serious fluorescence contributions can be measured as is illustrated by the subphthalocyanines.

References:

- [1] K. Clays and A. Persoons, *Rev. Sci. Instrum.* **63**, 3285 (1992)
- [2] M.C. Flipse, R.d. Jonge, R.H. Woudenberg, A.W. Marsman, C.A. van Walree and L.W. Jenneskens, *Chem. Phys. Lett.* **245**, 297 (1995).
- [3] N.W. Song, T.-I. Kang, S.C. Jeoung, S.-J. Jeon, B.R. Cho and D. Kim, *Chem. Phys. Lett.* **261**, 307 (1996).
- [4] G. Olbrechts, R. Strobbe, K. Clays, and A. Persoons, *Rev. Sci. Instrum.* **69**, 2233 (1998)
- [5] G. Olbrechts, K. Wostyn, K. Clays, and A. Persoons, *Opt. Lett.* **24**, 403 (1998)

Hyper-Rayleigh Scattering of Nonlinear Optical Chromophores at 1064 nm and 1907 nm

Jeffrey N. Woodford and C. H. Wang

Department of Chemistry, University of Nebraska-Lincoln, Lincoln, NE 68588-0304

jwoodfor@unlgrad1.unl.edu, chwang@unlinfo.unl.edu

Alex K.-Y. Jen

Department of Chemistry, Northeastern University, Boston, MA 02116

ajen@lynx.neu.edu

Over past decades, organic molecules have been extensively investigated for applications in nonlinear optical (NLO) devices. In contrast to inorganic materials (such as KDP and lithium niobate, etc.), a great variety of organic molecules can be devised for such applications because of the fast nonlinear optical response and flexibility of synthetic schemes. The many organic synthetic possibilities coupled with very fast optical response thus provide a rich background for molecular engineering to enhance optical nonlinearity. The essence of second-order NLO materials are molecules that exhibit large first hyperpolarizabilities, β .

Until recently, the only method in widespread use for measuring β was the electric field induced second harmonic generation (EFISHG) technique. This method involves the application of a static electric field to a liquid solution containing the chromophore, to induce polar order and thus permit second harmonic generation to be observed. The EFISHG technique is formally a third-order process, requiring a determination of the second hyperpolarizability (γ) as well. Furthermore, the EFISHG technique measures the projection of β onto the ground-state dipole moment ($\mu \cdot \beta$); thus a separate determination of μ is also required. And since the technique relies upon a static electric field to induce polar order, molecules lacking a ground state dipole moment, or ionic chromophores forming a conducting solution, may not be studied by the EFISHG technique.

An experimental technique based upon two-photon light scattering (TPS) has recently been reintroduced for the determination of β . TPS involves irradiating a sample with photons at frequency ω and detecting scattered photons at frequency 2ω . It is often referred to as hyper-Rayleigh scattering (HRS). Many of the experimental difficulties associated with EFISHG can be overcome by using the TPS technique instead: no static orienting field is required, no independent measurements of γ or μ are required, and both ionic and nonpolar chromophores may be studied via TPS. Since the conversion efficiency of second-order light scattering is low, a laser that produces short light pulses of high energy is required to generate

scattered photons at 2ω . The traditional laser used for TPS is the Nd:YAG operating at 1064 nm, with the scattered photons having a wavelength of 532 nm.

Theoretical studies and experimental results have shown that organic chromophores consisting of a strong electron donor and a strong electron acceptor separated by a π -electron conjugation path (D- π -A chromophores) can result in exceptionally large β values. Indeed a simple two-level quantum model for D- π -A type chromophores predicts β is proportional to the square of the transition dipole moment, and proportional to the difference in the dipole moments of the excited and ground states. Thus, chromophores with large absorption coefficients for the first excited state, and chromophores which have a large difference in the dipole moment between the ground state and the first excited state, will tend to have large values for the first hyperpolarizability.

However, increasing the ground state dipole moment by lengthening the π -electron chain tends to shift the wavelength of maximum absorption to the first excited state towards lower energies, and thus closer to the second harmonic of the excitation source. Thus, if the organic chromophore undergoes absorption the second harmonic, competing linear and nonlinear effects can also be generated. If the sample undergoes linear absorption at the second harmonic, the scattering intensity will be reduced. If the sample undergoes nonlinear absorption at the second harmonic, the generation of nonlinear fluorescence will increase the amount of light detected at the second harmonic. Furthermore, the location of a material resonance near the second harmonic of the incident light source will result in a large resonance enhancement of the measured β value, which will seriously overestimate the chromophore's NLO potential.

There have been several strategies developed in order to circumvent or eliminate these experimental difficulties. A simple Beer's Law correction may be used to compensate for linear absorption. A monochromator may be employed to scan around the second harmonic, to discriminate between the nonlinear fluorescence and the nonlinear scattering in the frequency domain. Another method involves using a picosecond or femtosecond laser to discriminate between the nonlinear fluorescence and the nonlinear scattering in the time domain. A third method is to use a femtosecond laser and modulate its repetition rate in order to suppress the nonlinear fluorescence entirely, so that only the nonlinear scattering is detected. While these methods are quite successful in properly correcting for the linear absorption and nonlinear fluorescence problems, none of them may be used to correct for the resonance enhancement of the measured β value. The aforementioned two-level quantum model (TLM) predicts β can be separated into an intrinsic molecular parameter, β_0 , times a dispersion factor,

$$D(\omega) = \left[\left(1 - \frac{\omega^2}{\omega_0^2} \right) \left(1 - \frac{4\omega^2}{\omega_0^2} \right) \right]^{-1}, \text{ where } \omega \text{ is the frequency of the incident laser source and } \omega_0 \text{ is the}$$

resonance frequency corresponding to the dipole transition between the ground state and the first excited state. However, recent experimental studies have cast doubt upon the validity of the TLM. In two separate studies, independent of our laboratory, the TLM has failed to predict correctly the β values measured at different wavelengths. Thus, we conclude that the resonance enhancement of the first hyperpolarizability may not be properly accounted for using current theoretical methods.

It appears, then, that one way to overcome the resonance enhancement problem is to avoid altogether the spectral region near the location of the material resonance. This may be accomplished by using a fundamental wavelength other than the traditional 1064 nm generated by a Nd:YAG laser, and shifting the incident wavelength further out into the infrared. We have accomplished this task by using a Nd:YAG-pumped H₂ Raman shifter, which generates ~100 mW of radiation at a wavelength of 1907 nm. This wavelength is far enough from the resonances of today's NLO chromophores that the competing process of two-photon absorption-induced fluorescence is absent. Furthermore, using this long wavelength to measure β results in a truer estimation of the NLO potential of these organic chromophores, since resonance enhancement is greatly reduced.

The development of radiation sources of multiple wavelengths results in the possibility to gather experimental data towards creating a more accurate dispersion model for β . The TLM, as originally proposed, neglects damping near the second harmonic; thus, as $\omega_0 \rightarrow 2\omega$, $\beta \rightarrow \infty$, a clearly unphysical result. Including the effects of resonant damping in the first excited state in the TLM yields an alternative expression for the dispersion factor, $D(\omega, \gamma)$, given as follows:

$$D(\omega, \gamma) = \frac{1}{3} \left\{ \left[\frac{2\omega_0}{\omega_0 + 2\omega} - \frac{\omega_0^2}{\omega_0^2 - \omega^2} + \frac{2(\omega_0^2 - 2\omega\omega_0 - \gamma^2)}{(\omega_0 - 2\omega)^2 + \gamma^2} \right]^2 + \frac{16\gamma^2(\omega_0 - \omega)^2}{[(\omega_0 - 2\omega)^2 + \gamma^2]^2} \right\}^{1/2}$$

where γ is the damping constant for the first excited state. As $\gamma \rightarrow 0$, $D(\omega, \gamma) \rightarrow D(\omega)$ of the simple TLM above. This presentation will discuss experimental results at the fundamental wavelengths of 1064 nm and 1907 nm for a series of novel NLO D- π -A chromophores. Structure-function relationships between the measured β value and the chemical structure of the NLO chromophores will be elucidated. The results upon application of the above dispersion model on the measured values of β will be presented.

Remarkable enhancement of first hyperpolarizabilities of Polynorbornenes studied by hyper-Rayleigh scattering. C. C. Hsu et al. Department of Physics, Chung Cheng University, Ming-Hsiung, Chia-Yi, Taiwan. Tel: 886-5-242-8173.

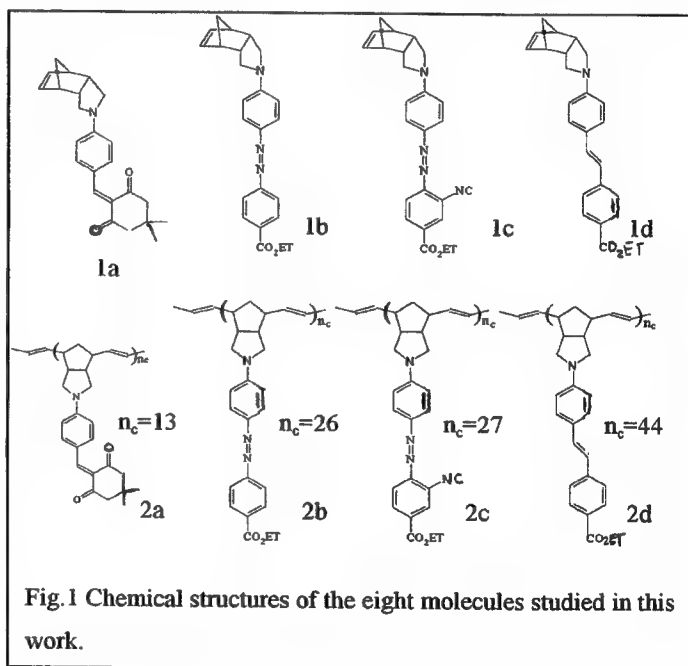
Hyper-Rayleigh scattering (HRS) has been shown to be a useful technique to determine the first hyperpolarizability (β) of nonlinear optical (NLO) chromophores [1-4]. Recently, Kauranen et al. have applied HRS to investigate the second order optical nonlinearity of polymers which contain NLO-chromophores as side groups [5-6]. The β values of the polymers were enhanced with respect to those of free NLO chromophores. This indicates that the polymer backbone is very rigid and the NLO-chromophores are attached to the polymer backbone in a non-centrosymmetric arrangement. Further, the NLO-chromophores are orientationally correlated and hence contribute coherently to the β value of polymers [5-6]. On the contrary, in other previous study no enhancement of the β value was reported for chromophores incorporated into other type of polymer with a flexible backbone [7]. It is learned from these results that the rigidity of the polymer backbone is essential to the enhancement of the β values of polymers. In this paper, the HRS technique is not only employed to study the rigidity but also used to investigate the conformation of the of the polynorbornenes polymers.

Fig. 1 shows the chemical structures of the samples. Samples 1a, 1b, 1c, and 1d, are the substituted norbornenes monomers. Samples 2a, 2b, 2c, and 2d, are the substituted poly-

norbornenes polymers that have in order 13, 26, 27, and 44, repeating units of the monomers shown above. The semi-empirical molecular orbital (MO) and open force field (OFF) calculations showed that the syndiotactic and isotactic forms are two possible conformations [8]. The calculations showed that the syndiotactic form has a stretched chain while the isotactic chain results in random coils [8]. The pendant NLO chromophores are orientationally correlated in the former structure and the β values of the polynorbornenes will be enhanced with this structure. On the contrary, no β enhancement will be observed with the random coiled isotactic structure.

Consequently, the HRS results can be used to estimate the structure of the polynorbornenes.

For all samples studied in this work we summarize in Table 1, the first hyperpolarizabilities β^{HRS} measured with the 1064 nm and 1480 nm lasers, and their dispersion-free counterpart β_0 calculated from the un-damped two states model. Also shown in the table are the molecular weight, the number of chromophores in a polymer chain n_c , and the absorption maximum λ_{max} in $CHCl_3$. The absorption spectra of the monomer and the polymer samples are similar although the λ_{max} values of the polymer samples are little blue shifted in comparison to those of the corresponding monomer samples. This agrees with the



conjecture that the electron conjugation localizes in the side chain NLO-chromophores of the polymers, therefrom the optical non-linearity mainly arises. As such the non-linearity contribution from the polymer backbone can be neglected. As shown in the Table 1, the β^{HRS} (1064 nm) values are much larger than the β^{HRS} (1480 nm) values for all the samples. This is attributed to more favorable one- and two-photon resonance enhancements on the first hyperpolarizability for the measurement using the 1064 nm laser. After correcting for the one- and two-photon resonance enhancements, the β_0 (1064 nm) and β_0 (1480 nm) values are close except for the samples 1b, 1c, and 1d. The larger β_0 (1064 nm) values of the samples 1b, 1c, and 1d are caused by the two-photon absorption induced fluorescence (TPF). The good agreement of the β_0 (1064 nm) and β_0 (1480 nm) values indicates that the un-damped two states model is valid for all the samples studied in this work. Although the TPF can enhance the β_0 (1064 nm) values of the monomer samples 1b, 1c, and 1d, large enhancement on the β_0 (1064 nm) values of the polymer samples are still observed. These β_0 enhancements help us to deduce the following conclusions. That is: (1) the conformation of the substituted polynorbornenes is syndiotactic; (2) the backbone of the substituted polynorbornenes is rigid; and (3) the pendant side group chromophores are orientationally correlated, and each chromophore contributes coherently to the hyperpolarizability of the polymer.

Table 1 Photo-physical properties of the samples.

sample	M_w g/mol	n_c	$\lambda_{max}(nm)$	β^{HRS} (1480nm) (10^{-30} esu)	β^{HRS} (1064nm) (10^{-30} esu)	β_0 (1480nm) (10^{-30} esu)	β_0 (1064nm) (10^{-30} esu)
1a	313		475	59	211	31	34
2a	4228	13	469	329	955	178	171
1b	387		450	108	416	54	97
2b	10000	26	435	874	1525	459	421
1c	432		495	65	758	32	80
2c	11700	27	487	557	2591	283	332
1d	385		393	42	229	28	90
2d	17000	44	384	726	1146	459	478

A plot of the β_0 (1480 nm) enhancement versus n_c , a linear dependence with a slope of 0.36 is obtained. Consequently, from this experimental result, the β_p^{HRS} can be written as

$$\beta_p^{HRS} = 0.36n_c\beta_{m,kkk} \quad (1)$$

Where β_p^{HRS} and $\beta_{m,kkk}$ are the dispersion free hyperpolarizabilities of the polymer and monomer samples, respectively. This indicates that each of the pendant chromophores contributes 36% of its monomeric value to that of the polymer. A simple theoretical syndiotactic structure for the polymer samples is used to find the theoretical relationship between β_p^{HRS} and $\beta_{m,kkk}$, and compare with the experimental result (Eq. 1). In this simple theoretical syndiotactic structure (Fig. 2) we assume the polymer backbone is stretched along the z-axis and the side chain chromophores are all perpendicularly attached to the polymer

backbone ($\theta=90^\circ$) and uniformly distributed, i.e. $-60^\circ < \phi < 60^\circ$. Since the non-linearity contribution is only from the pendant NLO-chromophores, the first hyperpolarizability of the polymer can be calculated from the vector sum of all contributions from the chromophores. By projecting the $\beta_{m,kkk}$ tensor of side chain chromophores onto the polymeric coordinate and vector summing over all of them, the non-vanishing polymeric β tensors in the polymeric coordinate are obtained. Using the Kleinman symmetry and transforming the polymeric β tensors from the polymeric coordinate to laboratory frame, we obtain the theoretical relationship between β_p^{HRS} and $\beta_{m,kkk}$,

$$\beta_p^{HRS} = 0.76n_c\beta_{m,kkk} \quad (2)$$

It indicates that each monomer contributes 76% of its β_0 value to that of the polymer, which is about twice the experimental observation. That the calculated result is higher likely arises from the assumptions made. First, the polymer is assumed to be syndiotactic with a stretched out backbone structure, to which the perpendicularly attached linear-chromophores are uniformly distributed between -60° and 60° . Second, we neglected the interaction between pendant chromophores, with which individual chromophores would have contributed less to the polymer's first-hyperpolarizability. It is noticed that, for poly-isocyanides polymer, the difference between experimental observation and theoretical prediction is somewhat larger [6]. Thus our assumption of the syndiotactic conformation of the substituted poly-norbornenes polymers is after all not unrealistic.

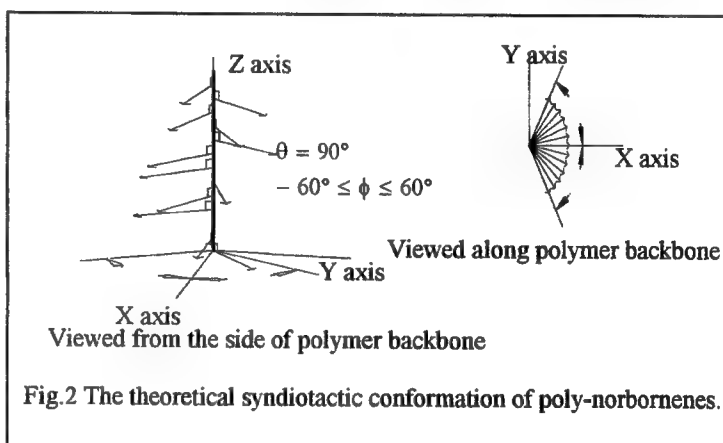


Fig.2 The theoretical syndiotactic conformation of poly-norbornenes.

References

1. K. Clays, and A. Persoons, Phys. Rev. Lett. **66**, 2980 (1991).
2. K. Clays, and A. Persoons, Rev. Sci. Instrum. **63**, 3285 (1992).
3. C. C. Hsu, T. H. Huang, Y. Z. Zang, J. L. Lin, Y. Y. Cheng, J. T. Lin, H. H. Wu, C. H. Wang, C. T. Kuo, and C. H. Chen, J. Appl. Phys. **80**, 5996 (1996).
4. C. C. Hsu, C.F. Shu, T. H. Huang, C. H. Wang, J. L. Lin, Y. K. Wang, and Y. L. Zang, Chem. Phys. Lett. **274**, 446 (1997).
5. M. Kauranen, T. Verbiest, C. Boutton, M. N. Teerenstra, K. Clays, A. J. Schouten, R. J. M. Nolte, and A. Persoons, Science **270**, 965 (1995).
6. T. Verbiest, C. Samyn, C. Boutton, S. Houbrechts, M. Kauranen, and A. Persoons, Adv. Matter, **8**, 756 (1996).
7. O. K. Song, J. N. Woodford, and C. H. Wang, J. Phys. Chem. **106**, 2819 (1997).
8. J. A. Sattigeri, C. W. Shiau, C. C. Hsu, F. F. Yeh, S. Liu, B. Y. Jin, and T. Y. Luh, J. Am. Chem. Soc., **121**, 1607, (1999).

Determining the Fifth Order Nonlinear Optical Susceptibility of a Polydiacetylene Film

Ke Yang and Jayant Kumar

Department of Physics, Center for Advanced Materials, University of Massachusetts Lowell, Lowell, MA 01854

Woohong Kim

Samsung Central Research Institute of Chemical technology, Taejon, Korea 305-380

Sukant Tripathy

Department of Chemistry, Center for Advanced Materials, University of Massachusetts Lowell, Lowell, MA 01854

Polydiacetylenes are known to possess large 3rd order nonlinearity due to their extensively delocalized π -electrons along the backbone.¹⁻⁶ It is expected that these π -conjugated molecules can generate measurable higher order NLO signal. It is very much interesting to investigate the higher order dispersions of NLO susceptibilities, as it helps us to obtain a better understanding of the NLO properties and to design the new materials. Electro-optical techniques⁷⁻²⁵ have been extensively used to characterize the electronic structures and the 2nd and 3rd order nonlinear optical properties of different materials involved in their electro-optical applications. These electro-optical techniques can be further applied to measure the higher order NLO susceptibilities. In this paper, we use electroabsorption spectroscopy to investigate the 5th order nonlinearity of one of the polydiacetylene, poly(BPOD), i.e. poly{[[[8-butoxy carbonyl] methyl urethane]1-(5-pyrimidyl)-octa-1, 3-diyne}.

A film of 3154 Å poly(BPOD) was spin coated on an ITO (indium tin oxide) glass substrate. A layer of Aluminum film was evaporated as the top electrode. The applied sinusoidal electric fields are 80V_{p-p} for both $\Delta I_{2\Omega}$ and $\Delta I_{4\Omega}$, 1kHz for $\Delta I_{2\Omega}$ and 500Hz for $\Delta I_{4\Omega}$. In order to increase the intensity of $\Delta I_{4\Omega}$, no polarizers were used in the measurement since the film has $C_{\infty v}$ symmetry. A beam of light, coming from a tungsten lamp or a xenon lamp through a monochromator, was incident normally on the sample. The electroabsorption signal $\Delta I_{2\Omega}$ and $\Delta I_{4\Omega}$, which are defined as the change in the output intensity I , was detected by a lock-in amplifier set at twice and four times the electrical modulation frequency. When the spectra are measured, a computer was used to synchronize the change of wavelength of the monochromator and the data reading of the lock-in amplifier.

It can be proved that:

$$\frac{\Delta I_{2\Omega}}{I} = -2\pi \cdot \frac{\omega}{c} t_k E_{ac0}^2 \cdot 3 \text{Im} \left[\frac{\chi_{1133}^{(3)}}{\tilde{n}} \right] \quad (1)$$

$$\text{and } \frac{\Delta I_{4\Omega}}{I} = -\frac{\pi}{2} \cdot \frac{\omega}{c} t_k E_{ac0}^4 \cdot 5 \text{Im} \left[\frac{\chi_{113333}^{(5)}}{\tilde{n}} \right] + \frac{\Delta I_{C4\Omega}}{I} \quad (2)$$

where t_k and E_{ac0} are thickness and the amplitude of the applied electric field, and the correction term is given by:

$$\frac{\Delta I_{C4\Omega}}{I} = \frac{1}{4} E_{ac0}^4 \left(2\pi \frac{\omega}{c} t_k 3 \text{Im} \left[\frac{\chi_{1133}^{(3)}}{\tilde{n}} \right] \right)^2 + \frac{9\pi^2 \omega}{2 c} t_k E_{ac0}^4 \text{Im} \left(\frac{[\chi_{1133}^{(3)}]^2}{\tilde{n}^3} \right) \quad (3)$$

The dispersion of $\Delta I_{4\Omega} / I$ and its $\chi^{(3)}$ correction $\Delta I_{4\Omega} / I - \Delta I_{C4\Omega} / I$ (see equation (2) and (3)), are shown in Figure 1. We confirm that the correction is necessary in this case. By performing the experiment and using the Kramers-Kronig relation, the complex spectra of $\chi_{1133}^{(3)}$ and $\chi_{113333}^{(5)}$ can be determined.

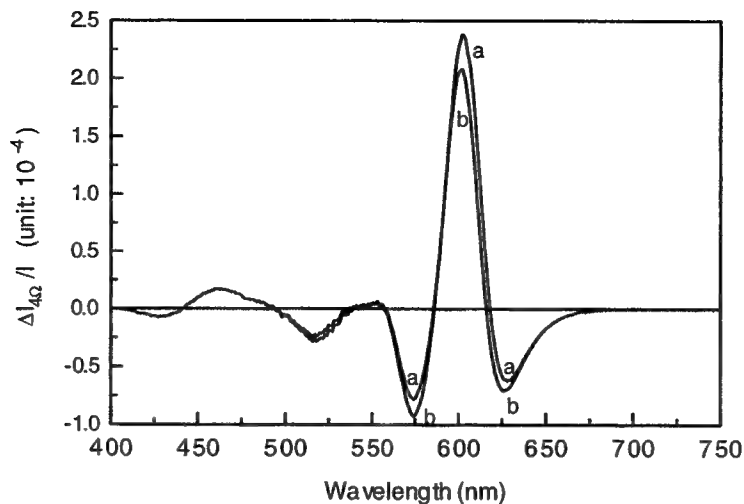


Figure 1. (a) The dispersion of $\Delta I_{4\Omega} / I$, and (b) $\Delta I_{4\Omega} / I - \Delta I_{C4\Omega} / I$, the result after $\chi^{(3)}$ correction.

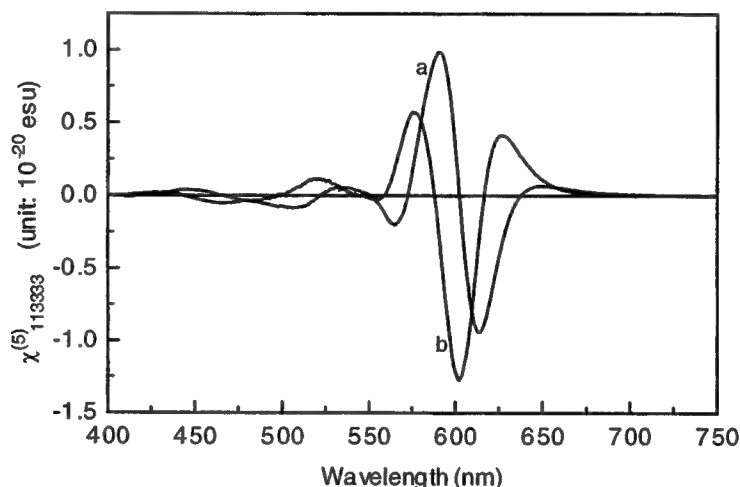


Figure 2. Dispersion of $\chi_{11333}^{(5)}(\omega; \omega, 0, 0, 0, 0)$; (a) is the real part; (b) is the imaginary part. Uncertainty: 6.4×10^{-22} esu.

The dispersions of the real and imaginary part of $\chi_{11333}^{(5)}$ are given in Figure 2. The peak values are of the magnitude of 10^{-20} esu. We can see that there is a sharp negative peak at 602nm and positive peaks near 625nm, 575nm, and 520nm in $\text{Im}[\chi_{11333}^{(5)}]$. Compared with the dispersions of $\text{Im}[\chi_{1133}^{(3)}]$ from 480nm to 750nm and the linear absorption spectrum, these behavior seem to be resonance responses of the two closely situated linear absorption peaks near 530nm and 575nm, which are 2.34 eV and 2.16 eV from the ground state. The behaviors near 440nm in $\text{Im}[\chi_{11333}^{(5)}]$, i.e. a positive peak at shorter wavelength and a negative peak at longer wavelength, are related to a positive peak around 440nm (2.82 eV from the ground state) in $\text{Im}[\chi_{1133}^{(3)}]$. However, there are no linear absorption peaks around 440nm. We believe this is a transition forbidden in linear absorption, activated by the applied electric field.

A model is under development to explain the observed electroabsorption spectra.

In conclusion, the dispersion of $\chi_{113333}^{(5)}(\omega; \omega, 0, 0, 0, 0)$ was determined through electroabsorption spectroscopy. The order of magnitude of $\chi_{113333}^{(5)}(\omega; \omega, 0, 0, 0, 0)$ is 10^{-20} esu. The contribution of $\chi_{3333}^{(3)}$ to $\Delta I_{4\Omega} / I$ is not negligible and needs to be subtracted.

Reference

1. F. Kajzar, J. Messier, J. Zyss, I. Ledoux, *Optics Communications* 45, p133-137(1983).
2. G. M. Carter, Y. J. Chen, S. K. Tripathy, *Appl. Phys. Lett.* 43, p891(1983).
3. C. Sauteret, J. P. Hermann, R. Frey, F. Pradere, J. Ducuing, R. H. Baughman, and R. R. Chance, *Phys. Rev. Lett.* 36, 956(1976).
4. B. J. Orchard, S. K. Tripathy, *Macromolecules* 19, p1844(1986).
5. S. B. Clough, S. Kumar, X. F. Sun, S. K. Tripathy, H. Matsuda, H. Nakanishi, S. Okada, M. Kato, *Nonlinear Optics of Organics and Semiconductors*, Springer-Verlag: Berlin, 1989, p149.
6. W. H. Kim, N. B. Kodali, J. Kumar and S. K. Tripathy, *Macromolecules* 27, p1819(1994).
7. Y. Kawabe, F. Jarka, N. Peygambarian, D. Guo, S. Mazumdar, S. N. Dixit, F. Kajzar, *Physical Review B* 44, 6530(1991).
8. C. Heldmann, L. Brombacher, D. Neher, M. Graf, *Thin Solid Films* 261, 241(1995).
9. K. Yang, W. Kim, J. Kumar, L. Li, S. Tripathy, *Optics Communications* 144, 252(1997).
10. K. Yang, D.-W. Cheong, S. Tripathy, J. Kumar, *Optics Communications* 144, 259(1997).
11. K. Yang, X. Wang, A. Jain, L. Li, S. Tripathy, J. Kumar, *Nonlinear Optics* 19, 215(1998).
12. K. Yang, S. Balasubramanian, X. Wang, J. Kumar, S. Tripathy, *Appl. Phys. Lett.* 73, 3345(1998).
13. C. C. Teng, H. T. Man, *Appl. Phys. Lett.* 56, 1734(1990).
14. J. S. Schildkraut, *Appl. Opt.* 29, 2839(1990).
15. P. Rohl, B. Andress, J. Nordmann, *Appl. Phys. Lett.* 59, 2793(1991).
16. M. Sigelle, R. Hierle, *J. Appl. Phys.* 52, 4199(1981).
17. R. A. Norwood, M. G. Kuzyk, R. A. Keosian, *J. Appl. Phys.* 75, 1869(1994).
18. K. D. Singer, M. G. Kuzyk, W. R. Holland, J. E. Sohn, S. J. Lalama, R. B. Comizzoli, H. E. Katz, M. L. Schilling, *Appl. Phys. Lett.* 53, 1800(1988).
19. M. G. Kuzyk, C. W. Dirk, *Appl. Phys. Lett.* 54, 1628(1989).
20. M. G. Kuzyk, K. D. Singer, H. E. Zahn, L. A. King, *J. Opt. Soc. Am. B* 6, 742(1989).
21. C. Poga, M. G. Kuzyk, C. W. Dirk, *J. Opt. Soc. Am. B* 11, 80(1994).
22. C. Poga, T. M. Brown, M. G. Kuzyk, C. W. Dirk, *J. Opt. Soc. Am. B* 12, 531(1995).
23. K. S. Mathis, M. G. Kuzyk, C. W. Dirk, A. Tan, S. Martinez, G. Gampos, *J. Opt. Soc. Am. B* 15, 871(1998).
24. F. Qiu, K. Misawa, X. Cheng, A. Ueki, T. Kobayashi, *Appl. Phys. Lett.* 65, 1605(1994).
25. H. Ono, K. Misawa, K. Minoshima, A. Ueki, T. Kobayashi, *J. Appl. Phys.* 77, 4935(1995).

Organic Thin Films for Photonics Applications

Poster Session

Saturday, 25 September 1999

SaE

5:45pm–7:00pm

California Ballroom Salons 1,2&3

Design guidelines for molecules with large hyperpolarizabilities for third-order nonlinear optics

U. Gubler, Ch. Bosshard, and P. Günter

Nonlinear Optics Laboratory, Institute of Quantum Electronics, Swiss Federal Institute of Technology ETH, ETH-Hönggerberg, CH-8093 Zürich, Switzerland
gubler@iqe.phys.ethz.ch

R. Martin, R. R. Tykwinski, and F. Diederich

Institute of Organic Chemistry, Swiss Federal Institute of Technology ETH, ETH Zürich, CH-8092 Zürich, Switzerland

V. Alain, M. Blanchard-Desce

Ecole Normale Supérieure, Département de Chimie, 24 rue Lhomond, 75231 Paris Cedex 05, France

The development of fiber and electro-optics led to a large increase in data rates over the last decade. Even higher transmission rates can be achieved in future modulation techniques by using optically induced refractive index changes in $\chi^{(3)}$ materials instead of electrically controlled refractive index changes.

The introduction of all-optical switching based on the nonlinear optical susceptibility $\chi^{(3)}$ critically depends on the development of suitable materials with a large enough nonlinear optical effect. Time responses of the nonlinearity $\chi^{(3)}$ on the femtosecond scale or below are necessary to offer an advantage over electro-optical techniques. Nonlinear susceptibilities $\chi^{(3)}$ created by thermal, orientational, vibrational or the photo-refractive effects are too slow. Excited state effects are potentially fast, but need too long to recover. The pure electronic effect is the only one to meet the ultimate speed requirements for fast all-optical switching and signal processing.

Besides semiconductors and glasses, organic materials with especially designed chromophores are the most promising candidates, offering advantages in material processing and costs, but also causing challenges in chemical and photo-stability. We present in this paper a detailed investigation of the third-order nonlinear optical properties of various molecular systems. From the results, we are able to give new rules for the optimization of the molecular structure and refinements of the established guidelines for the design of even better molecules.

The experimental methods we deployed to characterize the second-order hyperpolarizabilities γ of the molecules (nonlinear susceptibility $\chi^{(3)}$ per molecule) are third harmonic generation (THG) and degenerate four wave mixing (DFWM). In the THG experiment a fundamental wavelength of either 1.9 μm or 2.1 μm was used, in order to obtain the third harmonic wavelength outside the absorption band of the molecules. In the DFWM experiment at a wavelength of 1.047 μm , we used short laser pulses of 10 ps and a low repetition rate of 10 Hz to avoid orientational and thermal contributions to the signal. The measurements have been performed in chloroform solutions, guest-host polymer films, and pure polymeric films.

We focused our work on the two linearly conjugated systems polytriacetylene (PTA) and polyene (fig. 1), and the two-dimensionally conjugated tetraethynylethene (TEE). The monomer units were connected so that larger oligomers or even long polymer chains were built up. The endgroups were substituted by electron donating (D) and accepting (A) groups to tailor the nonlinear optical properties. The TEEs with their two-dimensional framework offer the potential to polymerize in one direction and to add the functionalized donor and acceptor groups laterally, maintaining strong interaction with the backbone conjugation.

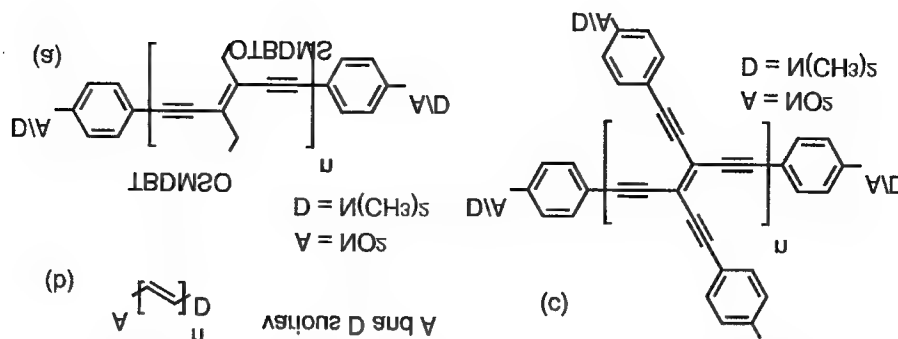
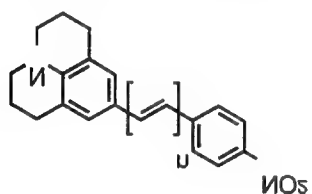


Fig. 1: Molecular systems under investigation: polytriacetylenes (a), polyenes (b), and tetraethynylethenes (c). D and A denote electron donating and accepting groups. The OTBDMS ((tert-butyl)dimethylsilyloxy) lateral groups enhance the solubility of the polytriacetylenes and have no direct influence on the nonlinearity.

For small molecules such as the polyenes the second-order hyperpolarizability γ is largest for asymmetric substituted molecules. The stronger the electron acceptor and donor the larger the nonlinearity. This rule has been assessed for over 20 molecules with no exception for THG. In DFWM the hyperpolarizabilities γ can reach a two photon resonance which enhances the nonlinearity dramatically, leading to the largest values for molecules matching the two photon resonance frequency. For hyperpolarizabilities γ off resonance the above asymmetry rule could also be confirmed. The elongation of the polyene conjugation leads to a superlinear increase, giving an additional path for optimization.



n	γ_{THG} 10^{-36} esu	γ_{DFWM} 10^{-36} esu	γ_{THG} $10^{-48} m^5/V^2$	γ_{DFWM} $10^{-48} m^5/V^2$
1	820	2500	12	35
2	1620	4000	23	56
3	3360	4500	47	63
4	5150	6400	72	89

Fig. 2: Example of a polyene series measured by third harmonic generation and degenerate four wave mixing. The nonlinearity increases with elongation of the polyene backbone. The experimental error is ± 10 percent.

The polytriacetylenes (PTAs) were measured first in the unsubstituted form for different conjugation lengths, what revealed a power law dependence of the second-order hyperpolarizability γ on the number of monomer units $\gamma \sim n^a$, for both THG and DFWM (fig. 3). The exponents a for both THG and DFWM are around 2.5 (fig. 3). The power law for the second-order hyperpolarizabilities measured by THG and DFWM saturates around 10 monomer units or 60 carbon-carbon bonds and increases only linearly for larger number of carbon bonds. The nonlinear susceptibility $\chi^{(3)} \sim \gamma/n$ experiences no further enhancement after saturation has been reached. Measurements on different conjugated molecular systems by other authors have shown similar behaviors with exponents a around 2.5 for off resonance nonlinearities and saturation around 60 carbon-carbon bonds (corresponds to a total length of 7.5 nm). This seems to be the upper boundary for the delocalization length of an electron in a conjugated molecule.

Substitution of the monomer by donor and acceptor groups yields the largest nonlinearity γ for the asymmetric geometry, similar to the polyenes discussed above. For the dimer, the asymmetric and symmetric donor substituted molecule show both the same value for the nonlinearity γ , raising doubts about the validity of the asymmetry optimization rule for longer molecules. Both THG and DFWM exhibit the same trends (fig. 3).

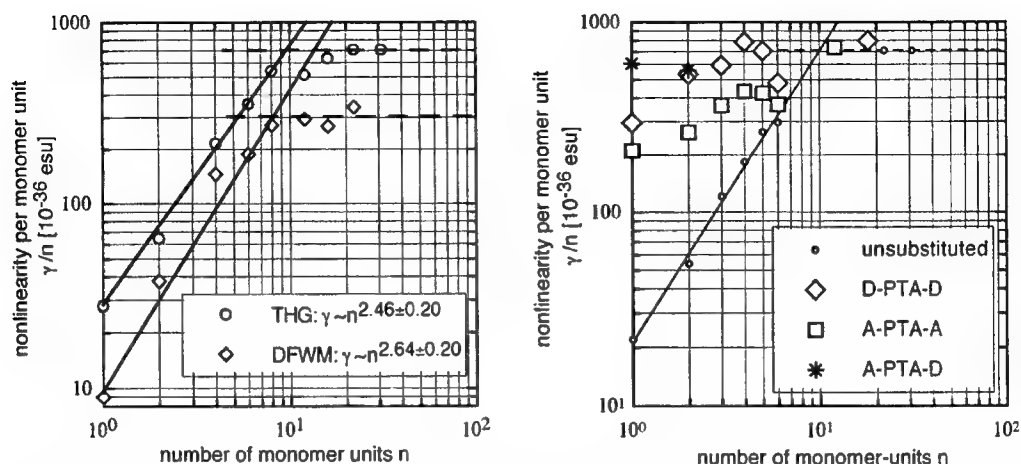
Design guidelines for molecules with large hyperpolarizabilities for 3rd-order NLO, U. Gubler, 3

Fig. 3: Power law scaling with saturation for unsubstituted polytriacylenes PTA measured by third harmonic generation and degenerate four wave mixing (left). Maximal nonlinearity of substituted PTAs for intermediate conjugation length, measured by THG (right). D and A denote electron accepting resp. donating groups, according to figure 1.

For the symmetrically substituted molecules the nonlinearity per monomer unit γ/n is maximal for oligomers of intermediate length (≈ 5 monomers), before reaching the same value as the unsubstituted PTAs in the limit of long molecules. In figure 3 the results by THG of the substituted PTAs are shown. The DFWM measurements (not shown for better legibility of the figure) show the same trends.

The two-dimensionally conjugated TEEs show generally one order of magnitude larger second-order hyperpolarizabilities than their PTA counterparts. For small molecules, the asymmetry rule also holds as observed experimentally and as has been described by a quantum mechanical treatment [1]. From the mono- to the dimer, the nonlinearity increases for all endsubstituted geometries by a factor of 2.5 to 4.5. The double donor species shows a much stronger enhancement than the asymmetric one (figure 4).

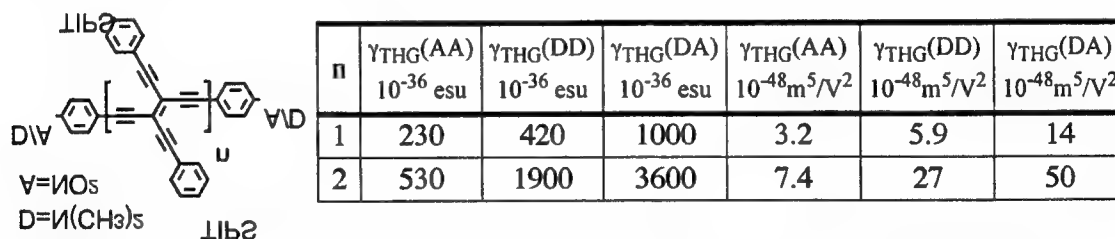


Fig. 4: Increase of the second-order hyperpolarizability γ for endsubstituted tetraethynylethenes going from monomers to dimers. The increase is most pronounced for the double donor substituted molecule (TIPS: triisopropylsilyl)

In conclusion, we have demonstrated the following guidelines for the design of molecules with enhanced third-order nonlinear optical properties within the PTA and TEE families. Optimized molecules should have:

- a long conjugation path, reaching the saturation of nonlinearity per molecule γ/n .
- for small molecules an asymmetric substitution with a strong donor and acceptor.
- two-dimensional conjugation, as the nonlinearity is enhanced and an additional degree of freedom is provided to functionalize the molecule.

Reference

[1] U. Gubler, R. Spreiter, Ch. Bosshard, P. Günter, R. Tykewinski, and F. Diederich, Appl. Phys. Lett. 73, 2396 (1998)

Polymer enhanced diffraction efficiency in an azo-dye doped liquid crystal

Gene Carlisle, Manlin Pei, and Yong-Jing Wang

Department of Physics

Texas A&M University

Canyon, TX 79016

Tel: (806) 651 2282 Fax: (806) 651-2733

gcarlisle@mail.wtamu.edu

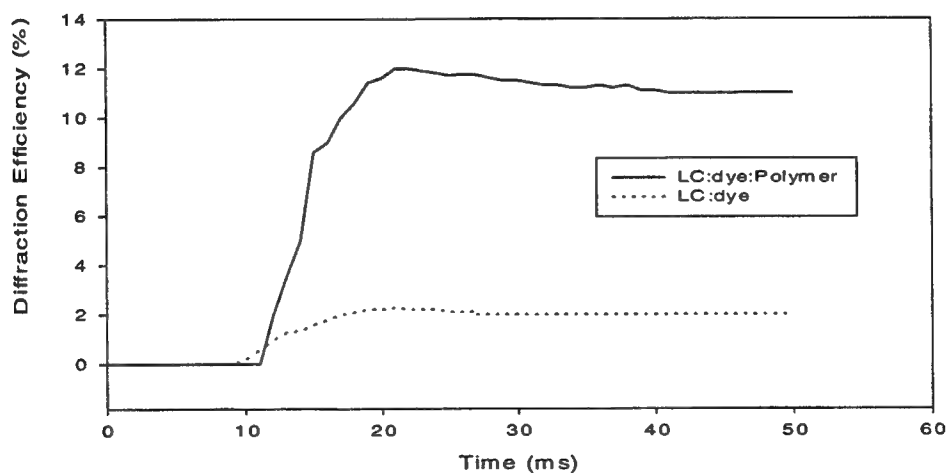
Because of their applications in optical devices for displays, storage, switching, and computing, photoresponsive liquid crystalline materials have been researched with great enthusiasm. The variations in LC material composition, device construction, optical geometry, and experimental objectives have led to many collaborative research efforts. Recently, there has been considerable interest in polymer-dispersed liquid crystals [1], polymer-stabilized liquid crystals [2], dye-doped liquid crystals [3], and liquid crystals that contain both dyes and polymers [4]. Investigations have concentrated on photorefractive and diffraction efficiency properties. Typically, the devices, ranging from 10 μm to 100 μm thick, require an applied dc voltage of about 1-2 V in order to observe wave-mixing effects. In this paper we investigate the diffraction efficiencies of liquid crystal devices that are dye-doped, contain only a very small amount of polymer, which enhances the diffraction efficiency, but do not require an applied dc or ac voltage.

The LC materials were prepared from homogeneous mixtures of the commercial nematic liquid crystal E7 (98% by weight), the azo-dye methyl red (1%), and the reactive diacrylate monomer 4,4'-bis(acryloylbiphenyl) (1%). The homogeneous solution was prepared by heating a stirring mixture of the components in a water bath at 80 °C. The mixtures were vacuum-loaded into cells made of indium tin oxide coated glass (25 mm x 15 mm x 1 mm) which had been spun-coated with polyimide, oven-baked at 240 °C for 1 hour and rubbed in a unidirectional manner for planar alignment of the liquid crystal. A cell gap of 22 μm obtained by using glass fiber spacers. Photopolymerization of the

monomers was performed by irradiating the cell for 10 minutes with 365-nm light with an intensity of 2 mW/cm^2 .

Using the basic configuration for phase conjugation, degenerate-four-wave-mixing experiments were performed using a diode-pumped YAG laser operating at 532 nm. The beam of linearly polarized light was divided into two coherent writing beams each having a power of 8 mW and a diameter of 2.0 mm. These p-polarized beams were overlapped parallel to the liquid crystal's director axis within the liquid crystal with an external intersection angle of 20° with the normal of the cell bisecting these beams. A p-polarized read beam having a power of 0.10 mW was launched counterpropagating one of the writing beams, and the power of the diffracted beam was detected with a photodiode and recorded as a function of time with a digitizing storage oscilloscope.

The diffraction efficiencies for the LC:dye:polymer and the LC:dye cells are shown in Fig. 1. As can



be seen in the figure the diffraction efficiency is enhanced about five-fold by the presence of only 1% polymer. The methyl red and LC molecules share similar rod shapes, and our polarized uv-vis

absorption measurements obtained on the cells clearly show that the dye molecules become oriented parallel to the LC director axis. Methyl red has an absorption maximum of 505 nm that is very near the laser line of 532 nm. Maximum absorption by the dye molecules occurs with the optical fields polarized along the long axis of the molecules. The mechanism for grating formation is believed to be due to the photo-induced *cis*-formation of the dye molecules [5]. The presence of the *cis*-form in the light regions of the grating causes reorientation of the LC molecules in that region giving rise to a refraction index grating in phase with the nonuniform light intensity. In the case of the LC:dye:polymer device, the presence of the polymer networks provides internal anchoring surfaces for the LC; the bulk LC is divided into many domains that can respond to local illumination independently and thus provide an enhancement of the diffraction efficiency.

Acknowledgement: This research was supported by The Welch Foundation and Advanced Display Systems.

References:

- [1] G. Cipparrone and A. Mazzula, *Opt. Lett.* **23**, 1505 (1998).
- [2] S. N. Lee, L. C. Chien, and S. Sprunt, *Appl. Phys. Lett.* **72**, 885 (1998).
- [3] I. C. Khoo, *Opt. Lett.* **20**, 2137 (1995).
- [4] S. Morino, A. Kaiho, and K. Ichimura, *Appl. Phys. Lett.* **73**, 1317 (1998).
- [5] A. G. Chen and D. j. Brady, *Opt. Lett.* **17**, 1723 (1994).

NEW STATES OF LIGHT IN NONLINEAR ORGANIC THIN FILMS AND POLYMERIC WAVEGUIDES

V.M. CHAPELA, J. PERCINO and V. N. SERKIN

Benemerita Universidad Autonoma de Puebla, Instituto de Ciencias

Blvd. 14 sur 6303, Ciudad Universitaria, Puebla, Pue., Mexico

tel: 52 (22) 45 62 07, fax: 52 (22) 32 60 67

e-mail address: vserkin@hotmail.com

EDUARD SCHMIDT

Institute of Theoretical Physics Friedrich-Schiller University, Jena, Germany

T. L. BELYAEVA

Lomonosov Moscow State University, Russia

1 INTRODUCTION

Nonlinear optical phenomena in organic thin films and polymeric materials are the subject of considerable interest motivated by their important applications to ultrafast optoelectronics and photonics [1]. Organic molecules with electron-donating and electron-accepting groups separated by a delocalized π -electron system have been the focus of much of the research on organic nonlinear optical materials. Recently G.Stegeman and co-authors [2-3] reported a large nonresonant nonlinearity in polydiacetylene *para*-toluene sulfonate (PTS) at 1600 nm that should yield 1D spatial solitons at a power of $P_s = 12W$, 40 times lower than in semiconductors and 30,000 times lower than in glass or CS_2 . Today PTS is the first solid-state material to show a strong cubic response with an observable quintic nonlinearity. PTS is a molecular quantum wire with a strong nonlinear optical response that is a consequence of the delocalization of π electrons along the conjugation axis of the material. Spatial soliton formation in the bulk single-crystal PTS has been studied experimentally in the paper [3]. Research efforts concentrate in the propagation and control of "pulse in space" (a narrow beam or fundamental soliton) because switching schemes proposed to date are based on them.

Due to spatial-temporal analogy both optical temporal solitons and optical spatial solitons are described by the nonlinear Schrodinger equation model (NSE) [4-7].

One of the fundamental problems that naturally arises is the problem of ultrashort pulse propagation in a organic materials with extremely strong nonlinearity. Theoretical investigations are also stimulated by the fact that up to date no answer has been obtained to the key question of the nonlinear optics of femtosecond pulses.

This question is what is the ultimate width of the pulse that can be produced and how to produce pulses with the width $\tau \sim T$, that is optical videopulse without a high-frequency field component?

To answer the above questions we used a direct computer modelling method based on the first principals and direct time integration of Maxwell's equations without using the NSE approximation. This method raises the limitation on the pulse duration, because it deals with real oscillations of the electromagnetic field as they are. The advantages of the Finite Difference Time Duration methods (FD-TD) consist in that it allows one both to approximate the starting equations without simplifications and to take into account quite easily the properties of various media. An improved algorithm of the difference scheme approximating Maxwell's equations and analyses the stability and dispersion properties of the difference scheme were presented in our papers [8,9].

2 MATHEMATICAL MODEL AND COMPUTER SIMULATIONS

Propagation of an electro-magnetic wave in a nonlinear dispersion medium is described by a system of nonlinear Maxwell's equations for electric field E and magnetic field H :

$$\frac{\partial H_y}{\partial t} = \frac{1}{\mu_0} \frac{\partial E_z}{\partial x} \quad (1)$$

$$\frac{\partial D_z}{\partial t} = \frac{\partial H_y}{\partial x} \quad (2)$$

Electrical induction D is related to the field by the non-linear material equation:

$$D_z = \varepsilon_0(\varepsilon_\infty E_z + F + \alpha \chi E_z^3 + \beta \chi E_z^5 + (1 - \alpha) \chi E_z G), \quad (3)$$

which allows for the medium dispersion, the electronic and nuclear contributions to the Kerr nonlinearities, and the effect of saturable nonlinearity.

For medium dispersion properties modelling we use harmonic oscillator response functions. The linear response for function F is:

$$F(t, z) = \int_0^\infty f(\tau) E_z(t - \tau, z) d\tau \quad (4)$$

$$f(\tau) = \omega_p^2 / \nu_0 \exp \left\{ -\frac{\delta \tau}{2} \right\} \sin(\nu_0 \tau), \quad (5)$$

$$\text{where } \omega_p^2 = \omega_0^2(\varepsilon_s - \varepsilon_\infty), \nu_0^2 = \omega_0^2 - \delta^2/4,$$

ω_0 is resonant frequency, δ is response of relaxation, linear index ε_0 is at $\omega = 0$, ε_∞ is at $\omega = \infty$. Nonlinear nuclear response for nonlinear function G is:

$$G(t, z) = \int_0^\infty g_3(\tau) E_z^2(t - \tau, z) d\tau \quad (6)$$

$$g_3(\tau) = \frac{\tau_1^2 + \tau_2^2}{\tau_1 \tau_2} \exp \{ -\tau / \tau_2 \} \sin(\tau / \tau_2), \quad (7)$$

where $1/\tau_1$ is the optical phonon frequency and τ_2 is the average phonon lifetime.

The computer simulation method described in this work is a powerful, practical instrument for investigating both well-known and new problems of femtosecond laser pulses interactions with different materials. First of all, in computer experiments the new soliton solutions of nonlinear Maxwell's equations were discovered, we called them Maxwell's electro-magnetic wave solitons. It was shown that in a nonlinear dispersive medium, the electron and nuclear mechanisms of nonlinearity, parametrically interacting with each other, lead to 10-20 femtosecond Maxwell's wave solitons forming (see Fig.1).

All the fundamental features of NSE envelope solitons including the particle like effects take place as well for Maxwell's wave solitons. Comparison of the dynamics of Maxwell's solitons and nonlinear Schrodinger solitons shows striking precision with which the main features of Schrodinger solitons coincide with those of Maxwell's solitons.

As follows from our computer simulations there exists the possibility to generate in organic and polymeric waveguides soliton-like pulses as short as 2-3T (see

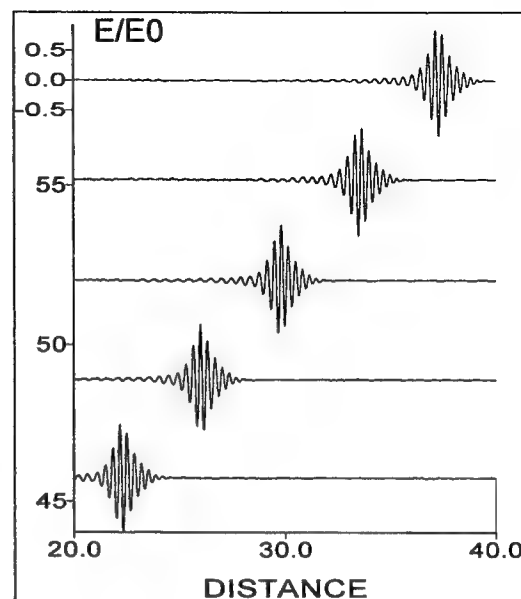


Figure 1 -

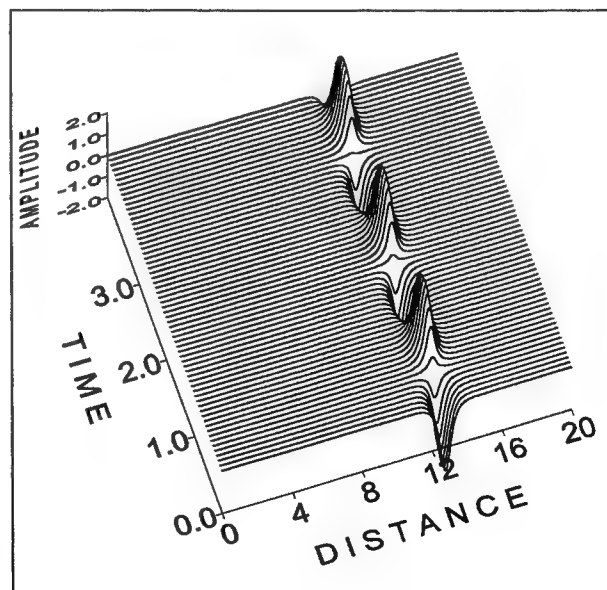


Figure 2 -

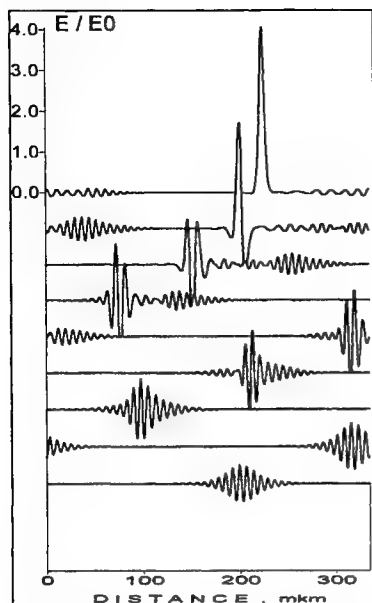


Figure 3 -

Fig.1). Their soliton behavior was confirmed by direct computer calculations which show practically elastic collision between them. Computer experiments predict also the possibility of generation of electromagnetic pulses with duration equals one period of optical oscillations and that is more, video-soliton pulses without a high frequency field components (see Fig.2). The dynamics of Maxwellian soliton transformation into optical video-soliton is shown on Fig.3.

Naturally, such pulses can be fully described only by the complete wave equation. Note also that in this situation, division of wave phenomena into self-actions and interactions, being traditional for nonlinear optics, loses its meaning. Indeed, a spectral width of the wave packet becomes comparable with the carrier frequency and consequently overlaps the interval between central frequencies of interacting pulses. In this case, the higher terms in the polarization expansion become comparable with, and even exceed, the lower terms. If nonlinearity is so great that the nonlinear length L_{nl} and phase mismatch Δk , caused by natural dispersion of the nonlinear medium, satisfy the inequality $L_{nl} \sim 1/\Delta k$, then a special choice of the phase matching conditions becomes redundant. In this case, generation of the higher harmonics does not depend on the phase matching conditions. The dynamics of higher harmonics generation induced by one period optical soliton is shown on Fig.4.

Optical video soliton which is asymptotically stable solitary wave without high frequency electromagnetic field components, is predicted in a strong nonlinear or-

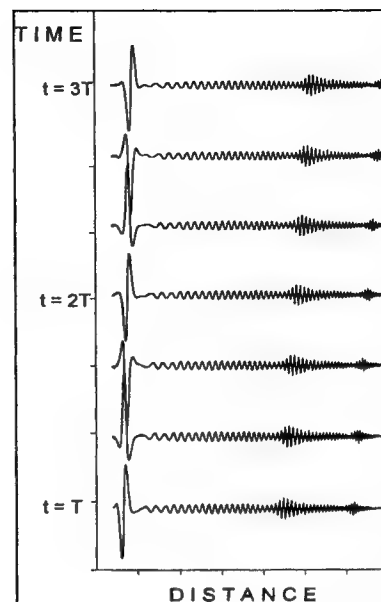


Figure 4 -

ganic polymers. The calculations were conducted using direct computer simulations on the first principals, i.e. based on the nonlinear Maxwell's equations. Dynamics of high harmonic generation induced by one period soliton pulse is also considered.

3 REFERENCES

1. G.I. Stegeman. Applications of Organic Materials in Third-Order Nonlinear Optics, CRC Press, Inc., p.799, 1997.
2. B. Lawrence, W.E. Torruellas, M. Cha, M.L. Sundheimer, G.I. Stegeman, J. Meth, S. Etemad and G. Baker, Phys. Rev. Lett., v.73, pp.597-600, 1994.
3. B.L. Lawrence and G.I. Stegeman, Opt. Lett., v. 23, pp. 591-593, 1998.
4. M. Segev and G.I. Stegeman, Self-Trapping of Optical Beams: Spatial Solitons, Physics Today, august 1998, pp. 42-48.
5. Akira Hasegawa. *Optical Solitons in Fibers*, Springer-Verlag, 1989.
6. E.M. Dianov, P.V. Mamyshev, A.M. Prokhorov, V.N. Serkin, *Nonlinear Effects in Optical Fibers*, Harwood Academic Publishers, 1989.
7. Govind P. Agrawal. *Nonlinear Fiber Optics*, Academic Press. Inc., 1995.
8. V.N. Serkin, E.M. Schmidt, E.V. Samarina, T.L. Belyaeva, SPIE Vol.2800, pp.310-318, 1996.
9. V.N. Serkin, E.M. Schmidt, T.L. Belyaeva, Quantum Electronics, v.27, pp.897-902, 1997.

SOLITON ATTRACTORS IN POLYMER FILM WAVEGUIDES

V.M. CHAPELA, J. PERCINO and V. N. SERKIN

Benemerita Universidad Autonoma de Puebla, Instituto de Ciencias

Blvd. 14 sur 6303, Ciudad Universitaria, Puebla, Pue., Mexico

tel: 52 (22) 45 62 07, fax: 52 (22) 32 60 67

e-mail address: vserkin@hotmail.com

T. L. BELYAEVA

Lomonosov Moscow State University, Russia

As earlier as in 1988 V.E.Zakharov et al. [1] discovered, for the first time, that in the conservative non-integrable systems the soliton is a statistical attractor. V.E.Zakharov et al. numerically integrated the nonlinear Scrodinger equation over large evolutions times for different degrees of nonlinearity and saturating nonlinearity as well. The results were very interesting and promising. The development of modulation instability gives rise to formation of a soliton grating. With further evolution, the system decays progressively into solitons and slightly nonlinear free waves. The interaction of solitons with each other and with free waves accounts for the gradual transfer of waves from the weak solitons to stronger solitons. At large time scales the system reaches a state in which it is a single soliton of small size and large amplitude. It has since been discovered that this phenomenon plays the most prominent role in the formation and interaction of optical solitons in the non-integrated modified nonlinear Schrodinger models. As was shown for the first time in [2] soliton attractors were formed in the processes of two and three solitons interactions in the frame of the model with higher order cubic-quintic nonlinearity of the saturating type. The first works dealing with nonintegrated "soliton" systems led to an outburst of scientific activity in this area [1-6] (see also recent review articles [7,8]).

From an experimental viewpoint the most attractive medium to discover soliton attractor experimentally is PTS crystals and thin films waveguides [3]. Polydiacetylene para-toluene sulfonate (PTS) is a material that has one of the largest cubic nonlinearities known to date and also exhibits a significant, negative quintic nonlinearity. The nonresonant nonlinear refractive indexes of PTS crystals have been reported to be $2.2 \times 10^{-3} \text{ cm}^2/\text{GW}$ and $-0.8 \times 10^{-3} \text{ cm}^4/\text{GW}^2$ [10,11]. At this case, at input soliton intensities as high as $2.75 \text{ GW}/\text{cm}^2$ the higher terms in the nonlinear polar-

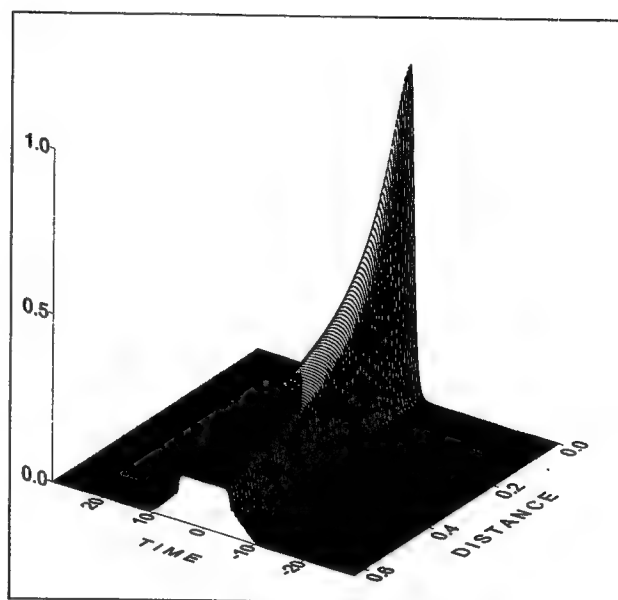


Figure 1 -

ization become comparable with, and even exceed, the lower terms. It is natural to ask how optical soliton-pulses propagate in organic polymers under this conditions. To answer this question we calculated in details the dynamics of soliton attractor described by the generalized NSE model:

$$i \frac{\partial \psi}{\partial z} + \frac{1}{2} k_2 \frac{\partial^2 \psi}{\partial \tau^2} + (R |\psi|^2 + \alpha |\psi|^4 + i\beta |\Psi|^2) \Psi = 0$$

which solution at $\beta = 0$ and $k_2=1$ is:

$$\psi(z, \tau) = \frac{\sqrt{2}\eta \exp[i(\eta^2 - \zeta^2)z/2 - i\zeta\tau]}{[1 + (1 + 8/3\alpha\eta^2)^{1/2} \cosh(2\eta(\tau + \zeta z))]^{1/2}}$$

Here, Ψ is the normalized field amplitude, τ is normalized transverse coordinate in the case of spatial solitons

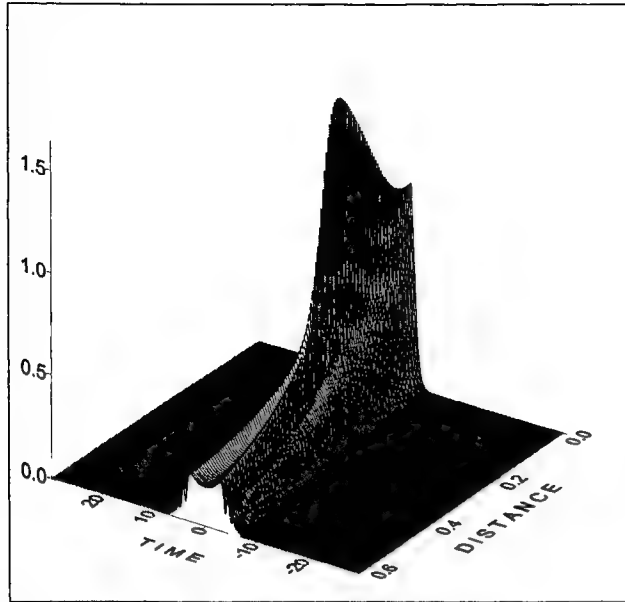


Figure 2 -

or retarded time in the case of temporal solitons. Parameters R and α are the cubic and fifth-order nonlinear parameters, β is the two-photon absorption coefficient, and k_2 is dispersion parameter.

In the absence of the quintic term, in the spectral range of positive GVD (parameter $k_2 = -1$) the large cubic nonlinearity is capable to produce a well known self-spreading and wave-breaking effects (see Fig.1.). High-order nonlinear term and two-photon absorption effects change cardinally the physical picture of high intensity pulse self-action. The intense and short peak is formed on the broad pedestal (see Fig.2) Cardinal changes in the dynamics of pulse self-action are connected with dominate influence of quintic nonlinearity.

The most important results obtained in the numerical experiments are connected with soliton attractor forming in the negative GVD spectral range. Fig. 3 illustrates the dynamics of $N=10$ solitons bound state self-compression. This multisoliton compression technics is widely used to provide a short femtosecond laser pulses. The dynamics of soliton attractor forming in the process of $N=10$ solitons bound states propagation is shown in Fig.4. One can see that the strong nucleation of multi-soliton pulses creates the possibility to generate the new (asymptotic state) soliton-like high energy pulse.

An optical soliton attractor can be produced in a thin organic film waveguides by injecting a train of a mode-locked laser pulses with an appropriate amplitudes. The dynamics of soliton attractor forming in this case is shown in Fig.5 and Fig.6. Fig.5 shows the process of

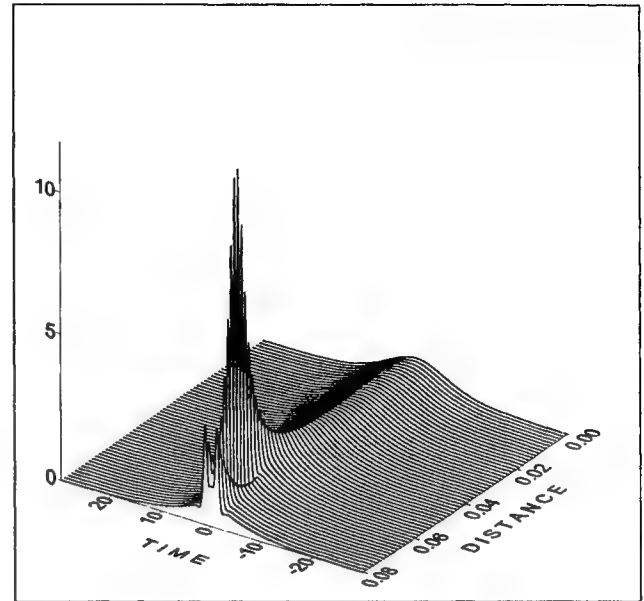


Figure 3 -

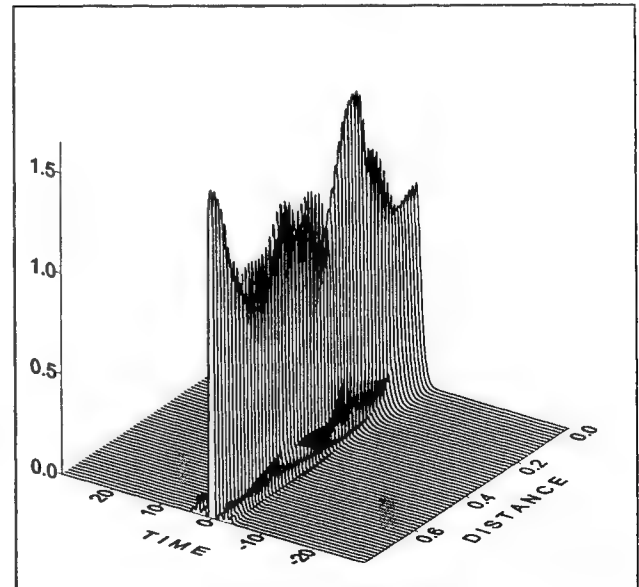


Figure 4 -

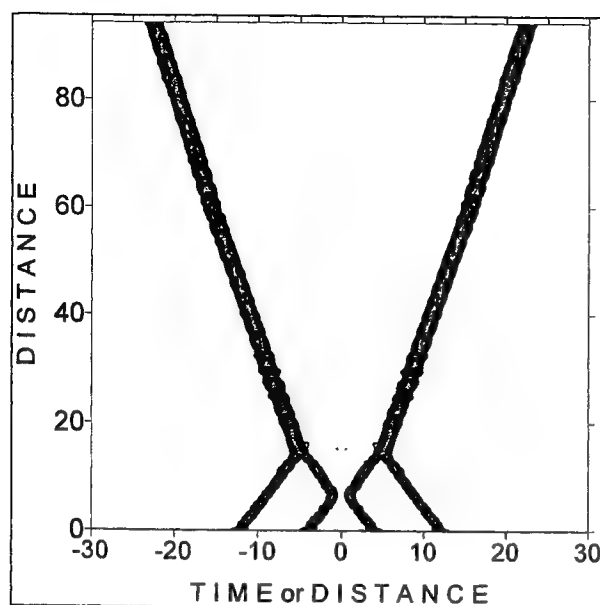


Figure 5 -

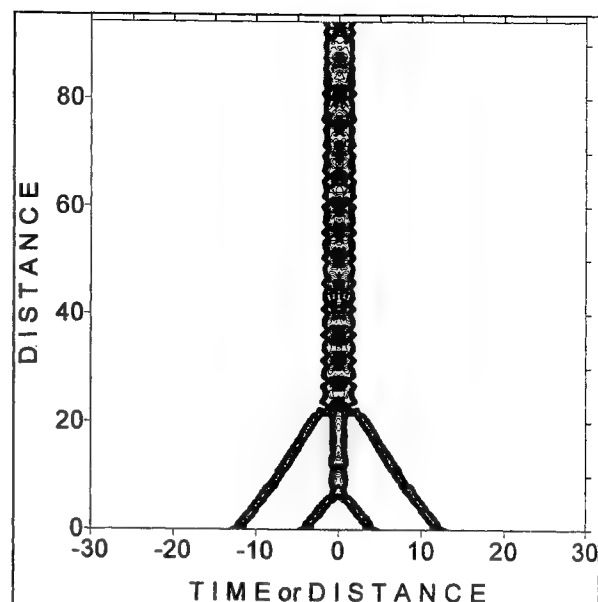


Figure 6 -

opposite phases soliton interaction and two soliton attractors formation due to the combine action of high-order nonlinearity and group velocity dispersion. Fig.6 shows the soliton attractor generation due to in phase soliton interaction.

Recently, spatial soliton formation in the bulk single-crystal PTS has been studied experimentally [11]. Investigations presented open the possibility to generate in PTS crystals temporal soliton attractors as well.

1 REFERENCES

- 1.V.E.Zakharov, A.N.Pushkarev, V.F.Shvets and V.V.Yan'kov, Soliton turbulence, JETP Lett., Vol.48, pp.83-87, 1988.
- 2.Z.S.Nikonova and V.N.Serkin, Femtosecond soliton attractors in optical fibers, in General Physics Institute Reports, pp.42-45, 1990.
- 3.B.S.Azimov, M.M.Sagatov and A.P.Sukhorukov, Sov. J. Quantum Electron., Vol. 21, pp.93-95, 1991.
- 4.S.Gatz and J.Herrmann, IEEE J. of Quantum. Electron., Vol.28, pp.1732-1738, 1992.
- 5.S.Gatz and J.Herrmann, Optics Letters, Vol.17, pp.484-486, 1992.
- 6.A.W.Snyder and A.P.Sheppard, Optics Letters, Vol.18, pp.482-484, 1993.
- 7.Mordechai Segev and George Stegeman, Self-Trapping of Optical Beams: Spatial Solitons, Physics Today, Aug. 1998, pp.42-48.
- 8.Allan W.Snyder and Francois Ladouceur, Light Guid-

ing Light, Optics&Photonics News, Vol.10, pp.35-39, 1999.

9.G.I. Stegeman. Applications of Organic Materials in Third-Order Nonlinear Optics, CRC Press, Inc., p.799, 1997.

10. B. Lawrence, W.E. Torruellas, M. Cha, M.L. Sundheimer, G.I. Stegeman, J. Meth, S. Etemad and G. Baker, Phys. Rev. Lett., v.73, pp.597-600, 1994.

11. B.L. Lawrence and G.I. Stegeman, Opt. Lett., v. 23, pp. 591-593, 1998.

Measurement techniques for the real and imaginary part of the third-order nonlinear optical susceptibility $\chi^{(3)}$

U. Gubler, Ch. Bosshard, and P. Günter

Nonlinear Optics Laboratory, Institute of Quantum Electronics, Swiss Federal Institute of Technology ETH, ETH-Hönggerberg, CH-8093 Zürich, Switzerland
gubler@iqe.phys.ethz.ch

R. Negres, D. Hagan

School of Optics, CREOL, University of Central Florida, Orlando, FL 32816, USA

We report about three measurement techniques yielding the real and imaginary part of the nonlinear optical susceptibility $\chi^{(3)}$, which have been applied for the first time to a whole series of molecular systems. A pump-probe technique, which is for the first time used to characterize the nonlinear optical properties of molecules, enables additionally to measure the wavelength dispersion of $\chi^{(3)}$ by a single experiment.

Under illumination with laser beams of high intensity any media exhibits a dependence of the refractive index n and the absorption α on the intensity I . By expanding the refractive index $n = n_0 + n_2 \cdot I$ and the absorption $\alpha = \alpha_0 + \alpha_2 \cdot I$ to the first order in the intensity, one can define a nonlinear refractive index n_2 and a nonlinear absorption coefficient α_2 . Materials with a large nonlinear refractive index are potential candidates for all optical signal processing and have therefore attracted a lot of interest in the past. The intensity loss through the nonlinear absorption α_2 is detrimental to these applications and should be kept small.

The origin of the nonlinear refractive index is the third-order nonlinear optical susceptibility $\chi^{(3)}$, which creates a nonlinear polarization P_i^{NL} in the media under investigation, with ϵ_0 being the dielectric constant and $K^{(3)}$ a factor dependent on the particularly considered nonlinear optical process.

$$P_i^{NL}(\omega_4) = \epsilon_0 \cdot K^{(3)} \cdot \chi_{ijkl}^{(3)}(\omega_4 = \omega_1 + \omega_2 + \omega_3, \omega_1, \omega_2, \omega_3) \cdot E_j(\omega_1)E_k(\omega_2)E_l(\omega_3) \quad (1)$$

Far from any resonance, the nonlinear susceptibility $\chi^{(3)}$ is a real number. Are the frequencies ω_m of one of the incident electric fields E_m tuned to a resonance, the nonlinearity $\chi^{(3)}$ starts to become complex, with an imaginary part portraying the resonance process. Due to the nonlinear nature of $\chi^{(3)}$ not only one photon resonances have to be considered, but also multi photon resonances as most prominent two photon absorption. In the case of the nonlinear refractive index, the frequencies in equation (1) are degenerate $-\omega_4 = \omega_1 = -\omega_2 = \omega_3 = \omega$ and the factor $K^{(3)} = 3/4$. The nonlinear refractive index n_2 and the nonlinear absorption α_2 are proportional to the real and imaginary part of the nonlinear susceptibility $\chi^{(3)}(-\omega, \omega, -\omega, \omega)$.

$$n_2 = \frac{3}{4\epsilon_0 n_0^2 c} \text{Re}(\chi^{(3)}(-\omega, \omega, -\omega, \omega)) \quad \alpha_2 = \frac{3\pi}{\epsilon_0 n_0^2 c \lambda} \text{Im}(\chi^{(3)}(-\omega, \omega, -\omega, \omega)) \quad (2),(3)$$

To produce a nonlinear phase shift $\Phi_{NL} = 2\pi/\lambda \cdot n_2 I$ the absorption should be sufficiently small. This can be expressed by two figures of merit W and T^{-1} for one and two photon absorption, which have to be both larger than one.

$$W = \frac{n_2 \cdot I}{\alpha_0 \cdot \lambda} > 1 \quad T^{-1} = \frac{n_2}{\alpha_2 \cdot \lambda} > 1 \quad (4),(5)$$

Using equations (2) and (3) and writing the nonlinearity $\chi^{(3)} = |\chi^{(3)}| \cdot e^{i\varphi^{(3)}}$ with an amplitude $|\chi^{(3)}|$ and

a phase $\varphi^{(3)}$ instead of the real and imaginary part, the two photon figure of merit can be rewritten.

$$\frac{\text{Re}(\chi^{(3)}(-\omega, \omega, -\omega, \omega))}{\text{Im}(\chi^{(3)}(-\omega, \omega, -\omega, \omega))} > 4\pi \quad \text{resp.} \quad \varphi^{(3)} < \tan\left(\frac{1}{4\pi}\right) \approx 4.55^\circ \quad (6),(7)$$

Equations (7) clearly shows, that for any nonlinear susceptibility $\chi^{(3)}$ with a phase $\varphi^{(3)}$ larger than 4.5° , the figures of merit can not be fulfilled and therefore no application relying on the nonlinear phase shift is possible. Consequently, two photon resonances have to be avoided. Often large nonlinearities $\chi^{(3)}$ are reported, which lie in a two-photon resonance without giving information on the phase $\varphi^{(3)}$ or the imaginary part of $\chi^{(3)}$. For any serious material characterization, the full knowledge of the complex nonlinear susceptibility $\chi^{(3)}$ is necessary, together with an evaluation of the timescale of the investigated nonlinearity.

In the first measurement technique, we use a standard degenerate four wave mixing DFWM setup in counterpropagating geometry (Fig. 1). A 10 ps Nd:YLF laser (1047 nm) was used with low repetition rate (10 Hz) to avoid orientational and thermal effects.

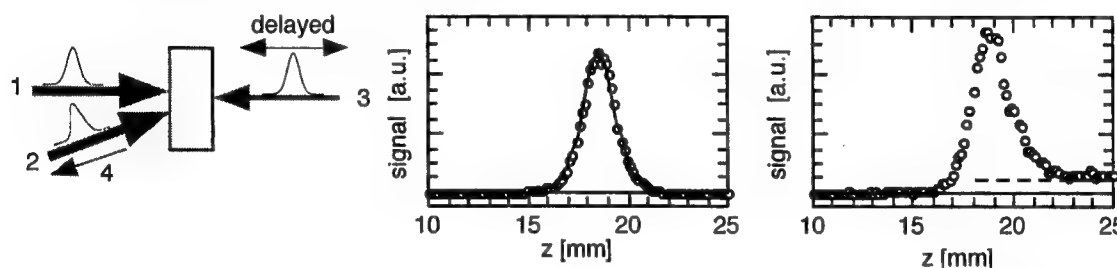


Fig. 1: Degenerate four wave mixing DFWM in counterpropagating geometry (left). The three incident beams create beam 4 through the nonlinear susceptibility $\chi^{(3)}$. The laser pulse 3 is delayed to read out the time response of the sample. Scans of an instantaneous response (middle) and one with some persistent contribution (right), created by two photon absorption. The remaining contribution originating from a grating of excited and ground state molecules decays on the timescale of nanoseconds.

When molecules with a second-order hyperpolarizability γ (nonlinear susceptibility $\chi^{(3)}$ per molecule) are diluted in a solvent, one usually sees a linear increase in the overall nonlinear susceptibility of the solution. If the phase $\varphi^{(3)}$ of the molecular second-order hyperpolarizability in the complex plane is different from zero, the contribution has to be added in the complex plane of the nonlinearity $\chi^{(3)}$, resulting in a curved dependence of the nonlinearity amplitude $|\chi^{(3)}|$ as depicted in figure 2. By measuring a concentration series of a molecule, the amplitude and the phase of the second-order hyperpolarizability γ can be calculated. For small phases of the nonlinearities, this measurement technique is rather insensitive.

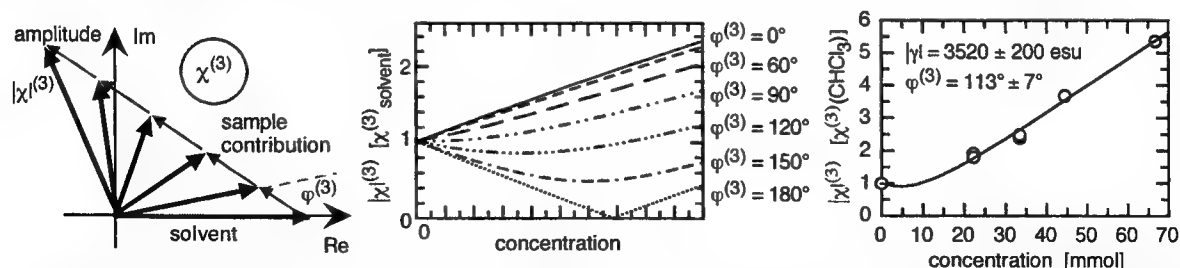


Fig. 2: Contribution from solvent and solute molecules have to be added in the complex plane of the nonlinear susceptibility $\chi^{(3)}$ (left) resulting in a nonlinear increase of the nonlinearity amplitude $|\chi^{(3)}|$ (middle). For small nonlinearity amplitudes $\varphi^{(3)}$ this approach is rather insensitive. Example of a typical measurement on a polyene sample (right).

In order to improve the resolution, we modified the DFWM setup and built an interferometer of the signal beam with a reference beam. The two beams are detected by a camera, showing a spatial interference pattern. If the signal beam has picked up a phase shift from the nonlinear susceptibility $\chi^{(3)}$, the interference fringes will shift spatially, disclosing the phase $\varphi^{(3)}$ of the nonlinear susceptibility. Phase zero is calibrated

with a measurement on the pure solvent and then the concentration of the molecules is step wise increased.

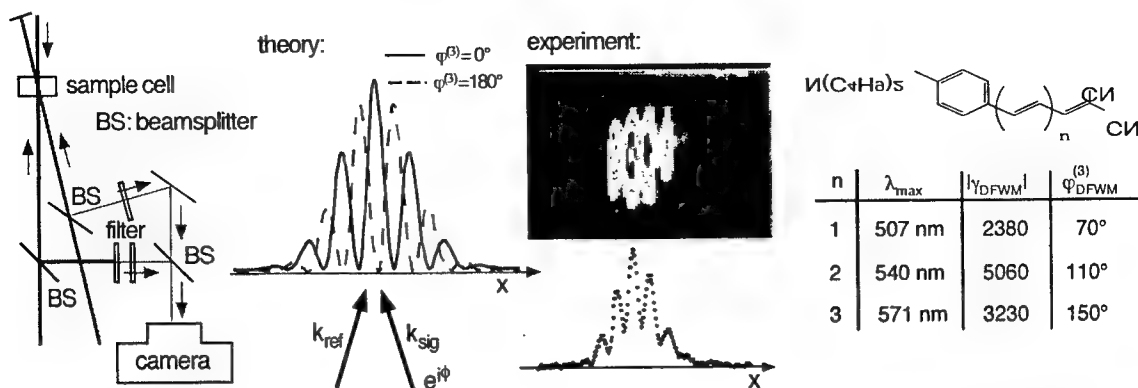


Fig. 3: Degenerate four wave mixing (DFWM) interferometer: the signal and reference beam are deflected from beam splitters through attenuation filters on a camera (left), where they interfere and show a spatial interference pattern (middle). A phase in the nonlinear susceptibility $\chi^{(3)}$ creates a phase shift in the signal and moves the peaks and valleys of the interference pattern. Example of a series of three polyene molecules, exhibiting increasing phase upon elongation of the molecule (right). λ_{\max} is the wavelength of maximal absorption.

In the third experimental method we used a pump-probe technique, which measures the two photon absorption spectra $\Delta\alpha = \alpha_2 I_e$, taking one photon from a strong pump beam (frequency ω_e , intensity I_e) and one photon from a weak, broad continuum. For fixed pump condition, the nonlinear Kramers Kroenig relations [1] can be used to calculate the change in the nonlinear refractive index $\Delta n = n_2 I_e$.

$$\Delta n(\omega, \omega_e, I_e) = \frac{c}{\pi} P \int_0^{\infty} \frac{\Delta\alpha(\omega', \omega_e, I_e)}{\omega'^2 - \omega^2} d\omega', \quad \Delta\alpha(\omega, \omega_e, I_e) = -\frac{4\omega^2}{\pi c} P \int_0^{\infty} \frac{\Delta n(\omega', \omega_e, I_e)}{\omega'^2 - \omega^2} d\omega' \quad (8)$$

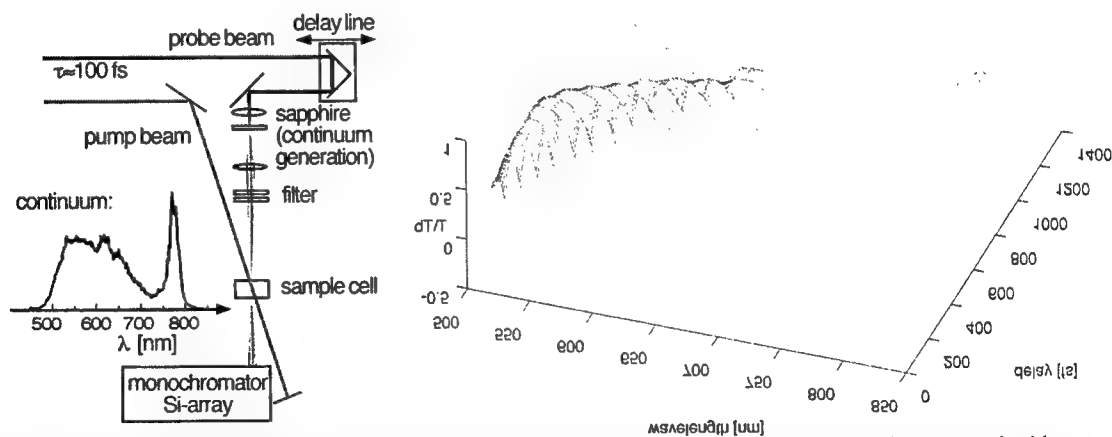


Fig. 4: Experimental setup of pump-probe measurements (left). The two photon absorption spectra is measured with a strong pump beam and a white light continuum for a broad spectral range in a single measurement. The spectra are measured for different delay times of the pump beam, resulting in a two dimensional data array (right). By deconvoluting the data array, the two photon absorption spectra and the continuum chirp are retrieved.

The measured two photon absorption coefficient α_2 and nonlinear refractive index n_2 are proportional to the imaginary resp. real part of the nonlinear optical susceptibility $\chi^{(3)}(-\omega, \omega, -\omega_e, \omega_e)$, leading again to a full characterization of the nonlinearity $\chi^{(3)}$. The main advantage is, that the $\chi^{(3)}$ can be retrieved over a broad range of frequencies ω , yielding also information about the wavelength dispersion. First results on several molecular systems will be shown in the presentation.

- [1] D. C. Hutchings, M. Sheik-Bahae, D. J. Hagan, E. W. van Stryland, Optical and Quantum Electronics 24 (1992), 1-30

Photoinduced birefringence in poled azo dyes doped side-chain polymers at 632.8 nm

Myung-Hyun Lee, Hyung-Jong Lee, and Min-Cheol Oh

Telecommunication Basic Research Lab, ETRI, 161 Kajong-Dong, Yusong-Gu, Taejeon 305-600, Korea

Tel. +82-42-860-5243, Fax. +82-42-860-6836, email. mhl@etri.re.kr

Introduction

Nonlinear optical (NLO) polymers give potential possibilities in the areas of optoelectronics, photonics, and optical signal processing and have the advantages of low dielectric constant and cost-effective fabricated process compared with those of inorganic electro-optic(EO) materials. Particularly, the azo dye doped polymers have been paid attention for EO (second-order NLO) modulation^{1,2}, polarization holography³, integrated optics⁴, optical data storage⁵, and molecular switching⁵.

In this paper, we report the photoinduced changes in the EO coefficients of the poled azo dyes doped side-chain polymers measured at room temperature with a He-Ne laser of 632.8 nm wavelength.

Experimental

Materials ; We used various side-chain polymers attached azo based disperse red 1 (DR1). Poly(methyl methacrylate) (PMMA), polyarylate (PA), and polyimide (PI) were used as backbone polymers.

The glass transition temperatures (T_g) obtained from differential scanning calorimetry (DSC) are 127 °C, 155 °C, and 225 °C for the PMMA-DR1, PA-DR1, and PI-DR1 side-chain polymers, respectively.

The peaks (λ_{max}) in the absorption band for the PMMA-DR1, PA-DR1, and PI-DR1 side-chain polymers occur at 471, 475, and 477 nm, respectively. It is noted that the DR1 based side-chain polymers have near absorption tails at 632.8 nm but they are transparent at 830, 1300, 1550 nm.

For the comparison, a PMMA based side-chain polymer with a 4-dimethylamino-4'-nitro- stilbene (DANS) chromophore (PMMA-DANS, λ_{max} = 425 nm) and polyurethane with disperse red 19 (PUR-DR19, λ_{max} = 479 nm) were used.

Sample Preparation ; Thin films with a thickness range of 1 ~ 3 μ m were prepared by spin-coating on an indium tin oxide (ITO) coated glass and dried in an oven under flowing nitrogen. Then a thin layer of gold was deposited onto the polymer film using a thermal evaporator. Electrode contact poling was performed at its glass transition temperature.

Measurement ; An experimental setup is a modified ellipsometric reflection technique, as shown in Fig. 1 (a). A He-Ne laser and three semiconductor lasers were used with the wavelengths of 632.8, 830, 1300 and 1550 nm. A laser beam was incident on the back of the glass substrate at the fixed angle $\theta = 45^\circ$. We detected the modulated EO signals, the phase difference, and the output intensity as a function of time using a photo detector, a lock-in amplifier, and a function generator. The output intensity as a function of phase retardation between the *s*- and *p*- wave is also shown in Fig. 1(b).

Results

Fig. 2 shows the variation of the modulated EO signals and the corresponding variation of the output intensity with a He-Ne laser of 632.8 nm as a function of time in the poled PMMA-DR1 sample. Also, Fig. 3 and Fig. 4 show the variation of the modulated EO signals and the corresponding variation of the lock-in angles at 632.8 nm as a function of time in the poled PA-DR1 and PI-DR1 samples, respectively. The changing rate of the EO signals is inversely proportional to the T_g as shown in Fig. 2, 3 and 4.

The magnitudes of the modulated EO signals, initially biased at the half maximum intensity (at point A in Fig. 1(b)) decrease rapidly to the changing position of the lock-in angle and/or to the maximum output intensity and increase rapidly to a certain extent and then decrease gradually again, as shown in Fig. 2.3. and 4.

It is noted that when the He-Ne laser is turned off, the initial state is recovered in a few days at room temperature. Besides, in the case of the poled PUR-DR19 sample, there is also a variation in the magnitude of the modulated EO signals at 632.8 nm. However, there are no variations in the magnitude of modulated EO signals in the poled azo dyes doped side-chain polymers at the wavelengths of 830 nm, 1300 nm and 1550 nm, as shown in Fig. 5. In the case of the poled PMMA-DANS sample, there is no variation in the magnitude of modulated EO signals at 632.8 nm.

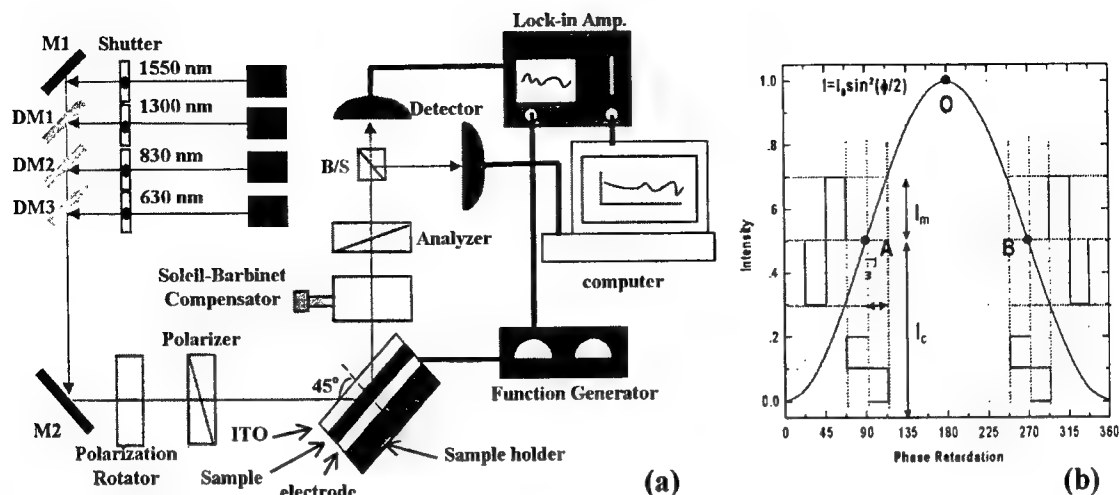


Fig.1 (a) Experimental configuration for the EO coefficients and (b) output intensity as a function of phase retardation between s- and p- wave.

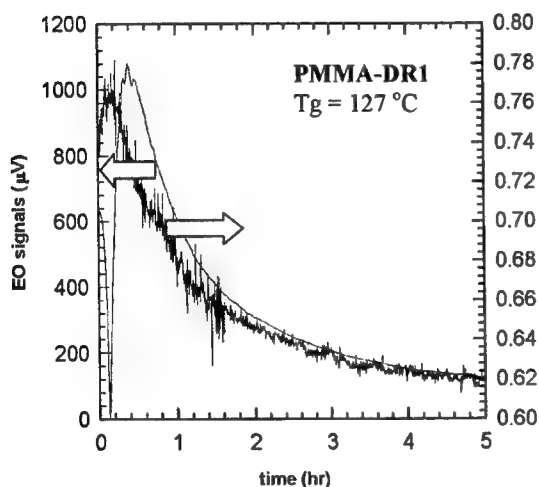


Fig. 2 Variations of EO signal and output intensity as a function of time

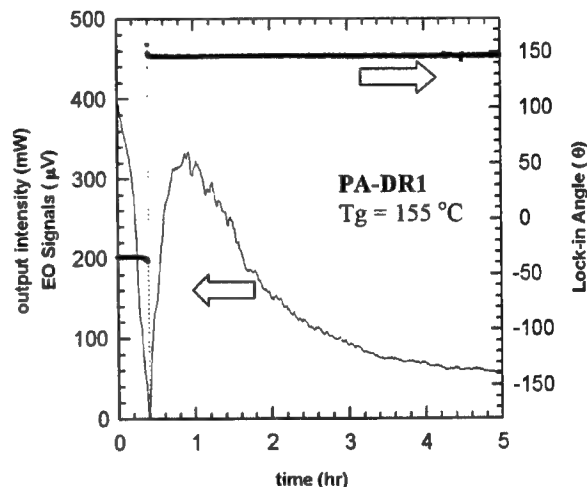


Fig. 3 Variations of EO signals and lock-in angle as a function of time

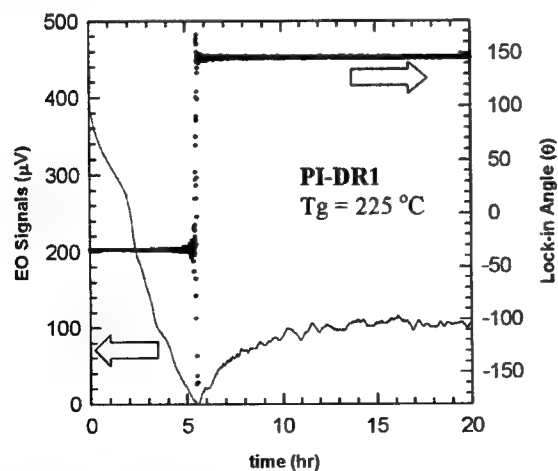


Fig. 4 Variations of EO signals and lock-in angle as a function of time

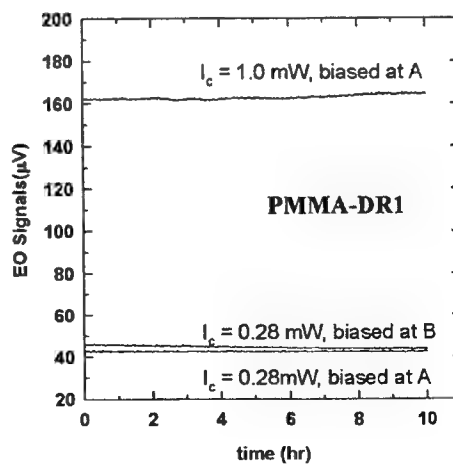


Fig. 5 There are no variations in EO signals at 830 nm as a function of time

Discussion

In azo dye doped polymeric films, the photo-induced orientation was well studied in ref. 7. As a pumping beam in order to cause the trans-cis photoisomerization of the azo group, a YAG laser with a 532 nm wavelength was used and a He-Ne laser with a 632.8 nm wavelength as a probing beam was used in many research groups^{7,8}. In this study, we used the He-Ne laser of 632.8 nm as the pumping and probing beam.

The origin of the variation of the EO signals is attributed to trans-cis photoisomerization of the azo group. During measurement, irradiating the poled azo dyes doped side-chain polymeric film with the He-Ne laser of 632.8 nm causes the trans-cis photoisomerization of azo molecules. The trans-cis process in azo molecules gives the photoinduced birefringence. The photoinduced birefringence affects the reflected intensity (output intensity). The change of the output intensity causes the changing of the biased points (point A to point B via point O in Fig. 1(b)) as shown in Fig. 2.

At point O in Fig. 1 (b), the magnitude of the modulated EO signal should be "0" and the phase difference of the modulated signals between the point A region and the point B region should be 180°. We confirmed these phenomena with measuring the modulated EO signals, the output intensities, and the lock-in angles as shown in Fig. 2,3, and 4.

As shown in Fig. 5, there is no change in the EO signals at the wavelengths of 830 nm, 1300 nm and 1550 nm, which are far from the absorption band of the azo group. Therefore, it is noteworthy that it should be very carefully considered when a He-Ne laser with the 632.8 nm wavelength is used in azo dye doped polymeric films as a probing beam.

Conclusions

The photoinduced changes in the EO coefficients of the poled azo dyes doped side-chain polymers are reported. During measurements, the magnitudes and the signs of the modulated EO signals measured with a He-Ne laser of 632.8 nm are changed as functions of time and glass transition temperature, but those measured at wavelengths of 830, 1300 and 1550 nm are not changed.

At the wavelength of 632.8 nm, the trans - cis photoisomerization occurs in the poled azo dyes doped side-chain polymers, causes the photoinduced birefringence and gives rise to the changes of the EO coefficients.

References

1. D. Chen, H. R. Fetterman, A. Chen, W. H. Steier, L. R. Dalton, W. Wang, and Y. Shi, *Appl. Phys. Lett.* 70(25) 3335 (1997).
2. J. I. Thackara, J. C. Chon, G. C. Bjorklund, W. Volksen, D. M. Burland, *Appl. Phys. Lett.* 67(26) 3874 (1995).
3. T. Todorov, L. Nikolova, and N. Tomova, *Appl. Opt.* 23, 4309(1984).
4. Y. Shi, W. H. Steier, L. Yu, M. Shen, and L. R. Dalton, *Appl. Phys. Lett.* 59, 2935 (1991).
5. T. Ikeda and O. Tsutsumi, *Science* Vol. 268 1873(1995).
6. C. C. Teng and H. T. Man, *Appl. Phys. Lett.* Vol. 56, No. 18, 1734(1990).
7. Z. Sekkat, J. Wood, E. F. Aust, W. Knoll, W. Volksen and R. D. Miller, *J. Opt. Soc. Am. B*, 13(8), 1713 (1996).
8. C. Wang, H. Fei, Y. Qiu, Y. Yang, Z. Wei, Y. Tian, Y. Chen, and Y. Zhao, *Appl. Phys. Lett.* 74(1) 19 (1999).

Optical Polymer-Amplifier Enhanced with Photo-Induced Periodic Gain Profile

Satoshi Tanaka, Takanori Kemanai, and Heihachi Sato

Department of Electrical Engineering, National Defense Academy

Hashirimizu 1-10-20, Yokosuka 239-8686, Japan

satoshi@cc.nda.ac.jp, heis@cc.nda.ac.jp

Seiichiro Hayakawa

Mitsubishi Chemical Corporation,

Chuo 8-3-1, Ami, Inashiki, Ibaraki 300-0332, Japan

3708949@cc.m-kagaku.co.jp

Photo-induced periodic gain[1,2] onto dye-doped organic polymer by using interference pattern of a frequency-doubled Nd:YAG (532 nm) laser leads to an extreme high-gain at a specific wavelength near 585 nm. In this paper we shall thus demonstrate an enhanced gain by use of ultraviolet(UV)-cured organic polymer[3] with doping Rhodamine 6G dye.

In Fig.1 the experimental apparatus is depicted: (a) the schematics and (b) the close-up for introducing a periodic gain profile. As pumping source a frequency-doubled Nd:YAG (532 nm) pulsed laser (Spectra Phys.: GCR 130-10) beam was incident through a beam splitter BS on a dye laser (Laser Ana. Sys.: LDL 20505), which provides us a

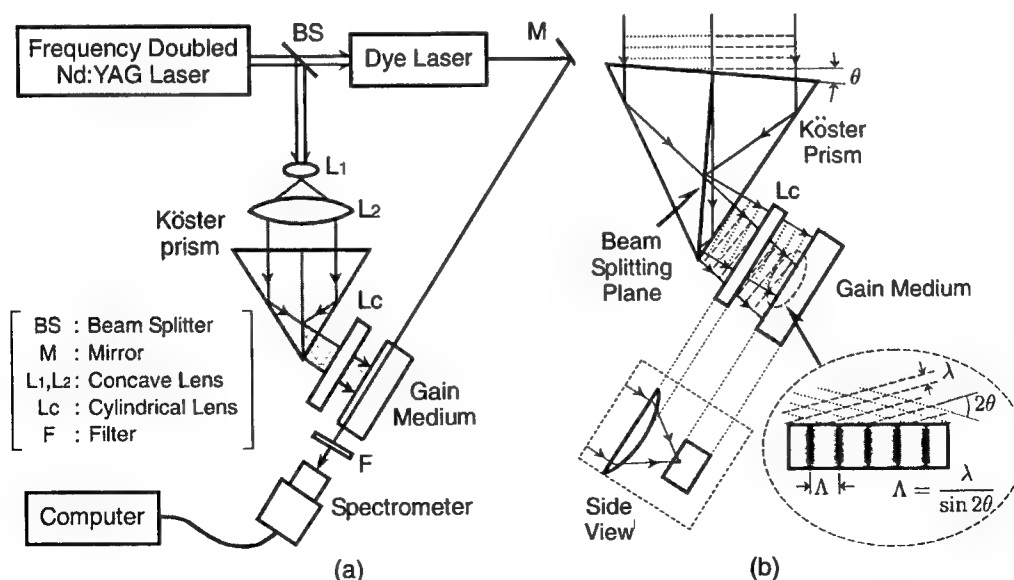


Fig. 1. Experimental setup: (a) the schematic diagram and (b) the close up for inducing a periodic gain corrugation.

signal beam ranging the wavelength from 580 to 595 nm. This signal beam was reflected back from a mirror M to direct to UV-cured organic polymer (called TEMA) with Rhodamine 6G (Rh-6G) dopant. The another 532 nm beam bypassed by the beam splitter BS was impinged on the Köster prism through a beam expander composed of lenses L_1 and L_2 . Using the Köster prism and a cylindrical lens L_c an interference of the 532 nm beam was made up as the pump source to induce a linear periodic gain profile optically inside the Rh-6G doped organic polymer. By slightly tilting the setting angle of the Köster prism by θ with respect to the equi-phase surface of the pumping beam enables us to vary the period Λ of gain-corrugation ($\Lambda = \lambda / \sin 2\theta$, λ : the wavelength) on the polymer as shown in Fig. 1 (b). The organic polymer used has been fabricated by UV curing technique with the Rh-6G dopant of 100 ppm. The length of specimen, i.e., polymer amplifier was 7 mm long with the thickness of 5 mm. The net gain of the amplifier was measured as a function of wavelength by a spectroscopic CCD array detector (ORIEL: Intraspec IV) with and without the interference pump beam, and processed and analyzed by a computer. It should be noted that the axis of signal beam must be exactly collinear to the focal line of interference pattern to make the amplifier effective.

Defining the net gain by the ratio of the output power with to without the pumping interference pattern, the typical results of the net gain G versus the wavelength were shown under the fixed pump energy of 0.15 mJ in Fig. 2 for different periods Λ of the interference pattern, where the net gain obtained for the uniform pumping irradiation was compared with dashed line. From the figure it is seen that the net gain is extremely enhanced at the wavelength 586 nm by the periodic interference pattern in comparison to that for the uniform irradiation, telling us a slight shift of the wavelength at the peak value towards a longer one as the interference period Λ is

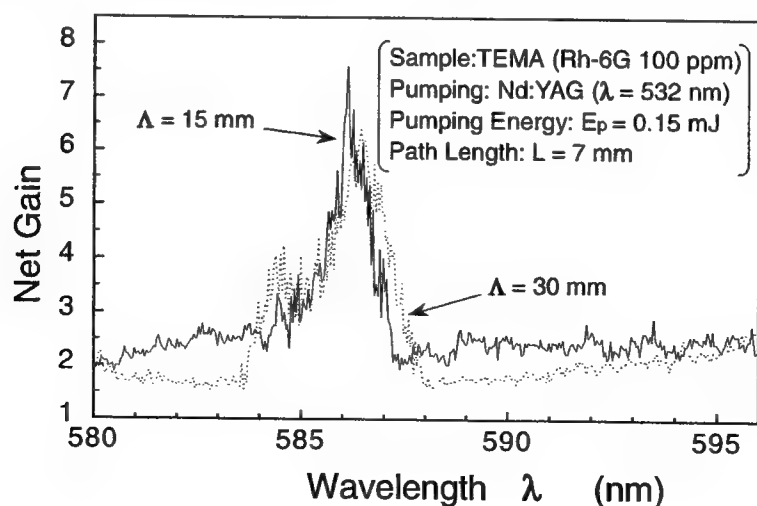


Fig. 2. Net gain G versus the wavelength under a fixed pump energy of 0.15 mJ.

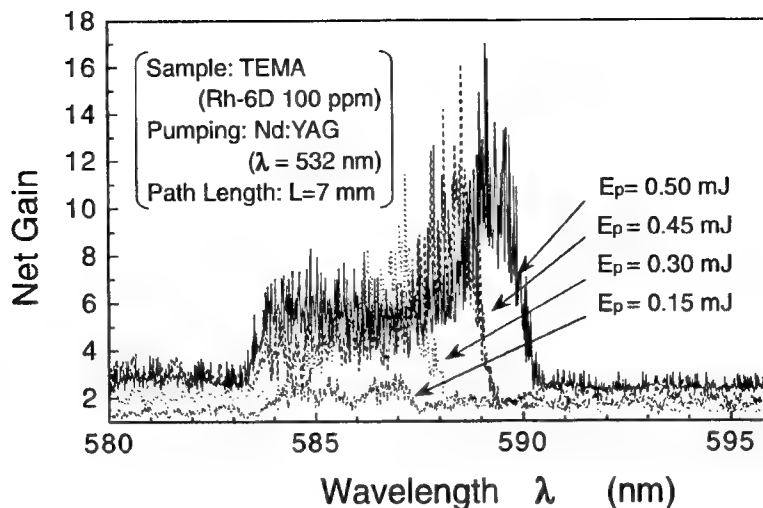


Fig. 3. Effect of the pump energy E_p on the net gain G .

changed from 15 to 30 μm . In Fig. 3 the effect of the pump energy E_p on the net gain G was depicted with uniform irradiation, indicating that the wavelength at the peak explicitly tends to be red shift. This fact implies that the line center of the amplifier with Rh-6G dopant will move to a longer wavelength due to photo-induced energy-gap shift with increasing the pump energy.

Based on the above results both the peak wavelength λ_p and the maximum net gain G_{max} are shown as a function of the pump energy E_p in Fig. 4 for the specimen of Rh-6G 100 ppm. It is found that both λ_p and G_{max} tend to almost linearly increase with the pump energy. At this moment the reason why these happens has not been specified, being left for the next study. However, the wavelength-selective high-gain greater than several times than that of the uniform irradiation has been obtained at the corrugation period Λ corresponding to the Bragg-condition. Similar net gain will be compared with the specimens with Rh-B dopant as well.

REFERENCES

- [1] H. Sato and Y. Azumai, CLEO Tech. Digest Series, **10**, 468 (1991).
- [2] H. Sato and Y. Azumai, Appl. Opt. **31**, 5822 (1992).
- [3] S. Miyoshi, S. Hayakawa, I. Seo, and H. Sato, Proc. SPIE, **2998**, 249 (1997).

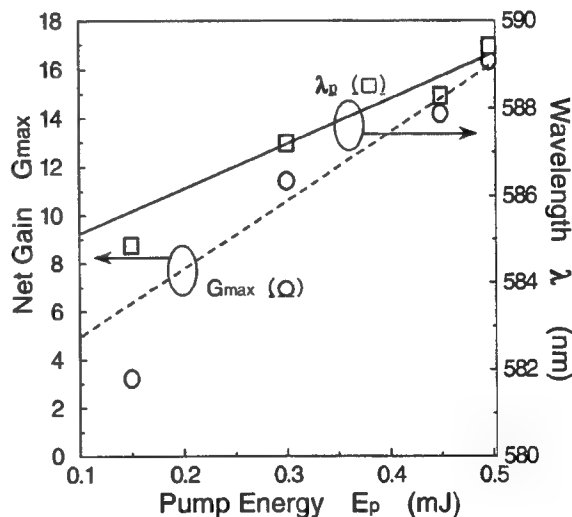


Fig. 4. Peak wavelength λ_p and the maximum net gain G_{max} are shown as a function of the pump energy E_p .

Unique two-dimensional effects in the first hyper-polarizability of molecules with carbazole donor groups

G. Berkovic[#], G. Meshulam, Z. Kotler

Optronic Materials Group, Electro-Optics Division, Soreq NRC, Yavne 81800 Israel

[#]e-mail: garry@ndc.soreq.gov.il

A. Ben-Asuly, L. Shapiro and V. Khodorkovsky

Dept. of Chemistry, Ben-Gurion University of the Negev, Beer-Sheva 84105 Israel

Organic molecules containing carbazole groups have generated interest as “multi-functional” molecules for electro-optic device applications which could combine the well known photo-conductivity of carbazoles with second order optical nonlinearity (NLO) and light emission [1]. Regarding second order NLO, substituted carbazoles appear particularly suitable at first glance, because numerous typical NLO molecules employ dialkyl or diaryl amino electron donors [2,3]; the carbazole group might be expected to act like a diphenyl-amino donor.

However, when characterizing the NLO efficiency β of conjugated molecules with indandione acceptors and the above donors, we found a drastic reduction in the EFISH values when a dialkyl- or diaryl- amino donor is replaced by a carbazole moiety (see Table 1). Whereas the dialkyl-amine derivatives show strong EFISH and large, positive $\mu\beta_0$ values in the range $200\text{--}800 \times 10^{-48}$ esu, the EFISH signals for solutions of carbazole molecules **1d**, **2d**, **3b** could barely be discerned from the pure solvent reference. Consequently we could deduce that the $\mu\beta_0$ values for the carbazole molecules must fall in the range of the small and often negative values given in the Table. A similar reduction is observed for molecule **4b** – the carbazole analog of **4a**, the classic NLO molecule DANS.

Since EFISH measures only the product $\mu\beta_0$, it is conceivable that this reduction comes from μ , and not β . Although we have not yet measured μ independently, high level quantum chemical calculations (using RHF/6-31G(d,p)//RHF/6-31G(d,p) model chemistries – Gaussian 98 Rev. A6) suggest that μ does not change considerably from the dialkyl- to the carbazole. A similar conclusion was also reached from solution IR absorption spectra: ionic character in the ground state will lengthen the indandione carbonyl bonds changing the overall bond-length alternation in the molecule [3]; however we found no differences in the carbonyl stretching frequencies in the two series of molecules.

The quantum chemical calculations further suggested that the differences in the two series of molecules

arose from a unique dimensionality effect. The dialkyl amino derivatives can be adequately represented as classical 1-D chromophores with dominant nonlinearity β_{zzz} along the molecular long axis. In the carbazole series, a significant, and negative, β_{zxx} component also appears due to transitions within the carbazole group. Recalling that an EFISH measurement determines the product of the β tensor with the μ vector, one extracts in this case $\beta^{\text{EFISH}} = \beta_{zzz} + \beta_{zxx}$. For molecule **1d** in the gas phase, the quantum chemical calculations gave $\mu=1.83$ D, $\beta_{zzz} = 18 \cdot 10^{-30}$ esu and $\beta_{zxx} = -30 \cdot 10^{-30}$ esu, giving $\mu\beta^{\text{EFISH}} = -24 \cdot 10^{-48}$ esu, in fair agreement with EFISH results.

An experimental check of this postulate is afforded by Hyper Rayleigh Scattering (HRS) which probes a different combination of β tensor elements than does EFISH. For a “two-dimensional” NLO molecule with β_{zzz} and β_{zxx} components, the total HRS signal is proportional to:

$$(\beta^{\text{HRS}})^2 = \frac{6}{35} \beta_{zzz}^2 + \frac{16}{105} \beta_{zzz} \beta_{zxx} + \frac{38}{105} \beta_{zxx}^2 \quad (1)$$

and the ratio β_{zxx}/β_{zzz} can be inferred from the HRS polarization ratio.

We have compared HRS signals of solutions of **1b** and **1d** irradiated with focussed 1.54 μm laser light. The dialkyl molecule **1b** gave a HRS signal with an experimental polarization ratio very close to the value of 5 expected for a 1-D molecule ($\beta_{zxx}=0$). Thus we could extract its β_{zzz} value by comparing its unpolarized HRS intensity with that of Disperse Red, a standard 1-D reference molecule. Extrapolating to zero frequency gave $\beta_{zzz}=50 \cdot 10^{-30}$ esu, which is consistent with the EFISH results since $\mu=3.7$ D [2].

Although the carbazole molecule **1d** showed no EFISH signal, its total HRS signal was quite similar to that of molecule **1b**, but the polarization ratio was significantly lower (around 2). This shows that molecule **1b** is not one-dimensional, and furthermore its polarization ratio is quite close to the value of 1.5 expected when $\beta_{zxx} \approx -\beta_{zzz}$. Solving for the HRS intensity in eq. (1) with $\beta_{zxx}/\beta_{zzz} = -1$ gave a zero frequency value $\beta_{zzz} = 30 \cdot 10^{-30}$ esu ; i.e. the long axis hyperpolarizability component is quite similar to that of the 1-D dialkyl amino analog.

In conclusion, we have presented evidence from several complementary techniques showing the second order nonlinearity of molecules with carbazole donor groups should be described in terms of two tensor components of opposite signs, which cancel out in an EFISH measurement.

References

- [1] Y. Zhang, L. Wang, T. Wada and H. Sasabe, Appl. Phys. Lett. 70 (1997) 2949.
- [2] C.R. Moylan, R.J. Twieg, V.Y. Lee, S.A. Swanson, K.M. Betterton and R.D. Miller, J. Amer. Chem. Soc. 115 (1993) 12599.
- [3] S.R. Marder, B.G. Tiemann, A.C. Friedli, E. Yang and L.-T. Cheng, Nonlinear Optics 9 (1995) 213.

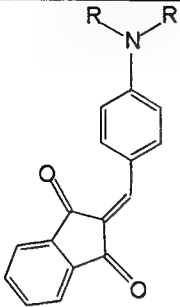
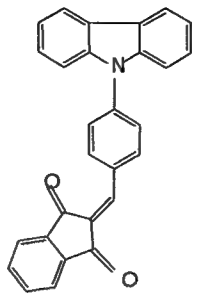
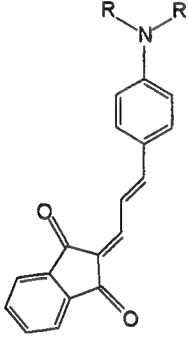
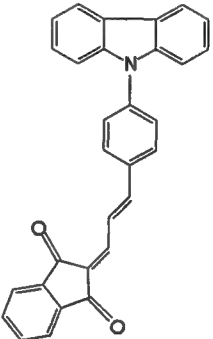
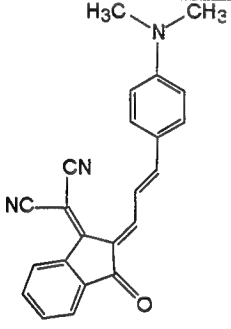
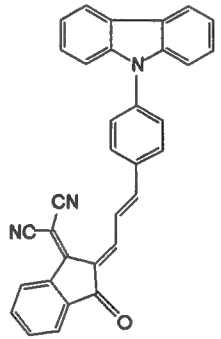
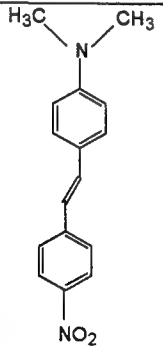
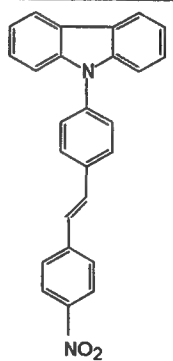
DIALKYL- OR DIARYL- AMINO DONOR	CARBAZOLE DONOR
 <p> 1a $R = CH_3$ $\mu\beta_0 = 130$ 1b $R = C_2H_5$ $\mu\beta_0 = 170$ 1c $R = C_6H_4-CH_3$ $\mu\beta_0 = 130$ </p>	 <p>1d $-10 < \mu\beta_0 < 0$</p>
 <p> 2a $R = CH_3$ $\mu\beta_0 = 300$ 2b $R = C_2H_5$ $\mu\beta_0 = 440$ 2c $R = C_6H_4-CH_3$ $\mu\beta_0 = 200$ </p>	 <p>2d $-50 < \mu\beta_0 < 20$</p>
 <p>3a $\mu\beta_0 = 790$</p>	 <p>3b $-25 < \mu\beta_0 < 25$</p>
 <p> 4a $\mu\beta_0 = 300$ (DANS) </p>	 <p>4b $\mu\beta_0 = 70$</p>

TABLE 1. Comparison of EFISH data (in units of 10^{-48} esu, and $\pm 20\%$ unless indicated otherwise) for molecules with a carbazole donor group with corresponding dialkyl or diaryl amine terminated molecules. Data for molecules **1c** and **2c** were taken from ref [2]; all other data were measured in this work. The EFISH experiments are performed on methylene chloride solutions, at $1.54 \mu m$; $\mu\beta_0$ values were calculated using the two-level model.

Synthesis and nonlinear optical properties of high glass transition polyimides and poly(maleimide-styrene)s.

Celest Samyn and Kurt Van den Broeck

Laboratory of Macromolecular and Physical Organic Chemistry,
University of Leuven, Celestijnenlaan 200F, B-3001 Leuven, Belgium

Tel: +32/(0)16/327438 Fax: +32/(0)16/327990

Celest.samyn@chem.kuleuven.ac.be, Kurt.vandenbroeck@chem.kuleuven.ac.be

Thierry Verbiest and André Persoons

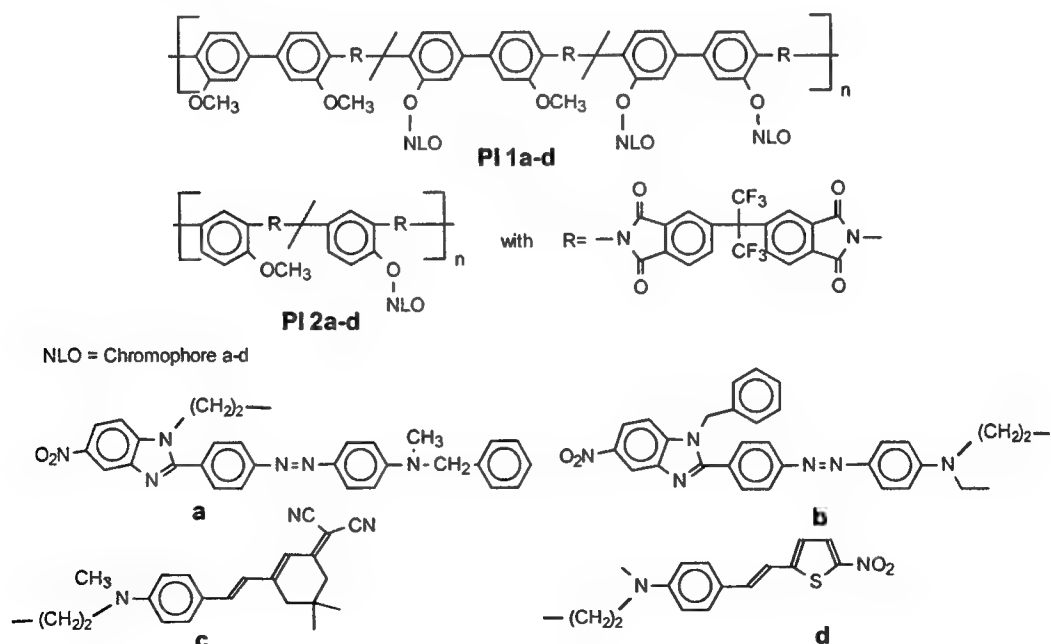
Laboratory of Chemical and Biological Dynamics and Center for Research on Molecular Electronics and Photonics,
University of Leuven, Celestijnenlaan 200D, B-3001 Leuven, Belgium.

Tel: +32/(0)16/327171 Fax: +32/(0)16/327982

Thierry.verbiest@fys.kuleuven.ac.be, Andre.Persoons@fys.kuleuven.ac.be

Organic nonlinear optical (NLO) polymers are of considerable interest in the development of second-order nonlinear optical materials, because of their potential applications for frequency doubling, optical storage devices, electro-optic switches and modulators¹. Long term stability of the NLO response is a major objective in the search for new polymer materials. The common method to suppress the reorientation of the aligned chromophores is to synthesize polymers exhibiting high glass transition (T_g) temperatures²⁻¹¹.

Polyimides show excellent thermal stabilities combined with good (nonlinear) optical properties, they were prepared by covalent binding of a chromophore (a-d) onto the polymer backbone of hydroxyl polyimide precursor polymers.



Glass transition temperatures for PI 1a-d polymers: 207-247°C and for PI 2a-d polymers: 264-275°C were obtained. The polymers were loaded with 34-62 wt% of chromophore. Six from the eight polymer systems could be spincoated onto ITO glass substrates, yielding high quality films. Noncentrosymmetry was induced by corona poling at a temperature of 10°C below T_g . Nonresonant $d_{33}(0)$ values up to 10 pm/V were obtained at 1064 nm of induced light.

A plot of $d_{33}(t)/d_{33}(t=0)$ as a function of time were $d_{33}(t)$ and $d_{33}(t=0)$ represent the second-harmonic coefficient at time t and time 0 respectively, at a temperature of 125°C is shown in Figures 1. and 2.

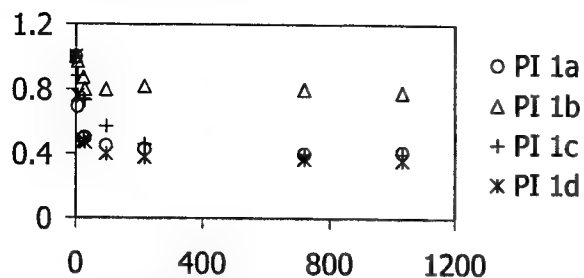


Fig. 1: $d_{33}(t)/d_{33}(t=0)$ in function of time(h) at 125°C for PI 1a-d.

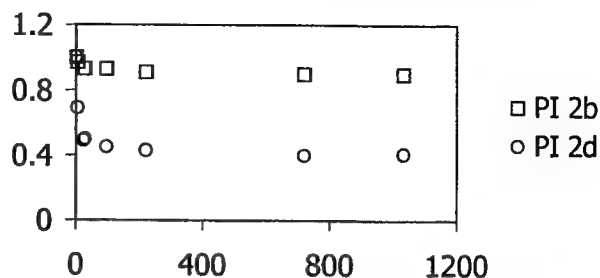
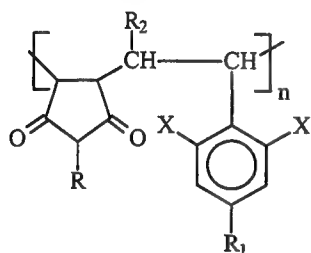


Fig. 2: $d_{33}(t)/d_{33}(t=0)$ in function of time(h) at 125°C for PI 2b and 2d.

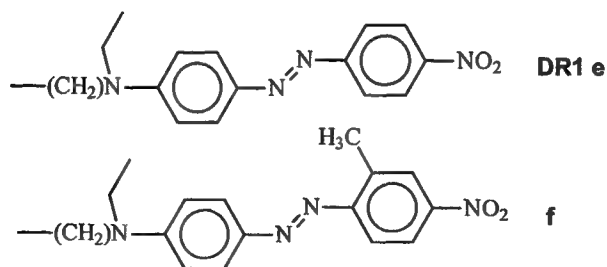
From this results, it can be seen that for polymers PI 1b and PI 2b after an initial decrease (28h), the nonlinearity does not significantly change over 1,000h, which finally results in 78% respectively 90% remaining NLO efficiency. The other systems initially show a larger decrease in the NLO response and stabilize at 36% to 56% after 1,000 h of heating.

Poly(maleimide-styrene) copolymers were prepared by polymer analogous reaction of maleic-anhydride copolymers with aminoalkyl-functionalized azo-chromophores a,e,f. Glass transition temperatures from 178-228°C could be obtained. The polymers were loaded with 36-54 wt% of chromophore.



P1-30-DR1(e): $R_2=H$, $X=H$, $R_1=-C_6H_5$
P2-42-DR1(e): $R_2=H$, $X=H$, $R_1=-C_6H_5$
P2-42-BIm(a): $R_2=H$, $X=H$, $R_1=-C_6H_5$
P1 a, e: $R_1=R_2=H$, $X=Cl$
Pp e, f: $R_1=O-CH_3$, $R_2=H$, $X=H$
Pβ f: $R_1=H$, $R_2=OCH_3$, $X=H$

Chromophores:



Poled films of the copolymers were measured for their second harmonic generation effect at 1064 nm of induced light, the highest obtained value of $d_{33}(0)$ was 12,5 pm/V. A plot of $d_{33}(t)/d_{33}(t=0)$ as a function of time at a temperature of 125°C is shown in figures 3. and 4.

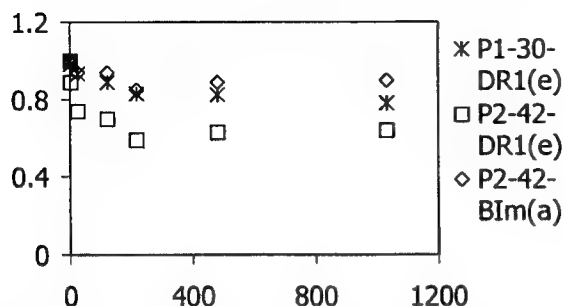


Fig. 3: $d_{33}(t)/d_{33}(t=0)$ in function of time(h) at 125°C for 4-Phenyl styrene systems.

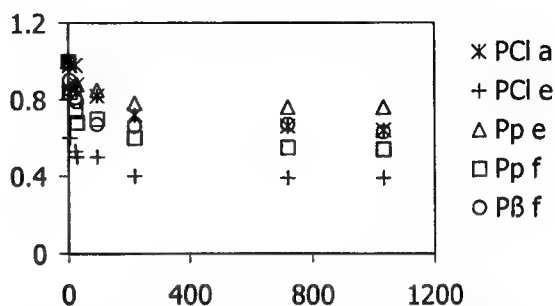


Fig. 4: $d_{33}(t)/d_{33}(t=0)$ in function of time(h) at 125°C for PCl, Pp and Pβ.

Poly(maleimide-4-phenyl styrene) copolymers show a poling order stability of 90% for the nitrobenzimidazole chromophore loaded copolymer, while the disperse red 1 loaded copolymers show stabilities up to 75% respectively 64% this depending on the chromophore content after 1,000 h of heating at 125°C.

The other copolymer systems give mostly a larger initial decrease (200h), which does not significantly change over 1,000 h. From the original value of the nonlinear optical response in polymer Pp e, 76% of the second-harmonic signal remained, while for PCl e only 40% remained, the other copolymers show poling order stabilities from 55-64%.

Our studies have shown that chromophore functionalized polyimides and copolymaleimides exhibit high glass transition temperatures, which result in a stable NLO-response at elevated temperatures. In addition the magnitude of the NLO-response suggests that these polymers could be useful for NLO-applications.

References:

- ¹⁾ D. M. Burland, R. D. Miller, C. A. Walsh, *Chem Rev.* **94**, 31 (1994)
- ²⁾ H.-J. Lee, M.-H. Lee, S. G. Han, H.-Y. Kim, J.-H. Ahn, E.-M. Lee, Y. H. Won, *J. Polym. Sci., Part A: Polym. Chem.* **36**, 301 (1998)
- ³⁾ D. Yu, A. Gharavi, L. Yu, *Appl. Phys. Lett.* **66**, 3005 (1995)
- ⁴⁾ D. Yu, A. Gharavi, L. Yu, *Macromolecules* **29**, 6139 (1996)
- ⁵⁾ Y. M. Cai, A. K.-Y. Jen, *Appl. Phys. Lett.* **67**, 299 (1995)
- ⁶⁾ T.-A. Chen, A. K.-Y. Jen, Y. Cai, *Macromolecules* **29**, 535 (1996)
- ⁷⁾ T. Verbiest, D. M. Burland, M. C. Jurich, V. Y. Lee, R. D. Miller, W. Volksen, *Macromolecules* **28**, 3005 (1995)
- ⁸⁾ T. Verbiest, D. M. Burland, M. C. Jurich, V. Y. Lee, R. D. Miller, W. Volksen, *Science* **268**, 1604 (1995)
- ⁹⁾ K. J. Drost, A. K.-Y. Jen, M. A. Drzewinski, *Polym Prepr. (Am. Chem. Soc. Div. Polym. Chem.)* **35**, 252 (1994)
- ¹⁰⁾ M. Ahlheim, F. Lehr, *Macromol. Chem. Phys.* **195**, 535 (1996)
- ¹¹⁾ T. Verbiest, C. Samyn, M. Van Beylen, A. Persoons, *Macromol. Rapid Commun.* **19**, 349 (1998)

Organic Photosensors for Ferroelectric Liquid Crystal Spatial Light Modulators

Scott Dickey, Blake Eliasson and Garret Model
 Department of Electrical and Computer Engineering
 University of Colorado, Campus box 425
 Boulder, CO 80309-0425
 Tel: (303) 492-1889, e-mail: model@colorado.edu

Introduction

We have combined organic charge generation (CG) and charge transport (CT) thin films to construct a bi-layer photosensor for use in an optically addressed spatial light modulator (OASLM). OASLMs have many applications including projection displays, incoherent to coherent image conversion, optical phase conjugation and reconfigurable optical fiber interconnects [1]. Current OASLM technology uses hydrogenated amorphous silicon (a-Si:H) as the photosensor [2]. Organic materials offer advantages over a-Si:H in that they potentially have higher resolution due to their low carrier mobility, are compatible with nearly any substrate, and have a low dielectric constant for better capacitance matching to the liquid crystal. Previously OASLMs were demonstrated using single-layer organic photosensors. One device used a polymer dispersed liquid crystal and required high voltage (70-90 Vrms) and low drive frequency (< 30 Hz) for operation [3]. Another employed a nematic liquid crystal, obtaining response times of 10^2 - 10^3 ms [4]. We present an improved photosensor for a high performance OASLM incorporating high-speed ferroelectric liquid crystals.

The device structure is shown in figure 1.

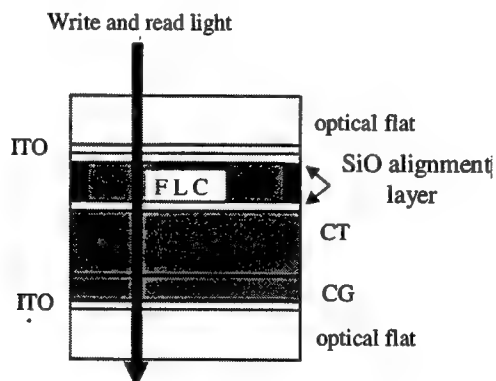


Figure 1: OASLM cross section

The optical absorption takes place within the thin (200 Å) CG layer, forming an electron-hole pair. In reverse bias the electron, with its lower mobility, is collected at the adjacent contact while the hole must drift to the photosensor-FLC interface. To facilitate this hole transport a CT material providing higher

hole mobility is incorporated. The photosensor must be significantly thicker than the CG layer in order to avoid switching the FLC in the absence of write-light illumination [2].

Fabrication

We prepared the charge generation layer by mixing 50% (by weight) titanylphthalocyanine (TiOPc) pigment into a host matrix of 40% polyvinyl butyral (PVB) and 10% N,N'-diphenyl-N,N'-bis(3-methylphenyl)-(1,1'-biphenyl)-4,4'-diamine (TPD), a p-type dopant, in a tetrahydrofuran solvent. This mixture was ball milled, spun onto ITO coated glass substrates to a thickness of approximately 200 Å, and dried in vacuum. We prepared the charge transfer layers by dissolving 70% TPD and 30% polystyrene, as the host matrix, in toluene. This mixture was spun onto the CG layer to a thickness of approximately 2 μm and dried in air at room temperature. Toluene was chosen as the CT solvent because of the low solubility of PVB in it, thus reducing mixing of the pigment from the CG layer. Electrical contact was made with gold electrodes evaporated onto the films.

Experimental Results

A typical current-voltage characteristic of the bi-layer photosensor appears in figure 2.

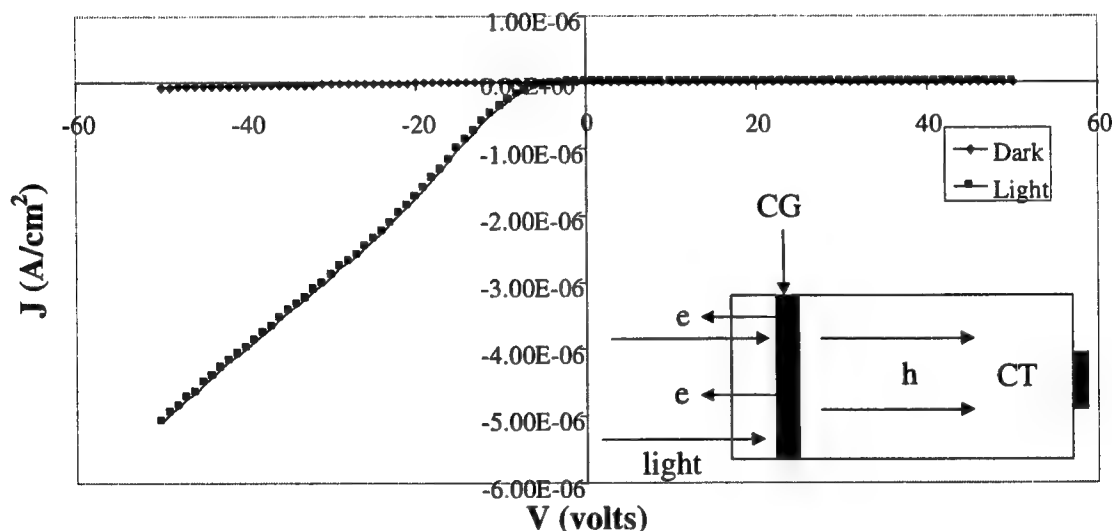


Figure 2: Typical I-V characteristic for a bi-layer system under 5 mW illumination.

The curve shows that the device has a non-linear photodiode-like characteristic. Because the reverse-bias current under illumination is voltage dependent, it appears that the mobility limits the hole collection.

An effective way to find the hole mobility is to measure the time of flight. Traditionally, this is done by optically pulsing the device and measuring the photocurrent decay over time. However, because of the low photocurrents another approach yields clearer response data. It is to measure the frequency response of the photocurrent, with results shown in figure 3.

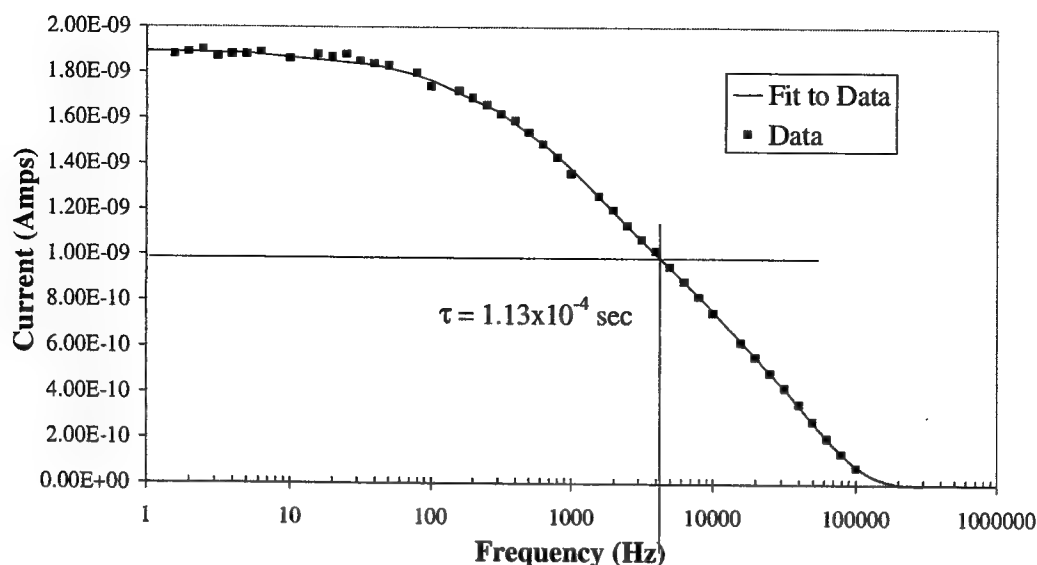


Figure 3: Frequency response indicating the half maximum point

The time required for a carrier to drift through the device (τ) is approximately $(2\pi f)^{-1}$, [5] where f is measured at the half maximum of the amplitude. For a 2- μm device biased at 20 volts the mobility, which is given by $d^2/V\tau$, is $2 \times 10^{-5} \text{ cm}^2/\text{V}\cdot\text{sec}$ (where d is the device thickness). With this mobility and response time we can operate an OASLM in the low kHz range, allowing us to drive high-speed ferroelectric liquid crystals.

Future Work

To further improve the transport properties of the photosensor, different material combinations in the CG and CT layers will be explored. Higher mobility dopants will be incorporated into the CT layer and the material purity issues will be improved. In construction of an improved OASLM, the polymer flatness over large enough areas is a critical issue that must be addressed.

References

- 1 *Spatial Light Modulator Technology: Materials, Devices, and Applications*, U. Efron, editor, (Marcel Dekker, New York, 1995) pp. 287-359.
2. "Thin-film photosensor design for liquid crystal spatial light modulators," P.R. Barbier, L. Wang, and G. Model, *Opt. Engr.*, 33, 1322-1329 (1994).
3. "Infrared- and Visible-Light Sensitive Spatial Light Modulator Using Pigment-Dispersed Organic Photoconductor," H. Fujikake, K. Takizawa, H. Kikuchi, J. Hirose, T Kobayashi and T. Matsumoto, *Japanese Journal of Applied Physics*, 1995, Vol. 34, pp. 4067-4073.
4. "Liquid Crystal Optically Addressed Spatial Light Modulators with the Organic Polymer Thin-Film Photoconductors," A. Parfenov, B Rumyantsev, L. Danilina, D. Pebalk, B. Kotov, *Proc. SPIE*, 1996, Vol. 2722, pp. 241-249.
5. "Photocurrent response times in undoped amorphous hydrogenated silicon," M.A. Parker and E.A. Schiff, *Applied Physics Letters*, 1986, Vol.48, pp. 1087-1089.

Bistable optical transmittivity in an ultrathin film of oriented molecular aggregates

K.-H. Feller and H. Glaeske

Fachhochschule Jena, Fachbereich Medizintechnik/Physikalische Technik, Tatzendpromenade 1b, D-07745 Jena, Germany

feller@mt.fh-jena.de, glaeske@stud.fh-jena.de

V.A. Malyshev

All-Russian Research Center "Vavilov State Optical Institute", Birzhevaya Liniya 12, 199034 Saint-Petersburg, Russia

In connection with the search for possibilities to create photonic devices working in the throughput regime the investigation of optical bistabilities in thin layers of organic molecular aggregates has been an active field of research in the last few years. An experimental realization of the bistable behavior of an aggregate would give us a real chance to create an all-optical switching unit which being integrated in an array could serve as a macro-unit of a logical all-optical device.

In¹⁻⁴ a mechanism of bistability attributed to an individual homogeneous aggregate or a localization segment was considered. But as has been shown in Refs.^{2,4} an aggregate of size less than the emission wavelength did not display any bistable behavior. This finding makes the above mechanism of the aggregate bistability to be hardly realizable at least for such well studied objects as J-aggregates in spite of that they normally incorporate to itself thousands of molecules having subsequently a size larger than an optical wavelength. In this connection the question can be risen whether an ensemble of localization segments just being shorter than the emission wavelength may display a bistable behavior. As was shown in Refs.^{5,6} a model system of homogeneously broadened two-level molecules elaborated in the form of a thin slab of a thickness smaller than an emission wavelength manifests a bistable behavior of transmittivity (or reflectivity) resulting from the coupling of molecules via the emission (far-zone) field. Note that the previous mechanism of bistability in fact originated from the near-zone intermolecular interaction^{2,3}.

We have shown that under the conditions of low-temperature experiments J-aggregated molecular systems can be modeled by an ensemble of inhomogeneously broadened two-level systems. Since the typical concentrations of molecules needed for the aggregation is rather high ($10^{-4} - 10^{-3} \text{ mol/dm}^3$) such that a square of linear size of the order of the emission wavelength incorporates many molecules a thin film comprised of J-aggregates may manifest a bistable behavior of transmittivity due to the coupling of localization segments via the emission field. Critical parameters for the occurrence of such a behavior seems to be achievable for J-aggregates of polymethine dyes.

The mathematical basis of the above mentioned concept implies the use of the standard set of semiclassical equations for the slowly varying (in time) amplitudes E and R respectively of the electric field and off-diagonal density matrix element as well as for the population difference between the one-exciton and ground states Z . For a sample in the form of a thin film of thickness L smaller than wavelength (considered along this Letter) it has the form

$$\dot{R}_N = -(i\Delta_N + \Gamma_N)R_N + \mu_N \Omega Z_N, \quad (1a)$$

$$\dot{Z}_N = -\frac{1}{2}\mu_N(\Omega R_N^* + \Omega^* R_N) - \gamma_N(Z_N + 1), \quad (1b)$$

$$\Omega = \Omega_i + \gamma_R \sum_N p(N) \mu_N R_N. \quad (1c)$$

Here the subscript N denotes the size of localization segment; $\Delta_N = \omega_N - \omega_i$ is the resonance detuning between the incident (ω_i) and transition (ω_N) frequencies; γ_N is the spontaneous emission constant of the

optically-active one-exciton state: $\gamma_N \approx \gamma_0 N$ with γ_0 being the analogous constant for an isolated molecule; $\Gamma_N = \gamma_N/2 + \Gamma_2$ is the dephasing constant including that (2) not connected with the spontaneous emission; $\Omega = d_N E/\hbar$ and $\Omega_i = d_N E_i/\hbar$ are the whole (also transmitted) and incident electric fields (in the frequency units) respectively, with d_N being the transition dipole moment for a segment of mean size N scaled as $d_N \approx d\sqrt{N}$ where d is the transition dipole moment of an isolated molecule; $\mu_N = d_N/d_N$; $p(N)$ is the distribution function of localization segments over sizes; $\gamma_R = 2\pi d_N^2 n k_i L/\hbar = 2\pi d^2 n_0 k L/\hbar$ where $k = \omega_N/c$ (c is speed of light) describes the superradiant radiative damping of an ensemble of two-level molecules and $n_0 = N/n$ is the original concentration of molecules in the film i.e. before aggregation.

For obtaining the parameter range for the possibility to get a bistable behavior of the system we investigate the steady-state solution of Eqs. (1) ($\dot{R}_N = 0 = \dot{Z}_N$) and obtain the following equation:

$$|\Omega|^2 \left[\left(1 + \gamma_R \sum_N p(N) \mu_N^2 \frac{\Gamma_N}{\Delta_N^2 + \Gamma_N^2 + \mu_N^2 \Gamma_N |\Omega|^2 / \gamma_N} \right)^2 + \left(\gamma_R \sum_N p(N) \mu_N^2 \frac{\Delta_N}{\Delta_N^2 + \Gamma_N^2 + \mu_N^2 \Gamma_N |\Omega|^2 / \gamma_N} \right)^2 \right] = \Omega_i^2. \quad (2)$$

By modelling the size distribution relative to which we have no real information by a Lorentz-shaped distribution we substitute in Eq. (2)

$$\sum_N p(N) \rightarrow \int_{-\infty}^{\infty} d\Delta p(\Delta) = \int_{-\infty}^{\infty} d\Delta \frac{G}{\pi} \frac{1}{(\Delta - \Delta_0)^2 + G^2},$$

where G plays the role of the J-band width and $\Delta_0 = \omega_0 - \omega_i$ is the deviation of the external frequency ω_i on the central frequency of the Lorentzian and replace all other quantities by their mean values.

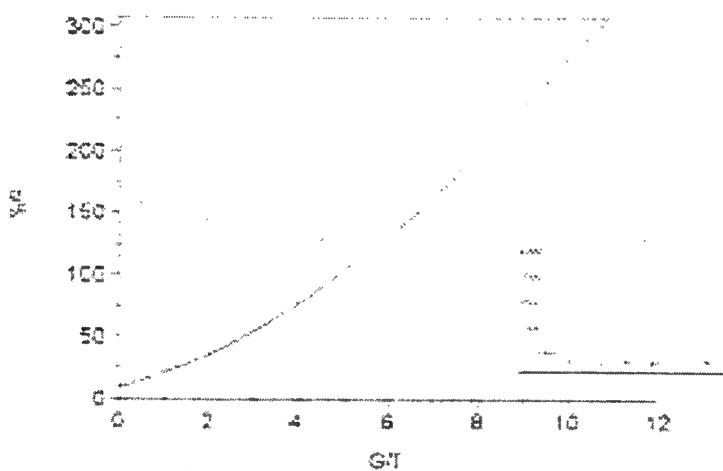


Fig. 1. Effect of the inhomogeneous broadening (or size dispersion) on the appearance of a three-valued solution to Eq. (2). The dashed region represents the domain of parameters G/Γ and γ_R/Γ where the bistable behavior can appear (same in the insert) only for a wider domain of G/Γ and γ_R/Γ .

In Fig. (1) the results of numerical solution of Eq. (2) are depicted showing the domain of parameters γ_R/Γ and G/Γ for which the bistable behavior can be realized (shadowed region). As is seen from this figure the threshold of bistability is $(\gamma_R/\Gamma)_c = 8$ (at $G = 0$)⁵. The dispersion of sizes acts in such a manner that the higher ratio G/Γ is the value of γ_R/Γ is required to get the bistability effect.

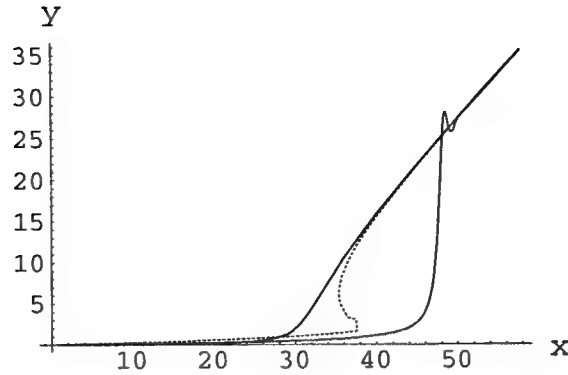


Fig. 2. Above-threshold ($\gamma_R/\Gamma = 10$) optical hysteresis loop of the output intensity $y = |\Omega|^2/\gamma\Gamma$ calculated using Eqs. (1) at adiabatic up-and-down scanning of the input intensity $x = \Omega_i^2/\gamma\Gamma$ (solid line). The dotted curve represents the stationary solution to the set of Eqs. (1). Detuning of resonance $\Delta = 0$.

Figure 2 represents the numerical solution of Eqs. (1) at adiabatic up-and-down scanning of the input intensity Ω_i^2 displaying the possibility of getting the hysteresis and high-contrast switching of transmittivity of the film. At zero detuning of the resonance slightly above the threshold an estimate gives $\Omega_i^2 \approx 27\gamma\Gamma$ which provides an image of the input field magnitude (in terms of relaxation constants) needed for switching of the transmittivity.

In conclusion let us discuss parameters of J-aggregates of PIC-Br as a real system one of the most studied in the last years. The width of the J-band is of the order of the blue shift of the transition from one-to-two exciton bands with respect to that from the ground state to the one exciton band for the red J-band ($\lambda = 576.1nm$) $\Gamma 30cm^{-1}$ or $G \approx 1ps^{-1}$ in frequency units. Taking $\gamma_0 = (1/3.7ns)$ $\Gamma n_0 = 2 \cdot 10^{18}cm^{-3}$ and $L \approx \lambda \approx 5.73 \cdot 10^{-5}cm$ Γ the superradiant damping constant can be estimated as $\gamma_R \approx 13ps^{-1}$ Γ i.e. Γ a magnitude that is remarkably larger than the width of the J-band G . Manipulating then the temperature Γ the required ratios of γ_R/Γ and G/Γ can be achieved to be within the bistable region (shown in Fig. 1 as shadowed).

-
1. V. V. Gusev Γ Adv. Mater. Opt. Electr. **1** 235 (1992).
 2. V. Malyshev and P. Moreno Γ Phys. Rev. A **53** 416 (1996).
 3. V. A. Malyshev Γ H. Glaeske and K.-H. Feller Γ Opt. Commun. **140** 83 (1997); J. Lumin. **76&77** 445 (1998).
 4. V. A. Malyshev Γ H. Glaeske and K.-H. Feller Γ Phys. Rev. A **58** 670 (1998).
 5. S. M. Zakharov and E. A. Manykin Γ 'Poverkhnost' (Moscow) **2** 137 (1988) [in Russian].
 6. A. M. Basharov Γ Zh. Exp. Teor. Fiz. **94** 12 (1988) [Engl. transl.: JETP **67** 1741 (1988)].

Paper withdrawn.

Optical Anisotropy of All Optically Induced $\chi^{(2)}$ Polar Structures

Naoto Tsutsumi* Masanori Imamura, Yoshiki Ikeyama,
Jun Yamamoto and Wataru Sakai

*Department of Polymer Science & Engineering, Kyoto Institute of Technology,
Matsugasaki, Sakyo, Kyoto 606-8585, Japan*

Tel: +81-756-724-7810; Fax: +81-75-724-7800; E-mail: tsutsumi@ipc.kit.ac.jp

Introduction

Nonlinear optical properties of organic materials have been of great interest because of their potential applications in frequency doubling for data storage, electro-optic modulation for telecommunication and optical interconnects, and integrated optics [1]. Large second-order optical nonlinearity in organic compound derived from the noncentrosymmetric alignment of π -conjugated compound with donor and acceptor sites. Langmuir Blodgett films or dipolar alignment by a static DC electric field in polymeric films is a common and widely used techniques to induce the noncentrosymmetric alignment of NLO dipoles. In recent years, photoinduced macroscopic $\chi^{(2)}$ structures has been demonstrated in a glass optical fiber [2] and in the polymeric materials with dipolar [3] or octupolar molecules [4]. This new technology opens up new way for developing noncentrosymmetric molecular orientation using all optical process [3,4,5]. Time averaged third-order optical nonlinearity of coherent superposition between fundamental and second harmonic lights is significantly responsible for the creation of the polar field which induces the noncentrosymmetric alignment of the dipolar molecules or moieties.

In this report, we present the noncentrosymmetric NLO dipolar orientation ($\chi^{(2)}$ structures) induced by the interference waves between fundamental and second harmonic lights in the polymeric materials embedded with azobenzene chromophores and investigate the optical anisotropy of $\chi^{(2)}$ structures.

Experimental

NLO material is Disperse Red 19 attached polyurethane (DR19-polyurethane). Schematic diagram of all optical poling is shown in Figure 1. Laser source is a Continuum model Surelite-10 Q-switched Nd:YAG pulse laser with 1064 nm *p*-polarized fundamental beam (320 mJ maximum energy, 7 ns pulse width and 10 Hz repeating rate). Second harmonic light from KTP crystal was supplied for seeding process. In the seeding (writing) process in Figure 1 (a), laser lights with fundamental (250 μ J) and doubled frequencies (1.25 μ J) were irradiated the sample films to create the noncentrosymmetric alignments of dipoles. In the reading process in Figure 1 (b), the second harmonic light was observed from the film sample using a

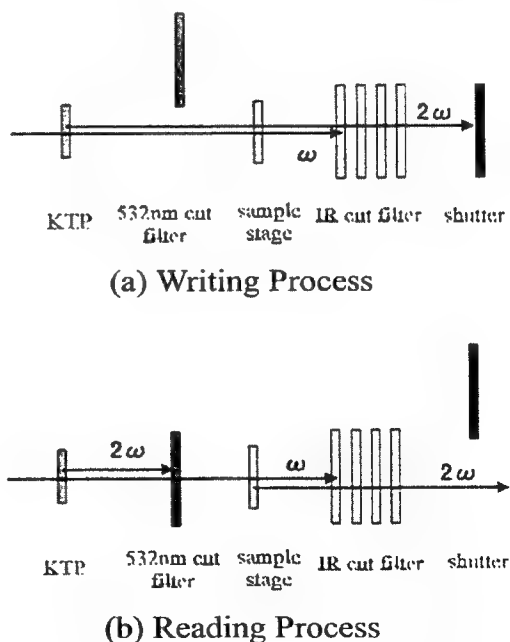


Figure 1. Schematic diagram of all optical poling

laser light with a fundamental frequency. In the optical poling process, computer controlled alternative writing and reading procedures was employed. Polarization direction (*p*-polarization and *s*-polarization) of writing and reading beams was controlled using a $\pi/2$ polarized plate putting on the optical path before entering KTP crystal.

Results and Discussion

Theoretical background of all optical poling process is relied on the optically induced polar field due to the cubic interference between fundamental and second harmonic waves. Photoinduced $\chi^{(2)}$ is proportional to the time averaged cubic interference of fundamental and second harmonic waves and given as follows [3]:

$$\chi_{ind}^{(2)} \propto \langle E^3(M,t) \rangle_t = \langle (E_\omega(z,t) + E_{2\omega}(z,t))^3 \rangle_t \quad (1)$$

where $\langle E^3(M,t) \rangle_t$ is a time averaged cubic interference beams. Assuming that the medium is transparent at fundamental frequency ω and taking α the absorption coefficient at 2ω frequency, this term writes:

$$\begin{aligned} \chi_{ind}^{(2)} &\propto \langle (E_\omega(z,t) + E_{2\omega}(z,t))^3 \rangle_t \\ &= (E_\omega^2 E_{2\omega}^* \exp(-i\Delta kz) + E_\omega^* E_{2\omega} \exp(i\Delta kz)) \exp(-\frac{\alpha}{2}z) \\ &= 2|E_\omega^2 E_{2\omega}^*| \cos\Delta kz \exp(-\frac{\alpha}{2}z) \end{aligned} \quad (2)$$

with $\Delta k = 2k_\omega - k_{2\omega}$ and where E_ω and $E_{2\omega}$ are the complex amplitudes of the optical fields at ω and 2ω frequencies. Taking $\Delta\Phi$ the relative phase difference between two writing beams, the equation (2) yields:

$$\chi_{ind}^{(2)} = |E_\omega^2 E_{2\omega}^*| \cos(\Delta\Phi + \Delta kz) \exp(-\frac{\alpha}{2}z) \quad (3)$$

Here, $\Delta\Phi$ was controlled by varying the tilt angle of a slide glass inserted in front of the sample.

The NLO dipole moments oriented by *p*-polarized interference beam in the writing process produced significant large *p*-polarized SH wave in the reading process. When *s*-polarized interference beam is used in the writing process, significant large *s*-polarized SH wave was observed in the reading process. Then the optical anisotropy of $\chi^{(2)}$ structures is measured by monitoring the intensity of the second harmonic wave with changing polarization direction of reading fundamental beam. Figure 2 shows the dependence of the generated second harmonic intensity on the polarization direction of the fundamental beam for all optically poled films. It is clearly shown that the NLO dipole moments are aligned along the polarization direction in the plane of film.

Reference

- 1) H. S. Nalwa, T. Watanabe, and S. Miyata, in *Nonlinear Optics of Organic Molecules and Polymers*, edited by H. S. Nalwa and S. Miyata (CRC, Boca Raton, 1997), Chap. 4, pp. 89-350.
- 2) U. Österberg and W. Margulis, *Optics Letters*, **11** 516 (1986).

- 3) C. Fiorini, F. Charra, J. M. Nunzi and P. Raimond, *Nonlinear Optics*, **9**, 339 (1995).
- 4) C. Fiorini, F. Charra, J. M. Nunzi, I. D. W. Samuel and J. Zyss, *Optics Letters*, **20**, 2469 (1995).
- 5) N. Tsutsumi, Y. Ikeyama and W. Sakai, *Nonlinear Optics*, in press.

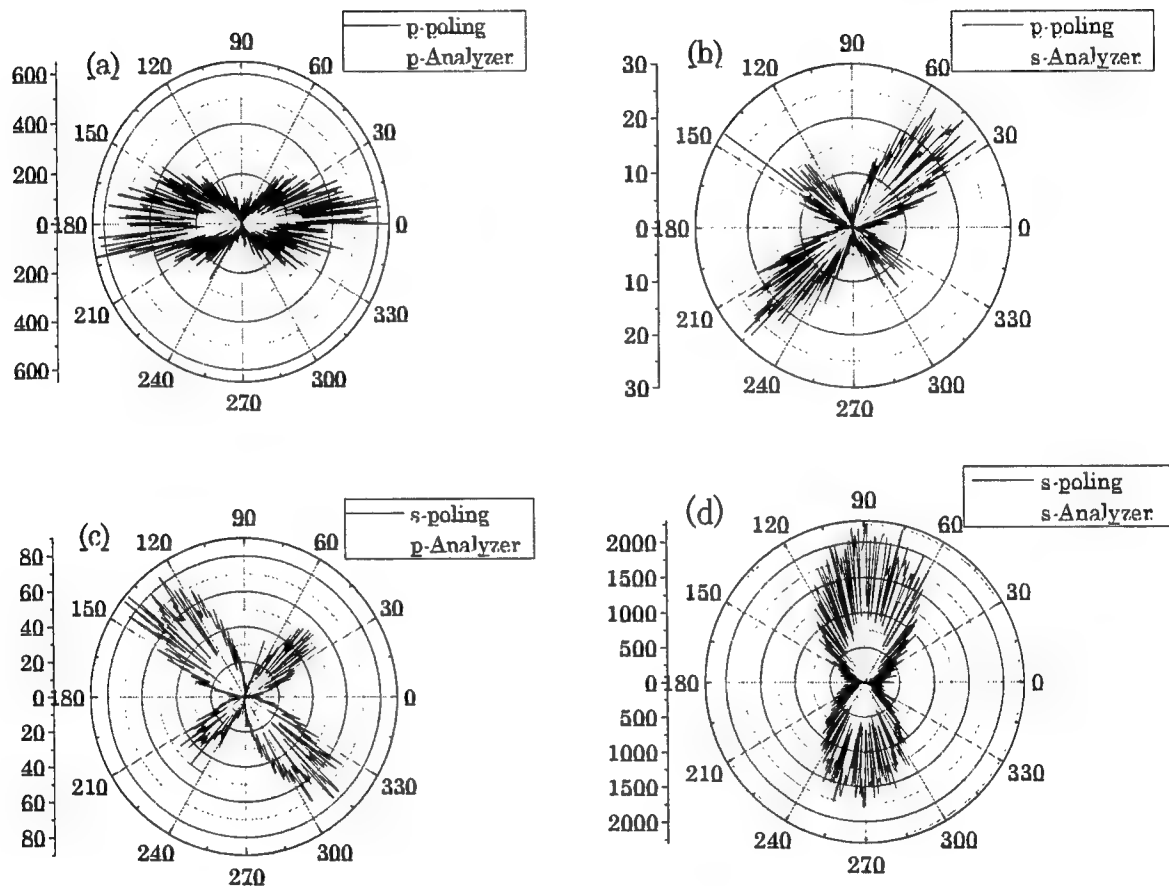


Figure 2. Dependence of SHG intensity on rotation angle of polarizer.

- (a) Poling: *p*-polarization fundamental and second harmonic waves;
Reading: *p*-polarized analyzer.
- (b) Poling: *p*-polarization fundamental and second harmonic waves;
Reading: *s*-polarized analyzer.
- (c) Poling: *s*-polarization fundamental and second harmonic waves;
Reading: *p*-polarized analyzer.
- (d) Poling: *s*-polarization fundamental and second harmonic waves;
Reading: *s*-polarized analyzer.

Photorefractive mechanisms in liquid crystal and polymer composites

Oksana Ostroverkhova, Jingwen Zhang, and Kenneth D. Singer

Department of Physics, Case Western Reserve University, Cleveland, OH 44106

Tel: +(216)-368-4017, email: kds4@po.cwru.edu

Ludmilla Sukhomlinova and Robert J. Twieg

Department of Chemistry, Kent State University, Kent, Ohio 44242

Tel: (330) 672-2791, Email: rtwieg@lci.kent.edu

High performance photorefractive polymer composites have been reported to possess large gain coefficients, high diffraction efficiencies, and short response times.[1,2] However, phase separation has been identified as a potential problem in these materials. Based on two considerations, maximization of the orientational enhancement effect[4] and inhibition of phase separation, we selected 4,4'-n-pentylcyanobiphenyl (5CB), which is a fluid (liquid crystal) at room temperature, as the nonlinear chromophore for a polymer composite. Choosing the host polymer poly[N-vinylcarbazole] (PVK) as the photoconductive agent, and C_{60} as a sensitizer, [5] a homogeneous single-phase composite with low light scattering, high speed, and high gain was formulated. No phase separation is observed in any samples up to this date, one and half years after fabrication, although no separate plasticizing agent is added.

Two-beam coupling experiments were performed to determine the gain and phase shift as a function of electric field. Large photorefractive gains of about 150/cm are observed with response times of the order of 1 second. Using the theory of photorefractive space charge formation and orientational enhancement, we fit our experimental results to determine the ratio of the orientational to the Pockels response (C_{BR}/C_{EO}) for the formation of the index of refraction replica. Using $\Lambda=3.0\mu m$, $T=300$, $\epsilon_r=6.5$ we find that $C_{BR}/C_{EO}\sim 2.9$. This is considerably less than the ratio of $C_{BR}/C_{EO}\sim 40$ that would be expected from the orientational response theory based on separately measured molecular parameters and freely rotating molecules. Thus chromophore orientation is inhibited in these samples as the temperature of measurement is about 15°C below the glass transition.

Temperature dependence of the gain was measured to study the influence of the nonlinear chromophore orientation on the magnitude of the gain coefficients and the ratio C_{BR}/C_{EO} . Typical data is shown in Fig.1

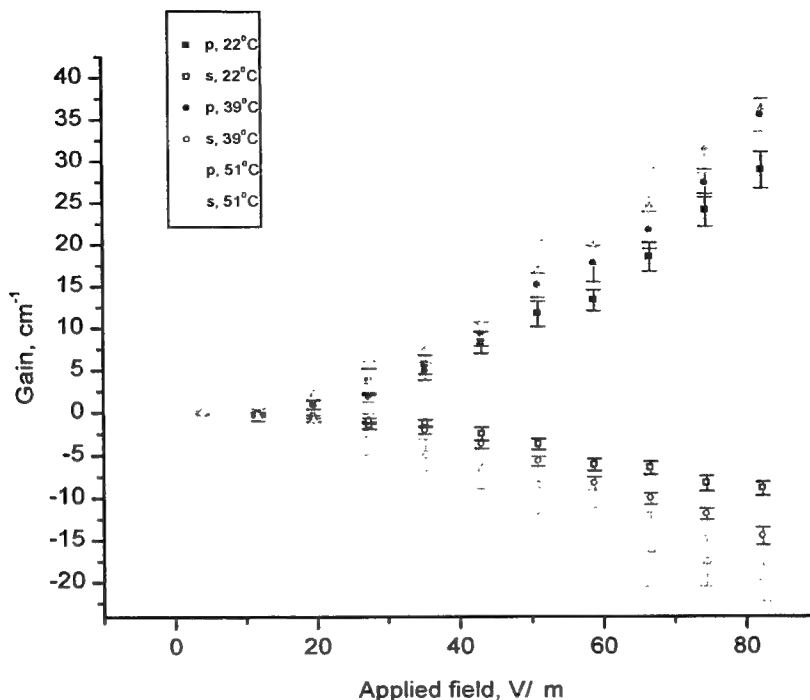


Fig.1. Temperature dependence of the gain coefficients.

We found that the gain increased for both p- and s-polarizations of the incident beams, with the s-polarization configuration being more sensitive to the change of the temperature. Also, the increase in the ratio C_{BR}/C_{EO} with a tendency to saturate at temperatures above the glass transition temperature was established. We found also that the establishment of the space charge field was temperature dependent due to occupancy of trap states.

Studies of chromophore concentration dependence and replacement of the chromophore with other nematic liquid crystals are being studied in order to verify the validity of the orientational enhancement model and to determine the optimum gain and response time.

Effort sponsored by the Air Force Office of Scientific Research, Air Force Materiel Command, USAF, under grant number F49620-96-1-0152 and by the NSF under Science and Technology Center Advanced Liquid Crystalline Optical Materials grant DMR89-20147.

1. W. E. Moerner, and S. M. Silence, *Chem. Rev.* **94**, 127 (1994)
2. W. E. Moerner, A. Grunnet-Jepsen, and C. L. Thompson, *Annu. Rev. Mater. Sci.* **27**, 585 (1997)
3. W.E. Moerner, S.M. Silence, F. Hache, and G.C. Bjorklund, *J. Opt. Soc. Am. B* **11**, 320 (1994)
4. J. Zhang and K. D. Singer, *Appl. Phys. Lett.* **72**, 2948 (1998)

Organic Thin Films for Photonics Applications

Polymer Integrated Optics: 1

Sunday, 26 September 1999

Robert A. Norwood, Photon-X, Inc., USA
Presider

SuA

8:30am–9:45am

California Ballroom Salons 4&5

Rare Earth Doped Polymer Optical Amplifiers

R. Gao and A. F. Garito

Department of Physics and Astronomy, University of Pennsylvania, Philadelphia, Pennsylvania 19104
garito@afgarito.physics.upenn.edu

Introduction

There has been much recent interest in rare earth doped systems for their application in photonics as fiber and waveguide amplifiers and lasers [1, 2]. Rare earth doped fibers and waveguides and their numerous applications constitute a major part of the ever-growing field of photonics. Applications range from signal amplifiers to fiber lasers and more recently to upconversion lasers. The simple principles behind their operation and the relative ease of fabrication have made rare earth doped systems both popular and accessible. Compact and efficient devices can be constructed by combining the optical gain of the rare earth ions with the high confinement of light intensity characteristic of single-mode fibers and waveguides. Rare earth-doped glass and crystal systems have been, and continue to be, extensively investigated, but studies of polymer systems are far fewer and have only recently become the focus of major investigations [3]. With the increasing awareness of the utility of polymer optical fibers (POFs) and waveguides [4, 5], rare earth doped polymer systems are also of interest. Rare earth ions can be introduced into polymers by encapsulating the ions by covalently bonded, physically insulating, organic ligands and then incorporating the resulting chromophores as guests, chains, or cross-links, in the polymer matrix. To evaluate the potential of these types of systems for amplification and lasing, it is essential to understand the radiative and nonradiative properties of the rare earth chromophores.

The property of a rare earth ion optical transition most influenced by the surrounding environment is the metastable state lifetime, which should be maximized for efficient optical performance. For a particular rare earth ion and host combination, the metastable state lifetime depends strongly on the organic ligands that coordinate to and encapsulate the ion. According to multiphonon theory, the lifetime can be increased upon reduction of the phonon energy spectrum surrounding the ion. In practice, this is accomplished by replacing bonds characterized by high vibrational energies with lower vibrational energy analogs [3]. Rare earth ions typically prefer eight- or nine-fold coordination [6], which can be achieved in a variety of ways. Tetrakis chromophores fully satisfy the bonding requirement, and hence shield the ion from the surrounding environment, as they possess four ligands with two coordinating oxygen atoms per ligand. Accordingly, tetrakis chromophores are usually favored over tris and fewer-ligand species, which do not effectively shield the rare earth ion.

Earlier, we have demonstrated [3] how to control the phonon spectrum and multiphonon decay through design and analysis of a series of chromophores, namely for example, the series comprised of the tetrakis species of D, BTF and HFA [3]. In each successive chromophore, one phenyl group containing high vibrational energy C-H bonds ($\sim 2950\text{ cm}^{-1}$) is replaced by a CF_3 group with low vibrational energy C-F bonds ($\sim 1200\text{ cm}^{-1}$). Accordingly, the chromophores having the lower energy vibrations suffer less nonradiative decay and, hence, possess longer lifetime, Table 1 displays the samarium (Sm^{3+}) $^4\text{G}_{5/2}$ metastable state lifetimes of the chromophore series in several hosts. The Sm^{3+} transition wavelength of interest is 650 nm because the central wavelength coincides with the window in the attenuation spectrum of PMMA. It is seen that the lifetimes increase from 3 μs for $\text{Sm}(\text{D})_4\text{NEt}_4$ to over 200 μs for $\text{Sm}(\text{HFA})_4\text{NEt}_4$. From these results, it is evident that the ligands directly influence nonradiative decay. Moreover, in this case, fluorination increases the metastable state lifetime by two orders of magnitude.

Host	Sm(D) ₄ NEt ₄ Lifetime (μ s)	Sm(BTF) ₄ NEt ₄ Lifetime (μ s)	Sm(HFA) ₄ NEt ₄ Lifetime (μ s)
Acetone-d ₆	3	157	257
PMMA	<1	88	104
PMMA-d ₈	<1	135	194

Table 1. Sm³⁺ ⁴G_{5/2} metastable state lifetimes of the chromophore series Sm(D)₄NEt₄, Sm(BTF)₄NEt₄, and Sm(HFA)₄NEt₄ in several hosts.

Importantly, we have observed [7] that in the process of incorporating tetrakis chromophores into polymers, the tetrakis species can dissociate into a tris form, containing three ligands, plus a free ligand. Since the tris chromophore only provides six coordinating oxygens, there remain two open sites which are usually occupied by two molecules of water or solvent [8,9]. Consequently, the tris species usually possesses a reduced metastable state lifetime because of the presence of the coordinating water or solvent molecules and their high vibrational energy O-H and C-H bonds. We overcame this deleterious dissociation effect by replacing the more highly fluorinated BTF ligand with the HFA ligand. Figure 1(a) is the dissociation curve of Sm(BTF)₄P chromophore. Figure 1(b) shows that there is no dissociation effects occurring in Sm(HFA)₄NEt₄ systems and that the increased fluorination results in increased rare earth chromophore stability.

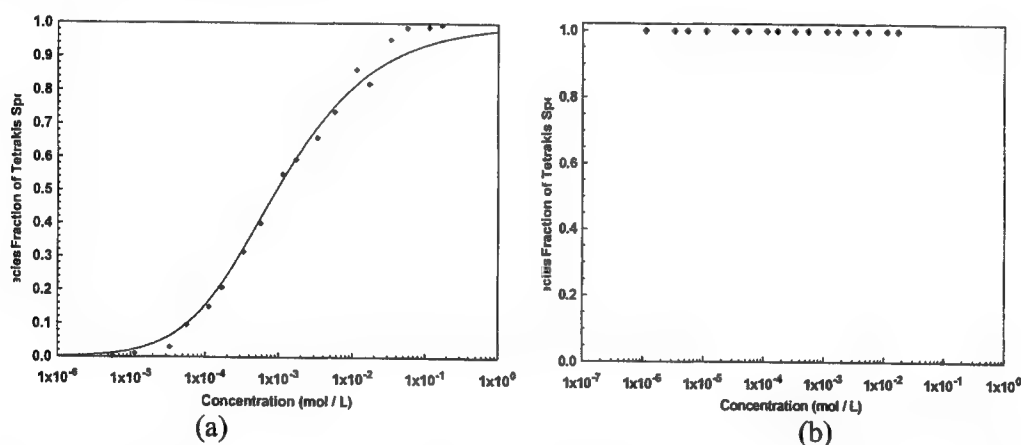


Figure 1. Dependence of the equilibrium fractions of tetrakis species of (a) Sm(BTF)₄P and (b) Sm(HFA)₄NEt₄ solutions in MMA monomer.

Amplifier Simulations

The viability of an amplifier system based on these rare earth polymer materials can be determined by calculating the single pass gain. Here, a Sm³⁺ chromophore-doped waveguide pumped by 488 nm light and operating at 650 nm is analyzed and simulated. The important quantity characterizing an amplifier is its single pass gain. The 650 nm samarium chromophore is modeled as a four-level system. With level 1 as the ground state, it is assumed that the lifetime of the pumped state (level 2) is much shorter than the metastable state (level 3) and, hence, the steady state population of level 2 is negligible. The evolution of the pump and signal beam intensities along the length of the waveguide in the z-direction can be derived. Under the assumption of no excited state absorption, the intensity equations are given by [1].

$$\int_0^{\infty} \int_0^{2\pi} \frac{dI_p}{dz} r dr d\phi = - \int_0^{\infty} \int_0^{2\pi} (n(r, \phi, z) \sigma_p N_1 - \alpha_p) I_p r dr d\phi \quad (1)$$

$$\int_0^{\infty} \int_0^{2\pi} \frac{dI_s}{dz} r dr d\phi = - \int_0^{\infty} \int_0^{2\pi} (n(r, \phi, z) \sigma_s N_3 - \alpha_s) I_s r dr d\phi$$

where $n(r, \phi, z)$ is the rare earth ion distribution, and α_p and α_s are the absorption coefficients of the undoped polymer waveguide at the pump and signal wavelengths, respectively. These first-order differential equations are coupled through the steady state population densities and can be solved by integrating the signal and pump wavefunctions over the waveguide cross-section and implementing a fourth-order Runge Kutta technique.

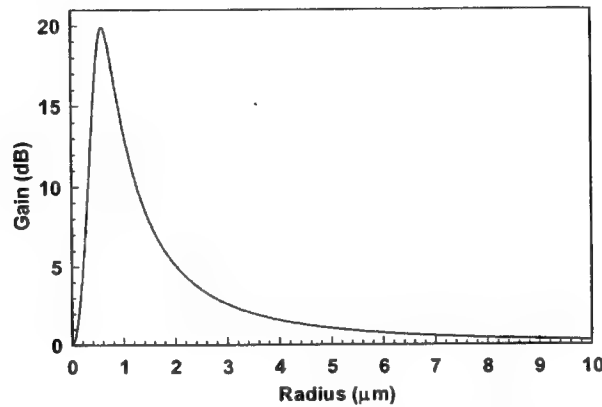


Figure 2. Gain dependence as function of guide radius for a $\text{Sm}(\text{HFA})_4\text{NEt}_4$ doped polymer waveguide amplifier, showing a maximum gain of about 20 dB for a 1.5 μm diameter guide.

In summary, we have demonstrated improvements of the optical properties of rare earth doped polymer systems for optical amplification. Numerical simulation shows the improved system can have high optical gain in short length optical fiber and waveguide structures.

-
- [1] Michel J. F. Digonnet ed, *Rare Earth Doped Fiber Lasers and Amplifiers*,. (Marcel Dekker, Inc., New York, 1993).
 - [2] E. Desurvire, *Erbium Doped Fiber Amplifiers* (John Wiley & Sons, Inc., New York, 1994).
 - [3] C. Koeppen, *Photonics Studies: Rare earth chromophores for polymer optical fiber and waveguide amplifiers*, Ph.D. dissertation, University of Pennsylvania, Philadelphia, PA, 1997.
 - [4] T. Kaino, "Polymer optical fibers," in *Polymers for lightwave and integrated optics*, L. Hornak, ed., Marcel Dekker, 1992.
 - [5] C. Koeppen, R. F. Shi, W. D. Chen, and A. F. Garito, "Properties of plastic optical fiber," *J. Opt. Soc. Am. B*, in press.
 - [6] T. Moeller, D. F. Martin, L. C. Thompson, R. Ferrus, G. R. Feistel, and W. J. Randall, *Chem. Rev.* **65**, 1 (1965).
 - [7] "Effects of chromophore dissociation on the optical properties of rare earth-doped polymers" R.Gao, C.Koeppen, G.Zheng, and A.F.Garito. *Appl. Opt.* **37**, 7100 (1998)
 - [8] R. G. Charles and A. Perotto, *J. Inorg. Nucl. Chem.* **26**, 373 (1964).
 - [9] H. Bauer, J. Blanc, and D. L. Ross, *J. Am. Chem. Soc.* **86**, 5126 (1964).

Photochromic media with sensitivity in the visible spectra

Igor Chapurin and Stephan Robu

Department of Physics and Department of Chemistry, State University of Moldova,
60 Mateevich str., Kishinev MD-2009, Moldova
chapurin@usm.md

Kazutaka Oba and Yeshaiahu Fainman

Department of Electrical and Computer Engineering, University of California, San Diego,
9500 Gilman Dr., La Jolla, CA 92093-0407
koba@ece.ucsd.edu, fainman@ece.ucsd.edu

INTRODUCTION

Organic photochromic compounds are of increasing importance for various optical technology applications (e.g., holography, optical data storage, and optical processing¹⁻³) due to their unique characteristics such as response time $<1ps$, spatial resolution $>5000mm^{-1}$, possibilities of data erasing and re-writing, etc. Most importantly, these materials can be easily fabricated in different formats and at low-cost. Typically, an organic photochromic compound consists of a host polymer and a photochromic dopant. One of the most commonly used photochromic dopant is spiropyran (SP). SPs are usually 2H-pyranes having a second heterocyclic ring system, attached to the 2-carbon atom of the pyran in a spiro-manner⁴. The SP is usually used as a dopant of methacrylate- or carbazole-contained materials such as poly-methylmethacrylate (PMMA) and poly-vinylcarbazole (PVK). As initially prepared, SP-doped organic compounds are colorless or yellowish in solutions as well as when they are converted into a solid film. When such a polymer compound is illuminated with UV light, it transforms into a dark-purple colored (merocyanine) form, with the maximum of the absorption spectra shifted to green-red range². This shift is suitable for realizing the write-read-erase (WRE) procedure³ cycles for over 10,000 times.

The commonly used writing procedure³ employs UV radiation from a Kr^+ laser operated at a wavelength of 350nm. The reading process employs absorption measurement using radiation of an Ar^+ laser in the blue-green spectral range at a wavelength of 488nm. More recently, a laser diode⁵ operated at a wavelength of 830nm has been used to detect the change in the index of refraction of the recorded media. For erasure of the recorded information, a common procedure uses radiation of a laser operating at a wavelength of 630-650nm. GaN laser diode has been also proposed⁶ for implementing both recording and erasing procedures employing pulsed and CW mode of laser operation, respectively. Detailed studies of photoreactions in SP-doped compounds report observation of both single- and two-photon induced fluorescence.^{2,7,8} Based on these research results it is possible to employ the photochromic compounds for realization of thin-film waveguides⁸ as well as 3D optical data storage systems.^{9,10}

In this paper we report a new photochromic composite polymer consisting of poly-epoxypropylcarbazole (PEPC) host with a SP dye dopant. Our research aimed to the finding photochromic compound sensitive in the visible spectra. Such a photochromic compound, called PEPC+SP, has been synthesized and experimentally characterized for optical holographic recording in visible spectral range. We use two-color (300-380nm and 632nm) recording procedure onto PEPC+SP film samples. Both recording and erasing procedures are possible using radiation from a blue line of an Ar^+ laser ($\lambda=458nm$).

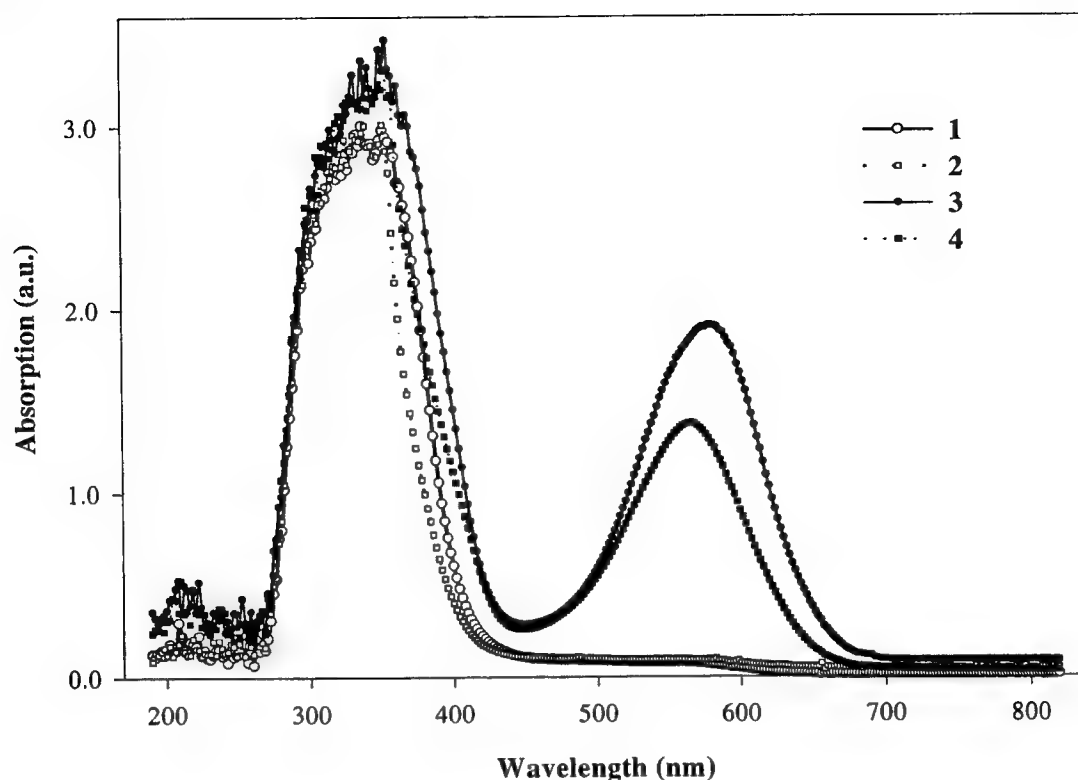


Figure 1. Absorption characteristics of photochromic compounds before (curves 1,2) and after (3,4) UV-irradiation: SP+PEPC (1,3) and SP+PVK (2,4)

EXPERIMENT

The PEPC+SP photochromic compound was prepared using a PEPC polymer hosts doped with 1,3',3'-trimethyl-6-nitrospiro-[2H-1-benzopyran-2,2'-indoline] SP. The SP was synthesized according to the well-known methods.⁴ Additionally, for comparison purposes, the same SP has been used for doping a PVK host polymer, that we call PVK+SP. Polymer films were cast on glass substrates from the toluene solutions of PEPC +SP and PVK+SP by setting at room temperature for 96 hours. Concentration and volume of the solutions were varied to obtain the desired thickness values in the range of 10-120 μm .

The experimental data on the absorption spectra of a 60 μm thick photochromic film of PEPC+SP and PVK+SP are shown in Fig. 1. The maximum absorption of the as prepared samples is observed in the range of 300 to 400 nm. Notice that the blue absorption edge of the PEPC+SP sample is shifted to the red in comparison with that of the PVK+SP sample. Next we illuminated both samples by UV radiation, which cause introduction of an additional maxima in absorption spectra at about 580 nm. The absorption spectrum of the PEPC+SP is higher and red-shifted in comparison to that of PVK+SP. It also should be noticed that irradiated samples of both types have an absorption minimum at about 430 nm (see Fig. 1). Finally, it should be noticed (see Fig. 1) that the main absorption spectra of the irradiated samples are red shifted (up to 30 nm) from that of the as prepared sample. Again, the blue edge of the UV-irradiated PEPC+SP sample has a red shift in comparison to that of the UV-irradiated PVK+SP sample. This spectral shift may become of practical importance for use with semiconductor blue laser sources.

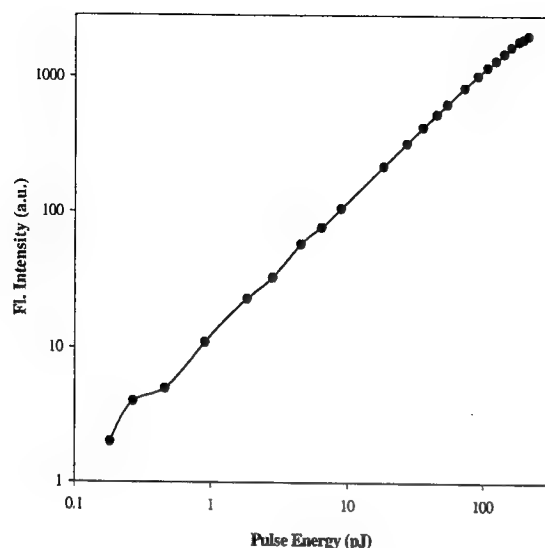


Figure 2. Fluorescence intensity vs excitation pulse

GRIOT Model 05-LPM-340-065) at 632nm. Both recording and erasing procedures were studied. We measured diffraction efficiencies of about 2.5% for a 60 μ m thick PEPC+SP film.

For the experimental measurements we use mode-locked Ti:Sapphire laser (Mira Model 900-F, Coherent) producing 200fs pulses at the center wavelength of 920nm with a repetition rate of 77MHz. The infrared (IR) radiation, 920nm, was frequency doubled using second harmonic generation producing pulses at a wavelength of 460nm. The measured intensity of the fluorescence flux vs the excitation pulse energy is shown in Fig. 2 in a log-log scale. The slope of the curve in Fig. 2 is about 1.0 (within the experimental error) indicating that PEPC+SP employs a typical single photon recording process. We also investigated PEPC+SP films using two-color recording procedure¹¹ by simultaneously exposing the samples to UV-lamp (ORIEL Instruments Model 6362) at 300-380nm and a He-Ne laser (MELLES

CONCLUSION

We report a new photochromic composite polymer material consisting of PEPC host with a SP dye dopant.. We have synthesized and experimentally characterized such a PEPC+SP photochromic polymer, which functional in the visible spectra. The experimental measurements of its absorption characteristics are evaluated in conjunction with its potential applications for optical holographic recording in visible spectral range. We use two-color (300-380nm and 632nm) recording procedure onto PEPC+SP film samples. Both recording and erasing procedures are possible using radiation from a blue line of an Ar⁺ laser ($\lambda=458$ nm). Simple diffraction gratings have been recorded in the PEPC+SP film of 60 μ m providing measured diffraction efficiencies of about 2.5%. We are currently investigating use of PEPC+SP for spectral holographic recording.

ACKNOWLEDGMENT

Authors are thankful for the NATO Science Committee's support under Linkage Grant HTECH.97-1684.

REFERENCES

1. A. Akella, S.L. Sochava, and L. Hesselink, *Opt. Lett.* **22**, 919 (1997).
2. A.S. Dvornikov and P.M. Rentzepis, *Proc. SPIE* **CR63** 240 (1996).
3. F. Ghailane, G. Manivannan, and R.A. Lessard, *Opt. Eng.*, **34**, 480 (1995).
4. J.C. Crano and R.J. Guglielmetti, Eds., *Organic Photochromics and Thermochromic Compounds* (Plenum Press, NY & London, 1999), pp.11-83.
5. A. Toriumi, J.M. Herrmann, and S. Kawata, *Opt. Lett.* **22**, 555 (1997).
6. T. Tsujioka, M. Kume, and M. Irie, *Jpn. J. Appl. Phys.*, **35**, L1532 (1996).
7. M.M. Wang, S.C. Esener, F.B. McCormick, et al., *Opt. Lett.* **22**, 558 (1997).
8. R. Piyaket, I. Çokgör, F.B. McCormick, et al., *Opt. Lett.* **21**, 1032 (1996).
9. D.A. Parthenopoulos and P.M. Rentzepis, *J. Appl. Phys.*, **68**, 5814 (1990).
10. F.B. McCormick, I. Çokgör, A.S. Dvornikov, et al., *Proc. SPIE* **3490**, 574 (1998).
11. V.V. Ivakhnik and V.I. Nikonov, *Opt. and Spectr.*, **83**, 446 (1997).

Fabrication of Polymeric Large-Core Optical Waveguides Using a Rubber Molding Process

Byung-Tak Lee, Min-Suk Kwon, Jun-Bo Yoon, and Sang-Yung Shin

Department of Electrical Engineering, Korea Advanced Institute of Science and Technology

373-1, Kusong-dong, Yusong-gu, Taejeon 305-701, Korea

bytelee@eeinfo.kaist.ac.kr, icarus@eeinfo.kaist.ac.kr, jbyoon@eeinfo.kaist.ac.kr, syshin@ee.kaist.ac.kr

I. Introduction

Optical interconnects have drawn much attention because they have the characteristics of wide bandwidth, low EMI, reduced cross-talk, low loss, and reduced size[1][2]. For optical interconnects, polymeric large-core waveguides are widely used. Their merits include large fabrication tolerance, low propagation loss, and easy alignment. To make polymeric large-core waveguides, reactive ion etching, direct laser drawing upon the photo-polymer, UV illumination upon the photo-polymer, and molding process have been investigated[2]. Among these methods, the molding process is promising because it is amenable to mass-production, insensitive to polymer selection, and low-cost. The method can be classified to the metal molding process[3] and the rubber molding process[4] according to the material of the mold. While the rubber molding process is not so well-known in comparison to the metal molding process, it has merits of flexibility, low-cost, and easy fabrication.

In this paper, we report a simple and low-cost fabrication of polymeric large-core optical waveguides using a rubber molding process. The molding method is composed of three steps: a master fabrication, a mold formation, and a transferring process to polymeric material. In the master fabrication, our newly developed process of the thick photoresist AZ9260 is used[5]. The polydimethylsiloxane (PDMS) elastomer, a kind of silicone rubber, is used as the mold. In the transferring process to polymeric material, we employ a modified microtransfer molding process[4]. All processes are simple and low-cost, so our fabrication method can be a cost-effective solution to the polymeric large-core optical waveguides of optical interconnects.

II. Fabrication and Measurement

The fabrication steps of optical waveguides using a molding method are illustrated in Fig. 1.

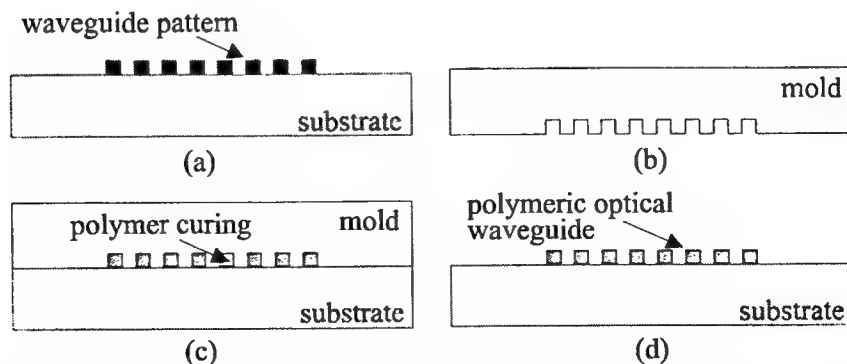


Fig. 1. Fabrication steps of optical waveguides using a molding method. (a) master fabrication. (b) mold formation. (c) transferring process to polymeric material. (d) fabricated optical waveguides.

To make the original master of the large-core optical waveguides, we use a positive thick photoresist. The photoresist AZ9260 (available from Hoechst) may be spin-coated with a thickness of about 100 μm . We can achieve the high-aspect-ratio (20:1) in the UV photolithography by using our two-step baking processes[5]. The first soft-baking is performed at an intermediate temperature upon an air-gapped hot plate with cover for several hours to evaporate large amounts of the solvent. Subsequently, the second soft-baking is performed at an elevated temperature upon an air-gapped hot plate for several minutes to enhance the aspect ratio. The cleaved images of the original master made from the photoresist are shown in Fig. 2. The dimension of a channel waveguide is 47 μm \times 41 μm (horizontal size \times vertical size). The channel width of an optical waveguide in the Cr mask is 50 μm but it is reduced to 47 μm because of the under-cut in developing photoresist.

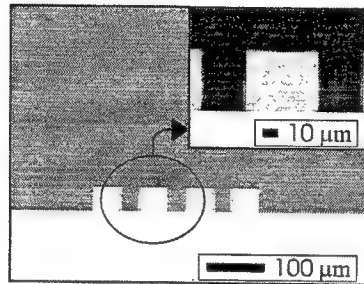


Fig. 2. Cleaved images of the original master made from the photoresist AZ 9260 (a top view).

We use the PDMS elastomer, a kind of silicone rubber, to make the mold. The PDMS elastomer (SylgardTM 184 available from Dow Corning) is supplied in the form of a curing agent (A) and a liquid silicone rubber base (B). We mix A and B with a ration of 1:10 and pour the mixture over the master. After several hours of stabilization, the mixture is cured at 50 $^{\circ}\text{C}$ for 3 hr. Because the cured PDMS elastomer is flexible, it can be easily peeled off from the original master. When peeled off, the PDMS mold has the complementary shape of the structure of the original master.

To make polymeric optical waveguides, we choose a thermo-curable epoxy, perfluorocyclobutane (PFCB)[6]. It has low propagation loss (0.25 dB/cm @1.3 μm , 0.2 dB/cm @1.55 μm), high thermal stability ($T_g = 400$ $^{\circ}\text{C}$), excellent resistance to solvents, and compatibility with IC fabrication processes. Therefore, this material is adequate for optical interconnects.

To transfer the shape of the mold to the polymer, PFCB (41 wt%), we follow the microtransfer molding method of Xia *et al*[4] except the step of placing the PDMS mold upon the SiO_2/Si wafer. When we place upon the substrate the mold filled with the polymer, the small air bubbles trapped between the mold and the substrate cause a problem. We solve it by slightly deforming the mold like a convex when placing the mold upon the substrate[7]. Then, the PDMS mold is pressed flat with a soft pressure during the curing process of the polymer. The first curing step is performed at 170 $^{\circ}\text{C}$ for 5 hr in the atmosphere of N_2 gas. After peeling off the PDMS mold, we perform the second curing step at 250 $^{\circ}\text{C}$ for 1 hr to achieve a full polymerization of PFCB. The cleaved images of polymeric optical waveguides are shown in Fig. 3. The polymeric optical waveguides (in Fig. 3) are well transferred from the original master (in Fig. 2) by our molding method. The molded polymer acts as a core. Both the SiO_2 layer (thickness = 2 μm) and the air act as cladding layers. The waveguide length is 1.6 cm after cleaving.

A multimode fiber (with a core diameter of 50 μm) is used to launch light into the waveguides. The output mode profiles of the fiber and the waveguide at the wavelength of 1.3 μm are shown in Fig. 4. The propagation loss is measured as 0.4 dB/cm @1.3 μm , 0.7 dB/cm @1.55 μm .

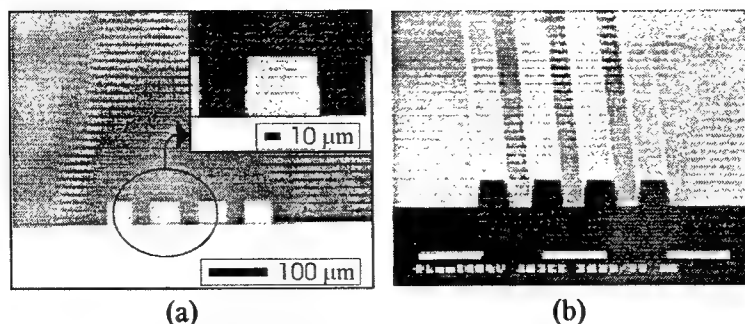


Fig. 3. Cleaved images of polymeric optical waveguides. (a) top view. (b) oblique view.

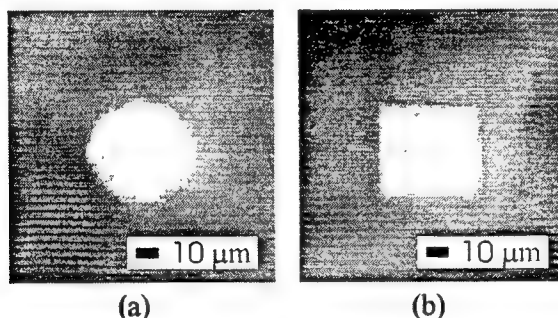


Fig. 4. Output mode profiles. (a) mode profile of the multimode fiber. (b) mode profile of the multimode waveguide

IV. Conclusion

We have developed a simple and low-cost fabrication method of polymeric large-core optical waveguides ($47\ \mu\text{m} \times 41\ \mu\text{m}$) using the rubber molding process. In the master fabrication, The two-step baking process of the photoresist AZ9260 is used. The mold is fabricated with the PDMS elastomer. In the transferring process to polymeric material, we employ the modified microtransfer molding process. The measured propagation loss is $0.4\ \text{dB/cm}$ @ $1.3\ \mu\text{m}$ and $0.7\ \text{dB/cm}$ @ $1.55\ \mu\text{m}$.

References

- [1] Y. S. Liu, W. B. Hennessy, R. Wojnarowski, J. P. Bristow, Y. Liu, J. Rowlette, J. Stack, J. Yardley, L. Eldada, R. M. Osgood, R. Scarmozzino, S. H. Lee, and S. Patra, *Proc. SPIE* **3005**, 2-10 (1997).
- [2] T. Li, S. Tang, R. Wickman, L. Wu, F. Li, M. Dubinovsky, and R. T. Chen, *Proc. SPIE* **3005**, 128-135 (1997).
- [3] L. Wu, F. Li, S. Tang, B. Bihari, and R. T. Cheng, *IEEE Photon. Technol. Lett.* **9**, 1601-1603 (1997).
- [4] Y. Xia and G. M. Whitesides, *Annu. Rev. Mater. Sci.* **28**, 153-184 (1998).
- [5] Jun-Bo Yoon, Chul-Hi Han, Euisik Yoon, and Choong-Ki Kim, *Proc. SPIE* **3512**, 316-325 (1998).
- [6] G. Fischbeck, R. Moosburger, C. Kostrzewa, A. Achen, and K. Petermann, *Electron. Lett.* **33**, 518-519 (1997).
- [7] H. C. Haverkorn van Rijsewijk, P. E. J. Legierse, and G. E. Thomas, *Philips tech. Rev.* **40**, 287-297 (1982).

Polarization Sensitive Surface Relief Gratings Formed on Amorphous Azopolymer Films

Nirmal K. Viswanathan^{a,c}, S. Balasubramanian^c, Jayant Kumar^{a,c}, Sukant K. Tripathy^{b,c*}

Department of Physics,^a Department of Chemistry,^b Center for Advanced Materials,^c One University Avenue, University of Massachusetts Lowell, Lowell, MA 01854.

Email: Sukant_Tripathy@uml.edu

Introduction:

Azobenzene chromophore functionalized polymer films belong to an important class of photoanisotropic materials [1]. Spatial variations of both intensity and polarization field patterns preferentially photoexcites and reorients the azo chromophores due to *trans-cis-trans* isomerization process making it a suitable candidate for forming birefringence gratings (BG) [2]. Since the demonstration of efficient fabrication of Surface Relief Gratings (SRGs) in thin films of these materials, a number of interesting photophysical effects continues to be reported [3-5]. Under appropriate conditions for the write and read beam polarization, it is possible to distinguish between the two grating formation processes. Effects due to the growth of SRG can cancel the BG effect resulting in a large difference in the diffraction efficiencies for orthogonally polarized read beams. The results of such a measurement have been advantageously utilized for making polarization optical elements (POE) such as polarization discriminators and polarization beamsplitters.

Experimental Details:

The experimental setup used to simultaneously write the birefringence grating and surface relief grating on thin azopolymer films is discussed in detail elsewhere [4-6]. It is a simple two-beam interferometer arrangement; formed by superposing two polarized Ar⁺ laser beams (488 nm). Different polarization combinations for the writing beams can be arranged by appropriately orienting the polarizers and polarization rotators ($\lambda/2$ and $\lambda/4$ waveplates). Different polarization combinations and interference angles (θ) for the writing beams have been carried out. Here we report the grating formation process due to the +45°: -45° combination with a periodicity of $\Lambda = 4 \mu\text{m}$. The grating formation is monitored by diffracting a polarized He-Ne laser beam (633 nm). The polarization of the read beam can be changed between s- and p- by rotating the $\lambda/2$ waveplate. The polarization vector for s- polarized read beam is parallel to grating grooves (perpendicular to grating vector) and for the p- polarized read beam it is in the perpendicular plane. The azopolymer is synthesized by post-azo coupling reaction [5]. The polymer is dissolved in DMF, spin coated onto a glass slide and vacuum dried to get good optical quality thin films.

Results and Discussion:

Recording an interference pattern due to polarized light beams, in a photoanisotropic azopolymer film, modulates the refractive index and the surface depending on the spatial variation of intensity and polarization. The recorded grating consequently is complex due to the simultaneous presence of both refractive index variations and surface modulations. The intensity modulation due to the superposed interference pattern and assuming a linear material response, the refractive index and surface modulations are given by

$$I = I_0 + \Delta I \cos(Kx); n = n_0 + \Delta n \cos(Kx); S = \Delta S \cos(Kx + \phi)$$

Where I_0 is the intensity of the two interfering beams, ΔI is the intensity modulation amplitude, grating vector $K = (2\pi/\Lambda)$, n_0 is the refractive index of the material before recording (1.63), Δn is the modulated refractive index or the induced birefringence, ΔS is the modulation depth of the SRG and ϕ is the arbitrary phase shift of the SRG with respect to the refractive index grating. A read light beam, traversing the grating, experiences a phase shift of $\Delta\Phi = (\pi\Delta n d/\lambda)$ due to the induced birefringence and a phase shift

of $\Delta\Psi = (\pi\Delta n\Delta S/\lambda)$ due both to the induced birefringence and surface relief part. Here, d is the thickness of the film before irradiation, (0.7 μm) and λ is the probe beam wavelength (633 nm). The induced birefringence ($\Delta n = n_{\parallel} - n_{\perp}$) is negative for an azopolymer. Thus, depending on the time development of Δn and ΔS , the effect of $\Delta\Psi$ can cancel the effect due to $\Delta\Phi$. Monitoring the +1 transmitted diffraction order with a polarized read beam it is possible to distinguish between the two grating processes. Variation of the diffraction efficiency (η) with the polarization angle (α) of the read beam is given by [7]

$$\eta = \eta_{\parallel} \cos^2 \alpha + \eta_{\perp} \sin^2 \alpha$$

where, η_{\parallel} and η_{\perp} are the diffraction efficiencies for the read beam polarized parallel (s-) and perpendicular (p-) to the grating grooves, corresponding to $\alpha = 0^\circ$ and 90° respectively. Probing the grating formation with orthogonally polarized (s- and p-) read beams can give us information about the exact nature of the birefringence and surface relief grating contribution.

Temporal behavior of the diffracted beam intensity for the writing beams with $+45^\circ : -45^\circ$ polarization probed by s- and p- polarized read beams is shown in Figure 1. Monitoring the grating formation process with s- polarized read beam, the diffracted beam intensity increases initially due to the photoinduced birefringence. The subsequent decrease in the diffracted beam intensity due to a simultaneous growth of the SRG is almost complete. This can be thought of as due to a complete cancellation of the photoinduced refractive index changes in the sample plane by the simultaneous increase in the SRG amplitude. The diffracted intensity due to p- polarized read beam, after the initial increase due to birefringence grating does not decrease but continues to increase until large diffraction efficiencies are achieved. Such a behavior can be explained based on the fact that the place where maximum birefringence is induced ($\Phi_{12} = 0$) is the place where the material gets piled up resulting in a surface maximum. This corresponds to the situation where there is no phase difference between the birefringence and surface relief maxima i.e., $\phi = 0$. Thus one records a continued increase in the diffracted beam intensity for the p- polarized read beam. $\eta_{\parallel} \approx 0.1\%$ at 1200 seconds and the corresponding value probed by the orthogonally polarized read beam is $\eta_{\perp} = 6\%$. The modulation depth of the SRG measured by an Atomic Force Microscope (AFM) is $\Delta S = 80$ nm. The grating formation is stopped at the point when $\eta_{\parallel} \approx 0$ (vertical line in Figure 1) and used for further characterization.

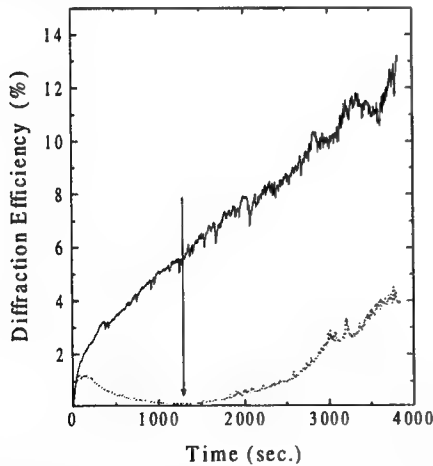


Figure 1: Diffraction efficiency as a function of time. Writing polarization: $+45^\circ : -45^\circ$; read beam polarizations: s- (dotted line) and p- (solid line).

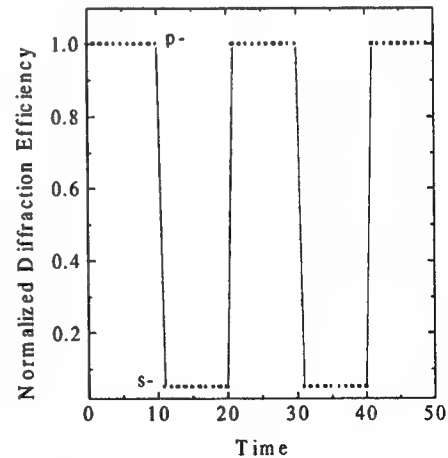


Figure 2: Normalized diffraction efficiency of the +1 order; polarization of the read beam is switched.

The diffraction efficiency of the SRG formed depends strongly on the polarization of the read light. As a natural outcome of this result, the polarization discrimination capability of the SRG is first measured.

Figure 2 shows the switching property of the fabricated SRG at 633 nm read beam wavelength. The polarization state of the read laser beam is changed periodically and the +1 order diffracted power is measured. If the input beam is s-polarized, there is very weak diffracted beam and if the input beam polarization is changed to p-, diffraction efficiency is the maximum. This property can be utilized in devices like polarization switches and for beam-steering applications.

Next, the polarization content of the diffracted and undiffracted beams transmitted through the same SRG is measured. An unpolarized He-Ne laser is used for this measurement. Polarization of each of the transmitted beams is recorded by rotating the analyzer. Schematic of the experimental setup and the measurements made are shown in Figure 3.

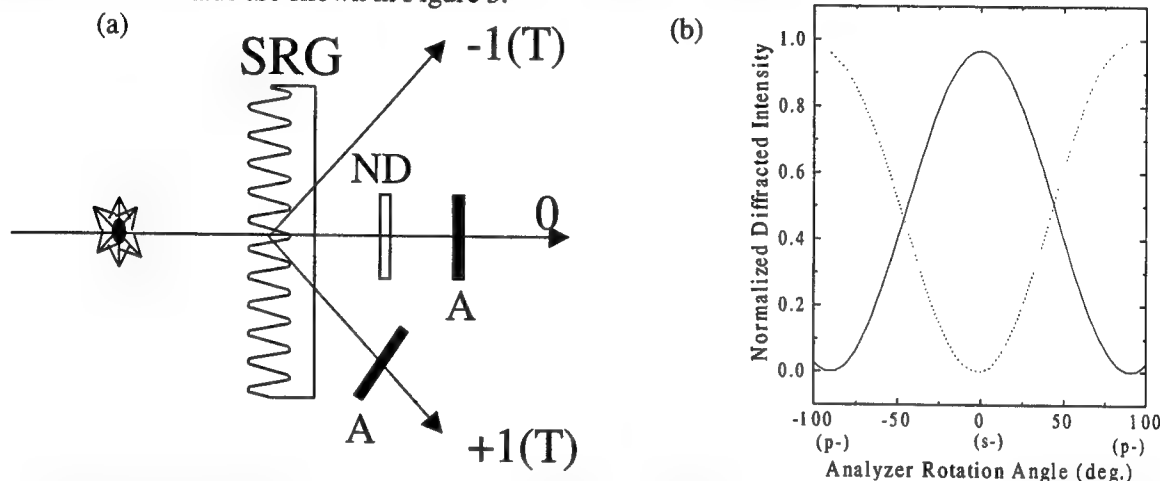


Figure 3: (a) Schematic of the experimental setup to measure the polarization content of the transmitted beams from the SRG. (b) Measurement for the 0th (solid line) and +1 order (dotted line) beams.

It is clear from the figure 3(b) that +1 order diffracted beams are predominantly horizontally polarized. The transmitted 0th order beam analyzed after reducing its intensity by a neutral density filter (ND) is found to have predominantly the vertical polarization component. Results suggest that the fabricated SRG can also be used as a polarization beamsplitter.

Conclusions:

The grating formation process in azo functionalized polymer films gives us a unique way to tailor the bulk and surface features. The planar and compact size of the polarization optical elements (POEs) fabricated are useful in integrated optics.

Acknowledgments:

Financial support from the ONR and the NSF are gratefully acknowledged.

References:

- [1] S. Xie, A. Natansohn, P. Rochon, *Chem. Mater.* **5**, 403, 1993.
- [2] T. Huang, K.H. Wagner, *J. Opt. Soc. Am. B* **13**, 282, 1996.
- [3] P. Rochon, E. Batalla, A. Natansohn, *Appl. Phys. Lett.* **66**, 136, 1995.
- [4] D.Y. Kim, S.K. Tripathy, L. Li, J. Kumar, *Appl. Phys. Lett.* **66**, 1166, 1995.
- [5] N.K. Viswanathan, D.Y. Kim, S. Bian, J. Williams, W. Liu, L. Li, L. Samuelson, J. Kumar, S.K. Tripathy, to appear in *J. Mater. Chem.* 1999.
- [6] N.K. Viswanathan, S. Balasubramanian, L. Li, S.K. Tripathy, J. Kumar, submitted to *Jpn. J. Appl. Phys.* 1999.
- [7] H. Haidner, P. Kipfer, J.T. Sheridan, J. Schwider, N. Streibl, J. Lindolf, M. Collischon, A. Lang, *J. Hutfless Opt. Eng.* **32**, 1860, 1993.

Organic Thin Films for Photonics Applications

Polymer Integrated Optics/ 2-Photon Absorption

Sunday, 26 September 1999

Lisa Dhar, Lucent Technologies, USA
Presider

SuB

10:15am–11:45am

California Ballroom Salons 4&5

Materials for Two-Photon 3D Lithography

Joseph W. Perry, Sundaravel Ananthavel, Kevin Cammack, Stephen M. Kuebler, Seth R. Marder, and Mariacristina Rumi

Department of Chemistry
The University of Arizona
Tucson, AZ 85721
jwperry@u.arizona.edu

Brian H. Cumpston, Ahmed A. Heikal, Jeffrey E. Ehrlich, Lael L. Erskine, Michael D. Levin, Matthew Lipson, Diane McCord-Maughon, and Harald Röckel

Division of Chemistry and Chemical Engineering and Beckman Institute
California Institute of Technology
Pasadena, CA 91125 U.S.A.

ABSTRACT

Conjugated organic chromophores with large two-photon absorption cross-sections have been developed and employed to prepare highly-sensitive nonlinear photopolymer systems, which can be used for 3D-microfabrication and optical data storage.

* To whom correspondence should be addressed; current address: Department of Chemistry, The University of Arizona, Tucson, AZ 85721.

SUMMARY

Two-photon excitation provides a means of activating chemical or physical processes with high spatial resolution in three dimensions and has enabled the development of three dimensional imaging, optical data storage, and microfabrication methods. These methods take advantage of the quadratic dependence of two-photon absorption on intensity, which allows, under tight-focusing conditions, the absorption to be confined to a small volume (of order λ^3) at the focus. Physical or chemical processes subsequent to such confined excitation can also be localized in this small volume. For instance, two-photon excitation can initiate chemical reactions such as radical generation and initiation of polymerization. The photosensitivity of such processes depends critically on the strength of the chromophore's two-photon absorptivity.

We have developed a wide array of chromophores which hold great promise for two-photon excited processes. These chromophores are based on donor- π -donor, donor-acceptor-donor, or acceptor-donor-acceptor structural designs. The magnitude of the two-photon absorption cross-section, δ , and the position of the two-photon absorption maximum can be controlled by varying the length of the conjugated bridge and by varying the strength of the donor/acceptor groups. Chromophores have been developed which exhibit strong two-photon absorption in the range of 500 - 975 nm, with cross sections as high as $4400 \times 10^{-50} \text{ cm}^4 \text{ s/photon-molecule}$.¹

We have shown for D- π -D molecules that two-photon excitation produces an excited state which has sufficient reducing strength for charge transfer reactions to occur with acrylate monomers. Such reactions can induce radical polymerization of these monomers and thus are useful in the formulation of two-photon absorbing nonlinear photopolymers. We have measured

polymerization rates under two-photon excitation with femtosecond laser pulses in the near infrared and found that our D- π -D two-photon chromophores display an order-of-magnitude increased photosensitivity over resins containing conventional photoinitiators. Two-photon excitable photopolymers based on these new initiators have been developed and used to demonstrate the fabrication of 3D micro-optical and micro-mechanical structures, including photonic-bandgap-type structures (Figure 1).² The two-photon microfabrication process can be extended to other material systems, such as metallic, ceramic, and composite materials, by using the fabricated 3D polymer structure as a template.

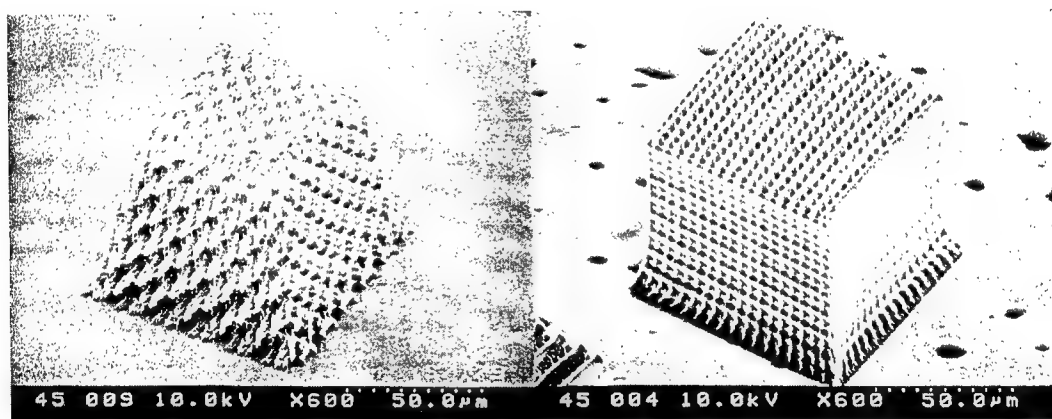


Figure 1. Scanning electron micrograph images of diamond lattice (left) and "stack-of-logs" (right) polymer microstructures fabricated by two-photon induced polymerization. These structures are about 75 μm on an edge.

We are investigating the use of highly sensitive two-photon chromophores in chemical processes for the 3D patterned photodeposition of nonpolymeric materials. In preliminary work, we have demonstrated that two-photon polymerization of a diacrylate aniline derivative can be used to form polymer structures which, when exposed to a solution of AgBF_4 , thermally reduce

silver ion to silver metal and form a metallic silver coating on the polymer structure. We have also demonstrated a one step process that allows the patterned photodeposition of silver micro- and nano-particles. In this case, a polymer gel containing a bis(phenyl,tolylamino)biphenyl two-photon chromophore and AgBF_4 forms localized regions containing silver metal particles, which appear as brown lines, upon laser exposure. These results indicate that, with efficient chromophores, there is great potential for the development of two-photon excitable materials systems which lead to the photodeposition of metals, and of other interesting materials systems.

References:

1. M. Albota, D. Beljonne, J.-L. Brédas, J. E. Ehrlich, J.-Y. Fu, A. A. Heikal, S. E. Hess, T. Kogej, M. D. Levin, S. R. Marder, D. McCord-Maughon, J. W. Perry, H. Röckel, M. Rumi, G. Subramaniam, W. W. Webb, X.-L. Wu, and C. Xu, *Science*, 281 (1998) 1653.
2. B. H. Cumpston, S. Ananthavel, S. Barlow, D. L. Dyer, J. E. Ehrlich, L. L. Erskine, A. A. Heikal, S. M. Kuebler, I.-Y. Sandy Lee, D. McCord-Maughon, J. Qin, H. Röckel, M. Rumi, X.-L. Wu, S. R. Marder and J. W. Perry, *Nature*, 398, (1999) 51-54.

Two-Photon Photoinitiated Polymer Processing and Microfabrication

Kevin D. Belfield,* Xiaobin Ren, David J. Hagan, Eric W. Van Stryland, Vladislav Dubikovsky, and Edward J. Miesak

Department of Chemistry, School of Optics/CREOL
University of Central Florida, P.O. Box 162366, Orlando, FL 32816-2366
(407) 823-1028 phone, (407) 823-2252 fax, kbelfiel@mail.ucf.edu

Introduction

Emerging device technologies such as microelectromechanical systems and integrated sensors are placing increased demands on the development of materials processing and fabrication techniques.^{1,2} In response, the characteristic three-dimensional (3-D) spatial resolution of the simultaneous two-photon absorption process is being harnessed for 3-D photoinitiated polymerization and microlithography. This is facilitated by the unique properties associated with simultaneous absorption of two-photons relative to single-photon mediated processes. There have been a limited number of reports of two-photon photopolymerization of commercial acrylate monomer systems, preformulated with UV photoinitiators.³⁻⁶ Efficient two-photon absorbing compounds based on phenylethenyl constructs bearing electron-donating and/or electron-withdrawing moieties have been reported.⁷ Among these are electron-rich derivatives that have been found to undergo a presumed two-photon induced electron transfer to acrylate monomers, initiating polymerization.^{8,9} The reportedly efficient two-photon photoinitiators, though more photosensitive than previously studied UV photoinitiators, are not commercially available and require rather involved syntheses. Thus, the practicality of their broader use is questionable. Herein, we report the near-IR two-photon induced polymerization of (meth)acrylate monomers using a commercially available photoinitiator system previously employed in single-photon visible photopolymerization.

Multiphoton absorption has been defined as simultaneous absorption of two or more photons via virtual states in a medium.¹⁰ The process requires high peak power, which is available from pulsed lasers. Even though multiphoton processes have been known for some time, materials that exhibit multiphoton absorption have yet to find widespread application. This may likely be due to the interdisciplinary nature of developing multiphoton-based techniques and processes, i.e., an understanding of photophysics, photochemistry, materials science, and optical science. A major feature that distinguishes single-photon absorption from two-photon absorption is the rate of energy (light) absorption as a function of incident intensity. In single or one-photon absorption, the rate of light absorption is directly proportional to the incident intensity ($dw/dt \propto I$), i.e., as the incident intensity is increased, the rate of photon absorption increases linearly for the molecule in question. By contrast, in simultaneous two-photon absorption (2PA), the rate of energy absorption is proportional to the square of the incident intensity ($dw/dt \propto I^2$).^{10,11}

The quadratic, or nonlinear, dependence of two-photon absorption as a function of light intensity has substantial implications. For example, in a medium containing one-photon absorbing chromophores, significant absorption occurs all along the path of a focused beam of suitable wavelength light, leading to out of focus absorption and associated processes. In a two-photon process, however, negligible absorption occurs except in the immediate vicinity of the focal point of a light beam of appropriate energy. This allows spatial resolution about the beam axis as well as radially, and is the principle basis for two-photon fluorescence imaging.¹²

The concept of miniaturization, successfully pioneered in the microelectronics industry for the fabrication of integrated circuits (IC), is now being extended to a number of other industrial sectors. The miniaturization of mechanical systems is developing under such names as micromachining, microsystems and nanosystems technology, or microelectromechanical systems (MEMS). It is widely believed that a "revolution" in miniaturization, particularly in the field of MEMS, is underway. It is projected that the design and manufacturing technology that will be developed for MEMS may rival, or even surpass, the far-reaching impact of ICs on society and the world's economy. At the forefront of techniques being

explored for 3-D spatially-resolved materials imaging and processing are methods based on 2PA. The use of longer wavelength light as the excitation source leads to deeper penetration depths than possible with conventional UV or visible excitation techniques. Since the absorption/excitation is confined to the focal volume in the 2PA process, there will be virtually no out of focus excitation/reaction, i.e., two-photon excitation falls off rapidly away from the focal volume.

Summary

We conducted two-photon initiated polymerization at 775 nm via direct excitation of a commercially available dye that undergoes a distinctly different electron-transfer free radical initiation process. The photoinitiator (5,7-diiodo-3-butoxy-6-fluorone, H-NU 470) was subjected to the 775 nm ultrafast laser pulses. According to the mechanism deduced from single-photon photochemical studies of the initiating system,¹³ electron transfer from the aromatic amine (N,N-dimethyl-2,6-diisopropylaniline) to the fluorone derivative, followed by proton transfer from the amine to the fluorone, resulted in formation of an arylamine bearing an free radical localized on the α -methylene carbon. This free radical species then initiated polymerization of (meth)acrylate derivatives. A diaryliodonium salt can be added to accelerate the rate of polymerization.¹³

The formation of polymeric microstructures with a variety of dimensions was accomplished, e.g., with 9 μm wide lines spaced 50 μm apart (as shown in Figures 1 using an ethoxylated bisphenol A dimethacrylate monomer (SR 349) from Sartomer). Microstructures were examined by optical reflection microscopy. Figure 1a depicts the microstructure formed in which the line width is 9 μm with relatively uniform 50 μm line spacing. Figure 1b shows the photograph of the same microstructure at higher magnification. Clearly evident in Figure 1b is a relatively uniform submicrostructure (nanostructure) likely due to the beam profile and repetition rate.

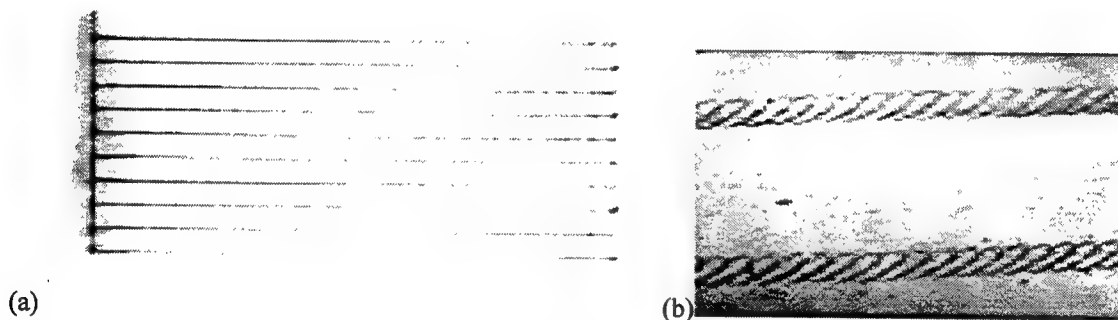


Fig. 1: (a) Micrograph of polymerized microstructure 9 μm line width and 50 μm line spacing. (b) Micrograph of the same microstructure depicted in Figure 1 at higher magnification. A uniform submicrostructure is clearly evident (9 μm line width and 50 μm line spacing).

Conclusions

We have demonstrated controlled two-photon induced photopolymerization, employing both commercial monomers and initiator system. Though the efficiency of initiation was not determined quantitatively, qualitatively it was observed that polymerization occurred rapidly, even at higher scan rates and lower power. This paves the way for three-dimensional microfabrication and lithography using readily available materials. Studies are currently underway to characterize the two-photon absorption spectrum and cross section for the fluorone initiator as well as other photoinitiators. Additional investigations in our laboratory are focused on control of the submicrostructure (nanostructure) and

extend the polymerization further in three-dimensions in an effort to create a variety of "functional microstructures".

Acknowledgments. This work is dedicated to Bruce A. Reinhardt (deceased) of the Air Force Research Laboratory, Polymer Branch, Materials Directorate. The authors gratefully acknowledge the Air Force Office of Scientific Research (AFOSR) and the National Science Foundation for partial support of this work. K.D.B. acknowledges AFOSR for a 1998 Summer Faculty Research Fellowship. We would also like to acknowledge Esschem, Inc. (in particular George F. Cowperthwaite) and Sartomer Co. for kindly providing the monomers, and Spectra Group Ltd., Inc. for the initiator used in this research.

References

1. See, e.g., Belfield, K. D.; Abdelrazzaq, F. B. *J. Polym. Sci.: Part A: Polym. Chem.* **1997**, *35*, 2207-2219.
2. See, e.g., Belfield, K. D.; Abdelrazzaq, F. B. *Macromolecules* **1997**, *30*, 6985-6988.
3. Strickler, J. H.; Webb, W. W. *Opt. Lett.* **1991**, *16*, 1780-1782.
4. Maruo, S.; Nakamura, O.; Kawata, S. *Opt. Lett.* **1997**, *22*, 132-134.
5. Borisov, R. A.; Dorojkina, G. N.; Koroteev, N. I.; Kozenkov, V. M.; Magnitskii, S. A.; Malakhov, D. V.; Tarasishin, A. V.; Zheltikov, A. M. *Appl. Phys. B* **1998**, *67*, 765-767.
6. Borisov, R. A.; Dorojkina, G. N.; Koroteev, N. I.; Kozenkov, V. M.; Magnitskii, S. A.; Malakhov, D. V.; Tarasishin, A. V.; Zheltikov, A. M. *Laser Phys.* **1998**, *8*, 1105-1108.
7. Albota, M.; Beljonne, D.; Bredas, J.-L.; Ehrlich, J. E.; Fu, J.-Y.; Heikal, A. A.; Hess, S. E.; Kogej, T.; Levin, M. D.; Marder, S. R.; McCord-Maughon, D.; Perry, J. W.; Rockel, H.; Rumi, M.; Subramaniam, G.; Webb, W. W.; Wu, X.-L.; Xu, C. *Science* **1998**, *281*, 1653-1656.
8. Cumpston, B. H.; Ananthavel, S. P.; Barlow, S.; Dyer, D. L.; Ehrlich, J. E.; Erskine, L. L.; Heikal, A. A.; Kuebler, S. M.; Lee, I.-Y. S.; McCord-Maughon, D.; Qin, J.; Rockel, H.; Rumi, M.; Wu, X.L.; Marder, S. R.; Perry, J. W. *Nature* **1999**, *398*, 51-54.
9. Joshi, M. P.; Pudavar, H. E.; Swiatkiewicz, J.; Prasad, P. N.; Reinhardt, B. A. *Appl. Phys. Lett.* **1999**, *74*, 170-172.
10. Goeppert-Mayer, M. **1931**, *9*, 273-294.
11. Kershaw, S. In *Characterization Techniques and Tabulations for Organic Nonlinear Optical Materials*; Kuzyk, M. G.; Dirk, C. W. Eds.; Marcel Dekker: New York, 1998, Chapter 7.
12. Denk, W.; Strickler, J. H.; Webb, W. W. *Science* **1990**, *248*, 73-76.
13. Hassoon, S.; Neckers, D. C. *J. Phys. Chem.* **1995**, *99*, 9416-9424.

Molecular hyperpolarizability in the two-photon resonance regime: Measurement and analysis

G. Berkovic[#], G. Meshulam, Z. Kotler

Optronic Materials Group, Electro-Optics Division, Soreq NRC, Yavne 81800 Israel

[#]e-mail: garry@ndc.soreq.gov.il

The hyperpolarizability, β , of organic nonlinear optical (NLO) molecules is a frequency dependent quantity. Comparison of hyperpolarizability under different conditions and for different molecules is most equitable when comparing values for the zero frequency hyperpolarizability, β_0 . For 1-dimensional NLO molecules, where the β_{zz} component dominates, the dispersion of this component - henceforth denoted $\beta(\omega)$ - has generally been taken to follow a two-level formula first given by Oudar and Chemla [1]. Using this formula, β_0 can be extrapolated from an experimental value of $\beta(\omega)$ determined from second harmonic generation according to:

$$\frac{\beta(\omega)}{\beta_0} = \frac{\omega_0^4}{(\omega_0^2 - \omega^2)(\omega_0^2 - 4\omega^2)} \quad (1)$$

where ω_0 is the energy of the first excited state. This formula, however, is not applicable under two-photon resonance, i.e. when $2\omega \rightarrow \omega_0$. In the resonance regime, the width (damping) of the transition, γ , should be included. This treatment leads to [2]

$$\frac{\beta(\omega)}{\beta_0} = \frac{\omega_0^2 (\omega_0 - i\gamma)^2}{[(\omega_0 - i\gamma)^2 - \omega^2][(\omega_0 - i\gamma)^2 - 4\omega^2]} \quad (2)$$

Equation (2) ensures that $\beta(\omega)$ remains finite and complex at the two-photon resonance. However, it explicitly assumes a homogeneously broadened transition, which is not particularly realistic for an organic molecule in solution. Thus, use of an inhomogeneously broadened version of equation (2) has been suggested [3], which we can write as:

$$\frac{\beta(\omega)}{\beta_0} = \int \frac{1}{\sqrt{\pi}G} e^{-y^2/G^2} F(\omega_0 + y) dy \quad (3)$$

where G is the inhomogeneous (Gaussian) width and $F(\omega_0)$ is the homogeneous ratio for $\beta(\omega)/\beta_0$ given—by equation (2). In Figure 1 we present simulations for the amplitude and phase of $\beta(\omega)/\beta_0$ obtained using equations (1–3). It is seen that all three equations predict the same enhancement off resonance, i.e. $\omega < 6500\text{cm}^{-1}$. At resonance, where equation (1) diverges, the peak amplitude enhancement given by equation (2) is approximately $2/3 (\omega_0/\text{HWHM})$; equation (3) predicts an enhancement larger by about an additional factor of $(\pi \ln 2)^{1/2}$. The latter two equations also show a continuous change of phase through $\pi/2$ at resonance.

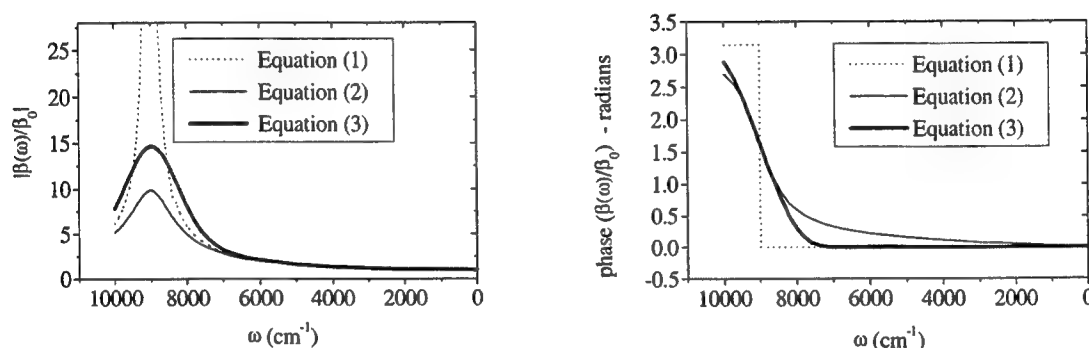


Figure 1. Amplitude and phase of $\beta(\omega)/\beta_0$ for a typical organic NLO molecule with an excited state of energy $\omega_0=18000\text{ cm}^{-1}$. Equation (1) is the non-resonant formula, while equations (2) and (3) include homogeneous and inhomogeneous broadening respectively, with a half width at half maximum of 1200cm^{-1} .

Experimental determination of β in the resonance regime can be performed with electric field induced second harmonic generation (EFISH), although the analysis is more complex than for an off-resonance determination. The characteristic fringes, obtained when the EFISH cell is translated in the laser, are washed out in a resonance experiment, and measurements must be performed on solutions of several different concentrations to extract a best fit value for the phase and amplitude of $\beta(\omega)$.

We have performed EFISH measurements on methylene chloride solutions of the NLO molecule known as IDLET (Figure 2) in both the off-resonance and resonance regions using $1.54\mu\text{m}$ and $1.064\mu\text{m}$ laser excitation. From the off-resonance measurement we found $\mu\beta_0=440\pm40 \times 10^{-48}\text{ esu}$, leading to $\beta_0=100\pm10 \times 10^{-30}\text{ esu}$ since $\mu=4.35\text{D}$ [4]. Using the resonance enhancement given by equation (3) we predict values of $6900\pm700 \times 10^{-48}\text{ esu}$ and $125\pm3^\circ$ for the amplitude and phase of $\mu\beta$ at $1.064\mu\text{m}$; our experimental results of $7600\pm700 \times 10^{-48}\text{ esu}$ and $125\pm3^\circ$ verify the correctness of equation (3) as the most suitable representation of the resonance enhancement of β .

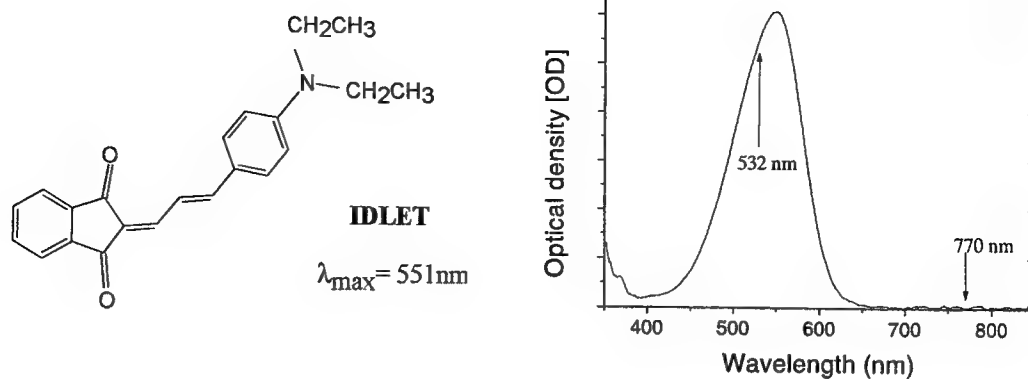


Figure 2. Structure and absorption of IDLET. The arrows show the energy of the harmonic wavelengths used in the on- and off- resonance EFISH measurements.

References

- [1] J.L. Oudar and D.S. Chemla, J. Chem. Phys. 66 (1977) 2664.
- [2] B.F. Levine, C.G. Bethea, E. Wasserman and L. Leenders, J. Chem. Phys. 68 (1978) 5042.
- [3] A. Otomo, G.I. Stegeman, M.C. Flipse, N.B.J. Diemeer, W.H.G. Horsthuis and G.R. M hlmann, J. Opt. Soc. Am. B. 15 (1998) 759.
- [4] C.R. Moylan, R.J. Twieg, V.Y. Lee, S.A. Swanson, K.M. Betterton and R.D. Miller, J. Amer. Chem. Soc. 115 (1993) 12599.

Polymer Photonic Components for WDM

C.L. Callender, J.-F. Viens, J.P. Noad

Communications Research Centre

P.O. Box 11490, Station H

Ottawa, Ontario, Canada K2H 8S2

claire.callender@crc.ca Tel: (613)-998-2726 Fax: (613)-990-8382

L. Eldada and R.A. Norwood

AlliedSignal Inc.

101 Columbia Road

Morristown, NJ 07962

louay.eldada@alliedsignal.com

Wavelength division multiplexing (WDM) has become one of the most promising methods of increasing the capacity of optical communications systems. Some components are now commercially available and implementation of prototype WDM systems is proceeding in the telecom networks of several countries. However, there still remains much research and development to be done on components to efficiently and cheaply achieve the various functions of an optical network, such as wavelength (de)multiplexing, routing, channel add/drop, and switching. Polymer waveguide technology can offer rugged, affordable, planar components with an easy interface to fiber to achieve many of these functions.

This paper will discuss the fabrication of polymer-based arrayed waveguide grating (AWG) (also known as PHASAR) devices.¹ AWGs are important elements for realizing demultiplexers, routers and more complex devices such as tunable filters and add/drop modules. This work was carried out using a planar waveguide technology based on acrylate polymers developed at AlliedSignal². The refractive index of each polymer layer in a waveguide structure can be tuned by mixing of monomer components prior to curing and patterning by conventional photolithography. Buried ridge waveguide structures can be made with dimensions ranging from 3 μm x 3 μm to 6 μm x 6 μm , ensuring single-mode operation at around 1.55 μm while minimizing device sizes and maintaining good overlap with optical fiber.

Arrayed Waveguide Gratings for dense WDM

For applications in telecom optical networks and "last-mile" access (delivery of services such as internet and cable tv to the home via optical fiber), we are currently developing dense WDM components with wavelength separations typically 1.6 nm or smaller based on arrayed waveguide gratings (AWGs).

The operation of an AWG device has been described in detail by Smit¹. Briefly, the device consists of a set of input and output waveguides, connected via two slab waveguide regions and a set of closely spaced array waveguides whose path lengths vary by an increment which is an integer number of wavelengths. Correct operation depends on the control of small phase differences in adjacent waveguides. This, coupled with stringent industry requirements for low cross-talk and insertion loss means that extremely good control over the thickness and flatness of layers, and precise photolithographic definition of waveguide dimensions must be achieved. A range of AWG devices has been designed and several of these designs have been fabricated on silicon substrates. For telecom applications we have targeted 8-channel wavelength routers, with a wavelength channel spacing of 1.6 nm (200GHz), centered at 1.55 μm . Figure 1 (a) shows the array region of such a device fabricated at CRC using the AlliedSignal standard acrylate polymers. Figure 1(b) shows an enlargement of the area where the array guides meet the slab region. In this design there are

76 array guides, each $3\text{ }\mu\text{m}$ wide by $3\text{ }\mu\text{m}$ thick, spaced $3\text{ }\mu\text{m}$ apart. The guides are all of excellent quality and by fine-tuning the exposure times and intensities, optimized photolithographic contrast and clean development of the closely spaced guides has been achieved. Larger guides with dimensions of $5\text{ }\mu\text{m} \times 5\text{ }\mu\text{m}$ and $6\text{ }\mu\text{m} \times 6\text{ }\mu\text{m}$ are also under investigation for these devices.

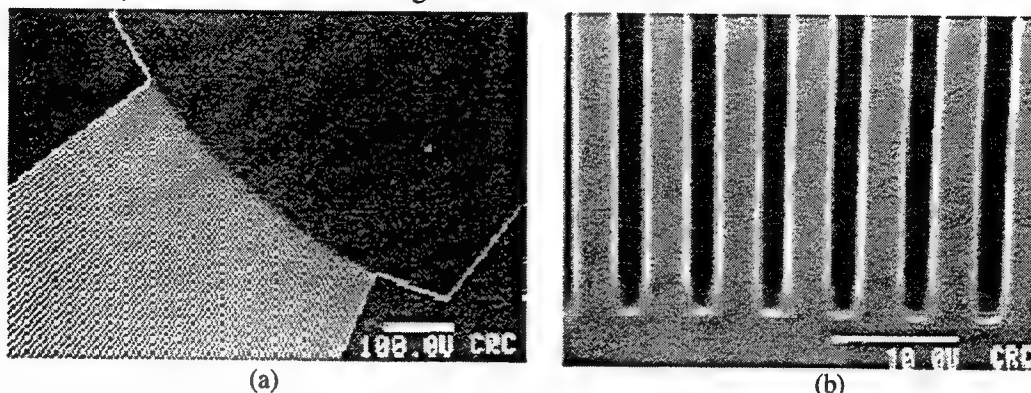


Fig. 1: SEM images of the array section of an AWG demultiplexer. 1(b) is a close-up view showing the high quality photolithographically defined polymer waveguides with widths and spacings of $3\text{ }\mu\text{m}$.

The devices were characterized using a tunable laser source with a wavelength range of 1.50 to $1.58\text{ }\mu\text{m}$. Figure 2 shows the output of an 8-channel AWG router with a channel spacing of 1.6 nm . The total insertion loss is around 12.5 dB (including unoptimized coupling losses), and the cross-talk is typically 20 dB . Side-lobes on the main transmission peaks are degrading the cross-talk. These are thought to be due to slight differences between the designed and actual values of the layer refractive indices and improvements are expected with further fine-tuning of the process. Propagation losses in the $3\text{ }\mu\text{m}$ wide single-mode buried ridge waveguides used to fabricate this device were typically 1 dB/cm at $1.55\text{ }\mu\text{m}$, of which 0.5 dB/cm is due to material loss. The length of the device is 40 mm .

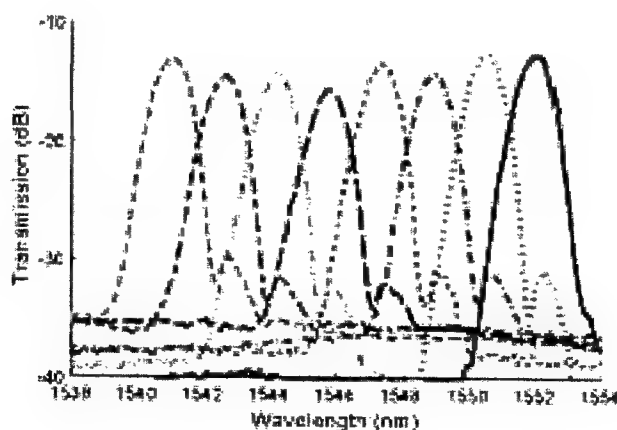


Fig. 2: Transmission of an 8-channel DWDM router as a function of wavelength.

The TM response was shifted typically 0.3 to 0.6 nm to shorter wavelengths relative to TE. This shift is dependent on process conditions. Reduction of the polarization sensitivity to an acceptable level (better than 0.1 nm) is currently under investigation. The use of halogenated materials² could substantially improve both the losses and the polarization sensitivity in AWG devices.

Broad-band demultiplexers

Another application currently of interest to CRC is the development of a small, lightweight, high bandwidth distribution link that can support multiple microwave frequencies and digital control signals for onboard spacecraft and ground terminal applications. By using WDM techniques many signals, each of which would require its own waveguide, coax or wire in current systems, could be carried on a single optical fiber, resulting in a significant size, weight and cost reduction. One approach under investigation is to use AWG technology to produce 2-channel, bi-directional wavelength routers, with channel separations of 10 to 30 nm. The targeted wavelength range is again around 1.55 μm , to exploit the widely available, cheap, narrow-linewidth laser sources that have become available as a result of the rapid developments in the telecom industry.

To achieve the channel separations of 10 nm and larger, the path length increment between array waveguides must be 20 to 30 μm , compared to $>70 \mu\text{m}$ for a typical DWDM device. To accommodate this, changes to the array geometry were required. Instead of the standard colinear input and output guides connected by a "loop" array, a design was formulated with offset input and output guides, mirror-imaged fanout regions, and a simple wedge-shaped region to achieve the smaller path length difference³. Several devices were fabricated, using the same waveguide layer systems as the DWDM routers described above. Figure 3 shows the response of a preliminary 2-channel AWG bi-directional router with a channel spacing of 20 nm. Cross-talk is currently around 15-18 dB, with potential for improvement through optimum control over layer refractive indices and process fine-tuning. The TM response is shifted 0.4 nm to shorter wavelength, which is acceptable for this application.

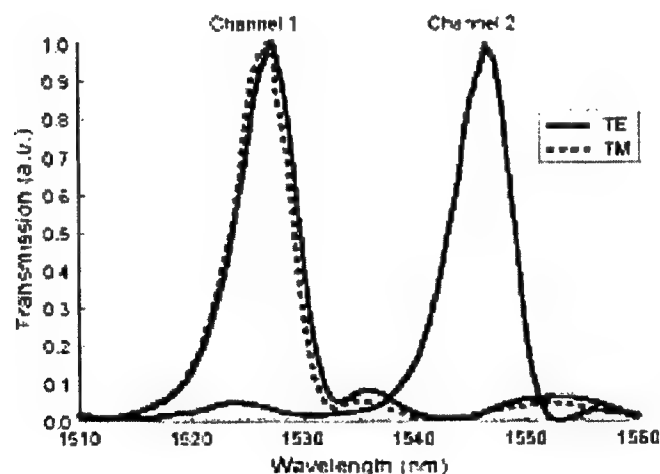


Fig. 3: Transmission of a 2-channel AWG bidirectional router with channel spacing of 20 nm.

References

1. M.K. Smit and C. van Dam, "PHASAR-Based WDM-Devices: Principles, Design and Applications", *IEEE J. Selected Topics in Quantum Electron.*, 2(2), 236-250 (1996).
2. L. Eldada, S. Yin, R.A. Norwood and J.T. Yardley, "Affordable WDM Components: the Polymer Solution", *Proc. SPIE* vol. 3234 161-174 (1997).
3. R. Adar, C.H. Henry, C. Dragone, R.C. Kistler and M.A. Milbrodt, "Broad-Band Multiplexers Made with Silica Waveguides on Silicon", *J. Lightwave Technol.*, 11(2), 212-219 (1993).

Organic Thin Films for Photonics Applications

Polymer Integrated Optics: 2

Sunday, 26 September 1999

TBA

Presider

SuC

1:30pm–2:45pm

California Ballroom Salons 4&5

Photopolymer Media for Holographic Data Storage

Lisa Dhar, Arturo Hale, Melinda Schnoes, Marcia Schilling, Howard Katz, Carol Boyd, Kevin Curtis,
Michael Tackitt, William Wilson, and Adrian Hill

Bell Laboratories, Lucent Technologies, 700 Mountain Avenue, Murray Hill, New Jersey 07974, USA
ldhar@lucent.com

The demand for increases in the capacity and speed of data storage tests the limits of conventional technologies and drives the search for new approaches. Optical holography has long held the promise of storage densities and data transfer rates far greater than those of traditional magnetic and optical systems¹. Its realization has been frustrated by the lack of suitable storage materials. Holographic media must satisfy stringent criteria, including high dynamic range, dimensional stability, optical clarity and flatness, and millimeter thickness. Here we describe a new design of materials for holography that has enabled substantial advances towards meeting these goals². These materials consist of solutions of two independently polymerizable and compatible chemical systems. One system polymerizes to form a thick, optically flat matrix; the other system remains dissolved in this matrix and polymerizes only during holographic writing. We demonstrate how this strategy yields recording media that exhibit an $M/\#$ ³ (a measure of the dynamic range) of 42, the highest yet reported, in a ~1 mm thick, optically flat format with low light scatter and that support the storage and recovery of high capacity digital data pages.

Holographic storage can achieve high transfer rates because data are written and recovered in a page-wise fashion; high storage densities are possible because many high capacity data pages can be recorded independently in the same volume of material. In order to enable simultaneously high storage densities and rapid data recovery rates, a material must have adequate refractive index contrast and thickness to support large numbers of holograms with sufficiently high diffraction efficiencies. The storage capacity of a holographic material is typically characterized by a parameter, $M/\#$, a measure of the number of holograms with diffraction efficiencies of one hundred percent that can be stored in the same volume. The $M/\#$ of iron-doped lithium niobate, the traditional choice for holography experiments, is typically 1-1.5 for 1 cm thick crystals. It is commonly believed that $M/\#$'s at least an order of magnitude higher will be required to achieve compelling storage densities and transfer rates. The thickness of the recording medium also independently determines how many holograms can be recorded in the same volume of material because of geometrical considerations. Thicknesses of at least 1 mm are thought to be required for high density applications. Recording media must undergo only limited changes in their dimensions and bulk refractive index as these changes can degrade the fidelity of data recovery and ultimately limit the storage density of a material. Holographic media must also be optically flat so that high capacity digital data pages can be imaged, recorded, and recovered with low probabilities of error.

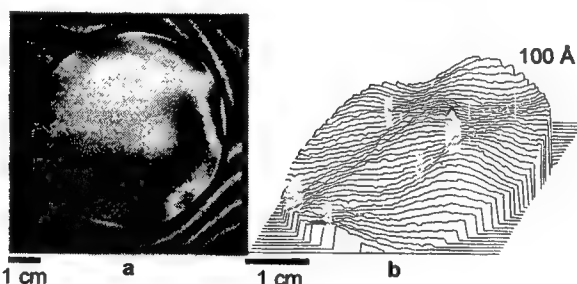
Photopolymer materials are attractive candidates for write-once-read-many times data storage applications because they can be designed to have large refractive index contrast and high photosensitivity, record permanent holograms, and be easily processed⁴. Holographic recording in photopolymer systems occurs through a spatial pattern of photoinitiated polymerization induced by the optical interference pattern generated during recording. The concentration gradient in the photosensitive species that results from the patterned polymerization leads to diffusion of the unpolymerized photosensitive species and creates a compositional pattern that converts the original optical interference into a refractive index modulation. Most of the currently available holographic photopolymers have been optimized for display applications that require only large refractive index contrasts ($\Delta n \sim 1 \times 10^{-2}$). Typically, these materials can be used only as thin ($\leq 200 \mu\text{m}$) layers and often exhibit significant

dimensional and bulk refractive index changes due to the polymerization of the photosensitive species that occurs during recording.

To better meet the needs of holographic data storage, we designed a new type of polymer system that is composed of two independently polymerizable and compatible chemical systems: low refractive index matrix precursors and high refractive index photopolymerizable monomers. The matrix of our media is formed by an *in-situ* polymerization to yield a cross-linked network in the presence of the photopolymerizable monomers, which remain dissolved and unreacted. Holographic exposure polymerizes the photoactive monomer(s); the unreacted monomers diffuse through the matrix producing a modulation in the refractive index that is determined by the difference between the refractive indices of the monomer and matrix. The most important aspects of this strategy which yield high performance holographic storage media are (i) preforming the matrix *in-situ* which allows media to be shaped into the required thick and flat formats, (ii) the creation of a cross-linked matrix as a support structure for stable holographic gratings, (iii) the choice of compatible matrix and monomer systems to yield media with good optical clarity and low levels of light scattering, and (iv) the design of independent matrix and monomer systems so as to avoid cross reactions that dilute the refractive index contrast. The fourth point ensures that the low refractive index of the "background" matrix is not detrimentally raised by the premature polymerization of the high refractive index monomer. Media with high refractive index contrast and high M/# can be fabricated using small amounts of the high index monomer thereby minimizing the photopolymerization-induced dimensional and bulk refractive index changes that occur during recording.

Figure 1 shows a transmission interferogram of typical 1 mm thick (polymer thickness) medium. (The polymer medium is contained between two glass substrates.) The data show flatness within 500 Å ($\lambda/10$) over the three inch diameter sample.

Figure 1(a) Transmission 1 mm thick photopolymer of the variation in the inner 4 cm of the sample. sample varies less than entire area of the medium.



interferogram of a typical medium. **(b)** Surface plot optical thickness of the. The optical flatness of the $\lambda/10$ /cm (~ 500 Å) over the

The strength of highlighted by the

optimize the dynamic range of the media. In general, the dynamic range of a photopolymer material increases with increasing concentration of the writing monomer. This approach, however, carries the penalty of increasing the changes in dimension and bulk refractive index that accompany recording. Our materials design strategy enables us to improve the dynamic range of media while keeping the effective dimensional changes fixed by simply varying the difference between the refractive indices of the matrix and the writing monomers.

separable chemistries is ability to controllably

In Figure 2(a), we show the M/#'s of a series of 200 μ m thick media that were fabricated using the same matrix but writing monomers of varying refractive index and varying size where the concentrations of the monomers were adjusted to yield equivalent levels of recording-induced changes in dimension and bulk refractive index. (Each of the samples underwent changes equivalent to $\sim 0.35\%$ in thickness and $\sim 2.1 \times 10^{-3}$ in the bulk refractive index for the complete reaction of the photoactive monomers.)

Increases in M/# from 2 to 11 were realized while maintaining the same level of effective dimensional stability of the media.

Media with high M/# were obtained by fabricating thick samples of our photopolymer materials. In Figure 2(b), we show how the M/# scales with thickness in media fabricated with a typical writing monomer. Data from three sets of samples are shown, with each set formulated with a different concentration of the monomer and therefore exhibiting levels of effective dimensional stability. The gains in M/# with increasing thickness are possible because of the low levels of light absorption and light scatter and the high level of effective dimensional stability of the media.

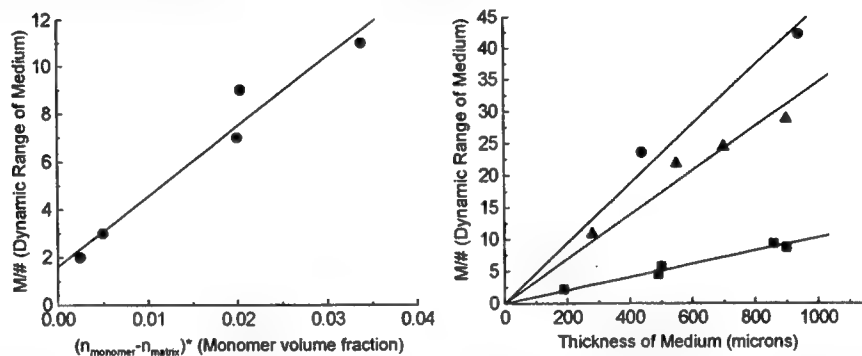


Figure 2(a) M/# versus the product of the difference between refractive indices of the photosensitive monomer and the matrix and the volume fraction of the monomer for five different resins. The molar number of reactive groups of the photoactive monomer in each of the media is adjusted to yield equivalent amounts of recording-induced rotations in the Bragg angle upon recovery. The media are all 200 μm thick. **(b)** M/# versus thickness for photopolymer media fabricated with a typical writing monomer: closed squares (triangles, circles), media exhibit $\sim 0.1\%$ (0.35% , 0.5%) change in thickness upon recording

We believe the observation of an M/# of 42 is the first demonstration of a holographic storage medium with dynamic range of this magnitude. Moreover, our strategy allows us flexibility in further optimization of our material. For example, media with higher M/#'s yet the same effective dimensional stability can be fabricated by using monomers with increased refractive index or monomers with higher molecular weights that would occupy larger volume fractions per reactive group.

As a preliminary demonstration of the capabilities of these media, they were used to store and recover multiple high capacity (480 kbit) digital data pages. Storage densities as high as 48 channel bits/ μm^2 or 31.5 channel Gbits/in 2 were demonstrated using established multiplexing techniques to record and recover 3000 digital data pages in a 750 μm thick medium. The data suggest that even greater storage densities are possible using the higher response versions of our materials.

The materials described here represent substantial advances in the development of recording media for holographic data storage. Their success, however, rests upon a few important issues. Ongoing work is focused on the temperature sensitivity of the polymer media and the long-term archival life of stored digital data. Nonetheless, the unprecedented M/#'s reported here, the demonstrated data storage capabilities of the systems, and the ability to further improve the material greatly enhance the promise of photopolymer media for holographic data storage.

References:

1. D. Psaltis and F. Mok., *Sci. Amer.* **273**, 52 (1995).
2. L. Dhar, A. Hale, H.E. Katz, M.L. Schilling, M.G. Schnoes, and F.C. Schilling, *Opt. Lett.* **24**, 487 (1998).
3. F. H. Mok, , G. W. Burr, and D. Psaltis, *Opt. Lett.* **21**, 896 (1996).
4. H. J. Bjelkagen, ed. *Selected Papers on Holographic Recording*, (SPIE Press) **MS 130** (1996).

RELIABLE POLYMERS FOR OADM APPLICATIONS

Constantina Poga and Robert Andrew Norwood

Telecom Photonics, AlliedSignal Inc., 101 Columbia Road, Morristown NJ 07962

constantina.poga@alliedsignal.com

Introduction

Dense Wavelength Division Multiplexing (DWDM) systems have been deployed because they cost-effectively address the need for increased capacity in long distance telecommunication networks. Polymeric materials provide a platform for variety of optical functions required for first and second generation DWDM systems, including filtering, switching, variable attenuation, and tunable filtering. For example, DWDM filter devices can be designed by using planar waveguides grating building blocks and these devices can be fabricated with low temperature processes and high throughput. Apart from exhibiting the desired optical performance, these components should be reliable and have a lifetime of 20-25 years as defined by industry standards. Optical add/drop multiplexers (OADM)¹ and, particularly, tunable OADM's² can be manufactured by using AlliedSignal's UV100 polymeric composite³. In this contribution, we focus on the reliability aspects of such a device by describing the proposed qualification process along with results of some of the intended tests.

Reliability program

Reliability issues for passive optical components are governed by various protocols such as the Bellcore 1209 and 1221⁴, 1209 focusing primarily on short-term reliability data and 1221 on the qualification of new class of devices. The reliability program for an OADM component can be represented by the following flow chart and is addressed individually below.

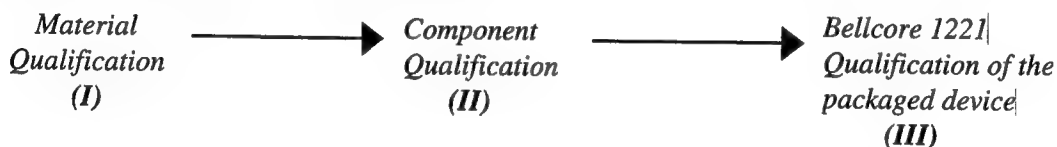


Figure 1: Schematic representation for the device qualification process.

I. Material Qualification:

Chemical Stability: In the material qualification stage, it is ensured that the material is chemically stable for the intended period of use (20 to 25 years) at the appropriate environmental conditions. These conditions are determined by the device's operating environment. For components that are intended for the office environment, these conditions are specified in the Bellcore 63 document and revisions thereto⁵ to be; temperatures from 0 to 60°C, and relative humidities from 5 to 85%.

A measure of polymer stability is given by thermogravimetric analysis (TGA) measurements where the weight loss of the material is measured as a function of time at some temperature. This temperature is usually well above the temperature of the intended use to accelerate the process, but below the material's decomposition temperature. TGA measurements give a measure of the degradation process that is usually described by the Arrhenius Law: $\text{Rate} \propto \exp[-(E_a/k_B T)]$ where T is the absolute temperature, k_B Boltzman's constant and E_a the activation energy for the chemical degradation process.

The AlliedSignal UV100 material used for the realization of these devices has a decomposition temperature of 366°C; we therefore ran TGA measurements at 230°C, 250°C, 270°C, 300°C and 340°C. These data were fit to an Arrhenius Law and the decay rates τ at various temperatures found and plotted against $1/T$. For temperatures up to 340°C, we found that the degradation rates are well described by

$$\ln(\tau) = -18.61216 + 1.39595 \cdot (k_B T)^{-1} \quad (1)$$

(1) can be used to determine the decay rate and therefore give a useful estimate of the lifetime of the material at use temperatures. For 60°C , which should represent the worst case for the device operation, we get a decay rate of $\tau_{60^{\circ}\text{C}} \equiv 21 \times 10^6$ years. This result shows that the material is chemically stable for time periods well above the intended period of use, at least for thermally activated decay processes.

Material's Pot Life: Another important factor in polymer device manufacturing is the material's pot life, defined as the time that the material can be kept on the shelf at typical storage temperatures without showing any degradation. As a measure of the degradation of UV100, we chose to measure the index of refraction, a key physical quantity for the operation of waveguide devices, in freshly prepared thin film samples of material that is either aging on the shelf or aging at an accelerated pace at 70°C . The results of this experiment are shown in Figure 2. The first thing to notice is that the index of refraction of the material that is kept at room temperature remains constant within experimental error during the period of the measurement. (The experimental error is given by the measurement accuracy that is of the order of 5×10^{-4} .) The other important feature is that the index of refraction of samples made by material kept at 70°C is the same, within measurement error, with the index measured in samples made by material kept at room temperature up to 47 days. The measurement that was done on Day 64 shows some deviation between the material that is kept at room temperature and that kept at 70°C . Thus, the most conservative estimate for the lifetime of the material kept at 70°C is 47 days. If, as a first approximation, we assume that reactions rates double for every 10°C ,⁶ we would roughly get a pot life of 2 years.

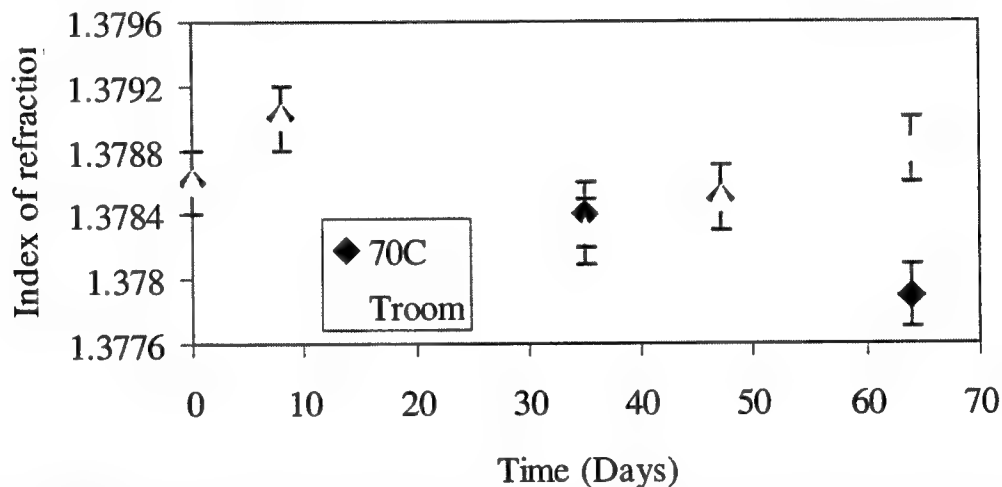


Figure 2: Refractive index of thin films made from material kept in glass bottles at room temperature and 70°C .

II. Component qualification:

The OADM design¹ consists of cascaded Mach-Zehnder interferometers with planar waveguide gratings. To simplify the testing procedure and aid in failure mode determination, individual building blocks, such as waveguides with gratings, are tested according to Bellcore 1209. The most challenging of the tests involves placing the optical component in an environment of 85°C and 85% relative humidity for several days. To accelerate even more the device's lifetime testing, we placed a UV-100 waveguide with a grating in an environment of 140°C ; the results are shown in Figure 3a. As shown in Fig. 3a, there are no significant changes in either the position or shape of the transmission spectrum for Days 2 and 13. Furthermore, the grating's strength, as is measured from the transmitted intensity, does not seem to deteriorate over time. Since the peak position, λ_B , is a very sensitive measure (to the 0.0001 level) of the index of refraction of the material, n , we see that the index remains unchanged for the time period measured. Further measurements showed the components to successfully withstand this environment for 20 days before changes in the spectrum occurred. These initial results strongly indicate that UV100 is environmentally stable; more extensive testing is underway.

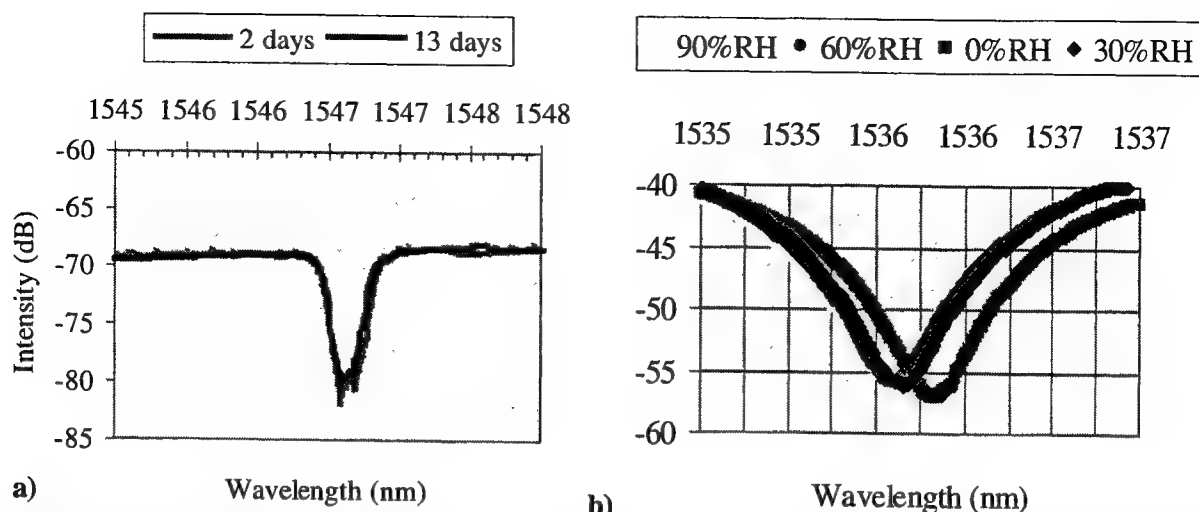


Figure 3: a) Grating transmission spectrum at Days 2 and 13; $T = 140^{\circ}\text{C}$ with the relative humidity uncontrolled. b) Grating transmission spectrum for 0% to 90% relative humidity (at $T = 50^{\circ}\text{C}$).

Figure 3b shows the shift of the transmission curve for a change of 90% in relative humidity for $T = 50^{\circ}\text{C}$. The Bragg wavelength shift is, in this case, 0.2 nm. This blue shift is consistent with a decrease in the material's effective index, likely a result of moisture absorption (polymer swelling). The size of this shift is important for device package considerations, and of course, reflects on its cost; if UV100 is used in devices with 1.6 nm channel spacing then hermetically sealing is not required. Industry standards recommend that the shift of the peak wavelength not exceed 20% of the channel spacing which is, for the 1.6 nm spacing, 0.3 nm. For narrower channel spacing it is necessary to provide a better seal. As an example, for 0.8 nm channel spacing, the allowed shift is 0.16 nm, slightly lower than the shift observed.

III. Bellcore 1221 qualification

As mentioned above, the packaged device should pass Bellcore 1221 testing. An important consideration for the package device is the degree of hermeticity required. We have performed humidity sensitivity measurements that indicate that UV-100 gratings would require only quasi-hermetic packaging to prevent humidity induced spectral shifts in operation. We are now completing the packaging design and will commence with full 1221 testing once packaged devices are completed.

References

- /1/ L. Eldada, S. Yin, C. Poga, C. Glass, R. Blomquist, and R. A. Norwood, *IEEE Photonics Technology Letters*, **10**, 1416 (1998).
- /2/ L. Eldada, R. Blomquist, M. Maxfield, D. Pant, G. Boudoughian, C. Poga, and R. A. Norwood, *IEEE Photonics Technology Letters*, **11**, 448 (1999).
- /3/ C. Poga, R. Blomquist, L. Eldada, and R. A. Norwood, *Diffraction/Holographic Technologies, Systems and Spatial Light Modulators VI*, Photonics West Symposium, San Jose, (1999).
- /4/ Bellcore GR-1209-CORE, "Generic Requirements for Fiber Optic Branching Components," (Bellcore, 1998). Bellcore GR-1221-CORE, "Generic Reliability Assurance Requirements to Fiber Optic Branching Components," (Bellcore, 1999).
- /5/ Bellcore GR-63-CORE, "Network Equipment-Building System (NEBS) Requirements: Physical Protection," (Bellcore, 1995).
- /6/ F. Brescia, J. Arents, H. Meislich, A. Turk, *Fundamentals of Chemistry*, 3rd ed., (New York, 1975) p 407.

Reversible Structuring of Optical Waveguides using Optical Switch Molecules

M. Jäger, S. Lecomte, U. Gubler, Ch. Bosshard, P. Günter
Institute of Quantum Electronics, Swiss Federal Institute of Technology,
CH-8093 Zürich, Switzerland
Phone +41 1 633-3166
Fax +41 1 633-1056
Email: mjaeger@iqe.phys.ethz.ch

L. Gobbi, F. Diederich
Institute of Organic Chemistry, Swiss Federal Institute of Technology
ETH Zentrum, Universitätsstr. 16
CH-8092 Zürich, Switzerland

Optical switch molecules are moieties undergoing reversible structural changes upon illumination. Associated with these chemical reactions the optical properties can be modified significantly. These materials have recently attracted a lot of attention as a possible medium for rewritable information storage [1]. We report on the investigation of optical switch molecules based on 2-(4-Iodophenyl)-1,1(8aH)-azulendicarbonitrile in solution as well as polymeric thin films. We also demonstrate rewritable waveguide structures employing these optical switches. As opposed to optical waveguides irreversibly structured by photobleaching [2], our waveguides can be thermally erased and again rewritten. Moreover, UV exposure results in an increased refractive index, such that the waveguide regions can be written by direct exposure.

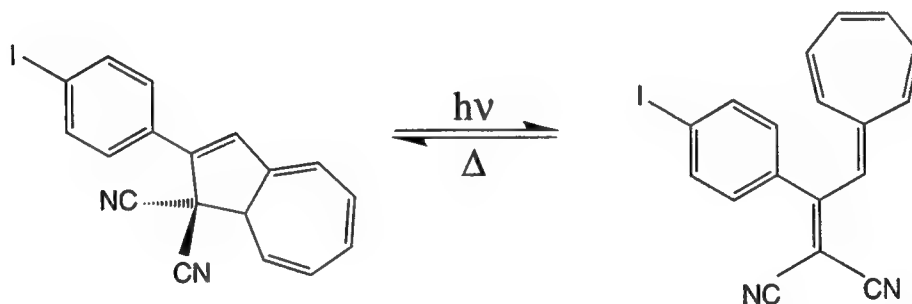


Fig. 1 Chemical structure of optical switch molecules: the UV illumination breaks the cyclic molecule **1** (left) and transforms it to form **2** (right).

The investigated molecular switch is based on a thermally reversible photo-retrocyclization (fig. 1). The photoreaction is activated by illumination with a wavelength near 360 nm, the absorption peak of the cyclic form **1** in the visible. The accumulation of form **2** is accompanied by a significant color change from light yellow to red according to the appearance of the absorption peak at 480 nm. The thermal relaxation back to **1** in solution was characterized by repeated absorption spectroscopy and is very well described by an exponential decay with the time constant of 5.4 hours at a temperature of 27°C (fig. 2).

Thin film samples of good quality were prepared using polysulfone as polymer host and dibromomethane as solvent. The absorption spectra of films with up to 15% chromophore content (by weight) showed no apparent sign of aggregation. As opposed to the relaxation (**2**

to 1) in solution the relaxation in thin films does not follow an exponential function. The decay occurs on a similar time scale as in the solution, but proceeds faster at first and slows down thereafter.

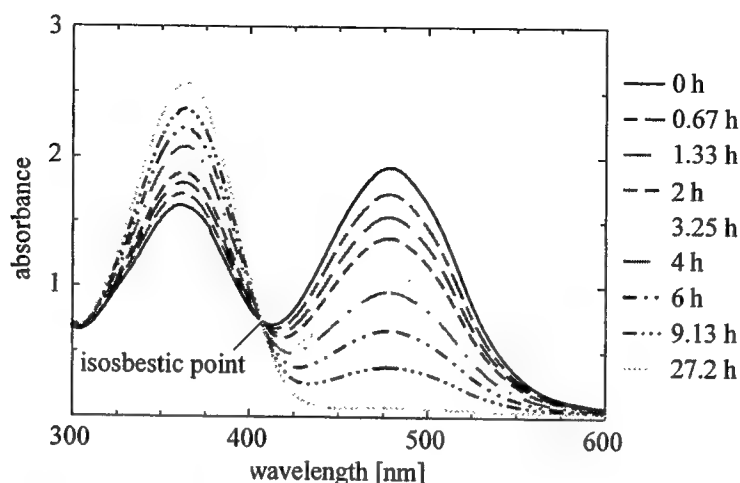


Fig. 2 Thermally activated relaxation of form 2 back to form 1 in chloroform with a time constant of 5.4 hours. An isosbestic point (i.e. a wavelength showing no change in absorbance) is evident at 407 nm.

The dynamics of the photoreaction (1 to 2) as well as the thermal relaxation (2 to 1) were also characterized using holographic gratings, because the large changes in the absorption (fig. 2) are accompanied by a refractive index change in the transparency region. For this purpose, two Argon ion laser beams ($\lambda=360$ nm, intensity of ca. 4 mW/cm^2 each) were crossed in the $1.2 \text{ }\mu\text{m}$ thick sample at an external angle of 20.8 degrees. The resulting grating of $1 \text{ }\mu\text{m}$ period was probed with a He-Ne laser ($\lambda=633$ nm) as a function of time. Fig. 3 shows the exponential build up of the grating with a time constant of 42s. With 14.7% chromophore content, the diffraction efficiency reaches 0.15% corresponding to a refractive index change of $6.5 \cdot 10^{-3}$. As expected, the build up time decreases with increasing intensity of the writing beams, which will be discussed in detail in the presentation. The thermal decay is again non-exponential and occurs with a time constant of about 6 hours, which is consistent with the absorption measurements mentioned above.

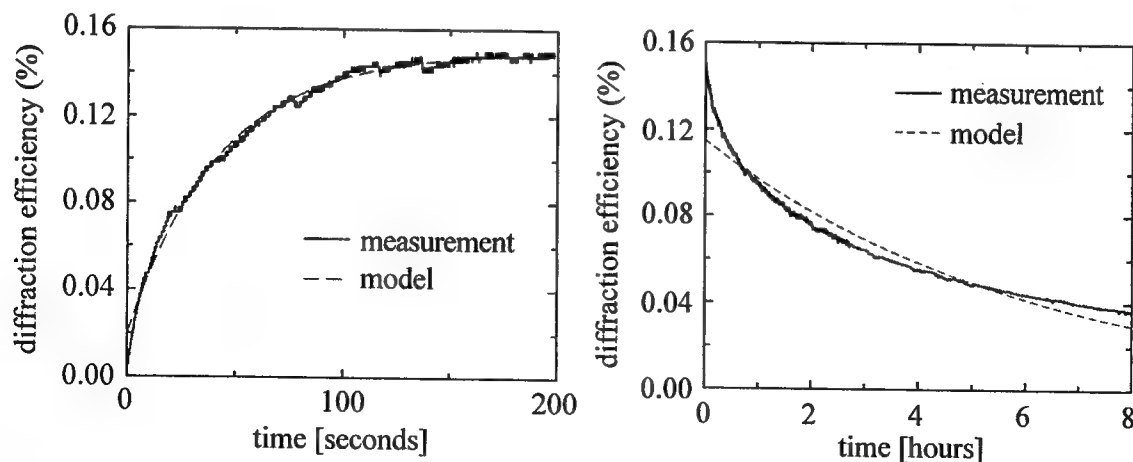


Fig. 3 Build up and decay of a holographic grating in a polymeric thin film (chromophore concentration of 14.7%) written with two laser beams. The theoretical model is described by an exponential function. (Note the different time scales)

The structural change of the molecular switches is also expected to alter not only the linear optical properties of the molecules, but also the nonlinear optical coefficients. This can be justified by the fact that form **2** has a conjugation of double bonds leading to the dicyano group, which represents a strong electron acceptor. However, this conjugation is missing in form **1**. First results of these nonlinear optical measurements (Third Harmonic Generation Maker fringes) will be given in the presentation.

Finally, the suitability of the employed material system for practical devices was tested. For this purpose, thin films of 1.5 μm with 8% chromophore content were spincoated on glass and coated silicon substrates. Subsequently, waveguide structures (8 μm wide channels and Y-junctions) were exposed into the doped film. Fig. 4 displays the microscope picture of these reversibly written waveguides.

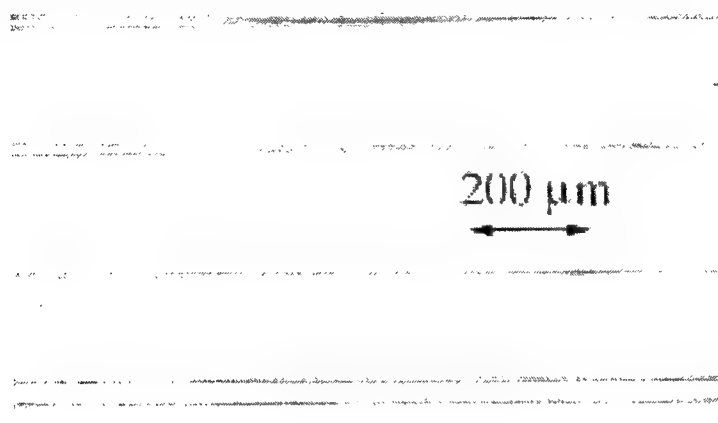


Fig. 4 Reversibly structured waveguides channels and Y-junctions with a width of 8 μm . The double arrow indicates a distance of 200 μm .

In conclusion, we have investigated the forward and backward chemical reaction of optical switch molecules in both solution and polymeric thin films. In particular, the changes in the linear and nonlinear optical properties were characterized. Furthermore, these photoswitches were employed for the demonstration of optical waveguide structures in thin polymeric films, which can be rewritten repeatedly. Further research will focus on the stability enhancement of form **2** and alternative (other than thermally activated) routes for the backreaction.

References:

- [1] J.-M. Lehn, *Supramolecular Chemistry*, VCH Weinheim (1995).
- [2] M.B.J. Diemeer, F.M.M. Suyten, and E.S. Trommel, A. Mc Donach, J.M. Copeland, L.W. Jenneskens, and W.H.G. Horsthuis, *Electron. Lett.* **26**, pp 379-380 (1990).

Low-loss optical polymer waveguide applications based on crosslinked fluorinated poly(arylene ether)s

Hyung-Jong Lee, Myung-Hyun Lee, Min-Cheol Oh, Joq-Heon Ahn, Wol-Yon Hwang, Seon Gyu Han

Telecommunication Basic Research Lab. Electronics and Telecommunications Research Institute, 161 Kajong-Dong, Yusong-Gu, Taejon 305-600, Korea. Tel.+82-42-860-4875, Fax. +82-42-860-6836, email. hjl@etri.re.kr.

Introduction

Recently, polymeric optical waveguide for optical telecommunications have been actively investigating because of their easy processibility and cost-effective technology. Based on low-loss polymer materials, various optical waveguide devices such as optical power splitter, digital optical switches, AWG wavelength multiplexers, and tunable wavelength filters have been demonstrated.¹⁻³ To obtain a polymer device with good performance, the polymer should be essentially required a low optical propagation loss at the telecommunication wavelength region of 1.3 and 1.55 μm , a sufficient thermal stability to withstand typical operation condition, and precise refractive index controllability. In addition to the polymers have an excellent film forming properties with various thickness, adhesion on substrate, chemical and environment resistance, and gapfilling ability for fabrication of optical waveguides. In our previous works, we reported on the synthesis of crosslinkable fluorinated poly(arylene ethers) and poly(ether ketone) having a crosslinkable ethynyl group at the chain end.⁴⁻⁵ In this article, we present our results on the characterization of newly synthesized crosslinkable fluorinated poly(arylene ether) derivatives for thermo-optic waveguide application.

Polymers synthesis.

We developed a thermally curable fluorinated poly(arylene ether)s (FPAE-EP) for an optical waveguide material with low propagation loss and good environmental stability. The FPAE-EP derivatives were synthesized from decafluorobiphenyl and 6F-BPA and/or resorcinol in the presence of potassium carbonate followed by adding 3-ethynylphenol (EP). The molecular weights (M_n) and polydispersities of the resulting prepolymers were in the range of 8,000 - 9,500 and 1.60 - 1.80 with polystyrene standards, respectively. The molecular weights of the precursor polymers were controlled by the monomer imbalance. For cladding and core materials in the optical waveguide, we used the FPAE-EP and their copolymers as shown in Fig. 1.

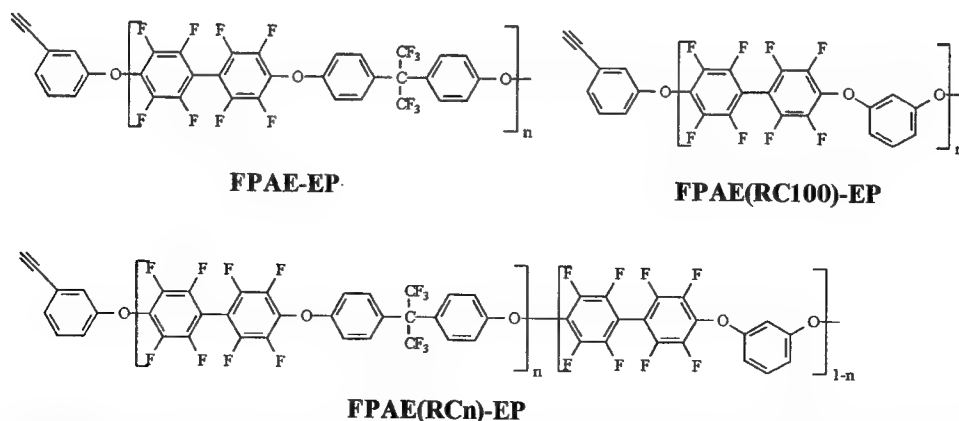


Fig. 1. Chemical structure of fluorinated poly(arylene ether)s with curable ethynyl group.

Films preparation and measurement.

FPAE-EP derivatives were dissolved in cyclohexanone at concentration of 20 - 40 wt %. The solution filtered with a syringe through a 0.2 μm Teflon membrane filter was spin coated on the Si wafer substrates with 2 μm SiO_2 layer. After coating, the film was cured at 250°C for 2 h on a hotplate to produce insoluble optical quality films with 0.5 - 10 μm thickness. A depth profiler (α -step 200) confirmed the film thickness. The refractive indices of TE and TM mode, n_{TE} and n_{TM} , of the polymer films at the 1.55 μm wavelength were determined from coupling angles of TE- or TM-optical guided modes with a gadolinium gallium garnet (GGG) prism.

Experimental results

For the fabrication of a waveguide device, a crosslinked FPAE-EP system using acetylene-terminated oligomer has several advantages such as increased thermal stability, chemical resistance, thickness controllability, gapfilling ability, and improved adhesion properties at the substrate. We synthesized the FPAE-EP copolymers for the refractive index control. It is important to control the refractive indices of the core and cladding materials when we design and fabricate single-mode waveguide devices. Fig.2 shows the dependence of the refractive indices for TE and TM mode polarization on the resorcinol content in copolymers at 1.55 μm wavelength. The refractive index of the polymer increases as the resorcinol content increases. Fig 2 indicates that the refractive index of polymers were able to control in the range of 1.495 - 1.535 at 1.55 μm by altering the copolymerization ratio of the monomers or blend between the FPAE-EP copolymers. The birefringence, which is the difference between n_{TE} and n_{TM} , was almost constant at low values of 0.003 - 0.004. Therefore, if the FPAE-EP copolymers with different resorcinol contents are used as the cladding and core materials, the difference between the refractive indices of the cladding and core for the TE polarization (Δn_{TE}) is almost the same as that for the TM polarization (Δn_{TM}). This is useful for designing the waveguide structures and fabricating them with low polarization dependent loss.

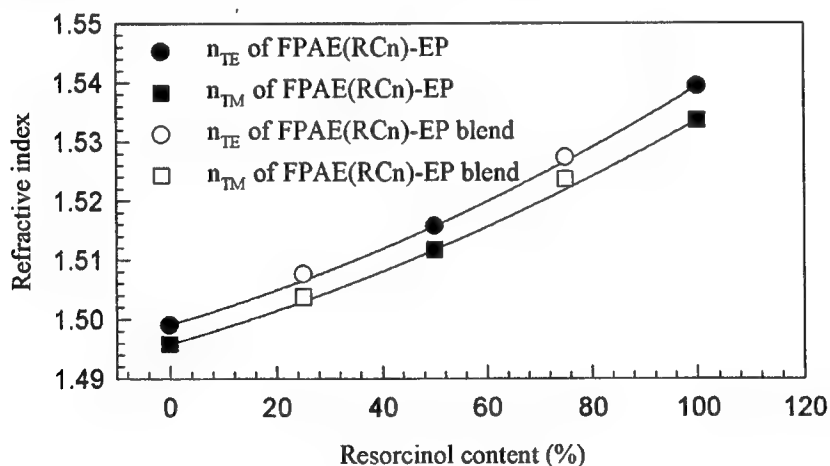


Fig. 2. Dependence of refractive index on resorcinol content of FPAE-EP copolymers.

The curing temperature and rate of the newly synthesized FPAE-EP derivatives was evaluated by a DSC and heat mounted FT-IR. DSC thermograms of FPAE-EP derivatives show an exothermic peak at maximum 280°C that is initiated at 235°C. As the curing proceeds, the acetylene C-H peak at 3308 cm^{-1} gradually disappeared. It is directly observed by heat mounted

FT-IR. This peak almost completely disappeared after curing at 250°C for 2 h. Cured films have good chemical resistance and high thermal stability.

Thermal stability is an important issue with regard to optical components. The thermal stability of polymers is essentially determined by the decomposition of the polymer itself. TGA thermograms of the polymers exhibit only 5% weight loss up to 510°C as shown in Fig. 3. Thermal stability was also evaluated by the refractive index variation at elevated temperature. Fig. 4. shows the change in the refractive index of the FPAE-EP and FPAE(RC25)-EP after being stored at 120 °C. It remains unchanged within 0.10% for over 700 h. Based on TGA and refractive index data, we think that FPAE-EP provides the good thermal stability.

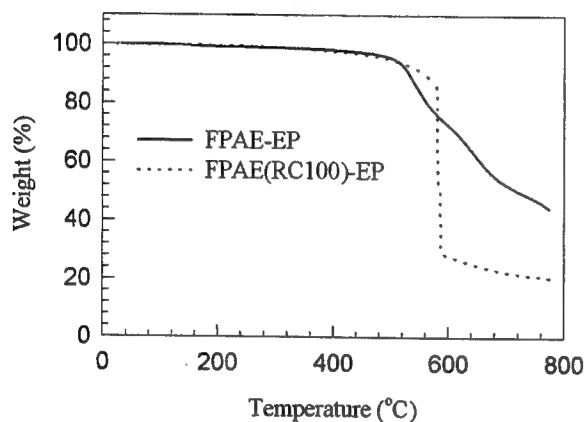


Fig. 3. TGA curve of the polymers.

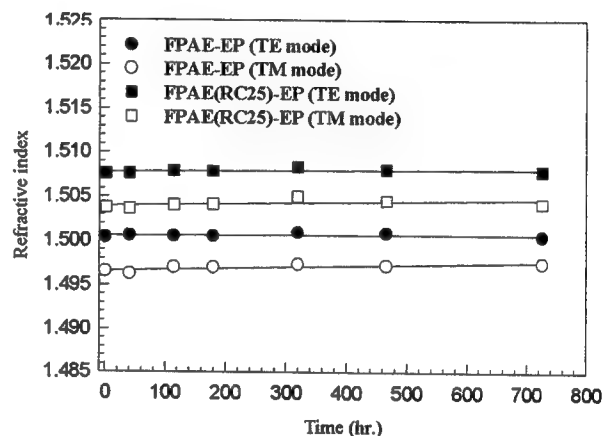


Fig. 4. Refractive index stability at elevated temperature.

For the optical waveguide fabrication, a single-mode channel waveguide was formed by spin coating of cladding/core/cladding and conventional photolithography and O₂ reactive ion etching for lateral confinement. The propagation loss is measured below 0.5 dB/cm at 1.55 μ m wavelength for TE and TM polarization by a cutback method. Using FPAE-EP and their copolymers, optical devices such as a thermo-optic switch, tunable attenuator are fabricated.

References.

1. M. -C. Oh, H. -J. Lee, M. H. Lee, J. -H. Ahn, S. G. Han, and H. G. Kim, *Appl. Phys. Lett.* **73** (18), 2543 (1998).
2. R. Yoshimura, M. Hikita, S. Tomaru, and S. Imamura, *IEEE, J. Lightwave Technol.*, **16** (6), 1030 (1998).
3. M. -C. Oh, H. -J. Lee, M. H. Lee, J. -H. Ahn, and S. G. Han, *IEEE Photon. Technol. Lett.*, **10** (6), 813 (1998).
4. H. -J. Lee, E.-M. Lee, M. H. Lee, M. -C. Oh, J. -H. Ahn, S. G. Han and H. G. Kim, *J. Polym. Sci.: Part A: Polym. Chem.*, **36**, 2881 (1998).
5. H. -J. Lee, M. H. Lee, M. -C. Oh, J. -H. Ahn, and S. G. Han, Accepted to *J. Polym. Sci.: Part A: Polym. Chem.* In press.

Organic Thin Films for Photonics Applications

Second/Third Order Nonlinear Optical Effects: 2

Sunday, 26 September 1999

André Pierre Persoons, University of Leuven, Belgium
Presider

SuD

3:15pm–5:15pm

California Ballroom Salons 4&5

Heterocyclic Liquid Crystals Designed for Organic Light Emitting Diode Applications

Robert J. Twieg, Shihai Gu, Ludmila Sukhomlinova
Chemistry Department, Kent State University
Kent, OH 44242-0001
rtwieg@lci.kent.edu , ph 330 672 2791 fax 330 672 3816

George G. Malliaras, Rong Fan, Dragana Culjkovic,
Department of Materials Science and Engineering, Cornell University
Ithaca, NY 14853-1501
george@msc.cornell.edu , ph 607 255 1956 fax 607 255 2365

Liquid crystals (LCs) represent an important and established area of technology while organic light emitting diodes (OLEDs) represent another important but emerging area of technology. It is of interest to attempt to merge features of liquid crystals and organic light emitting diodes as there appear to be several interesting opportunities to exploit. First of all, the charge mobilities in liquid crystalline materials are among the highest observed in any organic materials and this could lead to devices with low operating voltages. Second, unique function such as the emission of polarized light might be obtained in liquid crystalline OLEDs. And, third, since liquid crystal orientation in thin cells can be influenced by external fields, the opportunity exists to then develop OLEDs with some additional controllable properties.

Recently, polarized electroluminescence from the liquid crystalline oxadiazole derivative 2-[(4'-hexyloxyphenyl)-4-phenyl]-5-(4-hexyloxyphenyl)oxadiazole (HOBP-OXD) has been reported.[1,2] It was found that this molecule forms crystalline films at room temperature but at elevated temperatures it exhibits an unidentified smectic S_x mesophase characterized by very efficient electron transport with a drift mobility that approaches $10^{-3} \text{ cm}^2/\text{Vsec}$. Devices that had polarized EL emission were fabricated by sandwiching a $2\mu\text{m}$ thick HOBP-OXD film between two glass plates covered with the appropriate electrodes that were specially coated for alignment.

Here we report on the synthesis and mesogenic properties of liquid crystals containing one or two oxadiazole heterocyclic rings. This general class of materials is synthesized by very simple and well established routes. For example, in our preparation of HOBP-OXD (Fig. 1), the liquid crystal M18 (4-hexyloxy-4'-cyanobiphenyl) is treated with sodium azide to convert the nitrile group to a tetrazole intermediate that is subsequently reacted with 4-hexyloxybenzoyl chloride. The physical properties of the compound (K_1 116.3 K_2 125.3 K_3 127.4 S_A 170.1 N 180.3 I) we have prepared by this route differ somewhat from those reported previously. [1,2] We have now prepared numerous analogues of this substance and the detailed synthesis and structure-property relationships will be discussed.

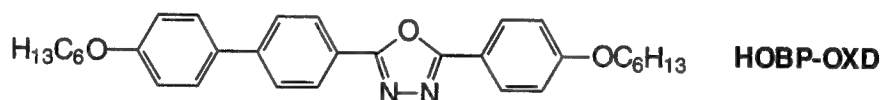


Fig. 1. An oxadiazole based liquid crystal, lumiphore and charge transporting molecule

We also report here on the fabrication and properties of single and bilayer devices based on HOBP-OXD which operate at room temperature. Since at ambient temperature HOBP-OXD is crystalline, thin devices can be fabricated by vacuum deposition of the organic layer(s) and the top electrodes just as in the case of other small molecule based organic light emitting diodes. Presently, the primary goal of our study is to characterize this mesogenic molecule in a standard crystalline device configuration, allowing comparison with other materials used in OLEDs. Subsequently, characterization of this molecule and its analogues in its liquid crystalline state will follow including results obtained in diodes where the HOBP-OXD is aligned by mechanically rubbing or other surface treatment to induce molecular orientation.

Light emission has been obtained from a variety of device configurations. Single layer devices were characterized by bad rectification and low currents indicative of poor transport

properties at room temperature. Better performance was achieved in devices built with TPD heterojunctions. For example, Fig. 2 shows the output of a 30 nm thick device biased at 22V with a maximum quantum efficiency of 0.02%. Deep-blue light was initially emitted, but in time it changed to white blue. The main peak at 400nm corresponds to emission from both the oxadiazole and TPD, while the broad peak centered at 500nm is characteristic of exciplex formation as is observed in other oxadiazole containing devices. The exciplex emission grows in time at the expense of the 400nm emission, decreasing the overall quantum efficiency.

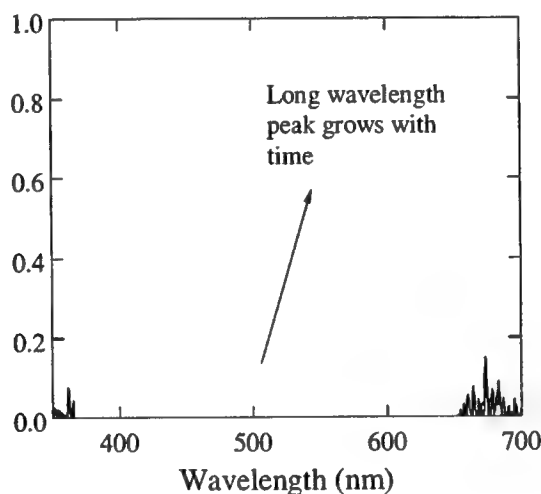


Fig. 2. Temporal evolution of the electroluminescence spectrum of a multi-layer TPD / HOBP-OXD diode (vertical scale in arbitrary intensity units)

Efforts on enhancing the multifunctional performance of the oxadiazole liquid crystals, especially the mesogenic range and fluorescence efficiency, and additional modifications of the overall device configurations are underway.

References:

- [1] H. Tokuhisa, M. Era, T. Tsutsui, *Adv. Mat.* **10**, 404 (1998).
- [2] H. Tokuhisa, M. Era, T. Tsutsui, *Appl. Phys. Lett.* **72**, 2639 (1998).

Monte Carlo Modeling Method for Light Transport in Organic Thin Film Light-Emitting Devices

Aldo Badano and Jerzy Kanicki

*Center for Integrated Microsystems, University of Michigan
2360 Bonisteel Blvd., Ann Arbor, MI 48109*

badano@umich.edu, kanicki@eecs.umich.edu

1. Introduction

Optical design of organic light-emitting devices (OLEDs) has been the focus of recent interest. In this work, we use a Monte Carlo simulation code (DETECT-II [1]) to study the effect of light transport processes on the optical performance of OLEDs. Monte Carlo methods track a large number of optical photons to describe the statistically averaged output. A unique advantage of this simulation method based on geometrical optics [2] is its ability to model absorption events, thin-film coatings and rough surfaces while keeping track of the photon polarization state [3].

Previously, we reported on the luminance spread functions of thin emissive displays showing that increased absorption in thin layers yield low veiling glare structures [4]. In this paper, we use DETECT-II to examine the effect of the optical properties of materials and surfaces on OLED optical performance.

2. Light transport Monte Carlo method

The current version of the simulation code models optically isotropic materials using a geometrical optics approach. At the optical boundaries, an analysis is performed depending on the surface type and material properties, using Fresnel's equations considering the polarization of the incoming photon. Light paths are assumed to apply to one single quanta (light photon). The reflection and transmission coefficients are therefore interpreted as probabilities. Naturally to Monte Carlo methods, bulk absorption in the structure materials is modeled with a linear coefficient.

To describe scattering events at rough surfaces we use an algorithm that randomly perturbs the surface normal within a solid angle that is associated with undulating profiles with low aspect ratio. The roughness is specified by defining a maximum cone within which surface normal tilting can occur. Current models for bulk absorption, refractive indices, and thin-film coatings include wavelength dependencies. For each photon history, a wavelength is selected. Photon sources can be mono-energetic, have a uniform wavelength distribution across the visible range, or be defined by a table corresponding to a specific spectral shape.

3. OLED structures studied

Two distinct OLED concepts were modeled using DETECT-II. The first structure is a typical OLED deposited on a transparent substrate pre-coated with a transparent conductive Indium Tin oxide (ITO) with a thickness of 200 nm, modeled as thin-film coating. The top electrode is a metallic reflective coating (i.e., Al alloy). We used a substrate thickness of 1 mm and a 200 nm-thick transparent organic layer for both structures. In the second structure, the top electrode consists of a transparent conductive oxide layer. An absorptive substrate constitutes the outer top layer. All simulations were performed for devices having a size of 1.0×1.0 cm.

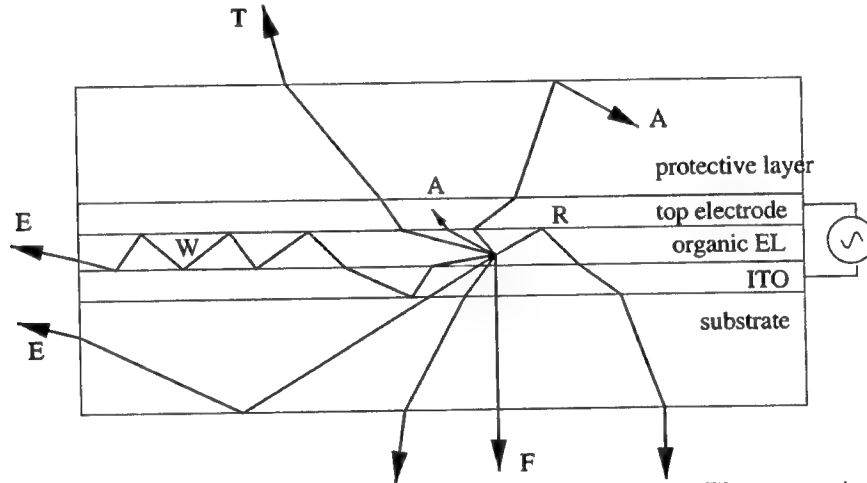


Figure 1. Typical OLED structure modeled in this work. The arrows indicate possible photon path directions. Key individual photon outcomes are depicted: absorption (A), reflection (R), light piping (P), emission through the front (F), top (T) or edge (E) surfaces.

4. Preliminary results

In this section, we present preliminary computational results on photon extraction efficiency and device diffuse reflectance for structures with varying absorption and surface roughness at the top electrode.

4.1 Photon extraction efficiency

From the isotropic emission at the luminescent center until the photons emerge, multiple scattering events take place within the OLED structure. It is traditionally understood that the external quantum efficiency (η_E) is dependent on carrier recombination efficiency (η_C) and photo-luminescent fraction (η_{PL}) [5]. However, the device external efficiency is better expressed as $\eta_E = \eta_C \eta_{PL} \eta_{PE}$, where η_{PE} is the photon extraction efficiency computed as the probability that a photon generated at the luminescent center would emerge through the front surface of the device. The value of η_{PE} depends strongly on the geometry of the stack, and on material and surface properties, and is always less than unity due to absorption, light piping and emissions through the edges and top surface.

According to our preliminary results, the roughness of the reflective coating seems to play a dominant role on the value of η_{PE} . An increase by a factor of 2 was predicted for coatings having more than 80% reflectivity, while a factor of 1.5 is obtained for a transparent electrode. The absorption in the top substrate when the electrode consists of a transparent thin film has no significant effect on η_{PE} .

4.2 Reflectance

To simulate device reflections, we use the same geometric descriptions used for efficiency calculations. In this case, a uniformly distributed planar isotropic light source with a uniform energy distribution in the visible range is placed outside the emissive structure in proximity to the display faceplate. Photons are binned within a small solid angle representative of the acceptance cone of the human eye. The ratio of the number of binned photons to the total number of histories is then associated with a diffuse reflection coefficient R_D , which has units of sr^{-1} . The simulation shows that decreasing the transmission at the metallic coating results in a linear increase of R_D . Improvements of 20 are predicted.

5. Summary

We have modeled the light transport processes that take place in multi-layered organic thin-film light-emitting devices using the Monte Carlo method. We show that optical design of the device structure and layers is essential to obtain high-efficiency devices. Moreover, the simulations can be used to investigate the performance of new device structures before their fabrication. Performance improvements of 2 for η_{PE} and 20 for R_D have been predicted.

References

- [1] A. Badano. *Image quality degradation by light scattering processes in high performance display devices for medical imaging*. PhD thesis, University of Michigan, 1999.
- [2] M. Born and E. Wolf. *Principles of optics*. Pergamon Press, 3rd. revised edition, 1965.
- [3] A. Badano and M. J. Flynn. Monte Carlo modeling of glare in cathode-ray tubes for medical imaging. *Proceedings of the Society for Information Display*, pages 495–498, 1998.
- [4] A. Badano and M. J. Flynn. Monte Carlo modeling of the luminance spread function in flat panel displays. *International Display Research Conference*, pages 382–385, 1997.
- [5] C. W. Tang and S. A. VanSlyke. Organic electroluminescent diodes. *Applied Physics Letters*, 51(12):913–915, September 1987.

Spectroscopy of the Instantaneous All-Optical Switching Nonlinearity of Thin Films

F.P. Strohkendl, R.J. Larsen, and L. R. Dalton
Department of Chemistry, University of Southern California, CA 90089-1062

Z.K. Kafafi
Naval Research Laboratory, Optical Sciences Division, Washington, DC 20375

Introduction

The third-order nonlinear optical susceptibility provides mechanisms for all-optical switching with potential for self-routing data packets in all-optical networks. Switching can be achieved through self-phase or cross-phase modulation and possibly frequency shifting, all of which can be related to the nonlinear refractive index n_2 . Here n_2 is defined such that a beam of intensity I will experience a change in refractive index Δn of the form

$$\Delta n = n_2 I. \quad (1)$$

The nonlinear refractive index may have contributions from mechanisms such as heating, nuclear alignment, distortion of the electronic wavefunction etc. All of these mechanisms have their own characteristic relaxation times. The fastest, and therefore the most interesting, mechanism for switching, is based on the distortion of the electronic wavefunction. Its relaxation time in solids is on the order of a few optical cycles and we refer to it as the "instantaneous" electronic nonlinearity. It is this fast "all-optical switching nonlinearity" and its dependence on the underlying electronic transitions which we are exploring here.

Our analysis is based on the third-order nonlinear optical susceptibility tensor $\chi^{(3)}$. It has four frequency arguments, $\chi^{(3)} = \chi^{(3)}(-\omega_4, \omega_3, \omega_2, \omega_1)$ of which ω_1, ω_2 , and ω_3 are frequencies of "input fields" and $\omega_4 = \omega_3 + \omega_2 + \omega_1$ is the frequency of the generated "output field." The nonlinear refractive index in $\text{erg}^{-1} \text{s cm}^2$ is related to the $\chi^{(3)}$ measured by degenerate four-wave mixing (DFWM) through

$$n_2 = \frac{48\pi^2}{n_0^2 c} \text{Re}[\chi_{1111}(-\omega, \omega, \omega, -\omega)] \quad (2)$$

where c is the speed of light in vacuum, and n_0 the linear refractive index. Fused silica, our reference standard, has a nonresonant χ_{1111} value of 3.95×10^{-14} esu [1,2].

The $\chi^{(3)}$ measured by DFWM exhibits one- and two-photon resonances. These resonances determine the all-optical switching behavior of a material at any wavelength. An understanding of these resonances may lead to molecular structure-property relationships for improved switching performance. Although DFWM is naturally related to all-optical switching, see Eq. (2), one finds that signals observed with long pulses often have large but slow nonelectronic components which overpower the instantaneous component. Experience has shown that experiments with 100 fs pulses, away from the linear absorption edge, measure the instantaneous $\chi^{(3)}$ while picosecond or longer pulses tend to show appreciable nonelectronic contributions [3, 4]. Close to the linear absorption edge even fs DFWM fails to measure the instantaneous electronic response, as we will show.

Here we implement nearly degenerate four-wave mixing (NDFWM) which measures $\chi^{(3)}[-(\omega-\Delta), \omega, \omega, -(\omega+\Delta)]$. Typically our frequency shift Δ is 0.1 eV which is smaller than typical absorption linewidths in thin films, but is large enough to suppress gratings based on sample excitation. Therefore, the nearly degenerate experiment measures in good approximation the instantaneous part of the DFWM $\chi^{(3)}$:

$$\chi_{\text{instantaneous}}^{(3)}(-\omega, \omega, \omega, -\omega) \cong \chi^{(3)}[-(\omega-\Delta), \omega, \omega, -(\omega+\Delta)]. \quad (3)$$

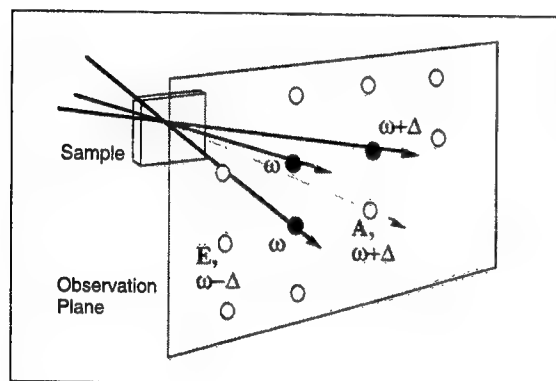


Fig.1: Beam geometry for nearly degenerate four-wave mixing in thin-film sample. Input beams (●) and signal beams (○) and their frequencies are indicated.

Experiment

Our four-wave mixing geometry is shown in Fig. 1. Three copropagating incident beams intersect inside a thin-film sample. All beams have the same linear polarization. Due to the third-order nonlinear interaction nine signal beams emerge. Beam A is the phase-matched signal beam which contains substrate and thin-film contributions [2]. All other signal beams are generated by the thin film with negligible substrate contributions due to phase-mismatch[2]. Here we use beam A to measure a reference signal in fused silica and beam E to measure the thin-film signal.

We have modified a travelling wave optical parametric amplifier which is pumped by 400 nm, 100 fs pulses to yield a double pulse where the first pulse is red shifted relative to the second. The pulses are 3 to 4 times transform-limited with spectral contents that would support a transform limited pulse duration of about 50 fs. The temporal pulse separation is on the order of 1 to 2 ps and the spectral separation is about 4 pulse line-widths. Further details on this device will be reported elsewhere. The double pulse is injected into the four-wave mixing set-up of Fig. 1. Through relative delay of the three input beams degenerate and nondegenerate signals can be generated. If we nominally call the first of the double pulses yellow and the second green, then nominal signal beam colors of blue, green, yellow, and red can be generated. The blue and red signals are only due to the instantaneous electronic response. We measured red signals in beam E, see Fig. 1.

Results

We have tested our method using C60 films for which a number of DFWM data exists. Data sets taken previously with ~1 ps [4] and 100 femtosecond pulses [3,5] are shown in Fig. 2. We also show three new NDFWM data points in the wavelength range 0.55 to 0.7 μm and a new DFWM point at 0.69 μm. The absorption at 0.55 μm is 14400 cm⁻¹ and ~1000 cm⁻¹ at 0.69 μm. The picosecond results give by far the highest χ_{1111} values, two orders of magnitude higher than the NDFWM data, due to strong sample excitation. Even the femtosecond result at 0.63 μm is a factor 15 above the NDFWM

result. We recorded a DFWM signal at 0.69 μm shown in Fig. 3. This signal seems to have an only moderate tail but yields a χ_{1111} value 5 times above the NDFWM result, see Fig. 2. The femtosecond DFWM data set which starts at 0.74 μm and extends towards longer wavelengths did *not* show any signal tails [3]. It was therefore assumed to reflect the instantaneous electronic response and was used to locate the lowest lying two-photon resonance of C_{60} , see Fig. 2. The smooth transition from these DFWM data to the new NDFWM data validates the assumptions made.

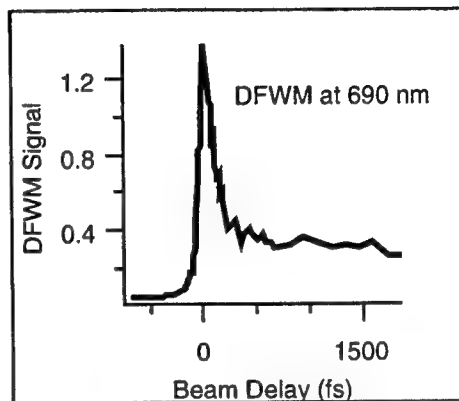
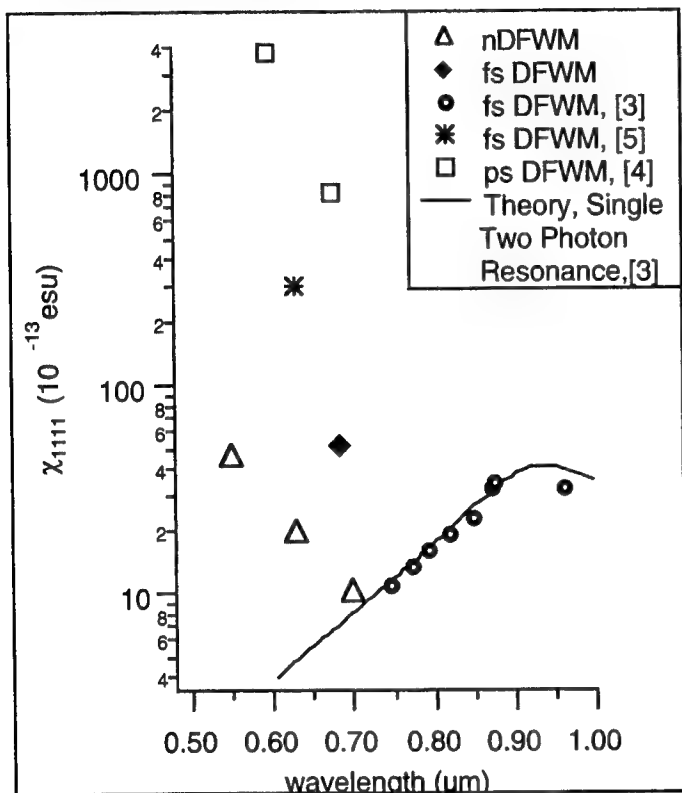


Fig. 3: Example of a DFWM signal which is unrelated to instantaneous electronic response. Measurement is shown as \blacklozenge in Fig. 2.

Fig. 2: χ_{1111} vs. wavelength. DFWM and NDFWM data with fs and ps pulses are shown.

Conclusion

We have demonstrated tunable femtosecond NDFWM and its ability to measure the instantaneous electronic response under resonant conditions. The instantaneous all-optical switching properties of materials are fully determined by their one- and two-photon resonances. Spectroscopy with NDFWM explores exactly these resonances and is therefore uniquely suited to establish all-optical-switching specific molecular structure-property relationships. Our present measurements were limited by sample absorption. The tuning range down to 0.45 μm of our present set-up may be explored with thinner samples and other sample systems in the future.

References

- [1] We follow the convention of Maker and Terhune for $\chi^{(3)}$: D. Maker and R. W. Terhune, Phys. Rev. **137**, A801 (1965).
- [2] F. P. Strohkendl, L. R. Dalton, R. W. Hellwarth, H. W. Sarkas and Z. H. Kafafi, J. Opt. Soc. Am. B **14**, 92 (1997);
- [3] F. P. Strohkendl, T. J. Axenson, R. J. Larsen, L. R. Dalton, R. W. Hellwarth, and Z. H. Kafafi, J. Phys. Chem. **101**, 8802 (1997).
- [4] S. R. Flom, R. G. S. Pong, F. J. Bartoli, and Z. H. Kafafi, Phys. Rev. B **46**, 15598 (1992).
- [5] M. J. Rosker, H. O. Marcy, and T. Y. Chang, Chem. Phys. Lett. **196**, 427 (1992).

Nonlinear Optical Properties of Phthalocyanine Aggregates

James S. Shirk, Steven R. Flom, Richard G.S. Pong, Dawn D. Dominguez, and Arthur W. Snow

Naval Research Laboratory, Washington DC 20375

shirk@nrl.navy.mil, flom @nrl.navy.mil, pong@sisyphus.nrl.navy.mil, snow@ccf.nrl.navy.mil

Heino Heckmann and Michael Hanack

Institut für Organische Chemie, Eberhard-Karls-Universität, D-72076 Tübingen, Germany

The phthalocyanines and naphthalocyanines can form ordered, stacked structures in thin films and in solutions at high concentrations. An illustration of these stacks is shown in Figure 1. In solution, the extent of the stacking is controlled by the concentration and the nature of the substituents, in films it may also depend on the deposition conditions and the substrate. Sometimes, the order is sufficient that liquid crystalline states have been identified. The size and structure of these aggregates determines the magnitude

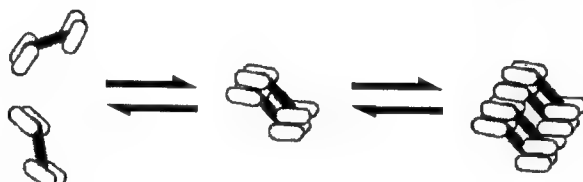


Figure 1. Supramolecular stacks in substituted phthalocyanine nonlinear optical materials

of the intermolecular couplings and hence the electronic states and their relaxation dynamics. For this reason, the nature of the intermolecular structure can have a substantial influence on the nonlinear optical properties of these materials.

Here we discuss the influence of the molecular structure on some concentration dependent effects that are crucial in determining the nonlinear absorption coefficient, α_{NL} . Large values of this coefficient are important in materials used for optical limiting. The formation of aggregates can introduce new relaxation pathways that deplete the excited state. These reduce the magnitude of nonlinear processes derived from populating an excited state. For example, it can reduce the nonlinear absorption in reverse saturable absorbing molecules that are useful in optical limiting.

Stacked structures have been identified in some cumylphenoxy substituted phthalocyanine materials. From the concentration dependence of the spectra we can identify the spectra of the monomers and dimers of $H_2Pc(\beta-CP)_4$ as shown in Figure 2. The dimer spectrum is broader and shifted to the blue

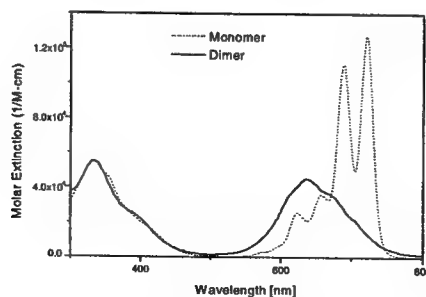


Figure 2 Spectra of monomers and dimers of $H_2Pc(\beta-CP)_4$

from the monomer. The intermolecular interactions responsible for these spectral shifts influence the relaxation rates of these materials. The upper state relaxation time of $\text{H}_2\text{Pc}(\beta\text{-CP})_4$ is shortened substantially by the formation of dimers and even more with higher aggregates. The concentration

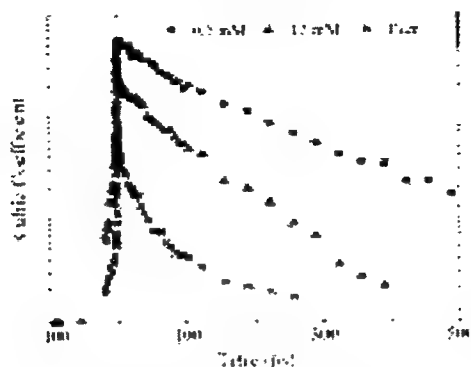


Figure 3 Time dependence of the degenerate four-wave mixing signal at different concentrations

dependence of the four-wave mixing signal for $\text{H}_2\text{Pc}(\beta\text{-CP})_4$ are shown in Figure 3. The decay of the signal is faster in more concentrated solutions. The decay times can be correlated with the aggregation to dimers and higher n-mers.

In the lead substituted $\text{PbPc}(\beta\text{-CP})_4$ evidence for higher order processes is seen at concentrations where dimers form. Figure 4 shows a series of open aperture Z-scans with increasing energy at a concentration where dimers are the predominant species in solution. These were recorded at 625 nm where the ground state absorption cross section is slightly larger than that of the first excited state.

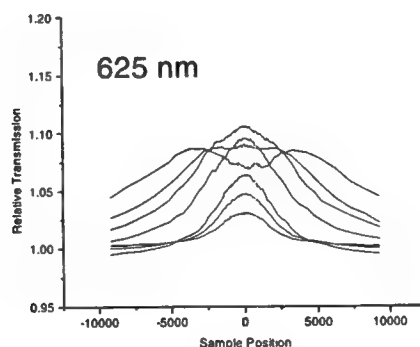


Figure 4. Open aperture Z-Scans at increasing incident fluences of a 20 mM solution of $\text{PbPc}(\beta\text{-CP})_4$ at 625 nm.

The progression of the data from strict saturable absorption at low excitation fluences to competing saturable and reverse saturable absorption at higher excitation fluences shows clearly a higher order process. At lower concentrations, this higher order process is not observed. This new process in dimers is assigned to strongly absorbing multiphoton states. These new states can enhance the nonlinear absorption at all visible wavelengths. The large dynamic range of concentration optimized optical limiters made from $\text{PbPc}(\beta\text{-CP})_4$ solutions is due to the presence of these states.

The new excited states in $\text{PbPc}(\beta\text{-CP})_4$ dimers mean that the nonlinear absorption coefficient increases with concentration, at least initially. In contrast, in materials where these higher excited states are not observed, e.g., $\text{H}_2\text{Pc}(\beta\text{-CP})_4$, the nonlinear absorption coefficient and consequently the optical limiting performance decreases monotonically with increasing concentration. This decrease is directly attributable in the observed decrease in the excited state lifetime.

To achieve the largest nonlinear absorption coefficients and increase the range before the nonlinearity saturates, we synthesized some materials where the molecular structure restricts the intermolecular aggregation to no more than dimers. The goal is to find materials that provide lower thresholds and increased dynamic range in optical limiting applications. One approach was an aryl substituted indium phthalocyanine whose structure is shown in Figure 5. The large axial substituent inhibits the formation of extensive stacks. While this material can aggregate to dimers in principle there was little evidence for any aggregation to a concentration of greater than 30 mM. It is possible that the molecular dipoles in these molecules inhibit the formation of dimers.

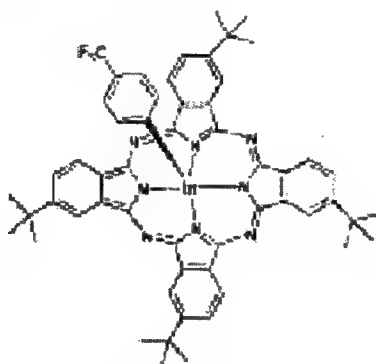


Figure 5 axially substituted Indium Pc's

The nonlinear absorption coefficient of this material was large in the visible due to the strong excited state absorption in the triplet state of the monomer. However, we see no evidence for the higher excited states found in $\text{PbPc}(\beta\text{-CP})_4$ dimers.

The recently synthesized capped phthalocyanine, shown in Figure 6, aggregates to dimers at concentrations of a few millimolar. The polyethylene oxide chains on one side of the molecule act as a barrier to aggregation beyond dimers. DFWM measurements show the lifetime of the first excited state is greater than 2 ns at 18 mM concentration for the metal free material. It is almost an order of magnitude longer than that observed in $\text{H}_2\text{Pc}(\beta\text{-CP})_4$.

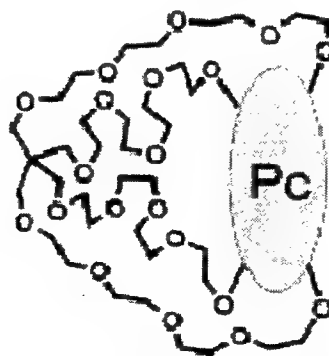


Figure 6 Polyethylene oxide capped Pc.

Nonlinear Optical Response of pTS Near the Band Edge

Steven R. Flom, J.R. Lindle and F.J. Bartoli

Optical Sciences Division, Code 5613, Naval Research Laboratory, Washington, DC 20375-5338
 flom@nrl.navy.mil, lindle@nrl.navy.mil, bartoli@nrl.navy.mil

Mingguo Liu and George I. Stegeman

Center for Research and Education in Optics and Lasers, University of Central Florida, Orlando, FL 32816
 mliu@steglab.creol.ucf.edu, george@mail.creol.ucf.edu

The highly nonlinear optical properties of the polydiacetylene (PDA), poly-[2,4 hexadiyne-1,6 diol-bis (p-toluenesulfonate)] (pTS) have caused it to be extensively investigated^{1, 2, 3, 4}. Here we present measurements of transient absorption, time-resolved degenerate four-wave mixing (DFWM) and nonlinear transmission (NLT) in pTS using picosecond excitation at wavelengths from 709 nm to 744 nm, near the band edge of pTS.

The single crystals of pTS were grown from saturated acetone solutions and thermally polymerized. The spectrum of the absorption coefficient for light polarized parallel to the polymer backbone is shown in Figure 1. The linear absorption in the 700-750 nm region is small but non-negligible. The refractive index ($n_1 = 1.87$ at 2 μm) and the crystal thickness were determined from the interference fringes observed in the absorption spectrum.

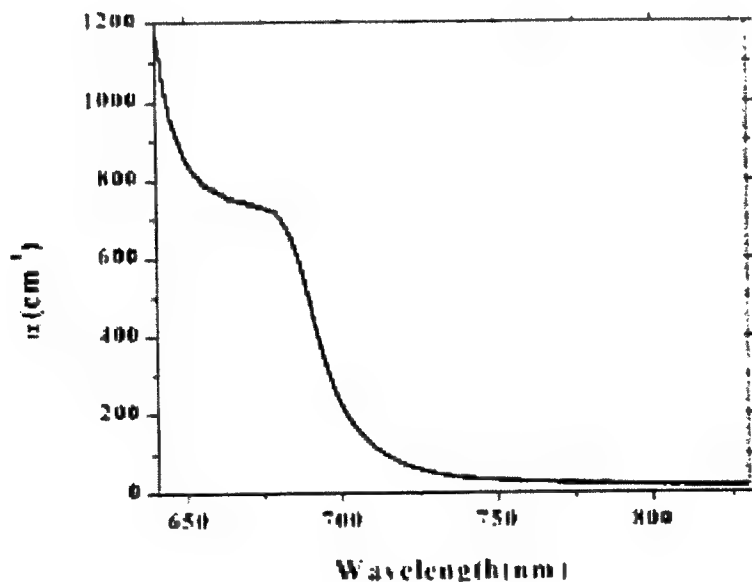


Figure 1 The spectrum of the absorption coefficient of pTS

Parallel-polarized transient absorption measurements were carried out in the near IR using ps pulses both to excite the sample and to generate a white light continuum probe. Figure 2 shows the observed changes in absorption at times within 10 ps of the arrival of the 725.5 nm excitation pulse. The two prominent negative peaks are consistent with stimulated Raman scattering. Their temporal profile and spectral linewidth are the same as those of the laser pulse. The peak shifted from the

excitation frequency by 1501 cm^{-1} exhibits a gain coefficient of 435 cm^{-1} while the peak shifted by 2102 cm^{-1} has a gain coefficient of 227 cm^{-1} . These frequencies are similar to C=C and C≡C Raman frequencies observed in another PDA⁵. Within experimental uncertainty the same stimulated Raman shifts were observed with 743.7 nm excitation.

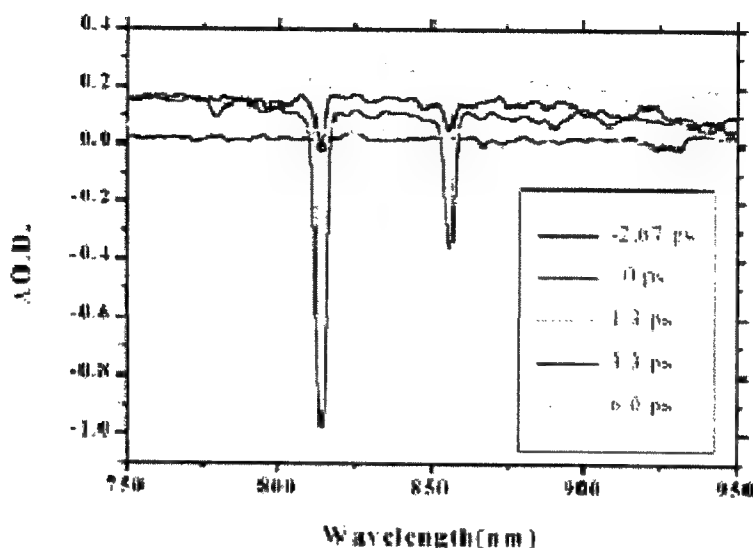


Figure 2 Transient absorption spectra of pTS. Spectra are taken using 5.5 GW/cm^2 excitation at 725.5 nm

The other prominent feature of the data presented in figure 2 is the large, spectrally broad, induced absorption which reaches its maximum value 1.3 ps after the stimulated Raman maximum. Within 6 ps the signal decays to a small residual value that persists to at least a ns. Similar dynamics are observed using DFWM at high intensities. At lower intensities the signal is nearly pulse width limited and decays to zero.

The variation of the NLT over nearly three orders of magnitude in intensity is illustrated

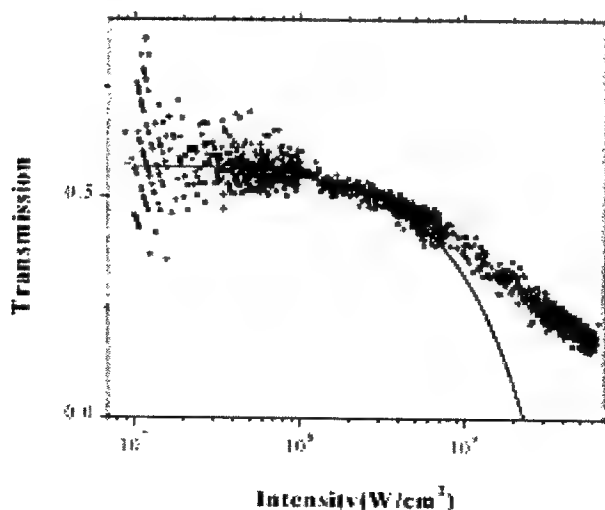


Figure 3 Nonlinear transmission from pTS at 725.5 nm

in figure 3 for 725.5 nm excitation. For comparison, the transient absorption data in figure 2 are taken at 5.5 GW/cm^2 . The variations of the nonlinear transmission with excitation pulse width indicate that the population responsible for the induced absorption arises from two photon excitation. The line drawn in figure 3 corresponds to a calculation of the nonlinear transmission expected using the linear absorption data of Figure 1 and a previously reported nonlinear absorption coefficient. This calculation clearly does not agree well at high intensities. More extensive modeling treating beam propagation through a nonlinear medium involving multiphoton processes and excited state populations will be presented. Effects of stimulated Raman scattering on the nonlinear transmission will be discussed.

The importance of the data presented here is that a substantial population of a short lived excited state is produced by off-resonant excitation of the single pTS crystals. This population contributes to the NLO response over a broad spectral region in the near infrared. Further, this same population may well be responsible for some of the higher order intensity dependence observed for pTS.

References:

1. G.M. Carter, M.K. Thakur, Y.J. Chen and J.V.Hryniewicz, *Appl. Phys. Lett.* **47**, 457 (1985), G.M. Carter, J.V. Hryniewicz, M.K. Thakur, Y.J. Chen and S.E. Meyler *Appl. Phys. Lett.* **49**, 998 (1986).
2. B.I.Greene, J. Orenstein, R.R. Millard and L.R. Williams, *Chem. Phys. Lett.* **139**, 381 (1987), B.I.Greene, J. Orenstein, R.R. Millard and L.R. Williams, *Phys.Rev. Lett.* **58**, 2750 (1987).
3. B. Lawrence, W.E. Torruellas, M. Cha, M.L. Sundheimer, G.I. Stegeman, J. Meth, S. Etemad, and G. Baker, *Phys. Rev. Lett.* **73**, 597 (1994).
4. W.E. Torruellas, B. Lawrence, G.I. Stegeman and G. Baker, *Opt. Lett.* **21**, 1777 (1996).
5. T.A. Pham, A. Daunois, J.-C. Merle, J.Le Moigne and J.-Y. Bigot, *Phys. Rev. Lett.* **74**, 904 (1995).

Mechanism of noncentrosymmetric alignment in spin-coated carbazole polymer films

Hiromi Kimura-Suda and Yadong Zhang

CREST, Japan Science and Technology Corporation (JST),
2-1 Hirosawa, Wako, Saitama 351-0198, Japan
Tel: +81-48-467-9601, Fax: +81-48-462-4695
kimura-suda@hypercrest.riken.go.jp

Takafumi Sassa

FRP, The Institute of Physical and Chemical Research (RIKEN),
2-1 Hirosawa, Wako, Saitama 351-0198, Japan

Tatsuo Wada and Hiroyuki Sasabe

CREST, Japan Science and Technology Corporation (JST),
FRP, The Institute of Physical and Chemical Research (RIKEN),
2-1 Hirosawa, Wako, Saitama 351-0198, Japan

Organic nonlinear optical (NLO) polymers are quite attractive due to their potential applications to integrated electro-optic devices. In order to exhibit second-order NLO responses, the polymeric materials are required to have a noncentrosymmetric arrangement. Electric field poling is commonly used to break the centrosymmetry of polymer films, and is accomplished by applying an electric field above a glass transition temperature (T_g) and cooling down the film in the presence of the field to freeze the chromophore alignment.¹ However, one major problem of poling is the thermal stability of the noncentrosymmetric alignment of chromophore which relaxes partially even below T_g .

Carbazole polymer is well-known to have multifunctional properties including second-order NLO responses. In our laboratory, several types of carbazole polymers, e.g. main-chain type, side-chain type and hyperbranched type, were synthesized to improve their performance for the thermal stability.² In previous work³, we succeeded in the preparation of polar film of carbazole polymers on substrates by flow casting, thermal treatment, and/or spin coating under one-dimensional flow, without electric field. The molecular orientation in polar films showed an in-plane polar anisotropy and parallel to the direction of the centrifugal force, and was stable even at an elevated temperature above T_g . It has been considered that the noncentrosymmetric alignment was achieved by the flow effect or the interfacial interaction between a substrate and the polymer. In this study, we have investigated the mechanism of noncentrosymmetric alignment in the spin-coated carbazole polymer

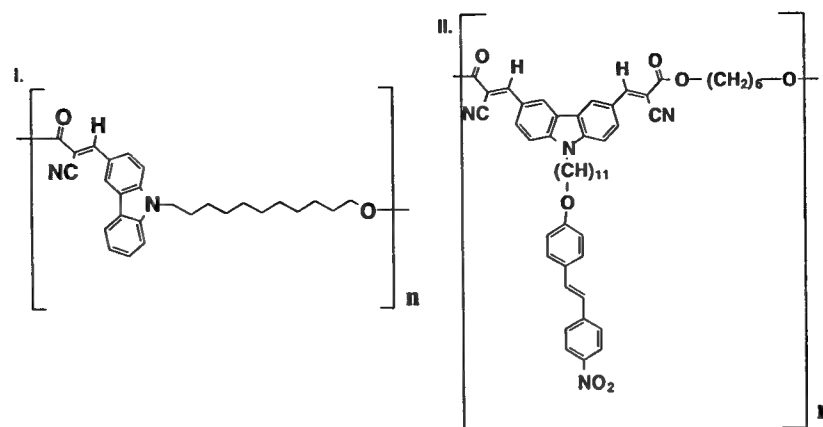


Fig. 1: Structure of carbazole polymers.

to optimize the molecular structure with very large NLO properties and thermal stability.

We used two types of carbazole polymers, a head-to-tail type (polymer I), and main-chain type (polymer II), as shown in Fig.1. Both polymers were dissolved in CHCl_3 , and the thin film was prepared by a spin coating under one-dimensional flow (Fig.2) on the two different types of substrate, e.g. a glass plate and a glass plate modified with silane coupling reagent, in order to check the interfacial interaction between the substrate and polymer chains.

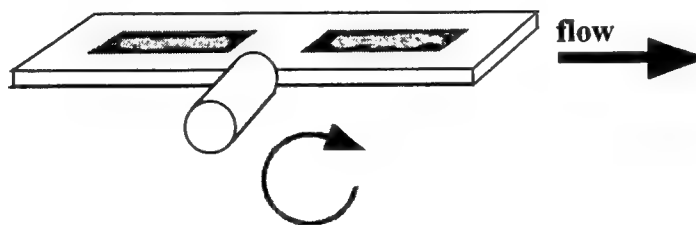


Fig. 2: Spin coating technique under one-dimensional flow.

The second-order coefficients of the films were determined by a rotational Maker fringe method. The fundamental beam was a p-polarized Q-switched Nd:YAG laser (1064 nm) and a p-polarized second-harmonic signal (532 nm) was detected. The absolute orientation of molecules in the spin-coated films were determined by an SHG phase measurement.³⁻⁵ In rotational Maker fringe measurement, SH signals were obtained for all films prepared. It follows that the molecular chains were well aligned due to the centrifugal force and showed an in-plane polar anisotropy.

Table 1: Second-order coefficients (d_{11}) of the spin-coated films.

	Tg (°C)	thickness (μm)	glass plate (pm/V)	modified glass plate (pm/V)
Polymer I	48	0.54	0.05	0.05
Polymer II	87	0.20	0.22	0.22

The second-order coefficients (d_{11}) of the spin-coated films were summarized in Table 1. The results indicated that noncentrosymmetric alignment in the spin-coated film was independent of the surface properties of substrates. Furthermore it was found that the orientation of main-chain was controlled during the spin coating (one-dimensional orientation), because even the spin-coated film of polymer I was aligned in an in-plane polar anisotropy. The spin-coated films were annealed above T_g for 24 hours. Polymer I sample showed undetectable decay of SH intensity, and polymer II showed approximately 10% decay of the initial value. On the other hand, it was found by SHG phase measurement that the absolute molecular orientation in polymer II was kept during annealing. These results indicate that the alignment of the side-chain groups was sustained during annealing. In conclusion, the main-chain alignment under one-dimensional shear flow is quite stable due to the tight chain packing, and it follows the stable side-chain alignment.

Reference

- 1 M. A. Pauley, H. W. Guan, and C. H. Wang, *J. Chem. Phys.*, **104**, 6834 (1996).
- 2 Y. -D. Zhang, L. -M. Wang, T. Wada, and H. Sasabe, *Macromolecules*, **29**, 1569 (1996).
- 3 H. Kimura-Suda, T. Wada, S. -A. Choi, Y. -D. Zhang, and H. Sasabe, *Mol. Cryst. Liq. Cryst.*, to be published.
- 4 K. Kemnitz, K. Bhattacharyya, J. M. Hicks, G. R. Pinto, K. B. Eisenthal, and T. F. Heinz, *Chem. Phys. Lett.*, **131**, 285 (1986).
- 5 H. Kimura-Suda, T. Wada, W. Liang, H. Nakahara, and H. Sasabe, *SPIE proceedings*, **3474**, 68 (1998).

ULTRAFAST NONLINEAR SWITCHING AND LOGIC BASED ON NONLINEAR TUNNELLING OF OPTICAL SOLITONS THROUGH ORGANIC THIN FILMS

V.M. CHAPELA, J. PERCINO and V. N. SERKIN

Benemerita Universidad Autonoma de Puebla, Instituto de Ciencias

Blvd. 14 sur 6303, Ciudad Universitaria, Puebla, Pue., Mexico

tel: 52 (22) 45 62 07, fax: 52 (22) 32 60 67

e-mail address: vserkin@hotmail.com

T. L. BELYAEVA

Lomonosov Moscow State University, Russia

Ultrafast all-optical switches and logic gates devices, to-day, are seriously considered for future applications for serial processing, to local and metropolitan area networks, computer systems for clock synchronization and communication between memory and processors, high-bit rate telecommunication applications and all-optical random-access memory for supercomputing. Ultrafast switching and logic means speeds greater than electronic systems may reach. It is well known that electronics logic and switching systems can operate at maximum speeds limited by 20-50 GHz because of fundamental considerations such as transit, relaxation and thermal diffusion times [1,2]. VLSI-like electronics as follows from [2] may be limited above 35 GHz. One of the main ideas to overcoming the electronics bottleneck is to use a terabit-rate logic systems based on optical soliton-dragging logic gates [3]. Soliton logic gates include soliton dragging, soliton trapping and billiard-ball soliton interaction gates. As was shown in previous works, soliton-dragging logic gates satisfy all requirements for a digital optical processor, including fan-out, cascability and Boolean completeness. And as follows from detailed analysis of M. N. Islam [3], today solitons are practically "natural" data bits.

Various types of optical switching devices have recently been proposed, based on the propagation and interaction of bright as well as dark temporal and spatial solitons. In this report we present a novel method of optical switching, based on the effect of nonlinear soliton tunnelling through strong nonlinear organic thin films. Recently G.Stegeman and co-authors [4-6] reported a large nonresonant nonlinearity in polydiacetylene *para*-

toluene sulfonate (PTS) at 1600 nm that should yield 1D spatial solitons at a power of $P_s = 12W$, 40 times lower than in semiconductors and 30,000 times lower than in glass or CS_2 . Today PTS is the first solid-state material to show a strong cubic response with an observable quintic nonlinearity.

The concept of linear tunnelling follows naturally from the linear wave equation.

$$u_{tt} - (c^2(x)u_x)_x + n^2(x)u = 0$$

Seeking solutions of the form $u(x, t) = \psi(x) \exp(-i\omega t)$, we obtain the Sturm-Liouville problem which is the ordinary Schrodinger equation with potential $n^2(x)$. The concept of nonlinear tunnelling follows from the nonlinear wave equation

$$u_{tt} - (c^2(x)u_x)_x + n^2(x) \sin(u) = 0$$

that leads to a nonlinear dispersion relation between k and ω .

The propagation of a soliton pulse towards a finite potential barrier was examined at the first time by Alan C. Newell [7] and it was found that in certain circumstances, depending on the ratio of soliton amplitude to barrier height, the soliton can tunnel through the barrier in a lossless manner.

The question we should like to discuss in this report is, what happens if the intensity of the input soliton is larger than the intensity of fundamental soliton tunnelling without losses? We predict the possibility of more than one soliton generation in tunnelling of powerful soliton through nonlinear barrier. In addition to

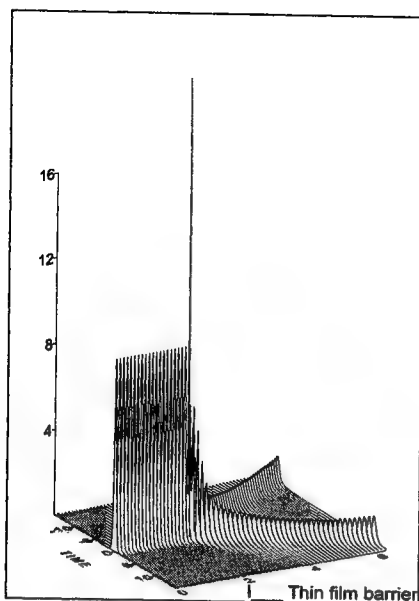


Figure 1 -

the Newell's tunnelling scenario with potential barrier $n^2(x)$ [7], we consider the nonlinear potential barrier depending on as coordinate and intensity of input soliton.

We show that the process of nonlinear tunnelling of optical soliton through strong intensity dependent barrier exhibits jump-like (nonadiabatical) evolution which eventually leads to the new solitons forming with different group velocities and frequencies, so called colored solitons (see Fig.1 and Fig.2). The model for the propagation of temporal or spatial solitons is the standard nonlinear Schrodinger (NLS) equation [8-11]. The high energy soliton dynamics in a thin strong nonlinear organic film can be described by the modified NLS equation which includes a nonlinear two-photon absorption term and a saturation nonlinear term.

Numerical simulations show that combine action of high-order nonlinearity and two-photon absorption leads to splitting of input soliton. Figure 1 shows the typical soliton evolution in process of tunnelling through the thin film. After the tunnelling two solitons formed with different frequencies. To get a deeper physical insight into this phenomenon, we numerically calculate the parameters of solitons formed, using the Zakharov-Shabat eigenvalue problem. Figures 3 and 4 show the dynamics of soliton profile and spectrum in the barrier region. This is the spectral range of positive group velocity dispersion forbidden for soliton propagation and due to the strong self-modulation effect the spectrum broadens up to one or two orders. It is this effect that causes new colored soliton formation (see Fig. 2). If the intensity of

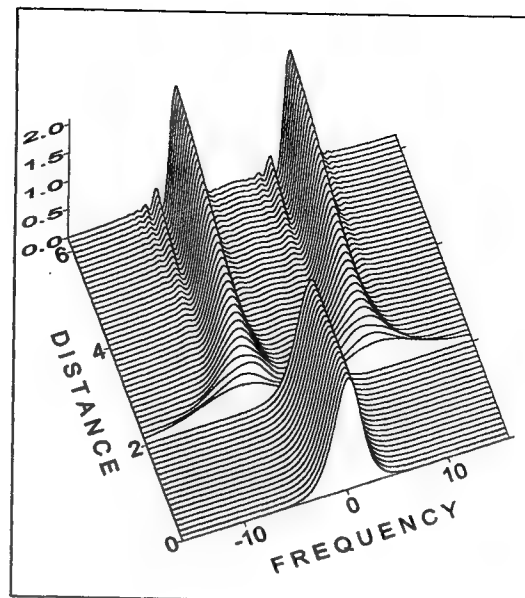
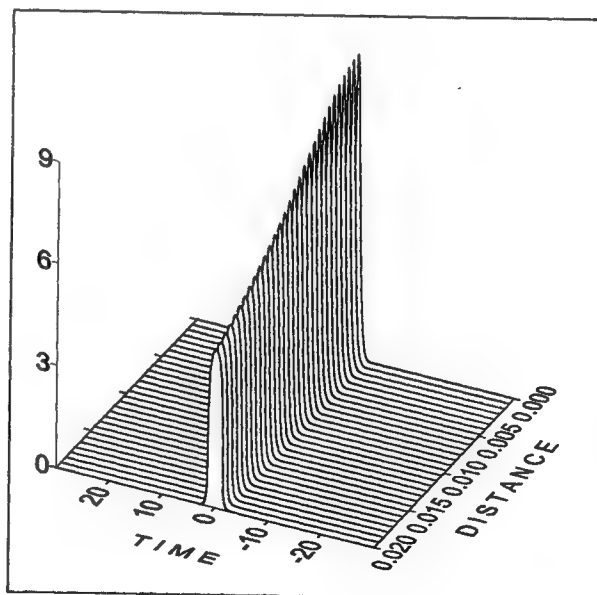


Figure 2 -

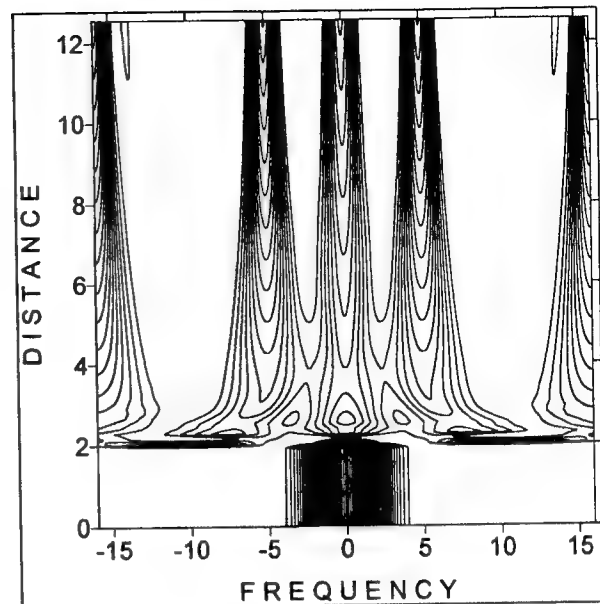
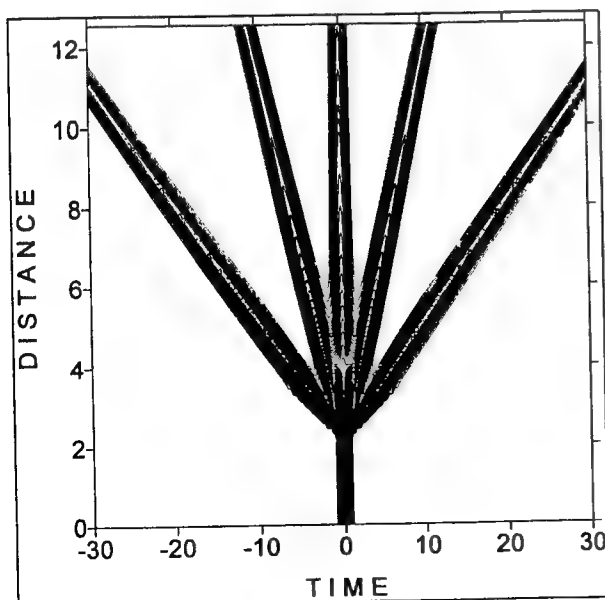
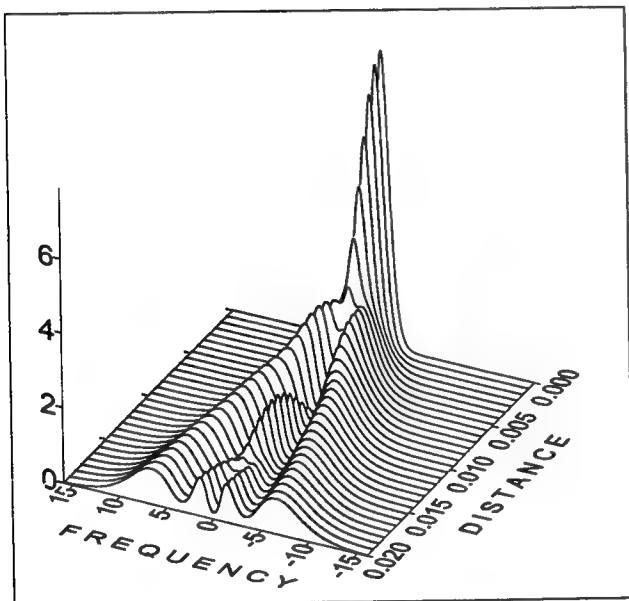
input soliton increases the number of solitons formed due to the process of nonlinear tunnelling also increases (see Fig. 5,6).



Different "reaction like" ultrafast switching processes are shown on Fig.1 and Fig. 5. There are several reasons why the "nonlinear optical reactions" calculated are particularly advantageous for tera-bit-rate switching and logic elements. First, the particle-like features of ultrafast pulses formed during "nonlinear reaction" can lead to very stable, low-energy switching. Second, terabit-

rate all-optical logic gates can operate due to several predicted properties of new solitons created, including modulation instability, elastic and non-elastic collisions, soliton dragging, tunnelling and trapping effects.

Finally, it seems very attractive to use the nonlinear soliton tunnelling effects predicted in developing a whole class of basically novel soliton logical devices. The most attractive medium to realize nonlinear reaction-like ultrafast soliton logic based on soliton tunnelling effect today is PTS thin films [4-6].



1 REFERENCES

- 1.D.A.B.Miller. SPIE, CR35, 68, 1990.
- 2.P.W.Smith, Bell System Tech. Jour., 61, 1975, 1982.
- 3.M.N.Islam, Ultrafast fiber switching devices and systems, Cambridge University Press, 1992.
- 4.G.I. Stegeman. Applications of Organic Materials in Third-Order Nonlinear Optics, CRC Press, Inc., p.799, 1997.
5. B. Lawrence, W.E. Torruellas, M. Cha, M.L. Sundheimer, G.I. Stegeman, J. Meth, S. Etemad and G. Baker, Phys. Rev. Lett., v.73, pp.597-600, 1994.
6. B.L. Lawrence and G.I. Stegeman, Opt. Lett., v. 23, pp. 591-593, 1998.
- 7.Alan C. Newell, J. Math. Phys., v. 19 (5), pp.1126-1133, 1978.
- 8.Akira Hasegawa. *Optical Solitons*, Springer, 1989.
- 9.E.M. Dianov, P.V. Mamyshev, A.M. Prokhorov, V.N. Serkin, *Nonlinear Effects in Optical Fibers*, Harwood Academic Publishers, 1989.
- 10.Govind P. Agrawal. *Nonlinear Fiber Optics*, Academic Press. Inc., 1995.
- 11.E.M. Dianov, A.B. Grudinin, A.M.Prokhorov, V.N. Serkin. *Optical solitons - theory and experiment*, ed. by J.R.Taylor, Cambridge Univ. Press, pp.197-265, 1992.

Fully atomistic modeling of a poled nonlinear optical polymer

L. Michael Hayden and Won-Kook Kim

Department of Physics, University of Maryland Baltimore County, Baltimore, MD 21250
hayden@umbc.edu, wkim@lancair.umbc.edu

The development of NLO polymer materials with simultaneous high nonlinearity and good thermal stability is the major impediment to marketing devices based on these materials. Understanding the physical mechanisms of chromophore orientation and/or re-orientation and the static properties of NLO polymers is essential to developing systems with high nonlinearity and excellent long term stability. α -type relaxation associated with the glass transition has been proposed as the mechanism responsible for chromophore re-orientation near and above T_g .¹ More recently, the influence of β -type relaxations on chromophore re-orientation in systems below T_g has been reported.² However, no conclusive evidence has been provided to elucidate the chromophore re-orientation mechanism at the molecular level.

Molecular modeling, using an empirically derived set of equations to describe the energy of a system as a function of atomic coordinates, has been applied to study the equilibrium properties as well as the kinetic physical properties for various polymer systems for a decade. Force field calculations such as these are required when the system size is too big to employ quantum mechanical calculations. From the detailed configurational coordinates, equilibrium properties such as free volume distribution,³ and time dependent properties such as polymer local dynamics⁴ and small molecule diffusion⁵ have been studied for several polymer systems. However, until now, no fully atomistic molecular dynamics have been employed to study the chromophore orientation mechanism in NLO polymers. Chromophore orientation under laboratory conditions, i.e., under moderate electric fields and temperatures, takes longer than nanoseconds to reach saturation, especially near or below T_g . This relatively long time scale can be a major handicap in utilizing molecular modeling, since simulation times longer than a few nanoseconds are not feasible with present computational power. This difficulty can be relieved somewhat by introducing considerably larger electric fields and temperature to the system.⁶

In this work, we used molecular modeling to investigate the static conformational properties, radial distribution functions, and energetics in poled and unpoled systems of poly(methylmethacrylate) (PMMA) doped with the NLO chromophore *N,N*-dimethyl-*p*-nitroaniline (DPNA). In addition, we studied the chromophore orientation process under the influence of an applied electric field. Eight independent molecular models of PMMA/DPNA at two different densities (HD and LD) were constructed and exposed to various electric fields. The higher density (HD) system corresponded to a sub- T_g state while the lower density (LD) system was above T_g .

The molecular dynamics and molecular mechanics in this study were performed using the molecular modeling package Discover (4.0.0)⁷ with the CVFF force field. The potential energy in the simulations contains the following terms, $E = E_{bond} + E_{angle} + E_{torsion} + E_{oop} + E_{nonbond} + (E_{field})$ where E_{oop} is the energy term for the out-of-plane interactions, and $E_{nonbond}$ comprises both the non-bonded van der Waals energy (E_{vdw}) and Coulombic (E_{Coul}) terms. E_{field} is the energy associated with the external electric field and was calculated from the summation of the dot products of the coordinates of each particle and the vector component of the product of the charge and the applied field,

$$E_{field} = \sum_{i=1}^n \mathbf{r}_i \cdot (q_i \mathbf{E}), \text{ where } i \text{ is the particle index. The } E_{field} \text{ term is only included in the potential energy}$$

calculation during the poling stage. The electric field was applied in the *z*-direction for the simulation. The charge groups were properly assigned to be neutral for the simulation. A group-based nonbond energy calculation method was employed with 9.5 Å cut-off distance. In the group-based method, all atom pairs in the groups are included in the Coulombic interactions if the distance between the switching atoms of two groups is shorter than 9.5 Å. In this way, artifacts due to the splitting of dipoles can be efficiently prevented.

Each simulation box contained a single atactic (50 : 50 of meso : racemic ratios) PMMA chain with 90 repeat units and two DPNA molecules so that the mass fraction of the DPNA contents was 3 %. Using a Monte-Carlo amorphous cell generation method^{8,9} eight independent initial HD structures were constructed in a cubic box, 23.60 Å on a side, resulting in a system density of 1.18 g/cm³. These initial structures were further relaxed by 100 ps of NVT molecular dynamics (MD) simulation at 500 K, recording the configuration at every ps. The lowest potential energy snapshot was chosen and minimized further using a conjugate gradient method of 500 iterations with 0.1 kcal mol⁻¹ Å⁻¹ as the convergence criteria. At this stage, the potential energy of each isolated system was higher by a few hundred kcal than that of a bulk system, which is evidence that the molecular models were physically acceptable cohesive structures. In these initial structures, the orientations of the dopants were fairly random with the value of $\langle \cos \theta \rangle$ of -0.1. The initial structures of the LD system were obtained by an additional 500 steps of energy minimization on the

unpoled HD static structures with $0.1 \text{ kcal mol}^{-1} \text{ \AA}^{-1}$ convergence in a cubic periodic box, 25.11 \AA on a side. Due to the larger box size, the resulting LD density was 0.98 g/cm^3 .

At 500 K, the HD system density of 1.18 g/cm^3 and the LD system density of 0.98 g/cm^3 correspond to an internal pressure of $\sim 10,000 \text{ atm}$ and $\sim 1 \text{ atm}$, respectively, as verified using NPT dynamics. In other words, the HD and LD densities are the appropriate ones for this force field at 500 K and those two pressures. Furthermore, it is well known experimentally that as pressure is applied to a polymeric system (hence increasing the density), the T_g increases. In fact, in PMMA, the T_g rises $\sim 22^\circ \text{ C}/1000 \text{ atm}$.¹⁰ Therefore, we qualitatively identify our 500 K HD system as a sub- T_g system and the 500 K LD system as one above T_g .

The smaller size of the periodic box in the HD system provides less free space for the atoms to fluctuate and results in a higher internal pressure. For this reason, higher electric fields were needed to pole the chromophores in the HD system. Eight independent structures at each density were poled to attain sound statistics. NVT molecular dynamics were performed for 1.5 ns using a 1 fs time step and the velocity Verlet method.¹¹ The temperature of the system was controlled by a velocity scaling method¹² with temperature windows of 20 K around the target temperature of 500 K. Configurational snapshots were recorded at every ps. The MD calculations were carried out on an SGI Challenge-XL server with 0.248 sec/step of CPU time for the MIPS R10000 processor.

The interaction between the DPNA chromophore and the PMMA matrix can be studied using the radial

distribution function, which is defined as $G_{ab}(r) = \frac{\langle n_{ab}(r) \rangle}{4\pi r^2 \Delta r \rho_{ab}}$ where $\langle n_{ab}(r) \rangle$ is the average number of atom pairs

in a spherical shell located between r and $r + \Delta r$, and ρ_{ab} is the number density of atom pairs of type ab . In Figure 1a, the radial distribution functions of pairs of -NO_2 and sub-units in PMMA as well as $\text{-N(CH}_3)_2$ and sub-units in PMMA for unpoled systems, averaged over the eight structures, are shown. Only four sub-atomic units in PMMA were considered in $G(r)$: CH_2 (ch2) units in the backbone, CH_3 (bch3) units bonded to the backbone alpha carbon atom, the COO (coo) side group, and the CH_3 (sch3) group bonded to oxygen. The coordinates of the center of mass of the atomic groups were employed and the minimum image convention periodic condition was used in the calculation of the separation distance between two pairs. The partial radial distribution functions reveal no appreciable order for relatively long separation distances ($> 6 \text{ \AA}$), which is typical for an amorphous system. Figure 1a shows that the DPNA molecules have a higher chance to be located near the side units of PMMA based on broad and large peaks near $\sim 4 \text{ \AA}$ separation distance. For poled structures, a similar behavior was found.

The final orientation of the DPNA molecules are affected not only by the applied field and bulk temperature but also by the local environment surrounding them, such as the local dynamics of the polymer matrix and the free volume size and shape near the chromophore. Therefore, the classical statistical treatment of dipole orientational ordering,¹³ which is based on an ideal gas like system and does not include the local polymer mobility or the surroundings of the chromophore, may not be sufficient to predict the dipole orientational order and eventually the susceptibility such as $\chi_{zz}^{(2)}$ and $\chi_{zzz}^{(2)}$. To elucidate this difficulty, we performed MD on a PMMA/DPNA guest-host NLO system under various applied electric field strengths at two different densities. For the HD system, we applied fields of $5 \text{ kV}/\mu\text{m}$, $10 \text{ kV}/\mu\text{m}$, and $50 \text{ kV}/\mu\text{m}$, while, for the LD system, we used fields of $0.5 \text{ kV}/\mu\text{m}$, $1 \text{ kV}/\mu\text{m}$, and $5 \text{ kV}/\mu\text{m}$. The field induced alignment of DPNA is shown in Figure 1b. Relatively rapid saturation of the dopant alignment was obtained for the $50 \text{ kV}/\mu\text{m}$ field in the HD system as well as the $5 \text{ kV}/\mu\text{m}$ field in the LD system. A great difference in order between the HD and LD systems for the $5 \text{ kV}/\mu\text{m}$ field is noticeable, indicating that chromophore orientation is greatly influenced by polymer mobility.

In the LD simulation, the rotational motion of each DPNA molecule involved a few "large" jumps (i.e., $\Delta\theta \geq 0.5 \text{ rad}$ or $\sim \pi/6$), which occurred in a fairly short time period. The HD system was similarly characterized except that the "large" jumps were less frequent and had smaller angular displacements in general. A comparison of the incidence of these large jumps to the value of the projection of the molecular dipole moment along the field direction, for a single dopant molecule, during the same time period reveals a qualitative correspondence. A model that accounts for these results is that the dopant orientation occurs chiefly through these relatively big rotational jumps rather than by a process consisting of many incremental motions. A corresponding analysis of the absolute translational displacement of the dopant showed that during the field induced orientation, the dopant translational jumps were only $1\text{--}2 \text{ \AA}$, suggesting that the orientation process is effected only by the dopant's immediate environment. This is in contrast to the observation by Hall et. al., that, during the average dopant reorientation time, near T_g , the dopant can translate (via diffusion) over 70 times its length.¹⁴ These studies of the translation-rotation paradox by Hall et. al. showed that reorientation times and diffusion times near T_g are very different, with reorientation times being much longer. Our simulation data suggests that the application of an electric field significantly decreases the orientational relaxation time such that little diffusion is seen during that time.

We also calculated the absolute displacement of the atoms in the polymer at every rotational jumping event as a function of their location from DPNA. Region I was assigned for the atoms located within 6 \AA from the center of mass of either the NO_2 or $\text{N(CH}_3)_2$ units, otherwise, region II is assigned. The absolute displacement was accumulated for each atom type and then normalized by their populations. The ratios of the normalized displacements

of the atoms between region I and region II were calculated. Every type of atom in region I had a higher absolute displacement than those in region II for both the HD and LD systems. For the HD system, which is in a sub- T_g state, the motion of the side group COOCH_3 unit is more responsible for DPNA orientation, while in the LD system, which is above T_g , motions of all atom types have nearly equal contributions to DPNA orientation. These results are in agreement with the arguments suggested by experimental work on sub- T_g states^{2,15,16} using SHG and EO techniques. Details of these calculations can be found elsewhere.¹⁷

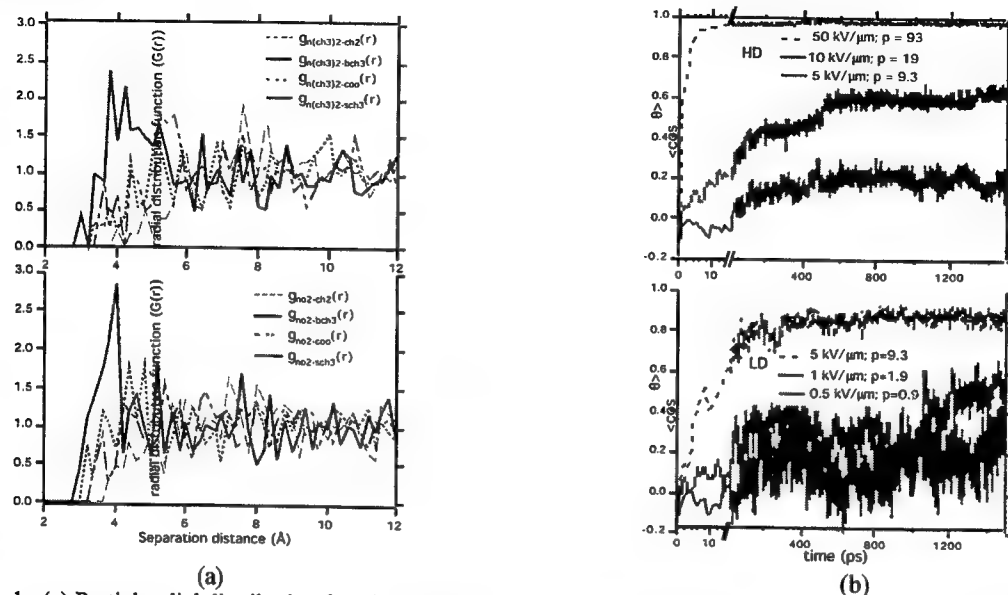


Figure 1. (a) Partial radial distribution functions between the center of mass of $\text{N(CH}_3)_2$ in DPNA and sub-units in PMMA and those between the center of mass of NO_2 in DPNA and sub-units in PMMA in unpoled static structures; (b) Average value of the dipole moment vector of DPNA along the field direction with respect to poling time for the HD (1.18 g/cm³) and LD (0.98 g/cm³) systems, respectively. The average value was obtained from 16 DPNA molecules.

Acknowledgment

This material is based on work supported by the National Science Foundation under Grant #DMR-9705800. The authors thank Dr. Kung for helpful discussions on btcl scripts for the E_{field} calculation.

References

1. A. Dhinojwala, G. K. Wong, and J. M. Torkelson, *Macromolecules* **26**, 5943 (1993).
2. F. Ghebremichael and H. S. Lackritz, *Applied Optics* **36**, 4081 (1997).
3. S. Misra and W. L. Mattice, *Macromolecules* **26**, 7274 (1993).
4. N. E. Moe and M. D. Ediger, *Macromolecules* **29**, 5484 (1996).
5. A. A. Gusev, U. W. Suter, and D. J. Moll, *Macromolecules* **28**, 2582 (1995).
6. J. A. Young, B. L. Farmer, and J. A. Hinkley, *Polymer* **40**, 2787 (1999).
7. *Insight II* (Molecular Simulation Inc., 9865 Scranton Road, San Diego, CA,).
8. *Amorphous Cell* (Molecular Simulation Inc., 9865 Scranton Road, San Diego, CA,).
9. H. Meirovitch, *Macromolecules* **18**, 569 (1985).
10. L. M. Hayden, S. C. Brower, and S. J. Strutz, *Macromolecules* **30**, 2734 (1997).
11. W. C. Swope, H. C. Anderson, P. H. Berens, and K. R. Wilson, *Journal of Chemical Physics* **76**, 637 (1982).
12. L. V. Woodcock, *Chemical Physics Letters* **10**, 257 (1971).
13. K. D. Singer, M. G. Kuzyk, and J. E. Sohn, *J. Opt. Soc. Am.* **4**, 968 (1987).
14. D. B. Hall, A. Dhinojwala, and J. M. Torkelson, *Phys. Rev. Lett.* **79**, 103 (1997).
15. F. Ghebremichael, M. G. Kuzyk, and C. W. Dirk, *Nonlinear Opt.* **6**, 123 (1993).
16. S. J. Strutz, S. C. Brower, and L. M. Hayden, *J. Polym. Sci., Part B: Polym. Phys.* **36**, 901 (1998).
17. W.-K. Kim and L. M. Hayden, submitted to *J. Chem. Phys.*

Organic Thin Films for Photonics Applications

Special Invited Speaker Presentation

Friday, 24 September 1999

SS

7:00pm

California Ballroom Salons 4&5

Spatial Light modulator using high Tg poled polymers

T. Yatagai

Institute of Applied Physics and Tsukuba Advanced Research Alliance (TARA)

University of Tsukuba

Tsukuba, Ibaraki, 305-8573, Japan

Tel&Fax: +81-298-53-5334

E-mail: yatagai@bk.tsukuba.ac.jp

Nonlinear organic materials have been of interest because their large optical nonlinearities and short response time. Polymeric materials are among the most promising organic materials for use in electrooptical applications. The advantage of these materials and development of spatial light modulators (SLMs) using them are discussed in this paper.

An electrically addressed SLM is designed here for optical information processing and display. It is composed of multipolymer dielectric mirrors, a polymer thin film, transparent electrodes, a planar layer and an LSI processor. The polymer films which have a large electrooptic coefficient make it possible to achieve a high modulation speed and a high contrast ratio. The use of a resonator structure is proposed to minimize the driving voltages because it increases the electrooptic effect of the material. The device has a sharp transmittance spectrum determined by the polymer film thickness and refractive index. The transmittance and reflectance of the device are controlled by the refractive index of the polymer material which is controlled by the applied voltage.

By using a corona-poled film sandwiched with multilayered dielectric mirrors, the transmittance change is observed by applying an ac voltage. A system consisting of azo dye disperse red 1 (DR1) doped poly-methyl-methacrylate (PMMA) is used as a polymeric material. The contrast ratio of the system is

70:1 at 1 kHz is obtained by applying a voltage of 11 Vrms. The maximum frequency response up to 10 MHz is performed. Side-chain molecules of poly-orange 6B isopropylideneisocyanate and N-phenylmaleimide, 4-isopropenylphenol and 4'-[N-ethyl-N-(4-isopropenylphenoxyethyl) amino]-4"-nitroazobenzene (PMPD) are also used for optical modulation. PMPD has a long decay time of more than 5000 hours of poling effect due to its high glass-transition temperature (T_g) of more than 190 °C.

Demonstration of spatial filtering using the poled polymer SLM has been successfully performed to make edge enhancement of 2-D images.

Key to Authors and Presiders

- Advincula, Rigoberto ■ FD2
 Ahn, Jpp-Heon ■ SuC4
 Ahyi, Ayayi C. ■ SaA2
 Alain, V. ■ SaE1
 Amarande, Stephen ■ SaE12
 Ananthavel, Sundaravel ■ SuB1
 Armstrong, Neal ■ FD1
 Badano, Aldo ■ SuD2
 Balasubramanian, S. ■ SuA4
 Bartoli, Filbert J. ■ SuD5
 Bechtel, James H ■ FB3
 Belfield, Kevin D. ■ SuB2
 Belyaeva, T.L. ■ SaE3, SaE4, SuD7
 Ben-Asuly, A. ■ SaE8
 Berkovic, Garry ■ SaE8, SuB3
 Bhowmik, Achintya ■ FA3, SaA2
 Blanchard-Desce, M. ■ SaE1
 Bloor, David ■ SaB5
 Bösch, M. ■ FA5, SaB4
 Bosshard, Christian ■ FA5, SaB4, SaE1, SaE5, SuC3
 Bouattou, Benharret ■ SaA3
 Boyd, Carol ■ SuC1
 Boyd, Joseph T. ■ SaA4
 Breckon, C.D. ■ SaC1
 Burcham, Kevin E. ■ SaA4
 Cai, C. ■ FA5, SaB4
 Callender, Claire L. ■ SuB4
 Cammack, Kevin ■ SuB1
 Canva, Michael ■ FB2, SaB1, SaB2, SaB3
 Carlisle, Gene ■ SaE2
 Casperson, J. D. ■ SaC5
 Chan, Kwok Pong ■ FC3, SaB3
 Chapela, V. M. ■ SaE3, SaE4, SuD7
 Chapurin, Igor ■ SuA2
 Chen, Antao ■ FB5
 Cheng, Hua ■ FC5
 Cho, Wook-Rae ■ FB2
 Chuyanov, Vadim ■ FB5, SaD2
 Clarson, Stephen J. ■ SaA4
 Clays, Koen ■ SaD4
 Cross, Graham H. ■ SaA3, SaB5
 Culjkovic, D. ■ SuD1
 Cumpston, Brian H. ■ SuB1
 Curtis, Kevin ■ SuC1
 Dalton, Larry R. ■ FA, FA1, FA2, FA5, FB1, SaD2, SuD3
 Davis, R.M. ■ SaD1
 Dhar, Lisa ■ SuB, SuC1
 Dickey, Scott ■ SaE10
 Diederich, F. ■ SaE1, SuC3
 Dominguez, Dawn D. ■ SuD4
 Dubikovsky, Vlasdislav ■ SuB2
 Dumont, Michel L. ■ FC2
 Ehrlich, Jeffrey E. ■ SuB1
 Eldada, L. ■ SuB4
 Eliasson, Blake ■ SaE10
 Erskine, Lael L. ■ SuB1
 Fainman, Yeshaiahu ■ SuA2
 Fan, R. ■ SuD1
 Feinberg, Jack ■ FB5
 Feller, Karl-Heinz ■ SaE11
 Figura, C. ■ SaD1
 Fischer, C. ■ SaB4
 Fischer, Michel ■ FC2
 Flom, Steven Robert ■ SuD4, SuD5
 Freeman, Neville J. ■ SaA3
 Galvan-Gonzalez, Adriana ■ SaB1, SaB2
 Gao, Renyuan ■ SuA1
 Garito, Anthony F ■ SuA1
 Garner, Sean ■ FB5, SaD2
 Garvey, Dennis W. ■ SaC1
 Glaeske, Holger ■ SaE11
 Gobbi, L. ■ SuC3
 Gu, S. ■ SuD1
 Gubler, Ulrich ■ SaE1, SaE5, SuC3
 Günter, Peter ■ FA5, SaB4, SaE1, SaE5, SuC3
 Hagan, David J. ■ SaE5, SuB2
 Hale, Arturo ■ SuC1
 Han, Seon Gyu ■ SuC4
 Hanack, Michael ■ SuD4
 Hayakawa, Seiichiro ■ SaE7
 Hayden, L. Michael ■ SaC6, SuD8
 Heckmann, Heino ■ SuD4
 Heflin, J. R. ■ FC, SaD1
 Heikal, Ahmed A. ■ SuB1
 Heinz, Tony F ■ FC1
 Hill, Adrian ■ SuC1
 Hirai, M. ■ SaC3
 Hsu, C. C. ■ SaD6
 Huang, Tzer-Hsiang ■ SaD6
 Hwang, Wol-Yon ■ SuC4
 Ikeyama, Yoshiki ■ SaE13
 Imamura, Masanori ■ SaE13
 Inaoka, Seiji ■ FD2
 Ishigure, T. ■ SaC2, SaC3
 Jabbour, G. E. ■ FD4
 Jäger, M. ■ FA5, SaB4, SuC3
 Jen, Alex K-Y. ■ FA2, FB, FD, SaD5
 Jin, Bih-Yaw ■ SaD6
 Kafafi, Zakya H. ■ SuD3
 Kagawa, Yasuyuki ■ SaB5
 Kajzar, Francois ■ FB2
 Kanicki, Jerzy ■ SuD2
 Kano, Mariko ■ SaC2
 Katz, Howard ■ SuC1
 Kauranen, Martti ■ FC5, SaD3
 Kemanai, Takanori ■ SaE7
 Khodorkovsky, V. ■ SaE8
 Kim, Won-Kook ■ SaD7, SuD8
 Kimura-Suda, Hiromi ■ SuD6
 Koike, Yasuhiro ■ SaC2, SaC3
 Kotler, Zvi ■ SaE8, SuB3
 Kowalczyk, Tony C ■ SaB1, SaB2
 Kubota, Yasuhiro ■ FB4
 Kuebler, Stephen M. ■ SuB1
 Kumar, Jayant ■ SaD7, SuA4
 Kuzyk, Mark G. ■ SaC1
 Kwon, Min-Suk ■ SuA3
 Lackritz, Hilary ■ SaB1, SaB2
 Larsen, R.J. ■ SuD3
 Le Duff, Anne-Claire ■ FB2, SaB3
 Lecomte, S. ■ SuC3
 Lee, Byung-Tak ■ SuA3
 Lee, Hyung-Jong ■ SaA5, SaE6, SuC4
 Lee, Myung-Hyun ■ SaA5, SaE6, SuC4
 Levin, Michael D. ■ SuB1
 Liakatas, I. ■ FA5, SaB4
 Lin, Weiping ■ FB3
 Lindle, James R ■ SuD5
 Lipson, Matthew ■ SuB1
 Liu, J. ■ FD3
 Liu, Mingguo ■ SuD5
 Liu, Sean ■ SaD6
 Liu, Sen ■ FA2
 Luh, Tien-Yau ■ SaD6
 Ma, Liang ■ FC5
 Ma, Hong ■ FA2
 Malliaras, G. G. ■ SuD1
 Malyshev, Victor ■ SaE11
 Marcu, D. ■ SaD1
 Marder, Seth ■ FA2, SaB1, SaB2, SuB1
 Martin, R. ■ SaE1
 McCord-Maughon, Diane ■ SuB1
 Meier, Joachim ■ FB2
 Meshulam, Guilia ■ SaE8, SuB3
 Miesak, Edward J. ■ SuB2
 Miller, M. ■ SaD1
 Mishra, Alpna ■ SaA2
 Moddel, Garret ■ SaE10
 Moerner, William E. ■ SaC5
 Murray, M.A. ■ SaD1
 Musick, Kwon Y. ■ FC5
 Naghschi, David ■ SaA4
 Nahata, Ajay ■ FC1
 Negres, Raluca ■ SaE5
 Neyman, P. J. ■ SaD1
 Noad, J. P. ■ SuB4
 Norwood, R. A. ■ SuA, SuB4, SuC2
 Oba, Kazutaka ■ SuA2
 Oh, Min-Cheol ■ SaA5, SaE6, SuC4
 Olbrechts, Geert ■ SaD4

- Olson, David J. ■ FB3
 Ostroverkhov, V. ■ FA4
 Ostroverkhova, O. ■ FA4, SaE14
- Pan, Feng ■ SaA1
 Pei, Manlin ■ SaE2
 Percino, J. ■ SaE3, SaE4, SuD7
 Perry, Joseph W. ■ SaD, SuB1
 Persoons, André ■ SuD, FC5, SaD3, SaD4, SaE9
 Petschek, R. G. ■ FA4
 Pliska, Tomas ■ FB2, SaB3
 Poga, Constantina ■ SuC2
 Pong, Richard G. S. ■ SuD4
 Pu, Lin ■ FC5
- Ravi, Mosurkal ■ SaB5
 Raymond, Paul ■ FB2
 Ren, Albert S. ■ SaD2
 Ren, Xiaobin ■ SuB2
 Ren, Yitao ■ SaA3
 Ricci, Vincent ■ FB2, FC3, SaB3
 Roberts, M. Joseph ■ FC4
 Robinson, Bruce ■ FA1
 Robu, Stephan ■ SuA2
 Rockel, Harald ■ SuB1
 Roitman, Daniel B. ■ FD2
 Rumi, Mariacristina ■ SuB1
- Sakai, Wataru ■ SaE13
 Samyn, Celest ■ SaE9
 Sasabe, Hiroyuki ■ SuD6
 Sassa, Takafumi ■ SuD6
 Sato, Heihachi ■ SaE7
 Sato, M. ■ SaC3
 Sattigeri, Jitendra A. ■ SaD6
 Schilling, Marcia ■ SuC1
 Schmidt, Eduard ■ SaE3
 Schnoes, Meldina ■ SuC1
 Serkin, Vladimir N. ■ SaE3, SaE4, SuD7
 Shapiro, L. ■ SaE8
 Shi, Yongqiang ■ FB3
 Shiau, Chung-Wai ■ SaD6
 Shin, Sang-Yung ■ SuA3
 Shirk, James S ■ SuD4
 Singer, Kenneth D. ■ FA4, SaE14
 Sioncke, Sonja ■ SaD3
 Sivaraman, Ram ■ SaA4
 Snow, Arthur W. ■ SuD4
 Sodah, Sunil ■ FA3
 Starodubov, Dmitry S. ■ FB5
 Stegeman, George I. ■ FB2, FC3, SaB, SaB1, SaB2, SaB3, SuD5
 Steier, William H. ■ SaA, FB5, SaD2
 Strohkendl, Friedrich P ■ SuD3
- Strutz, Shane J. ■ SaC6
 Sukhomlinova, L. ■ FA4, SaE14, SuD1
 Szablewski, Marek ■ SaB5
- Tackitt, Michael C. ■ SuC1
 Takatu, Ichiro ■ FB4
 Tan, Shida ■ FA3
 Tanaka, Satoshi ■ SaE7
 Thakur, Mrinal ■ FA3, SaA2
 Thayumanavan, S. ■ SaB1, SaB2
 Todorova, Galina ■ SaD2
 Toyama, Jiro ■ FB4
 Tripathy, Sukant K. ■ SaD7, SuA4
 Tsutsumi, Naoto ■ SaE13
 Twieg, R. J. ■ FA4, SaB1, SaB2, SaB3, SaC, SaC5, SaE14, SuD1
 Tykwinski, R. R. ■ SaE1
- Van den Broeck, Kurt ■ SaE9
 Van Elshocht, Sven ■ FC5, SaD3
 Van Stryland, Eric W. ■ SuB2
 Verbiest, Thierry ■ FC5, SaD3, SaE9
 Viens, J.-F. ■ SuB4
 Viswanathan, Nirmal K. ■ SuA4
- Wada, Tatsuo ■ SuD6
 Wang, C.H. ■ SaD5
 Wang, Wenshen ■ FB3
 Wang, Yong-Jing ■ SaE2
 Welker, David J. ■ SaC1
 Wilson, William ■ SuC1
 Woodford, Jeffrey N. ■ SaD5
 Wostyn, Kurt ■ SaD4
 Wright, D. ■ SaC5
 Wu, Jianyao ■ FA2
 Wu, Xiaoming ■ FA2
- Yacoubian, Araz ■ FB5, SaD2
 Yamada, Takeshi ■ FB4
 Yamamoto, Jun ■ SaE13
 Yang, Ke ■ SaD7
 Yang, Yang ■ FD3
 Yatagai, T. ■ SS1
 Yeh, Fen-Fen ■ SaD6
 Yoon, Jun-Bo ■ SuA3
 You, F. ■ SaC5
- Zhang, Cheng ■ FA5
 Zhang, Hua ■ SaD2
 Zhang, Jingwen ■ SaE14
 Zhang, Xuan Q. ■ SaB1
 Zhang, Yadong ■ SuD6

Organic Thin Films for Photonics Applications

Postdeadline Paper Session

Friday, September 24, 1999

PD

7:30pm-8:15pm

California Ballroom 4&5

Postdeadline Papers
California Ballroom Salons 4&5
Friday, September 24, 1999

PD1-1 7:30pm

Sense of chromophore orientation in APD films, *W.N. Herman, M. J. Roberts, G.A. Lindsay, U.S. Navy, USA*

The sense of orientation of the chromophores in two types of nonlinear optical films fabricated by alternating polyelectrolyte deposition is determined by second-harmonic phase measurements.

PD2-1 7:45pm

Practical Electro-optic polymer modulators using PC/CLD, *Min-Cheol Oh, Hua Zhang, Attila Szep, Vadim Chuyanov, William H. Steier, Cheng Zhang, Larry R. Dalton, Univ. Southern California, USA*

We fabricated a polymeric Mach-Zehnder modulator using a PC/CLD nonlinear optical polymer which satisfies the practical device requirements of excellent nonlinearity, high thermal stability, and low loss. The first device exhibited the V_{π} of 3.4 V, the extinction ratio of 26 dB and the insertion loss of 10.6 dB including the fiber coupling loss of about 5 dB.

PD3-1 8:00pm

Narrow line laser emission from Rhodamine B cored dendrimer waveguides, *Akira Otomo, Shiyoshi Yokoyama, Tatsuo Nakahama, Shinro Mashiko, Kansai Advanced Research Center, Japan*

Extremely narrow spectrum emission is observed in mirrorless polymer waveguides which contain Rhodamine B cored dendrimers. The bandwidth of the emission is less than 0.7nm

SENSE OF CHROMOPHORE ORIENTATION IN APD FILMS

W.N. HERMAN

U.S. Navy, NAWC AD, EO Sensors Branch, Patuxent River, MD 20670
 phone: 301-342-9112, fax: 301-342-0121, email: HermanWN@navair.navy.mil

M.J. ROBERTS and G.A LINDSAY

U.S. Navy, NAWC WD, Chemistry and Materials Division, China Lake, CA 93555

Alternating polyelectrolyte deposition (APD) is a promising technique for fabricating multilayer thin films at room temperature.¹ The substrate is alternately dipped in two different aqueous solutions — one containing a polycation and the other a polyanion. By incorporating chromophores in the polymer cation and/or anion, it has been demonstrated that the APD process can be used to make multilayer NLO polymer films.²⁻⁹ In addition, a recent encouraging discovery is that these films exhibit a high degree of thermal robustness.⁷⁻⁹

The structure of the stilbazolium-substituted polyepichlorohydrin (SPECH) side-chain polymer used in fabricating NLO APD films is shown in Figure 1. Results of orientation measurements on two types of films are reported here: the first had SPECH layers alternated with poly(sodium 4-styrenesulfonate) (PSS) and the second type with a weak polyanion - polyacrylic acid (PAA). These films were fabricated at room temperature in ambient air using a computer-interfaced Zeiss HMS Programmable Slide Stainer that was kept in a Class 100 clean room under UV/blue blocked fluorescent light. The SPECH/PSS films were deposited on hydrophobicized glass slides and the SPECH/PAA films on base-washed glass slides.¹⁰ Determination of the orientation of the chromophores in an NLO film is essential to understanding and improving the fabrication process in a new technique such as APD. Estimates of the tilt angle are useful for assessing the degree of polar order obtained in a particular film, but knowing which end of the chromophore is up is crucial to understanding the details of the deposition process. From ratios of different second-harmonic *d*-coefficients, for example, it is possible to extract a tilt angle

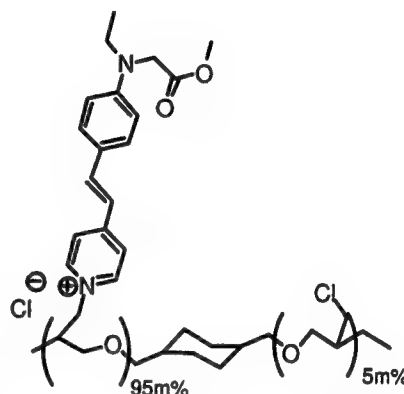


Figure 1. Structure of the SPECH polycation.

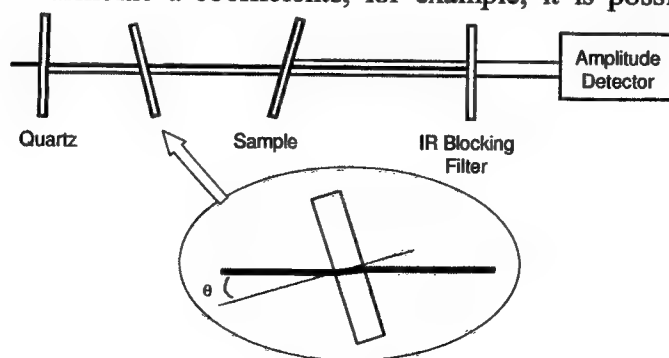


Figure 2. Arrangement for making SHG interference measurements. The glass slide blown up in the inset is rotated from -90° to $+90^\circ$ to vary the phase difference between the SHG from quartz and from the sample, which then interfere to produce an intensity modulation.

under the often-used assumption of a δ -function distribution.¹¹ The angle so obtained, however, is modulo 180° and as such does not determine “which end is up.” The absolute sense of orientation can be determined from second-harmonic generation (SHG) phase measurements^{12,13} using the setup depicted in Figure 2. The interference of the second harmonic (SH) generated by quartz with the SH generated by the sample can be varied using a glass plate as shown in the inset in Figure 2. Rotating the glass plate produces an intensity interferogram as a function of plate rotation angle. If the interferograms from two different films with similar chromophores are compared, they will be in phase if the absolute sense of orientation of the chromophores is the same (for example, acceptor ends of chromophores in both films are up) or be 180° out of phase if the absolute sense of orientation is opposite regardless of the tilt angle. The value of the tilt angle affects the relative magnitudes of SHG from the two films, but does not affect this phase issue. Effectively, the relative sign of $\chi^{(2)}$ with respect to a reference thin film is being measured and, for a chromophore with a 1-D charge transfer axis, $\chi^{(2)}$ is proportional to β_{zzz} . The 1319nm laser line of a diode pumped Nd:YAG was used as the fundamental for these SHG measurements.

For the reference, we used a 20-bilayer AB accordion polymer LBK film because the LB deposition process is well-established and MOPAC 7 simulations have been carried out for these polymers.^{14,15} When this film was placed at the position marked “sample” in Figure 2, the resulting interferograms are shown in Figure 3 indicated with solid-circle data points. The solid lines in the plots are least squares fits to the data to extract the phase ϕ_0 when the glass plate is perpendicular to the beam. The refractive index dispersion of both glass and air are required to fit the data. The interferogram for a 53 bilayer SPECH/PSS film is shown with open-circle data points in the top plot of Figure 3 and for a 51 bilayer SPECH/PAA film with open-circle data points in the bottom plot of Figure 3. The SPECH/PSS interferogram is clearly in phase with the 20-bilayer AB LBK interferogram, while the SPECH/PAA interferogram is out of phase with the

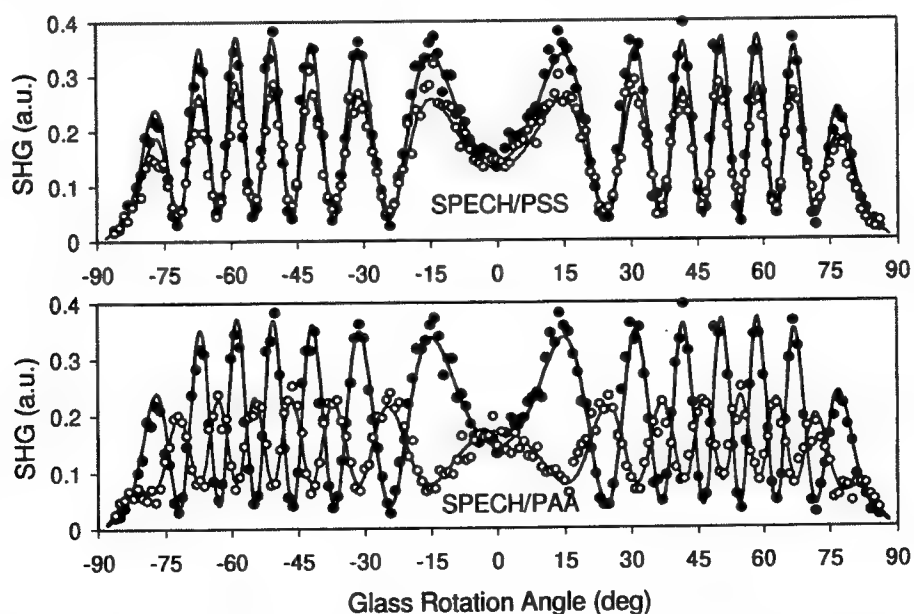


Figure 3. Superposition of SHG interferograms for 20-bilayer AB accordion polymer LBK film (solid circles, top and bottom plots) with 53-bilayer SPECH/PSS APD film (open circles, top plot) and 51-bilayer SPECH/PAA (open circles, bottom plot). The solid lines are least squares fits to the data.

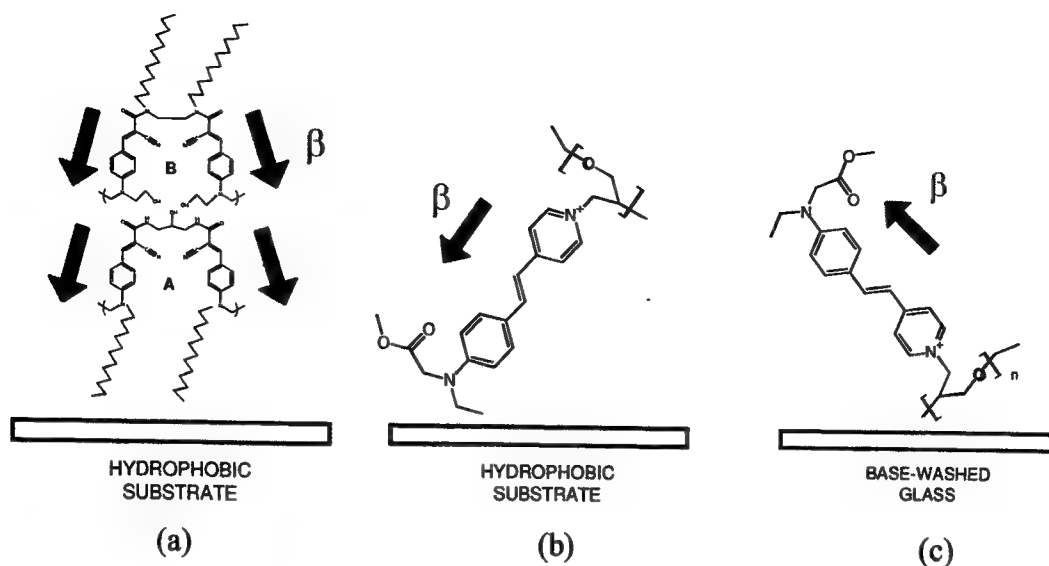


Figure 4. Orientations of the stilbazolium chromophore in (b) SPECH/PSS and (c) SPECH/PAA as deduced from comparison of interferograms with the reference (a) AB accordion polymer LBK film.

20-bilayer AB LBK interferogram. The least squares fits gave $\sim 0^\circ$ and $\sim 180^\circ$, respectively, for the phase differences. Thus, the absolute sense of orientation for the stilbazolium chromophore in the SPECH/PSS and SPECH/PAA films is as shown in Figure 4. The β -vectors shown in Figure 4 represent the irreducible vector part of the hyperpolarizability tensor.

These results confirm the expected sense of orientation.¹⁶ For SPECH/PSS on a hydrophobic substrate, the end of the chromophore with the pyridinium group near the backbone is relatively more hydrophilic than the opposite end of the chromophore. For SPECH/PAA on the base-washed glass, the orienting mechanism is thought to be ionic-attraction between the pyridinium and the negatively charged groups on the glass.

REFERENCES

1. J. H. Cheung, A. F. Fou, M. F. Rubner, *Thin Solid Films* **224**, 985 (1994).
2. Y. Lvov, S. Yamada, and T. Kunitake, *Thin Solid Films* **300**, 107(1997).
3. X. Wang, S. Balasubramanian, L. Li, X. Jiang, D.J. Sandman, M.F. Rubner, J. Kumar, S.K. Tripathy, *Macromol. Rapid Commun.* **18**, (451)1997.
4. J.R. Heflin, Y. Liu, C. Figura, D. Marciu, R.O. Claus, *Proc. SPIE* **3147**, 10(1997).
5. M.J. Roberts, J.D. Stenger-Smith, P. Zarras, G.A. Lindsay, R.A. Hollins, A.P. Chafin, R.Y. Yee, K.J. Wynne, *Proc. SPIE* **3281**, 126(1998).
6. C. Figura, D. Marciu, Y. Liu, Y. Wang, K. Lenahan, R. Claus, and J. Heflin, *Polym. Prepr.* **39**, 1126 (1998).
7. M.J. Roberts, G.A. Lindsay, W.N. Herman, and K.J. Wynne, *Polymer Preprints* **39**, 1122(1998).
8. M. Joseph Roberts, Geoffrey A. Lindsay, Warren N. Herman, Kenneth J. Wynne, *J. Am. Chem. Soc.*, **120**, 11202(1998).
9. J.R. Heflin, C. Figura, and D. Marciu, *Appl. Phys. Lett.* **74**, 497(1999).
10. For further details, see M.J. Roberts, paper FC4 in this conference.
11. A method for determining a more general orientational distribution function is given by B. Park, Y. Kinoshita, and H. Takezoe, *Phys. Rev. E* **57**, 6717(1998).
12. X. Liu, L. Liu, and X. Lu, *Thin solid films* **217**, 174(1992).
13. K. Kajikawa, H. Takezoe, and A. Fukuda, *Langmuir* **12**, 580(1996).
14. G. Lindsay, K. Wynne, W. Herman, A. Chafin, R. Hollins, J. Stenger-Smith, J. Hoover, J. Cline, and J. Roberts, *Nonlinear Optics B* **15**, 139(1996).
15. W.N. Herman, M. J. Roberts, J.D. Stenger-Smith, A.P. Chafin, R.A. Hollins, G.A Lindsay, and K.J. Wynne, *Polymer Preprints* **39**, 1105(1998).
16. Arising out of private conversation with K.J. Wynne.

Practical Electro-Optic Polymer Modulators Using PC/CLD

Min-Cheol Oh, Hua Zhang, Attila Szep, Vadim Chuyanov, William H. Steier

Department of Electrical Engineering, University of Southern California, Los Angeles, CA

Cheng Zhang, Larry R. Dalton

Chemistry Department, University of Southern California, Los Angeles, CA

Optical modulators made of electro-optic polymers have been investigated to demonstrate the wide modulation bandwidth over 100 GHz by virtue of the inherent low dispersion of the refractive index between optical and millimeter-wave frequencies [1]. Many kinds of electro-optic polymers have been synthesized to obtain the higher nonlinearity, and very recently the EO coefficient over 100 pm/V @ 1.06 μm has been realized in the guest-host system of PMMA and a highly nonlinear chromophore [2]. The PMMA host, however, can not guarantee the thermal stability which is essential for the practical polymer modulator.

To produce a device quality material with good thermal stability, a chromophore was incorporated into a thermo-set polyurethane system so that a MZ modulator with the V_π under 5 V was demonstrated for the 1.3 μm wavelength [1]. Nevertheless, the polyurethane system exhibited rather higher optical loss over 2 dB/cm compared to the loss of PMMA system, 1 dB/cm, and the efficiency of poling was much lower than that of PMMA.

In this work, we demonstrate a MZ modulator using a guest-host system of polycarbonate (PC) and CLD. The PC/CLD polymer satisfies the requirements for the practical polymer modulators. It has an excellent nonlinearity over 90 pm/V at the 1.06 μm wavelength, a thermal stability of 120 $^\circ\text{C}$, and a optical propagation loss of 1 dB/cm at the 1.3 μm wavelength. A special waveguide fabrication technique was introduced to compromise the weakness of PC/CLD against the chemicals like the photoresist and the developer. The first fabricated MZ modulator exhibited good performances required for the practical modulators such as a low V_π , high extinction ratio, and low insertion loss.

First of all, to find out the optimum poling temperature, we prepared some samples of PC/CLD coated on ITO glasses. The PC/CLD film was poled at some different temperatures for 30 min. by applying 8 kV at the needle of corona poling setup. The best EO coefficient over 90 pm/V was achieved at the poling temperature of 140 - 150 $^\circ\text{C}$ as shown in Fig. 1.

The thermal stability was obtained by the in-situ second harmonic measurement. Fig. 2 shows the decay of nonlinearity as the function of temperature. It is shown that the polymer has the thermal stability of about 120 $^\circ\text{C}$, which meets most systems requirements.

To measure the optical loss of the polymer, we prepared a planar waveguide structure by coating the PC/CLD on a 4 μm -thick oxide layer on a Si substrate. The propagation loss was measured by using the high-index liquid immersion technique [3]. From the output power variation depending on the immersion depth as shown in Fig. 3, the losses were found to be 1.2 dB/cm and 2.2 dB/cm for the 1.3 μm and 1.55 μm wavelength, respectively.

In spite of the excellent characteristics explained so far, the PC/CLD was difficult to process using the

standard photolithography because the polymer was dissolved during the photoresist coating. In order to protect the PC/CLD layer from the photoresist solvent, we coated an additional thin polymer of UV15 on the PC/CLD.

Fig. 4 shows the fabrication steps of the PC/CLD polymer waveguide. After coating the UV15 lower cladding and the PC/CLD core layer, the film was corona-poled at 140 °C for 30 min. by applying 8 kV. Then the diluted UV15 solution was coated to make a thin protection layer with a thickness of about 0.6 μm . The waveguide lines were patterned on the protection layer using a standard photolithography. By using the O_2 reactive ion etching (RIE), the UV15 protection layer was etched to make the rib structure of 0.5- μm depth. After the first RIE, the photoresist residue was removed by using a developer. Finally, the waveguide pattern made of UV15 was transferred into the PC/CLD layer by etching the whole areas with RIE. The rib height of the waveguide became 0.4 μm after the second RIE. The UV15 had the faster etch rate than the PC/CLD so that the final rib height became smaller than the first rib height on UV15. For the upper cladding layer, a UV curable epoxy, NOA73 was coated. The total thickness of the device became 9.0 μm with the core thickness of 2.4 μm . The end facet of the waveguide was diced with a nickel blade for the light coupling.

To measure the performance of the fabricated modulator, a single mode fiber was aligned to couple the TM polarized light of 1.3- μm wavelength into the waveguide. The output light was focused at a detector by using a 60x microscope objective lens. DC bias was applied to obtain the maximum output power by compensating the initial phase mismatch of the MZ modulator. The total insertion loss was measured to be 10.6 dB including the fiber coupling loss of about 5 dB due to the significant mode size mismatch. For the sample length of 3 cm, the propagation loss can be translated to 2 dB/cm, which is higher than the loss measured at the planar waveguide structure, 1.2 dB/cm. The excess loss of 0.8 dB/cm may be explained by the scattering from the minute roughness on the waveguide surface that was occurred after the waveguide RIE.

The electro-optic modulation response of the device was measured by applying an 1-kHz electrical signal with a sawtooth waveform. Fig. 5 shows the oscilloscope trace of the modulated optical signal. For the MZ modulator with a 2-cm long electrode, the V_π was measured to be 3.4 V, which is corresponding to an r_{33} of 40 pm/V at the 1.3 μm wavelength. The electro-optic coefficient is lower than the result obtained by the single PC/CLD layer poling. We believe this is due to the difference in electrical conductivity of the core and cladding at the poling temperature. If we optimize the poling by using a different cladding material with lower resistivity at the poling temperature, it should be possible to decrease the V_π to less than 2 V. The extinction ratio of the MZ modulator was as high as 26 dB, which means that the waveguide satisfies strictly single mode condition.

- [1] W. H. Steier et al., "Polymer electro-optic devices for integrated optics," *Chemical Physics*, vol. 245, pp. 487-506, 1999
- [2] L. R. Dalton et al., to be presented at the same conference, *Organic Thin Films for Photonics Applications*, Santa Clara, CA, Sept. 24-26, 1999.
- [3] C.-C. Teng, "Precision measurements of the optical attenuation profile along the propagation path in thin-film waveguides" *Applied Optics*, vol. 32, pp. 1051-1054, 1993.

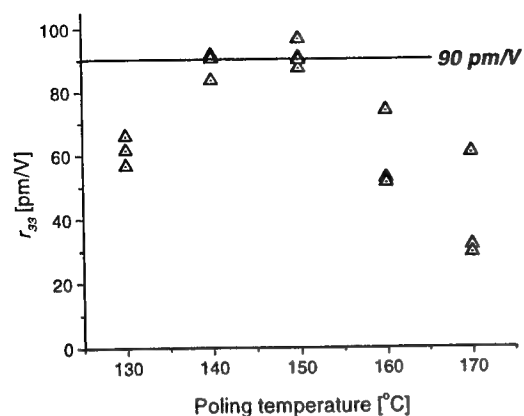


Fig. 1. Electro-optic coefficient measured for the different poling temperatures @ 1.06 μm wavelength.

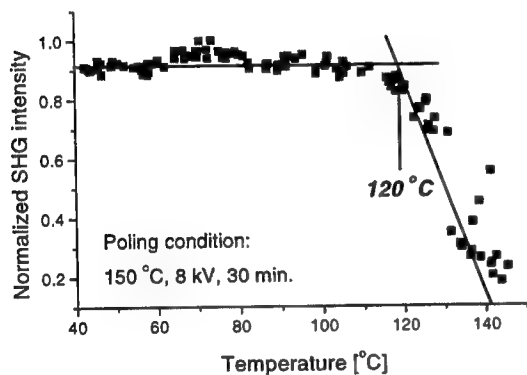


Fig. 2. Thermal stability of PC/CLD polymer measured by the second harmonic measurement.

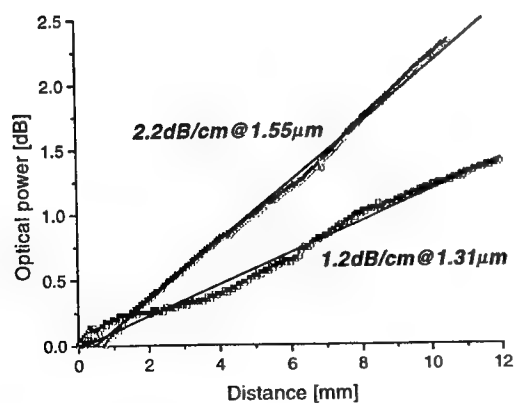


Fig. 3. Propagation loss of PC/CLD measured by the liquid immersion technique.

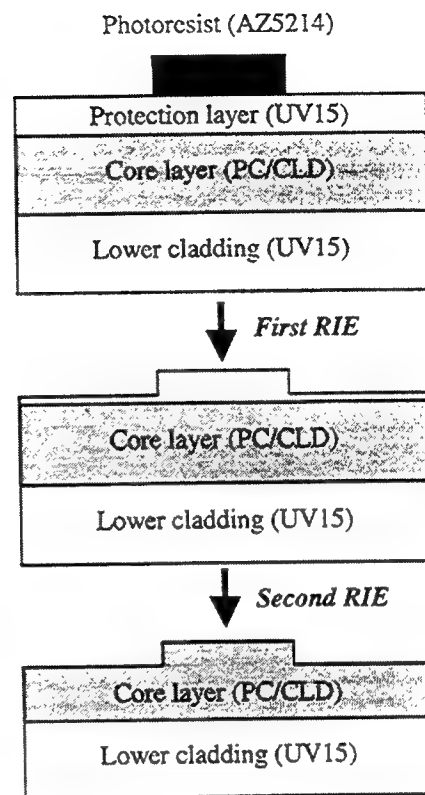


Fig. 4. Two step RIE of PC/CLD polymer waveguide fabrication with the protection layer.

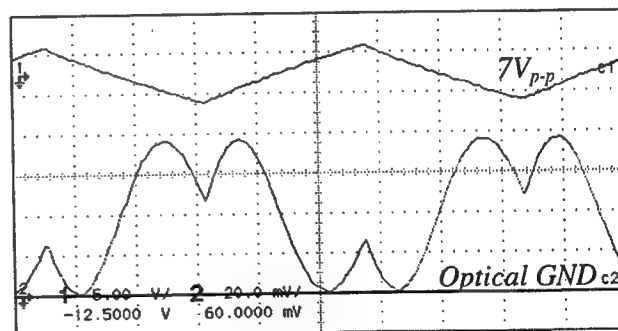


Fig. 5. Electro-optic modulation response of PC/CLD MZ-modulator at the 1.3 μm wavelength exhibiting a V_{π} of 3.4 V and an extinction ratio of 26 dB.

Narrow Line Laser Emission from Rhodamine B Cored Dendrimer Waveguides

Akira Otomo, Shiyoshi Yokoyama, Tatsuo Nakahama, and Shinro Mashiko
Kansai Advanced Research Center, Communications Research Laboratory
588-2 Iwaoka, Nishi-ku, Kobe 651-2401 Japan

Organic polymer mirrorless lasers have been investigated in various organic material systems, such as dye doped polymers,¹ conductive polymers,^{2,3} and scattering pigment solutions.⁴ Phenomenon of most of observed mirrorless lasing is amplified spontaneous emission (ASE), excepting a few cases claimed as superfluorescence. The bandwidths of the emission spectrum obtained from these mirrorless systems are rather broad (≈ 10 nm), even in long gain waveguide systems (1.7 nm).³ Narrow line emission from mirrorless systems has been reported in strongly scattered semiconductor films,⁵ and here we report amplified narrow line laser emission from weakly scattered PMMA waveguides containing Rhodamine B(RhB) cored dendrimers.

Dendrimers have attracted attentions because their branching architecture makes their three dimensional structures highly controllable. We synthesized RhB cored dendrimers in order to isolate the RhB from other molecules (Fig. 1). The RhB molecules in a concentrated solution tend to aggregate and become inactive for fluorescence. Since the shell surrounding a dendrimer core limits the interaction of the RhB molecules, aggregated dendrimers are still fluorescent. Moreover the shell can prevent some degradation reactions of the cored dye if it is covered by antioxidant molecules.

RhB dendrimer waveguides were formed by dispersing the dendrimers into host polymer, poly-methylmethacrilate (PMMA), films. The RhB dendrimers and PMMA were mixed and dissolved 10 w% in cyclohexanone and then spun onto fused silica substrates, that had been cut into 5-mm-wide rectangular shapes. The films thickness was adjusted as 700 – 800 nm for single mode waveguides at the emission wavelengths of the RhB (≈ 600 nm). The waveguides were optically pumped from the film surface using a frequency doubled Nd³⁺:YAG pulse laser (532 nm wavelength, 3 nsec pulse width, 10Hz repetition rate). The pumping region was a 0.1-mm-wide and 4-mm-long stripe shape formed by focusing with a cylindrical lens through a 4 mm slit. The fluorescence guided along the stripe in the film was collected by a 20x microscope objective and was separated from the substrate guided light by making an expanded image of the waveguide end face on the spectrometer input.

The dependence of the total emission from the waveguides on the pump fluence is shown for various RhB dendrimer densities in Fig. 2. The figure clearly shows the typical stimulated emission threshold behaviour for all the RhB dendrimer concentrations studied. The logarithmic plot in Fig. 2 shows the S-shaped transition characteristic of ASE. The evolution of the waveguide emission spectra with increasing pumping fluence is shown in Fig. 3. At low

pumping energies the fluorescence spectrum consists of a single broad spontaneous emission peak. As pumping energy increases, a narrow line emission appears suddenly and grows rapidly in the spectrum obtained from the film with the higher RhB dendrimer concentration. From its first appearance, the width of the emission line is less than 0.7 nm (FWHM). The observed linewidth is limited by the resolution of the spectrometer used. This behaviour (i.e. constant linewidth) is not found in ordinary ASE, in which case the linewidth gradually decreases as the pumping energy increases. The narrow line emission is not due to any macroscopic cavities formed in the waveguides. The end faces do not act as oscillator mirrors because the spincoating method results in the formation of very thick rips on the edges. That is also confirmed by the fact that the narrow line is still observed in the oblique end faces against the pumping stripe. When the pump energy increases further, other narrow peaks appear and combine together. The RhB/PMMA waveguide, in contrast, does not contain dendrimers and shows the ordinary spectral narrowing behaviour of ASE. Since the experimental conditions, except the presence or absence of the dendrimers, are the same for these two cases, no geometrical structure constructed physically or optically forms oscillators. Indeed, the presence of the dendrimer is the only cause of the narrow line laser emission. Moreover the narrow emission line was observed only in the spectra obtained from films in which the RhB dendrimer concentration was 0.5 w% or more. The films with lower RhB dendrimer concentrations show only the normal ASE behaviour. Here, the concentration is expressed for the chromophore, not

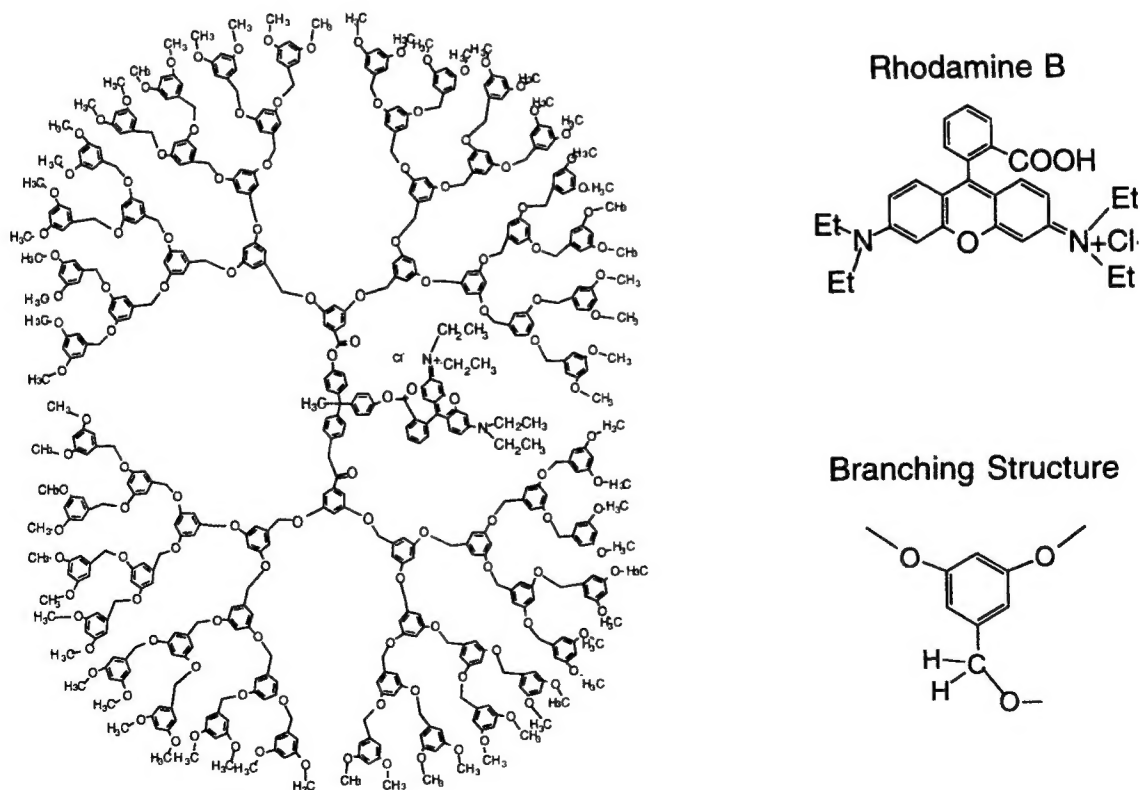


Fig. 1. The 4th generation rhodamine B cored dendrimer (RhB-G4ether).

for the dendrimer. There is some evidence that the weak scattering due to the aggregation of the RhB dendrimers causes the narrow line in the spectrum obtained from films with in the higher concentrations of RhB dendrimers. In the fluorescence lifetime measurement, the films with higher RhB dendrimer concentrations show lifetimes shorter than the films with lower concentrations. The same behaviour is found in the experiments with dispersed dendrimers and dendrimer aggregates on the substrate. This indicates that the dendrimers aggregate in the PMMA matrix and introduce scattering in the films with higher dendrimer concentrations. We have not yet clearly identified the mechanism of this narrow line emission.

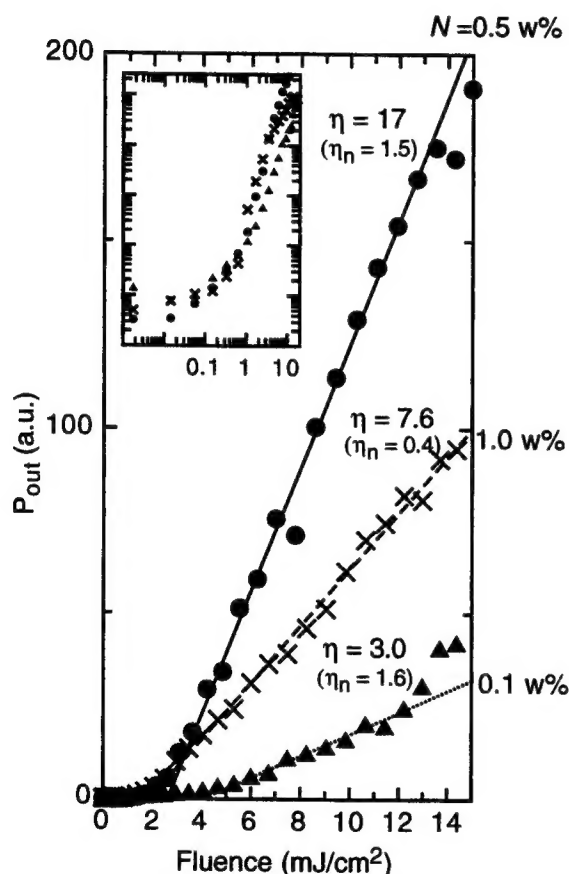


Fig. 2 Total emission from the RhB dendrimer/PMMA waveguides as a function of the pump fluence.

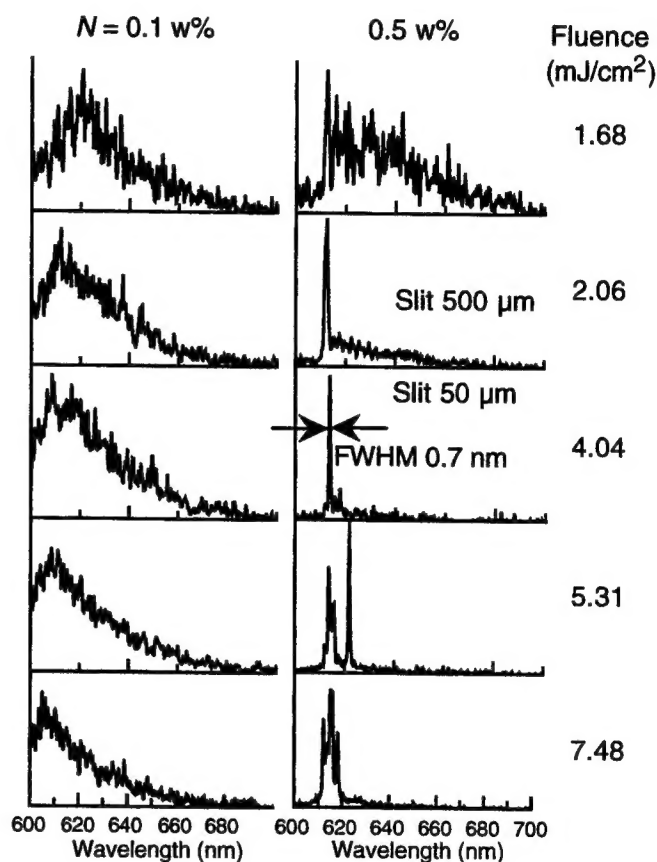


Fig. 3 Evolution of the emission spectra from the waveguides with increasing pump fluence.

References

1. R. E. Hermes, T. H. Allik, S. Chandra, and J. A. Hutchinson, *Appl. Phys. Lett.* **63**, 877 (1993).
2. F. Hide, M. A. Diaz-Garcia, B. J. Schwartz, M. R. Andersson, Q. Pei, and A. J. Heeger, *Science* **273**, 1833 (1996).
3. C. Zenz, W. Graupner, S. Tasch, G. Leising, K. Müllen, and U. Scherf, *Appl. Phys. Lett.* **71**, 2566 (1997).
4. N. M. Lawandy, R. M. Balachandran, A. S. L. Gomes, and E. Sauvain, *Nature* **368**, 436 (1994).
5. H. Cao, Y. G. Zhao, H. C. Ong, S. T. Ho, J. Y. Dai, J. Y. Wu, and R. P. H. Chang, *Appl. Phys. Lett.* **73**, 3656 (1998).

Key to Authors

Vadim Chuyanov
Larry R. Dalton
W.N. Herman
G.A. Lindsay
Shinro Mashiko
Tatsuo Nakahama
Min-Cheol Oh
Akira Otomo
M. J. Roberts
William H. Steier
Attila Szep
Shiyoshi Yokoyama
Cheng Zhang
Hua Zhang

Organic Thin Films for Photonics Applications

Technical Program Committee

William H. Steier, *Univ. Southern California, USA, General Chair*
Robert Twieg, *Kent State Univ., USA, General Chair*
Alex K-Y. Jen, *Northeastern Univ., USA, Program Chair*
Robert A. Norwood, *Photon-X, Inc., USA, Program Chair*
Paul Ashley, *US Army Missile Command, USA*
Larry Dalton, *Univ. of Washington, USA*
Louay Eldada, *AlliedSignal Inc., USA*
Susan Ermer, *Lockheed Martin Missiles & Space, USA*
Steve Forrest, *Princeton Univ., USA*
Zakya Kafafi, *Naval Res. Lab., USA*
Yasuhiro Koike, *Keio Univ., Japan*
Mark G. Kuzyk, *Washington State Univ., USA*
Hilary S. Lackritz, *Gemfire Corp., USA*
George F. Lipscomb, *Lightwave Microsystems, USA*
Robert D. Miller, *IBM Almaden Res. Ctr., USA*
Nasser Peyghambarian, *Univ. of Arizona, USA*
Xina Quan, *Lucent Tech./Bell Labs., USA*
Yongqiang Shi, *TACAN Corp., USA*
George I. Stegeman, *Univ. of Central Florida, USA*
Yang Yang, *Univ. of California, Los Angeles, USA*
Joseph Zyss, *École Normale Supérieure de Cachan, France*

International Advisory Committee

Richard Friend, *Cavendish Lab., UK*
Peter Günter, *Inst. of Quantum Electronics, ETH Zurich, Switzerland*
Alan Heeger, *Univ. of California, Santa Barbara, USA*
Toshikuni Kaino, *Tohoku Univ., Japan*
Barrie Keyworth, *JDS Fitel Inc., Canada*
Wolfgang Knoll, *Max-Planck-Inst. Für Polymerforschung, Germany*
Seizo Miyata, *Tokyo Univ. of Agriculture & Tech., Japan*
Almeria Natansohn, *Queen's Univ., Canada*
André P. Persoons, *Univ. of Leuven, Belgium*
HiroYuki Sasabe, *RIKEN, Japan*